HIGHER ORDER LAMINATED COMPOSITE PLATE ANALYSIS BY HYBRID FINITE ELEMENT METHOD

by

MING-SANG LI

B.S., National Cheng Kung University, Taiwan (1981)
M.A.Sc., University of Toronto, Canada (1984)

SUBMITTED TO THE DEPARTMENT OF
AERONAUTICS AND ASTRONAUICS
IN PARTIAL FULFILLMENT OF THE REQUIREMENTS
FOR THE DEGREE OF

DOCTOR OF PHILOSOPHY

at the

MASSACHUSEETS INSTITUTE OF TECHNOLOGY

June, 1989

Signature of Author _____
Department of Aeronautics and Astronautics
June 15, 1989

Certified by _____
Professor Theodore H.H. Pian
Thesis Supervisor

_____
Professor James W. Mar
Thesis Committee

_____
Professor Jerome Connor
Thesis Committee
Department of Civil Engineering

Accepted by _____
Professor Harold Y. Wachman
Chairman, Departmental Graduate Committee

To my parents

Kin and Hung Lin

HIGHER ORDER LAMINATED COMPOSITE PLATE ANALYSIS BY HYBRID FINITE ELEMENT METHOD

by

MING-SANG LI

Submitted to the
Department of Aeronautics and Astronautics
on June 15, 1989 in partial fulfillment of
the requirements for the Degree of
Doctor of Philosophy
in
Aeronautics and Astronautics

ABSTRACT

A development has been made of assumed stress hybrid elements for laminated composite plate analysis based on a mixed form of Hellinger-Reissner principle which is a function of three displacement components and three transverse stresses. The elements satisfy the stress continuity along the laminar boundaries and the traction free condition at the top and bottom surfaces of the laminates. Two families of elements are constructed. One is to assume the displacement field to be continuous function through the laminated thickness and the other is to be piecewise continuous function. A criterion for suppressing the kinematic deformation modes of the present elements has been established. The performances of these elements are verified by a large number of illustrative examples. The present mixed form hybrid stress elements have shown to be much more computationally efficient than the conventional hybrid stress elements.

The present mixed form element is also applied in conjunction with the global-local finite element method for the analyses of laminates with straight or curvilinear free edges and accurate results are obtained. Furthermore, various stress smoothing schemes for isotropic solids as well as laminated structures are also investigated using conventional hybrid stress elements. Such schemes are not as effective as the use of the present mixed form element.

Thesis Committee:

Theodore H.H. Pian
Professor of Aeronautics and Astronautics

James W. Mar
Professor of Aeronautics and Astronautics

Jerome Connor
Professor of Civil Engineering

ACKNOWLEDGEMENTS

To begin with, I would like to thank my family for their continuous support and encouragement.

I would like to express my sincere gratitude to Professor Theordore H.H. Pian, the Chairman of my thesis committee, for his continuous guidance, encouragement and support throughout the course of this study. He first introduced me the hybrid stress finite element method five years ago. Especially in the final stage of this work, he made many invaluable advice and suggestions and carefully check and corrected my writing. Also, I would like to thank Professor James W. Mar and Professor Jerome Connor for being a member of my thesis committee and for their continuous support, encouragement and advice. Their concern for my education in MIT was invaluable.

I would like to express my appreciation to Professor John Dugundji, Professor Paul A. Lagace and Professor Michael J. Graves for their carefully reading this text and suggestions. I would also like to thank Professor Andreas H. Von Flotow for his concern on my study.

I am also very grateful to the brothers and sisters in Boston Chinese Bible Study Group who made my years in Boston meaningful and enjoyable.

Finally, I would like to thank the Department of Aeronautics and Astronautics for continuously providing the financial support which made my education possible.

TABLE OF CONTENTS

LIST OF FIGURES

LIST OF TABLES

LIST OF SYMBOLS

Symbol

$\mathbf{B}$	strain-displacement interpolation matrix
$\mathbf{b}$	nodal strain parameters
$\mathbf{C}$	elasticity matrix
$\mathbf{D}$	differential operator matrix
$d_i(\zeta)$	interpolation polynomial of stresses
E	elasticity modulus
$\mathbf{e}$	column matrix of inplane or transverse strains
$\mathbf{F}$	column matrix of body forces
$f_i(\zeta)$	interpolation polynomial of displacements
f_j^i	transverse shear stress component of the i^{th} layer
$\mathbf{G}$	matrix in assumed stress finite element formulation
G	shear modulus
$g_i(\zeta)$	interpolation polynomial of displacements
$\mathbf{H}$	matrix in assumed stress finite element formulation
H	laminate thickness
h	laminate or layer thickness
$\mathbf{K}$	global stiffness matrix
$\mathbf{k}$	element stiffness matrix
k	arbitrary coefficient
L	length parameter
$l_i(\zeta)$	interpolation polynomial of displacements
$\mathbf{M}$	consistent matrix

$\mathbf{M}_L$	lumped matrix
$\mathbf{N}$	matrix of shape function
$\mathbf{P}$	matrix of assumed polynomials
P	mixed strain energy density
$\mathbf{p}$	nodal stress parameters
$\mathbf{Q}$	column matrix of nodal load
$\mathbf{Q}^i$	reduced material property matrix of layer i
$\mathbf{q}$	nodal displacements
$\Delta\mathbf{q}$	nodal displacement increments
$\mathbf{R}$	rigid body modes
R	radius of hole
r, θ, z	cylindrical coordinates (global)
$\mathbf{S}$	compliance matrix
S_u	prescribed displacement boundary
S_σ	prescribed traction boundary
$s_i(\zeta)$	interpolation polynomial of stresses
$\mathbf{T}$	column matrix of boundary tractions
$\mathbf{T}_i$	transformation matrix of layer i
t	laminate thickness
$\mathbf{t}$	column matrix of inplane or transverse stresses
$\mathbf{u}$	column matrix of displacements
U_d	element deformation energy
u, v, w	displacement components in Cartesian coordinates
u_0, v_0, w_0	the first terms in a power series expressions of u, v and w in the normal coordinate z
V	volume of the continuum

V_n	volume of element n
x, y, z	rectangular Cartesian coordinates (global)
α	deformation modes
β	set of stress parameters
ε	column matrix of strains
ε^*	continuous strain field
ε	extensional strain component
ϕ_x, ϕ_y	second terms in a power series expressions of u and v in the normal coordinate z
γ	shear strain component
ν	Poisson's ration
θ	ply angle or twisting angle per unit of length
π_R	Hellinger-Reissner principle
π_{mR}	mixed form Hellinger-Reissner principle
σ	column matrix of stresses
σ^*	continuous stress field
σ^{ij}	physical stress components
σ	extensional stress component
τ	shear stress component
τ^{ij}	stress tensor components
ξ, η, ζ	natural element coordinates (local)
ψ_x, ψ_y, ψ_z	the second terms in a power series expressions of u, v and w in the normal coordinate z

$\zeta_x, \zeta_y, \zeta_z$ the third terms in a power series expressions of u, v and w in the normal coordinate z

SUBSCRIPTS

c central axis or deformation modes related to coupling between inplane and transverse strains

i number of iterations or deformation modes related to inplane strain

i,j index of tensor

j number of node

L longitudinal fiber direction

p quantities related to inplane components

T transverse direction

t quantities related to transverse components or deformation related to transverse strain

x,y,z in the Cartesian coordinate direction

SUPERSCRIPTS

i number of element or sub-element

i,j,m,n index of tensor

MISCELLANEOUS

$(\bar{})$ prescribed quantities or normalized values

$(\tilde{})$ quantities corresponding to an uniform inplane strain

δ variational quantities

$\partial( )/\partial x$ partial derivative in x, etc.

CHAPTER ONE

INTRODUCTION

During the past two decades, advanced composite materials are being used increasingly in many engineering and civilian applications, ranging from fuselage of an aeroplane to the frame of a tennis racket. The fibre-reinforced composite possess two desirable features: one is their high stiffness-to-weight ratio, and the other is their anisotropic material property that can be tailored through variation of the fibre orientation and stacking sequence--a feature which gives the designer an added degree of flexibility.

In the analysis of laminated plates, studies [1,2] indicated that the transverse shear effect on the behavior of the plate is more pronounced that in isotropic plates due to the very large ratios of elastic modulus to shear modulus (e.g., of the order of 25 to 40, instead of 2.6 for typical isotropic materials). Due to the neglect of transverse shear strains in the analysis, the deflections are underpredicted and the natural frequencies and buckling loads are overpredicted.

On the other hand, experimental observations [3,4] on composite structures subjected to compressive loading and

foreign object impact also revealed some distinct failure modes which are unexpected in metallic material. A thorough knowledge of these mechanisms is necessary not only to avoid catastrophic failures, but also to create efficient and durable structures. Failures in these materials often begin as matrix microcraking and delamination. These modes of damage are essentially three-dimensional in nature, and interlaminar stresses are primarily response for them. Steep stress gradients are encountered in the vicinities of free edge, ply termination, zone of delamination, hole and in the regions subjected to impact loads. Efficient analytical and numerical methods are necessary not only for the precise estimation of these interlaminar stresses, but also for identifying the factors that affect directly the failure process.

Considerable attention has been given to the development various first and higher order shear deformation theories for homogeneous and laminated composite plates [5-22] that account for the effects of transverse shear and normal strains and the warping of cross section. However, many plate theories are required to introduce shear correction factors to account for the incorrect transverse shear stress assumptions across the thickness. While analytical methods are usually restricted to problems with simple geometries, loads, boundary conditions and cross ply laminates. The numerical method, namely finite element formulation, is a practical alternative way in dealing with complicated problems , for example, problems with irregular

geometries, general loadings, complex boundary conditions and anisotropy.

Considerable literature has been devoted to the finite element analysis of laminated composite plates [23-45]. However, it is noticed that limitations still exist such as most of the examples limited to 3 to 4 layers. Therefore, the first objective of this research is to find improved finite element methods to eliminate those limitations.

The second objective of this research is to determine the interlaminar stresses in the region where steep stress gradients are encountered. Study will put emphasis on the free edge problem even though a voluminous amount of results have already been reported in this problem [46-75]. However, the present investigation does not attempt to formulate a special element such as element including stress singularity or to develop a new approach, but rather to utilize the global-local modeling technique based on the proposed finite element methods to examine the computational efficiency and accuracy.

Based on these two objectives, two types of element are needed to be constructed. The first one designated as type I is based on the so-called 'effective' modulus plate theory in which the displacement approximations are assumed to be continuous functions across the entire laminate thickness as shown in Figure 1.1(a). The second one designated as type II is based on

the so-called 'effective' stiffness plate theory in which the displacement approximations are assumed to be linear or higher order function of z within each layer. Therefore, the assumed displacement field is piecewise linear or higher order function through the laminate thickness as shown in Figure 1.1(b).

The assumed stress finite element model is adopted for the present formulation because of its convenience in maintaining the continuity of transverse stresses along the laminar interfaces and in incorporating the traction free condition at the top and bottom surfaces of the laminate. The exact transverse shear behavior can be represented, hence it is not necessary to introduce any shear correction factors.

An alternative approach for maintaining stress continuity along the inter-element boundaries is the application of a stress 'smoothing' and iteration scheme in the post processing step of the finite element analysis [76]. Therefore, one focus in this study is to investigate various smoothing techniques for maintaining the continuity of interlaminar stresses along the interfaces of laminated composite plates.

An outline of the remainder of the thesis is as follows: Chapter 2 provides a review of theories of homogeneous and laminated plates, finite element formulations for various laminated plate problems. A summary of different methods that

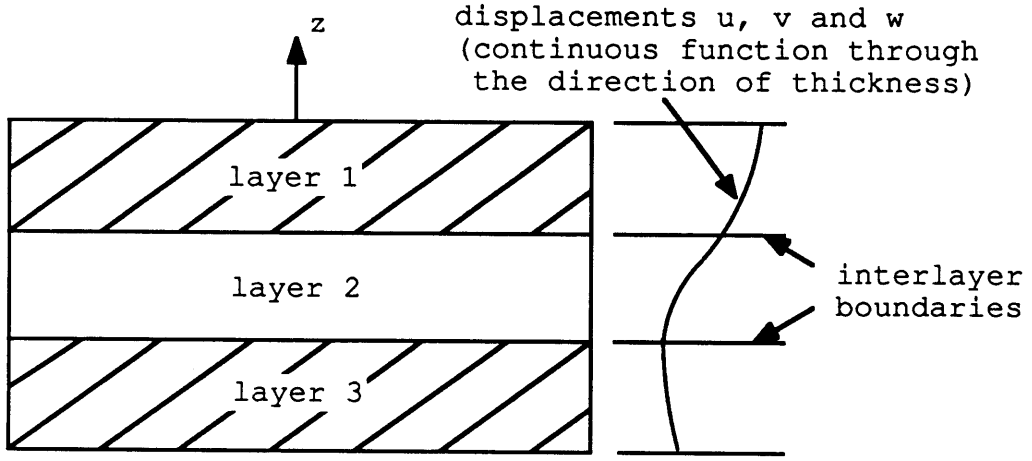

(a) type I element

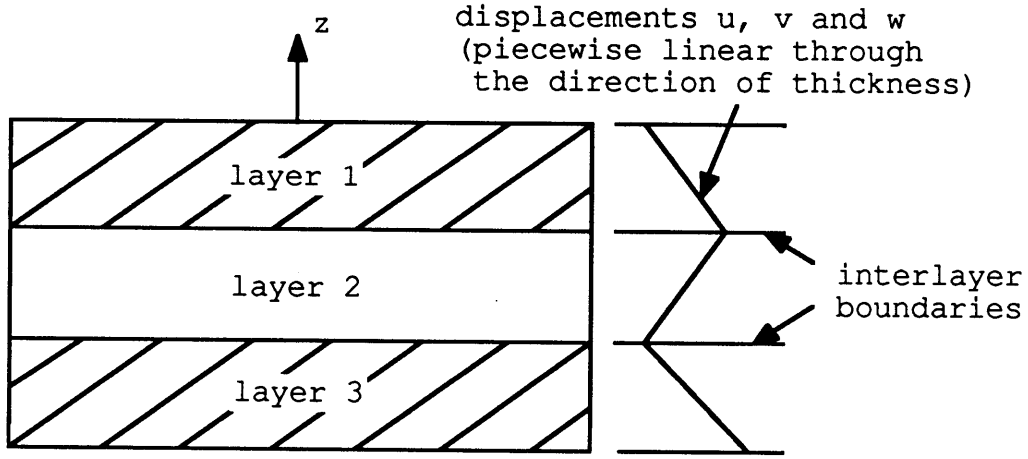

(b) type II element

Figure 1.1 Continuity of displacement function for element

have been used to solve a specific free edge problem is also included.

Chapter 3 presents the derivation of a new mixed form of Hellinger-Reissner principle and the formulation of the new mixed form hybrid stress elements. The later sections provide a guideline for selecting assumed stress field and assessments of the new elements.

Chapter 4 contains the study of the stress 'smoothing' and iteration techniques in the application of laminated plate problems using conventional hybrid stress elements. Assessments for these techniques are also included.

Chapter 5 presents the effectiveness of the global-local modeling technique in studying free edge problems with straight and curvilinear boundaries. A study of the effect of matrix thin layer is also provided.

Chapter 6 summarizes the conclusions drawn from this study and the suggestions for future research.

All the numerical calculations in this study are carried over on a Macintosh SE personal computer.

CHAPTER TWO

REVIEW OF LAMINATED PLATE THEORIES, FINITE ELEMENTS AND STRAIGHT FREE EDGE PROBLEMS

Before going into detailed discussions of the formulation of the new mixed form hybrid stress laminated plate element and the results of numerical studies, a review of the first and high order shear deformation theories for homogeneous and laminated plates, various finite element formulations for laminated plate problems and their limitations are presented in this chapter. Another objective here is also to briefly review the many important ideas and publications which have addressed the free edge problems of laminates subjected to uniform tension or extension and to assess its current state and solution.

2.1 First Order Shear Deformation Plate Theory

The classical laminated plate theory by Reissner and Stavsky [5], for which the normals to the midsurface before deformation are assumed to remain straight and normal to the plane after deformation and the transverse shear deformation effect is ignored, is inadequate for the analysis of thick laminated plates.

Refined theory for homogeneous plates due to Reissner [6] and Mindlin [7] is improvements of the classical plate theory by including the effect of transverse shear deformation. It is based on the assumption that the normals to the midplane before deformation remain straight but no longer remain normal to the midplane after deformation. Its kinematic assumptions are of the form

$$\begin{aligned} u &= u_0 + z\,\psi_x \\ v &= v_0 + z\,\psi_y \\ w &= w_0 \end{aligned} \tag{2.1}$$

where

z = the coordinate normal to the midplane

and u_0, v_0, ψ_x, ψ_y and w_0 are dependent on the inplane coordinates x and y and time t

Reissner assumed a consistent forms for the stress distributions across the thickness and employed a variational theorem to determine both the equations of equilibrium and the stress-strain relations. Without introducing corresponding stress distribution assumptions, Mindlin directly obtained the governing equations from the corresponding three-dimensional equations by appropriate integrations with respect to z, in conjunction with the displacement assumptions of Eq. (2.1). In Mindlin's derivation, it was necessary to introduce a shear

correction factor to account for the incorrect uniform shear stress assumptions across the thickness.

Yang, Norris and Stavsky [8] extended the Reissner-Mindlin theory based on the same kinematic assumptions of Eq. (2.1) to laminated plates for studying the propagation of harmonic waves in a two-layer of two isotropic materials. Following Mindlin's derivation procedure, the governing equations were obtained but arbitrary correction factors to the transverse shear stiffness are required.

Although the Yang-Norris-Stavsky (YNS) theory is adequate for predicting the overall responses such as transverse deflections, natural frequencies and buckling loadings (first few modes) of laminated composite plates, they do not adequately predict responses relating to interlaminar stresses in the edge zone or near a delamination in composites. These can be addressed only by the higher order theories which account for transverse shear deformation, transverse normal strain and warping of cross section.

2.2 High Order Plate Theory

If we consider that the classical theory is merely a special case of the shear deformation theory such that the transverse shear deformation is small and can be neglected, Eq.

(2.1) applies to both the classical plate theory as well as the Reissner-Mindlin theory. Thus, they are of the same order of approximation considering the terms in Eq. (2.1) as the first terms in a power series expressions in the normal coordinate z.

There have been many theories proposed which are of higher order than those based on Eq. (2.1). A brief review of some of the theories are presented. It should be noted that the term "high order theory" refers to the level of truncation of terms in a power series expansion for displacement assumptions, rather than to the order of the final system of differential equations.

Essenburg [9] derived the next higher order one-dimensional homogeneous plate theory based on the following displacement assumptions,

$$u = u_0 + z\,\psi_x$$
$$v = v_0 + z\,\psi_y \qquad (2.2)$$
$$w = w_0 + z\,\psi_z + z^2\,\zeta_z$$

where

ψ_z and ζ_z are dependent on the inplane coordinates x and y and time t

This includes the effect of transverse shear and normal strains but does not allow warping of cross section. Based on the stress distribution assumptions across the thickness,

corresponding to Eq. (2.2) the governing equations can be obtained. Essenburg has demonstrated the advantage to use the theory based on Eq. (2.2) over lower order theories in the context of contact problems.

Whitney and Sun [10] developed a similar level shear deformation theory for laminated plates. The assumed displacements are extended to include the first order of the transverse normal strain and the warping of cross section and are of the form

$$\begin{aligned} u &= u_0 + z\,\psi_x + z^2\,\zeta_x \\ v &= v_0 + z\,\psi_y + z^2\,\zeta_y \\ w &= w_0 + z\,\psi_z \end{aligned} \qquad (2.3)$$

The governing equations are derived from the Hamilton principle and shear correction factors of the same type as employed by Mindlin were used. The theory has been used to study one-dimensional wave propagation problem for laminated plates and to compare to exact solutions obtained from dynamic elasticity theory. The theory yields improved results for extensional motions.

Nelson and Lorch [11] has presented a theory of next higher order for modeling laminated plates and is based on the following assumed displacements

$$u = u_0 + z\,\psi_x + z^2\,\zeta_x$$
$$v = v_0 + z\,\psi_y + z^2\,\zeta_y \qquad (2.4)$$
$$w = w_0 + z\,\psi_z + z^2\,\zeta_z$$

It includes all higher order effects of the transverse shear and normal strains and the warping of cross section. The Hamilton principle is again used to formulate the displacement equations of motion with appropriate boundary and initial conditions. Like previous theory, shear correction factors must be introduced. The theory is capable to accurately model the static and dynamic behavior of laminated orthotropic plates.

A high order theory for homogeneous plates involving the lower order correction for the effect of out-of-plane deformation to Eq. (2.1) was given by Reissner [12]. The displacements are in the form

$$u = z\,\psi_x + z^3\,\phi_x$$
$$v = z\,\psi_y + z^3\,\phi_y \qquad (2.5)$$
$$w = w_0 + z^2\,\zeta_z$$

which the inplane deformation along the midplane is neglected. Reissner has shown that for the bending of a plate with a

circular hole this theory gives very accurate results compared to the elasticity solution.

Lo, Christensen and Wu [13,14] have extended Reissner theory by including both inplane and out-of-plane effects to investigate homogeneous and laminated composite plates. The theory is based on

$$
\begin{aligned}
u &= u_0 + z\,\psi_x + z^2\,\zeta_x + z^3\,\phi_x \\
v &= v_0 + z\,\psi_y + z^2\,\zeta_y + z^3\,\phi_y \\
w &= w_0 + z\,\psi_z + z^2\,\zeta_z
\end{aligned}
\qquad (2.6)
$$

The governing equations were derived with the help of the principle of stationary potential energy. Assessment has been made for a simply supported thick isotropic and laminated plates subjected to cylindrical bending.

Since 1980, a new class of high order theories began to appear in the literature. The inplane displacements u and v are assumed to be the same order as that given in Eq. (2.6) but the transverse displacement w is assumed to be constant through the thickness. Thus, the effect of normal strain is neglected. The main feature of these theories is that the number of dependent unknowns can be successfully reduced to the same number as the first order shear deformation theory. They are achieved by satisfying the condition of zero transverse shear stresses on

the top and bottom surfaces of the laminate, and consequently, there is no need to use any shear correction factors. The displacements are reduced to the form

$$u = u_0 + z \left[\psi_x - \frac{4}{3} \left(\frac{z}{h}\right)^2 \left(\psi_x + \frac{\partial w}{\partial x}\right) \right]$$

$$v = v_0 + z \left[\psi_y - \frac{4}{3} \left(\frac{z}{h}\right)^2 \left(\psi_y + \frac{\partial w}{\partial y}\right) \right] \qquad (2.7)$$

$$w = w_0$$

where

h is the total thickness of the laminate

The theory which involves the displacement assumptions of Eq. (2.7) was first presented by Levinson [15] for isotropic plates. To assess the validity of the theory, torsion of a rectangular plate was studied and compared to Reissner's results [6]. Murthy [16] extended the theory to laminated plates. Instead of directly using Eq. (2.7), he used "average" displacements u, v and w and "average" rotations of a line normal to middle surface β_x and β_y as unknowns. He has shown that the present theory is more accurate than other first order shear deformation theory.

Their derivations involve a displacement approach like that in Mindlin theory and its straight forward extensions. The constitutive equations which relate the forces and moments to displacements and rotations are obtained by integration through

the thickness. But the equations are derived by using the equilibrium equations of the first order shear deformation theory instead of through the variational principle. These equations which are derived from the principle of virtual displacement based on the displacement assumptions of Eq. (2.1) are variational inconsistent with their displacement assumptions. The correct forms of differential equations and boundary conditions based on this displacement field have been derived by Reddy [17].

Based on the same displacement assumptions, Reddy [17] has presented a geometrically nonlinear theory by simply introducing the von Karmain (nonlinear) strains instead of the linear strains. He derived the equilibrium equations by applying the Hamilton Principle. He has shown that the linear version of his theory is more accurate to predict the deflections, stresses and frequencies when compared to the Reissner-Mindlin first-order theory. Reddy [18] also presented a linear high order theory of laminated composite plates based on the displacement assumptions of Eq. (2.7).

Bhimaraddi and Stevens [19] has employed another set of displacement assumption similar to those of Eq. (2.7). They are

$$u = u_0 + z \left(1 - \frac{4z^2}{3h^2}\right) \psi_x - z \frac{\partial w}{\partial x}$$

$$v = v_0 + z\left(1 - \frac{4z^2}{3h^2}\right)\psi_y - z\frac{\partial w}{\partial y} \qquad (2.8)$$

$$w = w_0$$

The assumed displacement field of classical plate theory can be obtained as a special case from Eq. (2.8) but not from Eq. (2.7). They also employed the Hamilton principle to derive the equations of motion. The superiority of the theory has been demonstrated by comparing the results obtained by Reissner-Mindlin plate theory in the context of free vibration analysis of isotropic and laminated plates.

The next higher order theory is to extend the previous theory by including the normal strain effect. Krishna Murty and Vellaichamy [20] presented a theory for symmetric laminated plates and loading are assumed to be applied at the top and bottom surfaces of the plates. The displacement assumptions are of the forms

$$u = u_0 + z\left(1 - \frac{4z^2}{3h^2}\right)\psi_x - z\frac{\partial w}{\partial x}$$

$$v = v_0 + z\left(1 - \frac{4z^2}{3h^2}\right)\psi_y - z\frac{\partial w}{\partial y} \qquad (2.9)$$

$$w = w_0 + h^2\left(1 - \frac{4z^2}{h^2}\right)\zeta_z$$

The governing equations and boundary conditions were derived with the help of the principle of virtual displacement. The theory provided good estimates of the deflections, and the inplane stresses.

The prominent common feature of the theories discussed in the previous paragraphs is to assume each displacement component as smooth continuous function across the entire plate thickness. For laminated plates, they are the so-called 'effective' modulus theories in replacing the composite by a homogeneous anisotropic material.

All the first order and some high order shear deformation theories for laminated plates require an arbitrary correction factor to the transverse shear stiffness. The determination of the shear correction factors is still a controversy among authors. For example, the usual procedure for determining the correction factor in a dynamic problem is to match specific frequencies from the approximate theory to frequencies obtained from dynamic elasticity. For the general case of a laminate this procedure becomes very tedious as the value of the factor will depend on the stacking sequence and the number of the plies. The high order theories with the traction free condition enforced on the top and bottom surfaces of the laminate resolve this difficulty.

However, the assumption of smooth continuous displacements

across the entire thickness will lead to discontinuous transverse shears at the interlaminar surfaces. Although the transverse shear and normal strains and the warping of cross-section are included in many high order theories, they are adequate for predicting the global responses but still inadequate for predicting the interlaminar stresses because they cannot satisfy the equilibrium of each layer, especially around the free edge region.

Another class of high order laminated plate theories is the so-called 'effective' stiffness theory and is based upon the assumption that the displacement field is linear functions of z within each layer.

Sun and Whitney [21] and Srinivas [22] presented a theory based on this kind of assumptions. The displacement field in the k^{th} layer is assumed to be of the form

$$\begin{aligned} u^k &= u_0^k + \zeta^k \phi_x^k \\ v^k &= v_0^k + \zeta^k \phi_y^k \\ w^k &= w_0^k = w_0 \end{aligned} \qquad (2.10)$$

where

ζ^k = local thickness-coordinate of layer k

u_0^k, v_0^k, w_0^k, ϕ_x^k and ϕ_y^k are nodal displacements at the midplane of layer k

The continuity conditions of displacement and transverse stress at the laminar interfaces are satisfied. The equations of motion were derived again by applying the Hamilton principle and Srinivas also provided a procedure for obtaining the general solution in the form of hyperbolic-trigonometric series. Sun and Whitney assessed the theory by studying the wave propagation problems and compared the results with the exact three-dimensional elasticity solutions. Srinivs assessed the theory by studying free vibrations and flexure of simply supported rectangular laminates and compared with the exact solutions.

The 'effective' stiffness theories yield more detailed informations about the laminate than the 'effective' modulus theories. However, they still cannot satisfy the layer equilibrium around the free edge in order to predict the interlaminar stresses accurately because the theories are lack of equations to enforce the boundary conditions and the transverse normal strain is also ignored. On the other hand, the theories become intractable as the number of layers becomes large.

2.3 Laminated Plate Finite Elements

In the last decade, there has been considerable effort directed toward the development of shear-flexible, multilayered

anisotropic plate elements based on the first or high order plate theories. The objective of this section is to review the formulations of those multilayer plate elements appeared in the literature. This type of elements is classified into two groups, type I element and type II element.

2.3.1 Type I Laminated Plate Elements

Based on the different methodologies used in the formulation, the type I multilayer plate elements can be further divided into displacement model, mixed model and hybrid stress or strain model.

2.3.1.1 Displacement Model

Pryor and Barker [23] constructed a conventional displacement finite element based on the YNS theory [8] to analyze thick laminated composite plates. The element is a 4-node rectangular element and has 7 degrees of freedom (three displacements, two total rotations and two shear rotations) per node. The transverse stresses in each lamina are obtained by utilizing the local equilibrium equations rather than by directly estimating from the displacement solution through the use of the strain-displacement and stress-strain relations.

The procedure is as follows

1) Use the displacement solutions to deduce the inplane stresses σ_x, σ_y and τ_{xy}.

2) Insert these inplane stress solutions into the following equilibrium equations for layer i

$$\tau^i_{xz,z} = -\left(\sigma^i_{x,x} + \tau^i_{xy,y}\right) \qquad (2.11)$$

$$\tau^i_{yz,z} = -\left(\sigma^i_{y,y} + \tau^i_{xy,x}\right)$$

3) Solve for the transverse stresses τ_{xz} and τ_{yz} by integration.

The integration is done by assuming that there are no shear stresses at the top and bottom surfaces of the laminate and the transverse stresses are continuous between layer boundaries. Several simply supported square two- to four-layer cross ply laminated plates subjected to sinusoidal loading or cylindrical bending were tested. The transverse stresses are in reasonable agreement with the elasticity solutions if no severe warping of cross section occurs.

Noor and Mathers [24] studied two aspects of the finite element analysis of symmetrical laminated composite plates. The first is to exploit the symmetries exhibited by anisotropic plates for various loadings and boundary conditions. A simple

procedure was outlined and saving in cost of computations can be resulted by considering the symmetries.

The second aspect is to study the effects of anisotropy and shear deformation on the accuracy and convergence of five quadrilateral shear-flexible finite elements based on the YNS theory [8]. They are two serendipity-type elements with quadratic and cubic interpolation functions, two Lagrangian elements with bi-quadratic and bi-cubic functions, and one Hermitian element. All elements satisfy continuity requirements of the type C^0 and have both displacements and displacement derivatives as nodal parameters. Numerical studies on global responses of the plates have shown that the accuracy and convergence of the first three elements are strongly dependent on both the transverse shear flexibility and degree of anisotropy of the plate. On the other hand, the higher order elements, bi-cubic and Hermitian, are less sensitive to variations in these effects.

By eliminating the two shear rotation degrees of freedom at each node of Pryor and Barker's element [23], Panda and Natarajan [25] developed an 8-node quadrilateral C^0 laminated plate element with five degrees of freedom (three displacements and two rotations) per node. The element is also based on YNS theory but no shear correction factor is used. Several simply supported laminated plates under sinusoidal loading or cylindrical loading were tested. Compared to the elasticity

solutions, the element gives good predicting in the maximum deflection and inplane stresses for thin plate. However, the accuracy of the solutions begin to deteriorate when the span-to-thickness ratio is lower than 10.

Reddy [26] developed an 8-node quadrilateral C^0 element also based on the YNS theory for laminated composite plates. The element contains five degrees of freedom (three displacements and two rotations) per node. Instead of directly utilizing the YNS theory, Reddy employed a penalty function formulation. For a thin plate limit, the normals to the midplane before deformation remain straight and normal to the midplane after deformation implies that

$$\psi_x = -\frac{\partial w}{\partial x} \quad \text{and} \quad \psi_y = -\frac{\partial w}{\partial y} \tag{2.12}$$

The problem of finding the solution (u, v, w) to the thin plate equations can be viewed as one of finding (u, v, w, ψ_x, ψ_y) subject to the constraint equations of Eq. (2.12). Reddy showed that this can be achieved by using a penalty function to the equations governing the thin plate theory that resembles the YNS theory. Assessment of the element has been made for the bending and free vibration analysis of rectangular laminated plates with various loadings and boundary conditions. Results in deflections, inplane stresses and natural frequencies are in

good agreement with the exact solutions for thin plates and in reasonable results for thick plates.

A higher order shear-flexible triangular element for laminated plates based on the YNS theory was formulated by Lakshminarayana and Murthy [27]. The element has three nodes located at its vertices and 15 degrees of freedom per node. The three displacements and two rotations along with their first derivatives are selected as the nodal parameters. In order to approximate the displacement field by complete cubic polynomials, centroidal values of three displacements and two rotations are used during evaluation of element matrices but are eliminated by static condensation.

Numerical assessments include many geometries, loading conditions, support conditions, laminated configurations, regions of stress concentration and singularity. The results has shown that element has accurate prediction in displacements and stress resultants. His study also indicates that the elements which do not include the effect of transverse shear deformation may be highly inaccurate in the analysis of laminated composite plates.

Instead of focussing on the prediction of the global responses for the laminated plates, Engblom and Ochoa [28,29] attempted to predict through-the-thickness stress distributions by using the displacement model. They followed the idea

originally due to Pryor and Barker [23]. Inplane stresses are first determined by utilizing the layer constitutive equations and then the transverse stresses are determined by integrating the first two equations of equilibrium in the transverse direction.

Two quadrilateral high order displacement elements were presented in Reference 28. The inplane displacement field is described by Eq. (2.3) and the transverse displacement w is constant through the thickness. The first one is an 8-node element with 7 d.o.f. (three displacements, two rotations and two high order terms for inplane displacements) per corner node and 3 d.o.f. (transverse displacement and two rotation) per mid-side node. The second one is a simplified version of the first one where the mid-nodes are omitted. Because quadratic variation of the transverse shear strains through the thickness are used, no shear correction factor is required. An eight-node quadrilateral element was presented in Reference 29. The three displacements, two total rotations and two shear rotations are chosen as nodal parameters at each corner node similar to Pryor's element and one transverse displacement at each mid-side node. Reasonable results in inplane and transverse stress distributions are obtained if the laminates are in moderately span-to-thickness ratio.

Pandya and Kant [30] presented a high order C^0 plate element based on the assumed displacement field of Eq. (2.5) for

symmetrical laminates. It is a 9-node Lagrangian isoparametric plate bending element with six d.o.f. (one transverse displacement, two rotations, three higher order terms for displacement) per node. The element is account for quadratic and linear variations of the transverse shear strains and normal strain, respectively. Therefore, no shear correction factor is required and the element includes all six components of strain. Symmetrical laminates with various loadings, boundary conditions and laminated configurations has been tested. Results in deflections and stresses are in good agreement with the exact solutions.

2.3.1.2 Mixed Model

If the displacement-based finite element model is based on the high order theory of Eq. (2.7) in which the assumed displacement field satisfies the zero transverse shear stress boundary conditions at the top and bottom surfaces of the laminate, no shear correction factor is required but the resulting formulation contains second order derivatives of the transverse displacement in the total potential energy and consequently the formulation requires the use of C^1 continuous shape functions. However, if in addition to the three displacements and two rotations the moment resultants are also used as variables, the resulting governing equations will not include the second derivatives of the transverse displacement.

Therefore, the requirement of the inter-element displacement C^1 continuity based on these mixed variables can be relaxed.

Putcha and Reddy [31] has developed two mixed shear flexible C^0 plate elements with relaxed inter-element displacement continuity based on the previous discussion for geometrically linear and nonlinear analysis of laminated composite plates. The elements are a 4-node linear and a 9-node quadratic elements with eleven d.o.f. (three displacements, two rotations, three moment resultants and two higher order moment resultants) per node. They has evaluated the element by studying the problems of bending of laminated rectangular plates with different laminated configurations, loadings and edge supports. It has demonstrated that the global responses predicted by the element are in accuracy compared with other available results.

Kwon and Akin [32] presented a mixed shear flexible element based on the assumed displacement field of Eq. (2.2). Applying the traction free conditions at the top and bottom surfaces of the laminate to the assumed displacement field and using the three moment resultants along with the three displacements, the high order terms of transverse displacement and the two rotations are eliminated. The element has 4-node with six d.o.f. (three displacements and three moment resultants) per node. Only the deflections for three simply supported rectangular laminated plates subjected to sinusoidal loading

were presented. However, they has demonstrated the advantage over other elements based on the YNS theory.

2.3.1.3 Hybrid Stress or Strain Model

Spilker and his colleagues [33] presented a four-node quadrilateral hybrid stress element with five degrees of freedom (three displacements and two rotations) per node. It is based on a modified complementary energy principle. The choice of assumed stress field is as follows. First, the inplane strains ε_x, ε_y and γ_{xy} for the entire laminate are expressed as

$$\mathbf{e}_p = \mathbf{P}^* \beta \tag{2.13}$$

where

$$\mathbf{e}_p = \{\varepsilon_x, \varepsilon_y, \gamma_{xy}\}^T$$

$\mathbf{P}^*$ = matrix of assumed polynomials

β = set of undetermined parameters

Then the inplane stresses σ_x, σ_y and τ_{xy} for the i^{th} layer are related to the strains in the form

$$\mathbf{t}_p = \mathbf{Q}^i \mathbf{e}_p = \mathbf{Q}^i \mathbf{P}^* \beta \tag{2.14}$$

where

$$\mathbf{t}_p = \{\sigma_x, \sigma_y, \tau_{xy}\}^T$$

$\mathbf{Q}^i$ = reduced material property matrix of layer i to a plane stress state

The remaining transverse stresses τ_{xz}, τ_{yz} and σ_z in the i^{th} layer are obtained by integrating the equations of equilibrium and enforcing the stress continuity conditions. As a result, the assumed stress field satisfies the equilibrium exactly. Corresponding to the assumed displacement field, a linear interpolation of the inplane strain in the interior of the element is used. Assessments have been made for some simply supported laminated plates under cylindrical bending. However, though-the-thickness stress predictions are similar to those obtained by displacement model with the help of integration of local equilibrium equations.

Spilker and Jakobs [34] extended the previous 4-node hybrid stress element to an 8-node quadrilateral element with the same 5 d.o.f. per node. A scheme which is to identify all the similar terms in the integrations is used to reduce computational effort. The reduction for thin plates is accomplished by ignoring the contributions of the transverse stresses to the complementary energy. Several simply supported laminated plates subjected to cylindrical bending have been tested to assess the accuracy of the element.

A nine-node hybrid strain element for laminated composite plates and shells was developed by Haas and Lee [35]. Three

displacements and two rotations are chosen as nodal parameters at each node. The element is a degenerate solid type of shell element based on a modified Hellinger-Reissner principle with independent inplane and transverse shear strains. The assumed strain field is in terms of 24 undetermined strain parameters. Based on the hybrid strain model, the element has eliminated the shear locking phenomenon while modelling thin plates and shells. Several simply supported rectangular laminated plates with regular and distorted meshes have been study to assess the accuracy of the element.

2.3.1.4 Limitations of Type I Laminated Plate Elements

There are several limitations for the type I laminated plate elements. Many are related to those of the displacement-based laminated plate theory. First, arbitrary shear correction factors are needed to account for the assumption of uniform transverse shear stress distributions if the element is based on the YNS theory.

Second, elements based on the formulation other than the hybrid stress model guarantee discontinuous transverse stresses at the laminar interfaces.

Third, elements, in general, are adequate for predicting the deflections, maximum inplane stresses and natural

frequencies but inadequate for predicting through-the-thickness stress distributions. If no severe warping of cross section occurs, reasonable results in through-the-thickness stress distributions can be obtained by integrating the local equilibrium equations for the displacement, mixed and hybrid strain models. However, considerable amount of computational effort is required if the number of layers becomes moderately large.

Fourth, elements are incapable to model warping of the cross section and most of the elements do not include the effect of transverse normal strain. Therefore, they cannot be used to model the region subjected to severe stress concentration, for example, free edge and delamination zone.

Fifth, elements based on the high order displacement field which satisfy the traction free condition at the top and bottom surfaces of the laminate are required to use the moment resultants as nodal parameters in order to relax the condition of inter-element displacement continuity.

2.3.2 Type II Laminated Plate Elements

Two formulations have been used in deriving type II laminated plate elements. There are displacement and hybrid stress models.

2.3.2.1 Displacement Model

Mawnya and Davies [36] developed an 8-node quadratic multilayer plate element which permits individual layer to deform locally. The effects of transverse shear deformation are included by allowing warping of cross section. Three displacements of the midplane and two normal rotations of each constitutant layer of the laminate are chosen as nodal parameters at each node. However, it is equivalent to two inplane nodal displacements at each interlayer boundary including the top and bottom surfaces of the laminate as shown in Fig. 2.1(b) and one transverse nodal displacement at the midplane. Therefore, the number of degrees of freedom per node is 2N + 3 where N is the number of layers of the laminate.

Results for simply supported laminates under sinusoidal loading have demonstrated the convergence of global responses with the element. However, the span-to-thickness ratio for their numerical studies is not smaller than 20. Many type I elements have been shown their good performance in predicting the global responses for thin and moderately thick laminated plates. Therefore, the use of type II element is not cost effective if only the global responses are sought.

A 6-node shear flexible laminated plate triangular element

has been presented by Chaudhuri [37]. The displacement field is assumed to be piecewise linear in inplane displacements u and v and constant in transverse displacement w across the thickness which is equivalent to Mawenya's element. Through-the-thickness predictions of interlaminar shear stresses are calculated at the centroid of the triangular surface which has been proved to be the point of exceptional accuracy for the interlaminar shear stresses. The Pryor and Baker's method which is based on the integrations of equilibrium equations to predict the interlaminar shear stresses is used. Using the type II piecewise linear displacement-based element and the equilibrium equation has shown that the accuracy results in through-the-thickness interlaminar shear stress distribution can be obtained for symmetrical laminates.

However, the transverse shear stresses, as computed by the equilibrium method will not, in general, simultaneously vanish at both the top and bottom surfaces of an unsymmetrical laminated composite plates. The method needs to solve a overdetermined system. Chaudhuri and Seide [38] refined the equilibrium method by an approximate semi-analytical method.

They used the same 6-node shear flexible triangular element with the same d.o.f. as before. Instead of directly applying the equilibrium approach to predict the transverse shear stresses at the centroid of the triangular surface, they adopt

the following approach. The transverse shear stress $\tau^i_{xz}(z)$ of layer i are assumed to be of the form

$$\tau^i_{xz}(z) = \sum_{j=1}^{3} N_j(z)\ f^i_j \qquad (2.15)$$

where

$N_j(z)$ = one-dimensional quadratic shape functions

f^i_j, j = 1,2,3 designate $\tau^i_{xz}(z)$ at the bottom, middle and top surfaces of the i^{th} layer, respectively

Therefore, it requires 3N equations to solve for 3N unknowns where N is the number of layers. The equations are chosen by (i) forcing τ_{xz} to be zero at the top and bottom surfaces of the laminate (2 equations), (ii) satisfying continuity condition at each interface (N-1 equations), (iii) identifying τ_{xz} as computed by directly estimating from the displacement solution through the use of the strain-displacement and stress-strain relations at the midplane of individual layer (N equations), (iv) computing jump in τ_{xz} at each interface utilizing the first two equilibrium equations in terms of the stresses (N-1 equations). Following an identical procedure, a similar expression for $\tau^i_{yz}(z)$ can be obtained.

The refined method has been demonstrated to be superior to the equilibrium method and the predicted transverse shear

stresses are in close agreement with the exact solution for a 3-layer cross ply laminate under cylindrical bending.

Owen and Li [39,40] presented an 8-node quadrilateral multilayer element with the same through-the-thickness displacement assumptions as those displacement-based type II elements. In order to reduce the computational effort in solving the global system equations for thick laminate, a substructure technique eliminating of internal degrees of freedom after assembly is used. Assessments have been made by using the element to study the static bending, vibration and buckling problem of laminates with various thickness and modulus ratio.

On the other hand, the maximum transverse shear stresses are calculated by a so-called 'local' smoothing technique. The transverse shear stresses are calculated at the 2x2x2 Gauss points, where are known to be the optimum location for stress sampling, by directly estimating from the constitutive relations. Then the transverse shear stresses at the element boundary are obtained by interpolating the Gauss point solutions.

2.3.2.2 Hybrid Stress Model

A four-node general quadrilateral multilayer plate element

was developed by Mau, Tong and Pian [41]. The assumed through-the-thickness displacement field is the same as those assumptions in previous displacement-based type II elements in which the inplane displacements u and v are assumed to be piecewise linear and the transverse deflection w is assumed to be constant across the layer thickness. The element is based on a modified complementary energy principle in which the interlayer stress compatibility conditions are enforced by Lagrange multipliers. The assumed stress field within each layer is related to a set of 20 stress parameters and satisfies the equilibrium equations exactly. Accurate results in through-the-thickness stress distributions have been obtained for thick laminates subjected to sinusoidal loading or cylindrical bending.

Spilker [42] presented a 2-node two-dimensional multilayer plane strain element with high order through-the-thickness distributions for both stress and displacement in individual layer. The element is based on a modified complimentary energy principle wherein the continuity of inter-element tractions and the mechanical boundary conditions have been relaxed by using the Lagrange multipliers. The assumed displacement field is assumed to be linear between two node-lines and high order through-the-thickness distributions within each layer by allowing displacement u to be of order z^3 and w to be of order z^2. After enforcing the displacement continuity between layers,

the total degrees of freedom for laminate having N laminae is 10N + 4.

Corresponding to the high order through-the-thickness assumption of displacement field, the assumed stress field which satisfies the equilibrium condition in each layer is in terms of total 21 stress parameters. He begin by assuming the inplane stress σ_x to be of order z^3 and y^3. The remaining stress components are chosen via the equilibrium equations. Thus, the transverse shear stress τ_{xz} is of order z^4 and y^2 and the transverse normal stress σ_z is of order z^5 and y. The continuity condition at the lamina interfaces and traction free condition at the top and bottom surfaces of the laminate reduce the total number of stress parameters to 16N - 3. Because the large computational effort is required to generate the element stiffness matrix, numerical tests were restricted to problems of cylindrical bending of 2 and 3 layers cross ply laminates. However, the results in through-the-thickness distribution are in close agreement with the exact solution for the span-to-thickness ratio as small as 1.

An invariant eight-node hybrid stress element for multilayer plate element was presented by Spilker in Reference 43. Through-the-thickness displacement field within individual layer is assumed to be piecewise linear in the inplane displacements u and v and constant in the transverse deflection w across the layer thickness. In order to maintain the

invariant property of the element, the inplane stresses are assumed to be complete cubic polynomial in x and y for both bending (order z) and stretching (constant) within each layer. The remaining three components of transverse stress are obtained via the equilibrium equations. Finally, a total of 67 stress parameters is used in each layer. However, after enforcing the stress continuity and traction free conditions, the total number of stress parameters for the element is 56N - 10 where N is the number of layers.

The total degrees of freedom of the element is 16N + 24 and the minimum number of stress parameters is 16N + 18. Therefore, the total number of β's will be excessive large compared to the minimum number of β's when the number of layers is greater than 2. For example, if the number of layers is 2, the total number of β's is 102 and the minimum number is 50. A three layers cross ply laminates under cylindrical bending has been tested to assess the performance of the element.

Liou and Sun [44] has presented an 8-node hybrid stress multilayer plate element based on a modified complementary energy principle. All the three components of displacement u, v and w are assumed to vary linearly through the thickness of each lamina. Therefore, the element can account for all six components of strain. The assumed stress field which satisfies the equilibrium condition within each layer is interpolated in terms of stress polynomials with 55 β's. The element does not

have invariant property. On the other hand, the number of β's is greatly reduced compared with the previous Spilker's element. The total number of stress parameters for the element is (55-14)N - 10 after enforcing the traction free and continuity conditions of the stresses. Good accuracy and convergence are observed in the numerical results of several cross ply laminates subjected to sinusoidal loading or cylindrical bending.

Moriya [45] developed an 8-node shear flexible laminated plate and shell element. The assumption displacement field is the same as those in Liou and Sun's element. However, the element is not based on any conventional modified complimentary energy principle but rather based on a new form of mixed Hellinger-Reissner principle [45,81-83]. This new mixed principle is adopted in this study and will be re-derived in a more concise and clearer manner in the next chapter. It is in terms of all three components of displacement and three components of transverse stress. Therefore, no assumed stress field is required for inplane stresses. The total number of stress parameters being used is greatly reduced, and consequently, considerable computational effort has been saved.

Assumed transverse stresses within each layer are in terms of 36 uncoupled stress parameters and applying the idea originally due to Pian and Chen [84], the third equation of equilibrium is enforced in an integral sense through the use of three internal transverse displacement w_λ's. A simply supported

three layers cross ply laminate under sinusoidal loading with various span-to-thickness ratio, a free edge problem of a four layers symmetrical cross ply laminate and a two layers cross ply laminated cylindrical shell subjected to two concentration forces were tested to assess the performance of the element.

2.3.2.3 Limitations of Type II Laminated Plate Elements

Accurate results in the global and local responses of thick laminates can be obtained by these elements. However, it is obvious to see that any type II element is required extensive computational effort deriving the element stiffness matrix and solving the global equation because of large bandwidth of the system when the number of layers becomes moderately large. Most of the numerical tests on these elements in the literature are limited to laminates having 3 to 4 layers and the highest order element developed by Spilker [42] is formulated only for two-dimensional analysis.

Elements based on the displacement model will lead to discontinuous transverse stresses at the laminar interfaces. Through-the-thickness stress distribution of transverse stresses can be obtained by using the integration of the first two equilibrium equations or the semi-analytic method suggested by Chaudhuri and Seide [38]. On the other hand, considerable

amount of computational effort is required if the number of layers becomes moderately large.

For hybrid stress element, no extensive computational effort is required to compute the transverse stresses. However, using the conventional hybrid stress approach, a large number of stress parameters is used if the number of layers becomes large. Because the computational effort in deriving the element stiffness matrix is proportional to the number of stress parameters being used, the effort increases rapidly as the number of layers becomes moderately large.

2.4 Laminated Free Edge Problem

As mentioned earlier, catastrophic failures in laminated composite plates often begin as delamination and matrix microcracking. Interlaminar stresses are primarily response for these failures and numerous attempts have been made to predict the interlaminar stress distributions around the free edges. The model which has widely been used in studying the problems is a finite width laminate subjected to uniform axial strain. Reviewed here, the majority of analytical and numerical studies are based on modeling each layer as a homogeneous anisotropic material. As a more realistic models, the interface is characterized as a separate layer, but still maintain distinct layer interfaces.

2.4.1 Finite Difference Method

An elasticity solution for a finite width laminate under a uniform axial strain was first developed by Pipes and Pagano [46]. By assuming that the stresses are not varying along the axial direction, the resulting differential equations are functions of two space variables instead of three. They employed the finite difference method to solve the problem for a symmetrical four layers laminate and reported a sharp rise in all three interlaminar stresses near the free edge. It is suggested that a stress singularity exists at the free edge.

On the other hand, Altus, Rotem and Shmueli [47] did not employed this approximation and established the resulting different equations in terms of all the three space variables u, v and w. Then, they adopted the three-dimensional finite difference scheme to study several four layer symmetrical angle ply laminates. The results have shown that peeling stresses may be a significant factor for delamination.

However, it has been indicated that the results obtained by the finite difference scheme near the interlayer boundary and the free edge may not be reliable. Therefore, the conclusions drawn from these results are questionable. More in depth discussions will be presented at the end of this section.

2.4.2 Finite Element Method

Rybicki [48] derived a three-dimensional equilibrium finite element for the solutions of some finite width symmetrical cross ply laminates under uniaxial strain. He first approximated the assumed stress field within each layer which satisfies the equilibrium equations by three sets of Maxwell stress function with 648 unknown coefficients associated with each discrete element. After satisfying the stress boundary and compatibility conditions along the interlayer boundaries, the number of unknown is reduced and they are determined by minimizing the complementary energy. Similar results compared with Pagano and Pipes [46] were obtained.

Wang and Crossman [49] studied the Pagano-Pipes quasi-three-dimensional problem by utilizing constant strain, triangular displacement-based finite elements. Numerical results for five types of laminated configuration have been reported and emphasis is placed on assessing the stress singularity in the regions close to laminar interfaces and free edge.

On the other hand, they [50] also proposed a finite element substructuring scheme to study thick laminates composed of many layers. The idea is to model the layers distant from the region of interest by a single element having effective material

properties as 'effective' modulus plate theory, while the region of interest is modeled by a dense population of elements which are capable to capture the high stress gradients around the region of interest, for example the free edge zone of laminates.

A special hybrid stress element which satisfies the traction free edge condition exactly based on the high order hybrid stress laminated plate element [42] was presented by Spilker [51] to study the effect of traction free edge condition. He employed the element to a 4-layer cross ply laminated structure. Based on his study, the effect of satisfying the traction-free-edge condition exactly on the stresses is limited to a very narrow region near the free edge. However, the element does not have good performance in predicting stresses for the free edge problem because of its poor assumed stress field. The conclusion is questionable.

Raju and Crews [52] studied the quasi-three-dimensional free edge problem by applying large number of eight-node isoparametric elements. Seven laminates belonging to a family $[\theta/(\theta-90)]_s$, $0 \leq \theta \leq 90$ were considered. Three rectangular meshes were used and the fine mesh had 1833 nodes and 576 elements which is the finest mesh in finite element analysis has ever reported in the literature for a two layers model. Near the laminar interfaces and the free edge, the transverse normal stress σ_z is tensile for the cross ply laminates and compressive for all other five laminates considered. The transverse shear

stress σ_{xz} where x is the direction of prescribed strain is much larger than the normal stress σ_z for laminates except for the cross ply laminates in which σ_{xz} is zero. Convergence studies again indicate the existence of weak stress singularity at the intersection of the interface and the free edge. A log-linear curve fitting procedure has been used to evaluate the power of the singularities. For the graphite/epoxy laminates of $[\theta/(\theta-90)]_s$ $0 \leq \theta \leq 90$ family, the power of the singularity in σ_{xz} is found to be about 0.17 along the interface.

Although in reality the stress singularity does not exist, to capture this weak stress singularity is still of great interest. There exist two hybrid stress elements and one displacement-based element in which the singular stress field is included.

Wang and Yuan [53] presented a special hybrid stress element which includes the stress singularity in the assumed stress field and exactly satisfies the stress free edge condition and the stress continuity condition along the interlaminar boundaries. The element based on a modified hybrid functional and eigenfunction solution of a pair of linear governing partial differential equations derived from the theory of anisotropic elasticity and Lekhnitskii's stress potentials [54,55]. The singular hybrid element along with 8-node isoparametric displacement-based elements was used. The results for a $[\pm 45]_s$ laminate confirmed the results obtained by Raju and

Crews [52]. The finite element mesh has 273 nodes and 78 elements and has reduced drastically compared with the one used by Raju and Crews which does not include any singular element.

Independently, Lee, Rhiu and Wong [56] developed a singular hybrid stress element along with conventional hybrid stress elements to study the problem. The singular element is also based on the same modified hybrid functional as in Wang and Yuan [53] and Lekhnitskii's stress potential solutions for the free edge anisotropic elasticity problem. Numerical results indicated fast convergence compared with the solutions obtained by other finite element without embedded the stress singularity.

Yeh and Tadjbakhsh [57] developed a singular displacement finite element based on a singularity transformation which was original suggested by Yamada and Okumura [58]. First the singular element is derived and then the order of stress singularity is computed. It is interesting to note that for a singular hybrid element, the order of stress singularity is first computed before the singular element is derived. Good agreement between the present results and the analytical solutions was obtained.

Murthy and Chamis [59] abandoned the model used by many investigators that laminate is characterized as combinations of distinct material layers with distinct interfaces. They considered the interface as a separate matrix thin layer, but

still maintaining distinct layer interfaces. They adopted three-dimensional 20-node brick isoparametric elements to study the interply layer effect on the free edge stress field of symmetric angle ply laminates subjected to uniform tensile stress. A total of 1365 and 224 brick elements were used to model the primary structure and the free edge region, respectively. The results have shown that the effect of interply layer reduces the stress intensity at the free edge significantly. The peel off stress σ_z is not significant and not likely to initiate edge delaminations in $[\pm\theta]_s$ angle ply laminates. However, the interlaminar shear stress could become substantial in the interply layer free edge region and may initiate edge delaminations.

2.4.3 Perturbation And Series Solution Method

Tang [60] and Tang and Levy [61] developed a plane stress boundary layer theory from the three-dimensional theory of anisotropic elasticity. By expanding the stresses, displacements, body forces, and surface tractions in power series of the half-thickness of a layer in the equations of equilibrium, compatibility and boundary conditions, a set of system equations was obtained. They employed the zeroth order approximation of the theory to study the unidirectional extension of a finite width $[\pm\theta]_s$ laminates. Tang [62] has also

extended his boundary layer theory to analyze a laminated plate with a circular cutout.

Hsu and Herakovich [63] matched the classical lamination plate theory solution in the interior region to a boundary region solution by a perturbation technique. They also employed the zeroth order approximation of the theory to analyze the unidirectional extension of a finite width $[\pm\theta]_s$ laminates. Interlaminar stress distributions were obtained as a function of the laminate thickness-to-width and compared to finite difference results [46].

Bar-Yoseph and Avrashi [64,65] presented a variational asymptotic formulation for the free edge problem. It is based on the singular perturbation techniques. Instead of directly finding variational approximations for the high order asymptotic approximations, they employed the Hellinger-Reissner variational principle and derived a modified hybrid stress element to analyze the stress singularity at the free edge region. Results indicate that the stress singularity is very closely approximated by log r instead of $r^{-\alpha}$.

On the other hand, they and their colleagues [66,67] have extended the singularity perturbation techniques to analyze the interlaminar stress distribution for laminated plates containing a curvilinear hole and the effect of material non-linearity on the interlaminar stress field.

Wang and Choi [54,55] developed a eigenfunction expansion method to analyze the problem. The method is based on Lekhnitskii's stress potentials and the theory of anisotropic elasticity which lead to a pair of coupled governing partial differential equations. The solution are obtained by solving the homogeneous solution for the governing P.D.E.'s in terms of eigenfunction series and applied a collocation technique at each interlaminar surfaces to ensure the stress continuity. However, the completeness of the eigenfunction solution is questioned by some investigators [68].

2.4.4 Variational Method

Pagano [69] presented a high order theory in which all six stress components are non-zero and displacement and traction continuity conditions at laminar interfaces are satisfied. The theory in which layer equilibrium conditions can be enforced is derived form Hellinger-Reissner variational principle based on assumed inplane stress functions linear in the z within each layer and the transverse stresses evolved from equilibrium consideration. The theory consists 13N field equations and 7N edge conditions for each layer where N is the number of layers. Results agree quite well with those of Wang and Crossman [49]. However, in the establishment of the layer equilibrium, conditions of vanishing force and moment per unit length of

layer thickness are imposed rather than pointwise traction free edge conditions. Hence the model approaches the classical elasticity model only as the layer thickness approaches zero.

In order to have good predictions of interlaminar stresses, it requires two to three sub-layers to model individual physical laminae for the free-edge problem. Like other local models which the number of variables depend on the number of layers, it rapidly becomes intractable as the number of layers becomes moderately large. However, Pagano and his colleague have presented a global-local model to resolve this difficulty [70]. They divided the laminates into global and local regions. For the global regions in which the interlaminar stresses are not interested, they employed the conventional 'effective' modulus plate theory. For the local regions in which the interlaminar stresses are interested, they employed the high order plate theory developed in Reference 69. The displacement and stress continuity conditions along the boundaries between the two regions are derived by a variational functional.

A extended Galerkin procedure was used by Wang and Dickson [71] to study the problem. The method is to minimize the potential energy for individual layer by analytical substituting the admissible solutions of interlaminar stresses and displacements in terms of Legendre polynomials and numerically solving a resulting system of simultaneous algebraic equations.

Again, good agreement with Wang and Crossman [49] for cross ply structure was shown.

Mandell [72] presented an approximated theory of anisotropic laminates for studying the free edge problem. The theory is based on the assumed stress field which is in terms of exponential functions with a 'boundary-layer-thickness' parameter. The assumed stress field satisfies equilibrium and the traction free edge condition exactly and is decay to the far field stresses predicted by the classical lamination theory. The exponential parameter is then determined by applying the principle of minimum complementary energy. He has used the theory to study 4-layer balanced angle plies and cross ply structures.

Kassapoglou and Lagace [73,74] also developed a simple and efficient method to determine the interlaminar stresses in a symmetric laminates under uniaxial loading and the method is served as a primary design tool. Again, the assumed stress field is in terms of exponential functions with two exponential parameters. The force and moment equilibrium are satisfied in an integral sense and the displacement and traction continuities between interlayer boundaries are satisfied exactly. The assumed stress field is also asymptotic to the interior solutions obtained by the classical lamination plate theory and the two exponential parameters are again determined by minimizing the complementary energy.

2.4.5 Discussion

It is interesting to note that for the angle ply laminate, [±45]s, the interlaminar normal stress distributions obtained by various numerical methods disagree in both magnitude and sign. A finite difference solution [46] and perturbation method [63] predicted a tensile σ_z very near the free edge along the interface between the $+45^0$ and -45^0 plies, while the displacement-based finite element methods [49,52] predicted a compressive stress. The differences in magnitude of the peak stress were expected but not the difference in sign.

The cause of the difference has been investigated by Whitcomb, Raju and Goree [77] and they concluded that it was attributed to the unsymmetrical stress tensor at the singular point. The finite difference and perturbation solutions [46,63] in the literature may have predicted an incorrect sign for the stress σ_z because of the assumption of a symmetric stress tensor combined with stress boundary conditions at the singular point. On the other hand, the displacement-based finite element solution did not explicitly prescribe the traction free condition at the interface corner. Instead it prescribed the normal and tangential forces on each of the element sides that lie along the free edge to be zero. Although symmetric stress tensors are still used in the formulation, the displacement-

based finite element method showed accurate solutions everywhere except in a region involving the two elements closest to the stress singularity. Numerical solutions by the displacement-based finite elements [78] have also indicated that it is better to leave the natural (force) boundary conditions to nature in some cases.

On the other hand, the special hybrid stress element [53] which includes the stress singularity in the assumed stress field and exactly satisfies the stress free edge condition and the stress continuity condition along the interlaminar boundaries does predict a compressive σ_z very near the free edge along the interface between the $+45^0$ and -45^0 plies.

Nishioka and Atluri [75] developed a special-hole-element to study the stress field of laminate structures with a circular hole. The special element which includes the analytical asymptotic solution for the stress field near a hole as well as satisfying the traction free edge condition exactly along the hole performs better than the conventional assumed displacement elements. It is also found that the element satisfying the traction boundary conditions on the surface of a crack exactly along with some forms of analytical asymptotic solution in the assumed stress field is essential for obtaining accurate stress results [79,80].

CHAPTER THREE

THE MIXED FORM HYBRID STRESS ELEMENT

In the conventional finite element formulation, mixed forms of Hellinger-Reissner principle have been used to remove locking difficulties by splitting the strain energy into two parts. For example, strain energy is split into spherical and deviatoric parts to avoid incompressibility locking, bending and transverse shear parts for beams, plates and shells to avoid shear locking, and bending and membrane strains for shells to avoid inextension locking.

A family of mixed form hybrid stress elements for laminated composite plate analysis based on a new mixed form of Hellinger-Reissner principle is formulated. The new mixed principle is based on the splitting of the strain energy into inplane and transverse parts and on a variational functional which is a function of all the components of displacement but only the transverse components of stress. In this chapter, the mixed variational principle is first introduced and the formulation of the new element is followed. Because a successful hybrid element does strongly depend on the assumed stresses, a section will address the issues of selecting assumed stresses. A family

of two- and three-dimensional elements, numerical examples and a summary are presented at the later sections.

3.1 Variational Principle

It has been well established that the variational method [85], which involves the finding a stationary value among the group of admissible functions of a finite number of variables, provides a powerful and systematic tools for derivation of the governing equation for the finite element methods. The hybrid stress elements can be derived based on the Hellinger-Reissner principle which has both element displacements and stresses as variables. It is to note that the equilibrium equations are not the prerequisite condition of the principle. However, if the assumed stresses satisfy the equilibrium conditions exactly, the complementary energy principle can be used and the stresses in the element and displacements along the element boundary are the variables [84,86,87]. When the Hellinger-Reissner principle is used, the compatibility of displacement on the inter-element boundaries can also be relaxed by using the Lagrange multipliers.

The basic thoughts in the formulation of a mixed theorem [45,81-83] are (1) that it is inconvenient to use approximations for the inplane stresses σ_x, σ_y and τ_{xy} in the analysis of laminated plates because of their discontinuity in the direction

of the plate thickness in general and (2) that it is more important to make approximate assumptions concerning transverse stresses τ_{yz}, τ_{zx} and σ_z such that the stress-free condition at the top and bottom surfaces and the stress continuity condition along the laminar interfaces can be satisfied.

We begin with the original version of the Hellinger-Reissner principle which involves all displacements and stresses, in the form

$$\pi_R(\mathbf{u},\sigma)=\int_V [-\frac{1}{2}\sigma^T\mathbf{S}\,\sigma+\sigma^T(\mathbf{Du})-\bar{\mathbf{F}}^T\mathbf{u}]\,dV-\int_{S_u}\mathbf{T}^T(\mathbf{u}-\bar{\mathbf{u}})\,dS$$

$$-\int_{S_\sigma}\bar{\mathbf{T}}^T\mathbf{u}\;dS = \text{stationary} \qquad (3.1)$$

where

σ = column matrix of stresses

$\mathbf{S} = \mathbf{C}^{-1}$ = compliance matrix

$\mathbf{D}$ = differential operator matrix

$\mathbf{u}$ = column matrix of displacements

$\mathbf{F}$ = column matrix of body forces

$\mathbf{T}$ = column matrix of boundary tractions

V = volume of the continuum

S_u = prescribed displacement boundary

S_σ = prescribed traction boundary

and a matrix with a bar overhead is to indicate prescribed quantity.

Since the body forces, and the prescribed tractions and displacements do not affect the derivation of the element stiffness matrices, they are ignored in the present development. We begin by dividing the stresses σ and stains ε into the inplane and transverse parts, as

$$\sigma = \begin{bmatrix} \mathbf{t}_p \\ \mathbf{t}_t \end{bmatrix} \tag{3.2.a}$$

$$\varepsilon = \mathbf{D}\mathbf{u} = \begin{bmatrix} \mathbf{e}_p \\ \mathbf{e}_t \end{bmatrix} \tag{3.2.b}$$

$$\mathbf{t}_p = \{\sigma_x, \sigma_y, \tau_{xy}\}^T \tag{3.2.c}$$

$$\mathbf{t}_t = \{\tau_{yz}, \tau_{zx}, \sigma_z\}^T \tag{3.2.d}$$

$$\mathbf{e}_p = \{\varepsilon_x, \varepsilon_y, \gamma_{xy}\}^T = \mathbf{D}_p\mathbf{u} \tag{3.2.e}$$

$$\mathbf{e}_t = \{\gamma_{yz}, \gamma_{zx}, \varepsilon_z\}^T = \mathbf{D}_t\mathbf{u} \tag{3.2.f}$$

where

$$\mathbf{D}_p = \begin{bmatrix} \frac{\partial}{\partial x} & 0 & 0 \\ 0 & \frac{\partial}{\partial y} & 0 \\ \frac{\partial}{\partial y} & \frac{\partial}{\partial x} & 0 \end{bmatrix} \tag{3.2.g}$$

$$\mathbf{D}_t = \begin{bmatrix} 0 & \frac{\partial}{\partial z} & \frac{\partial}{\partial y} \\ \frac{\partial}{\partial z} & 0 & \frac{\partial}{\partial x} \\ 0 & 0 & \frac{\partial}{\partial z} \end{bmatrix} \tag{3.2.h}$$

The stress-strain relation can be expressed as

$$\begin{bmatrix} \mathbf{e}_p \\ \mathbf{e}_t \end{bmatrix} = \begin{bmatrix} \mathbf{S}_p & \mathbf{S}_{pt} \\ \mathbf{S}_{pt}^T & \mathbf{S}_t \end{bmatrix} \begin{bmatrix} \mathbf{t}_p \\ \mathbf{t}_t \end{bmatrix} \tag{3.3}$$

Substituting Eqs. (3.2) and (3.3) into Eq. (3.1), we get

$$\pi_R(\mathbf{u}, \mathbf{t}_p, \mathbf{t}_t) = \int_V [-\frac{1}{2}\mathbf{t}_p^T\mathbf{S}_p\mathbf{t}_p - \mathbf{t}_p^T\mathbf{S}_{pt}\mathbf{t}_t - \frac{1}{2}\mathbf{t}_t^T\mathbf{S}_t\mathbf{t}_t + \mathbf{t}_p^T\mathbf{e}_p + \mathbf{t}_t^T\mathbf{e}_t]\,dV \tag{3.4}$$

From the first half of Eq. (3.3), we can solve for $\mathbf{t}_p$ in terms of $\mathbf{e}_p$ and $\mathbf{t}_t$

$$\mathbf{t}_p = \mathbf{C}_p\mathbf{e}_p + \mathbf{C}_{pt}\mathbf{t}_t \tag{3.5.a}$$

where

$$\mathbf{C}_p = \mathbf{S}_p^{-1} \tag{3.5.b}$$

$$\mathbf{C}_{pt} = -\mathbf{C}_p\mathbf{S}_{pt} = \mathbf{C}_{tp}^T \tag{3.5.c}$$

Substitution of Eq. (3.5.a) into Eq. (3.4), yields the

following mixed variational functional for which involves displacements and transverse stresses

$$\pi_{mR}(\mathbf{u},\mathbf{t}_t) = \int_V [\frac{1}{2}\mathbf{e}_p^T\mathbf{C}_p\mathbf{e}_p + \mathbf{t}_t^T\mathbf{C}_{tp}\mathbf{e}_p - \frac{1}{2}\mathbf{t}_t^T\mathbf{S}_t^*\mathbf{t}_t + \mathbf{t}_t^T\mathbf{e}_t]dV \qquad (3.6.a)$$

$$= \int_V [P(\mathbf{e}_p,\mathbf{t}_t) + \mathbf{t}_t^T\mathbf{e}_t]dV \qquad (3.6.b)$$

where

$$P(\mathbf{e}_p,\mathbf{t}_t) = \text{'mixed strain energy density'}$$

$$= \frac{1}{2}\mathbf{e}_p^T\mathbf{C}_p\mathbf{e}_p + \mathbf{t}_t^T\mathbf{C}_{tp}\mathbf{e}_p - \frac{1}{2}\mathbf{t}_t^T\mathbf{S}_t^*\mathbf{t}_t \qquad (3.6.c)$$

$$\mathbf{S}_t^* = \mathbf{S}_t - \mathbf{S}_{pt}^T\mathbf{C}_p\mathbf{S}_{pt} \qquad (3.6.d)$$

with the constraint equations (3.2.e), (3.2.f) and (3.5.a). We can see from Eqs. (3.6.c) and (3.5.a),

$$\mathbf{t}_p = \frac{\partial P(\mathbf{e}_p,\mathbf{t}_t)}{\partial \mathbf{e}_p} \qquad (3.7)$$

The present mixed variation principle was first suggested by Reissner in 1984 [81]. He started with the principle of potential energy. With the help of Lagrange multipliers to relax the transverse part of strain-displacement relation and the introducing of a complementary function through a partial Legendre transformation, Eq. (3.6.a) was obtained. In 1986, He re-derived the same theorem by a more concise way [82]. He began with Hellinger-Reissner principle and then introduced the

'semi-complementary energy density' to arrive the mix variational theorem.

Independently, Moriya [45] arrived the same functional in 1986. He began with the Hu-Washizu principle and introduced the constraint Eqs. (3.2.e), (3.2.f) and (3.5.a) into the principle to eliminate the undesirable inplane stress terms. Huang [83] re-derived the theorem by means of the weighted residual scheme corresponding to some governing equations which are based on displacements and transverse stresses.

It appears that the present derivation is the most concise and clearest way to arrive the resulting mixed principle. We can verify Eq. (3.6.b) by taking its variation with respect to $\mathbf{e}_t$, $\mathbf{e}_p$ and $\mathbf{t}_t$ that is,

$$\delta\pi_{mR} = \int_V [\delta\mathbf{e}_p^T \frac{\partial P}{\partial \mathbf{e}_p} + \delta\mathbf{t}_t^T \frac{\partial P}{\partial \mathbf{t}_t} + \delta\mathbf{t}_t^T \mathbf{e}_t + \delta\mathbf{e}_t^T \mathbf{t}_t] dV = 0 \quad (3.8)$$

Substituting Eqs. (3.2.e), (3.2.f), (3.5.a) and (3.7) into above equation and applying integration by parts, Eq. (3.8) is reduced to the form

$$\delta\pi_{mR} = \int_V [-\delta\mathbf{u}^T (\mathbf{D}_p^T \mathbf{t}_p + \mathbf{D}_t^T \mathbf{t}_t) + \delta\mathbf{t}_t^T (\frac{\partial P}{\partial \mathbf{t}_t} + \mathbf{e}_t)] dV = 0 \quad (3.9)$$

Thus, the resulting Euler equations are the constitutive equations

$$\mathbf{e}_t = - \frac{\partial P}{\partial \mathbf{t}_t} \qquad (3.10.a)$$

which gives $\mathbf{e}_t$ and function of $\mathbf{e}_p$ and $\mathbf{t}_t$, and the three equilibrium equations

$$\mathbf{D}_p^T \mathbf{t}_p + \mathbf{D}_t^T \mathbf{t}_t = \mathbf{0} \qquad (3.10.b)$$

3.2 Element Stiffness Formulation

A new mixed form hybrid stress element based on the mixed variational principle is derived in the present section. The formulation of the conventional hybrid stress element is also included for comparison because of their similarities. A discussion on the advantage and efficiency and the method of implementation will follow.

3.2.1 Derivation

We rewrite the Hellinger-Reissner principle, Eq. (3.1), and the mixed variational principle, Eq. (3.6.a), into a

modified form for finite element formulation and assume that the prescribed boundary displacements are satisfied

$$\pi_R^* = \sum_n \{ \int_{V_n} [-\frac{1}{2}\sigma^T \mathbf{S}\,\sigma + \sigma^T(\mathbf{Du}) - \bar{\mathbf{F}}^T\mathbf{u}]\,dV - \int_{S_\sigma} \bar{\mathbf{T}}^T\mathbf{u}\,dS \} \qquad (3.11)$$

and

$$\pi_{mR}^* = \sum_n \{ \int_{V_n} [\frac{1}{2}\mathbf{e}_p^T\mathbf{C}_p\mathbf{e}_p + \mathbf{t}_t^T\mathbf{C}_{tp}\mathbf{e}_p - \frac{1}{2}\mathbf{t}_t^T\mathbf{S}_t^*\mathbf{t}_t - \bar{\mathbf{F}}^T\mathbf{u}]\,dV - \int_{S_\sigma} \bar{\mathbf{T}}^T\mathbf{u}\,dS \} \qquad (3.12)$$

where

n = number of element

V_n = spatial domain of element n

The definition and notation of the matrices used below are standard in most literature concerning conventional hybrid stress element. A similar definition and notation are used for the present mixed form element to make it easy to observe the similarities between the two formulations.

In the conventional formulation all six stresses σ are approximated by a finite number of undetermined parameters β and in the present mixed form formulation only three transverse stresses $\mathbf{t}_t$ are approximated. For a type I element, the stress field is expressed as

$$\boldsymbol{\sigma} = \mathbf{P}\ \beta \tag{3.13.a}$$

for the conventional hybrid stress element and

$$\mathbf{t}_t = \mathbf{P}\ \beta \tag{3.13.b}$$

for the present mixed form hybrid stress element, where

$\mathbf{P}$ = matrix of assumed polynomials

β = set of stress parameters

The displacements $\mathbf{u}$ which are the same for the two formulations are approximated by interpolation functions in terms of nodal displacements $\mathbf{q}$.

$$\mathbf{u} = \mathbf{N}\ \mathbf{q} \tag{3.14}$$

where

$\mathbf{N}$ = matrix of shape functions

$\mathbf{q}$ = nodal displacements

Introducing Eqs. (3.13.a) and (3.14) into Eq. (3.11), the functional is reduced to the form

$$\pi_R^* = \sum_n \left\{ -\frac{1}{2}\beta^T \mathbf{H}\,\beta + \beta^T \mathbf{G}\,\mathbf{q} - \mathbf{q}^T \mathbf{Q} \right\} \tag{3.15.a}$$

where

$$\mathbf{G} = \int_{V_n} \mathbf{P}^T (\mathbf{DN})\ dV = \int_{V_n} \mathbf{P}^T \begin{bmatrix} \mathbf{D}_p \\ \mathbf{D}_t \end{bmatrix} \mathbf{N}\ dV \qquad (3.15.b)$$

$$\mathbf{H} = \int_{V_n} \mathbf{P}^T \mathbf{S}\, \mathbf{P}\ dV \qquad (3.15.c)$$

$$\mathbf{Q} = \int_{V_n} \mathbf{N}^T \overline{\mathbf{F}}\, dV + \int_{S_\sigma} \mathbf{N}^T \overline{\mathbf{T}}\, dS \qquad (3.15.d)$$

and introducing Eqs. (3.13.b) and (3.14) into Eq. (3.12), the functional is reduced to

$$\pi^*_{mR} = \sum_n \left\{ \frac{1}{2} \mathbf{q}^T \mathbf{k}_p \mathbf{q} + \beta^T \mathbf{G}\, \mathbf{q} - \frac{1}{2} \beta^T \mathbf{H}\, \beta - \mathbf{q}^T \mathbf{Q} \right\} \qquad (3.16.a)$$

where

$$\mathbf{k}_p = \int_{V_n} (\mathbf{D}_p \mathbf{N})^T\ \mathbf{C}_p\ (\mathbf{D}_p \mathbf{N})\ dV \qquad (3.16.b)$$

$$\mathbf{G} = \int_{V_n} \mathbf{P}^T [\mathbf{C}_{tp} (\mathbf{D}_p \mathbf{N}) + (\mathbf{D}_t \mathbf{N})]\ dV \qquad (3.16.c)$$

$$\mathbf{H} = \int_{V_n} \mathbf{P}^T \mathbf{S}_t^* \mathbf{P}\ dV \qquad (3.16.d)$$

and $\mathbf{Q}$ is given by Eq. (3.15.d)

Applying the stationary condition to Eq. (3.15.a) or (3.16.a) with respect to β, i.e. $\partial\pi/\partial\beta = \mathbf{0}$, we obtain

$$\mathbf{G}\, \mathbf{q} - \mathbf{H}\, \beta = \mathbf{0}$$

and rewritten as

$$\boldsymbol{\beta} = \mathbf{H}^{-1}\ \mathbf{G}\ \mathbf{q} \tag{3.17}$$

Substituting Eq. (3.17) into Eq. (3.15.a) or (3.16.a) and applying the stationary condition with respect to $\mathbf{q}$, i.e. $\partial\pi/\partial\mathbf{q} = \mathbf{0}$, we obtain

$$\mathbf{K}\ \mathbf{q} = \mathbf{Q} \tag{3.18.a}$$

where

$\mathbf{K}$, $\mathbf{q}$ and $\mathbf{Q}$ are global matrices assembled from element matrices

$$\mathbf{k} = \mathbf{G}^{T}\ \mathbf{H}^{-1}\ \mathbf{G} \tag{3.18.b}$$

for the conventional hybrid stress element and

$$\mathbf{k} = \mathbf{k}_{p} + \mathbf{G}^{T}\ \mathbf{H}^{-1}\ \mathbf{G} \tag{3.18.c}$$

for the present mixed form hybrid stress element

After solving Eq. (3.18.a), the stress calculations can be carried out by using Eqs. (3.17) and (3.13.a) for the conventional hybrid stress element or by using Eqs. (3.17), (3.13.b) and (3.16.a) for the new mixed form hybrid stress element.

For a type II sub-element, the stress field in the ith sub-element is expressed in local stress parameters β^{i}

$$\boldsymbol{\sigma}^i = \mathbf{P}^i \, \beta^i \tag{3.19.a}$$

for the conventional hybrid stress element and

$$\mathbf{t}_t^i = \mathbf{P}^i \, \beta^i \tag{3.19.b}$$

for the present mixed form hybrid stress element

and the displacement field $\mathbf{u}^i$ is also expressed in terms of nodal displacements $\mathbf{q}^i$

$$\mathbf{u}^i = \mathbf{N}^i \, \mathbf{q}^i \tag{3.20}$$

Therefore, Eqs. (3.15.b) to (3.15.d) can be rewritten as

$$\mathbf{G} = \sum_N \left\{ \int_{V_{ni}} (\mathbf{P}^i)^T (\mathbf{D}\mathbf{N}^i) \, dV \right\} \tag{3.21.a}$$

$$\mathbf{H} = \sum_N \left\{ \int_{V_{ni}} (\mathbf{P}^i)^T \mathbf{S}^i \mathbf{P}^i \, dV \right\} \tag{3.21.b}$$

$$\mathbf{Q} = \sum_N \left\{ \int_{V_{ni}} (\mathbf{N}^i)^T \bar{\mathbf{F}} \, dV + \int_{S_{ni}} (\mathbf{N}^i)^T \bar{\mathbf{T}} \, dS \right\} \tag{3.21.c}$$

for the conventional hybrid stress element and

$$\mathbf{k}_p = \sum_N \left\{ \int_{V_{ni}} (\mathbf{D}_p \mathbf{N}^i)^T \mathbf{C}_p^i (\mathbf{D}_p \mathbf{N}^i) \, dV \right\} \qquad (3.22.a)$$

$$\mathbf{G} = \sum_N \left\{ \int_{V_{ni}} (\mathbf{P}^i)^T [\mathbf{C}_{tp}^i (\mathbf{D}_p \mathbf{N}^i) + (\mathbf{D}_t \mathbf{N}^i)] \, dV \right\} \qquad (3.22.b)$$

$$\mathbf{H} = \sum_N \left\{ \int_{V_{ni}} (\mathbf{P}^i)^T \mathbf{S}_t^{*i} \mathbf{P}^i \, dV \right\} \qquad (3.22.c)$$

for the present mixed form hybrid stress element, where

N = number of sub-elements thru the laminate which equals to the number of laminae or less

Finally, the element stiffness matrix can be obtained by either Eq. (3.18.a) or Eq. (3.18.b).

Because the nodal displacement $\mathbf{q}^i$ include parameters on the laminar interfaces, continuity of the displacements across such interfaces will be guaranteed after 'assembly' of the layers for the sub-element. On the other hand, the stresses in the i^{th} sub-element are subdivided into the following form

$$\beta^i = \begin{bmatrix} {}^t\beta^i \\ {}^i\beta^i \\ {}^b\beta^i \end{bmatrix} \qquad (3.23)$$

where

${}^t\beta^i$ = stress parameters which are associated with the top surface of the i^{th} sub-element

$^{i}\beta^{i}$ = stress parameters which are associated only within the i^{th} sub-element

$^{b}\beta^{i}$ = stress parameters which are associated with the bottom surface of the i^{th} sub-element

Enforcing the continuity of transverse shear and normal stresses at the interlayer boundaries and the traction free condition at the upper and lower surfaces of laminate can be done easily by only relating the parameter β^{i} at the appropriate top and bottom surfaces of that sub-element and setting some parameters to be zero, respectively.

Looking at the two formulations, we can see that the kinematic assumptions are identical. The matrices **G** and **H** are very similar except that a smaller matrix **P** is used and an elasticity matrix is inside the integral of matrix **G** for the new mixed form model.

The obvious result separated the stresses into two parts is that the element stiffness matrix **k** for the new mixed form element is also divided. The first-half $\mathbf{k}_p$ is related to the inplane deformation energy and the expression is very similar to a element based on the displacement model. The second-half $\mathbf{G}^T \mathbf{H}^{-1} \mathbf{G}$ is related to the transverse and coupling between inplane and transverse deformation energy. The formula is similar to the conventional hybrid stress element.

Several advantages by using the new formulation are cited as follows: First, the number of stress parameters β used is less in comparison with the conventional element, and therefore the dimensions of matrices **G** and **H** are smaller. Since the computational effort is proportional to the dimensions of **G** and **H** in the order of cubic, considerable computational effort will be saved by reducing the number of β's.

Second, any element based on displacement model will violate the continuity of interlaminar stresses along the laminar interfaces. Any type I element and type II element with appropriate stress assumptions based on the present mixed form formulation will satisfy the continuity of interlaminar stress condition along the interfaces.

Third, no extensive computational time is required to calculate the transverse stresses in the present mixed form model.

Fourth, the order of inplane stresses in the present mixed form model is higher than the one in a displacement model with the same order of degrees of freedom. It is because the calculation of inplane stresses, Eq. (3.5.a), includes the transverse stresses which are higher order in the new mixed form model.

3.2.2 Implementation

Each layer in the laminate is assumed to be in a three-dimensional stress state, so that the stress-strain relation for a typical lamina i with reference to its material axes 1, 2 and 3 is shown in Figure 3.1 and can be rewritten as

$$\begin{bmatrix} \varepsilon_1 \\ \varepsilon_2 \\ \varepsilon_3 \\ \gamma_{23} \\ \gamma_{31} \\ \gamma_{12} \end{bmatrix}^i = \begin{bmatrix} S_{11} & S_{12} & S_{13} & 0 & 0 & 0 \\ S_{12} & S_{22} & S_{23} & 0 & 0 & 0 \\ S_{13} & S_{23} & S_{33} & 0 & 0 & 0 \\ 0 & 0 & 0 & S_{44} & 0 & 0 \\ 0 & 0 & 0 & 0 & S_{55} & 0 \\ 0 & 0 & 0 & 0 & 0 & S_{66} \end{bmatrix}^i \begin{bmatrix} \sigma_1 \\ \sigma_2 \\ \sigma_3 \\ \tau_{23} \\ \tau_{31} \\ \tau_{12} \end{bmatrix}^i \qquad (3.24)$$

As in the case of a fiber reinforced composite, the material is transversely isotropic about axis 1, the direction of the fiber. The element S_{ij} are given by

$$S_{11} = \frac{1}{E_L} \qquad S_{22} = S_{33} = \frac{1}{E_T}$$

$$S_{12} = S_{13} = -\frac{\nu_{LT}}{E_L} \qquad S_{23} = -\frac{\nu_{ZT}}{E_T} \tag{3.25}$$

$$S_{55} = S_{66} = \frac{1}{G_{LT}} \qquad S_{44} = \frac{1}{G_{ZT}}$$

where

E_L = longitudinal modulus

E_T = transverse modulus

G_{LT} = shear modulus for the LT plane

G_{ZT} = shear modulus for the ZT plane

ν_{LT} = Poisson's ration measuring strain in the transverse direction under uniaxial normal stress in the axis L

ν_{ZT} = Poisson's ration measuring strain in the transverse direction under uniaxial normal stress in the axis Z

The stress-strain relation with respect to the plate axes x, y and z is obtained by applying a coordinate transformation law

$$\boldsymbol{\varepsilon}^i = \mathbf{T}_i^T \, \mathbf{S}^i \, \mathbf{T}_i \, \boldsymbol{\sigma}^i \tag{3.26.a}$$

$$= \bar{\mathbf{S}}^i \, \boldsymbol{\sigma}^i \tag{3.26.b}$$

where

$\mathbf{T}_i$ = transformation matrix of layer i [88]

For this particular case of a fiber-reinforced composite,

let the direction 1 (parallel to the fiber direction L) make an angle θ with the x axis as shown in Figure 3.1 and direction 3 remain parallel to the z axis, then the transformation matrix becomes

$$\mathbf{T}_i = \begin{bmatrix} c^2 & s^2 & 0 & 0 & 0 & -2cs \\ s^2 & c^2 & 0 & 0 & 0 & 2cs \\ 0 & 0 & 1 & 0 & 0 & 0 \\ 0 & 0 & 0 & c & s & 0 \\ 0 & 0 & 0 & -s & c & 0 \\ cs & -cs & 0 & 0 & 0 & c^2-s^2 \end{bmatrix} \tag{3.27}$$

where

$$c = \cos\theta$$

$$s = \sin\theta$$

Eq. (3.26) defines the elasticity matrix for any particular lamina i. It is obvious that the elasticity matrix is dependent on fibre orientation and, in general, is different for each lamina.

The integrals in Eqs. (3.15), (3.16), (3.21) and (3.22) are evaluated by Gaussian quadrature numerical integration. However, the elasticity matrix is different from layer to layer and is not a continuous function of ζ. For the integrations it is necessary to split the integration limits through each layer. Furthermore, the displacements and assumed stresses of type II

sub-element are in local sub-element natural coordinate ξ, η and ζ_i rather than global natural coordinate ξ, η and ζ as shown in Figure 3.2. Modifying the variable ζ to ζ_i in any i^{th} layer or sub-element is needed before applying the Gaussian quadrature. This all can be achieved by the change of variable. It is obtained from

$$\zeta = \frac{\bar{\zeta}_i + \bar{\zeta}_{i+1}}{2} + \frac{\bar{\zeta}_i - \bar{\zeta}_{i+1}}{2} \zeta_i \qquad (3.28.a)$$

$$d\zeta = \frac{\bar{\zeta}_i - \bar{\zeta}_{i+1}}{2} d\zeta_i \qquad (3.28.b)$$

where

$\bar{\zeta}_i = \zeta$ coordinate of the top surface of i^{th} layer or sub-element

$\bar{\zeta}_{i+1} = \zeta$ coordinate of the bottom surface i^{th} layer or sub-element

With this substitution, the numerical integrations can be carried out as usual.

3.3 Assumed Stress

Appropriately selecting the assumed stresses is the key to achieve a satisfactory hybrid element. Within this content, considerations will be focus on the plate elements. The first

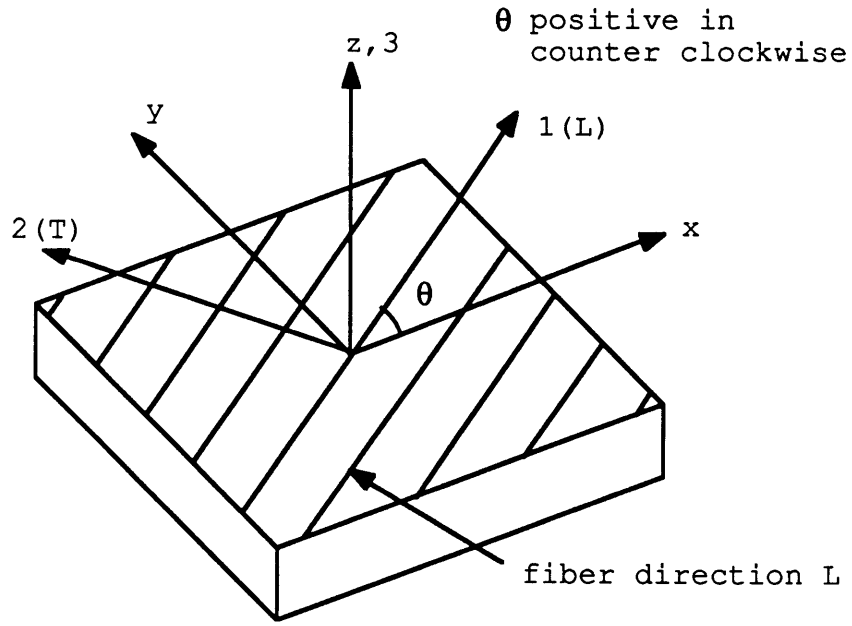

Figure 3.1 Fiber direction with respect to plate axes

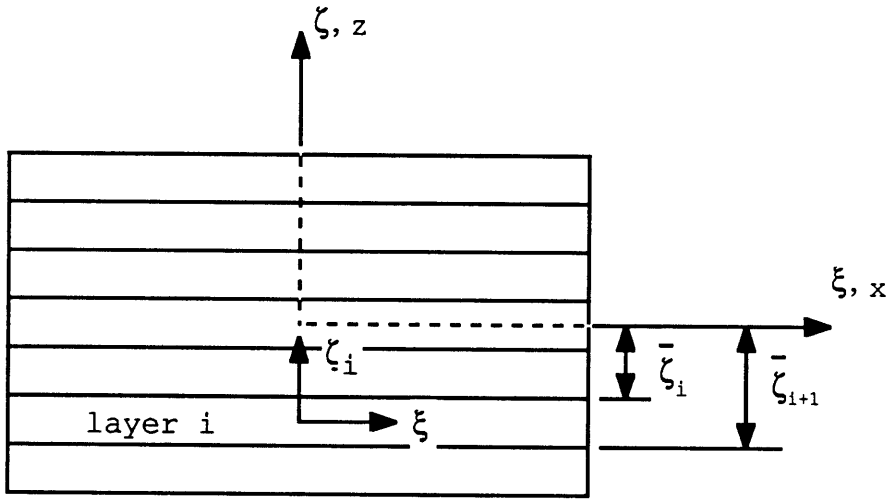

Figure 3.2 Local element natural coordinates for layer i

consideration is to choose the assumed stress field satisfying the equilibrium condition. While selecting the stresses to satisfying the equilibrium, three other considerations should be taken into account. They are satisfying the invariant property, suppressing the kinematic modes and avoiding the shear locking.

3.3.1 Equilibrium Condition

As we mentioned before, if the hybrid stress element is based on the Hellinger-Reissner principle, the equilibrium equations are not the prerequisite condition of the principle. The global equilibrium is enforced in an integral sense through the variation of the functional, strictly speaking, the local equilibrium on each element can be relaxed.

However, a hybrid/mixed element having a 'sufficiently' large number of stress parameters and without constraint by equilibrium equations will eventually lead to results identical to those of displacement-based model, according to a limitation principle due to Fraeijs de Veubeke [89,90]. Furthermore, study [91] has shown that the hybrid stress element satisfying the equilibrium equations will perform better than the one that it does not.

Therefore, the assumed stress field should satisfy the equilibrium equations exactly if the global Cartesian

coordinates are used or in an integral sense if the natural coordinates are used in order to get better performance. Two alternative approaches are available to achieve this. First, the assumed stress field is initially approximated by a number of uncoupled stress parameters β's while we directly apply the equilibrium equations on the assumed stress field to enforce the condition. In this process, the number of β's will be reduced and they are no longer to be uncoupled [92].

The alternative approach is still first approximated the assumed stress field by a number of uncoupled β's while we indirectly enforce the equilibrium condition through the application of constraint conditions with internal displacements as Lagrange multipliers. The element, in general, will not satisfy the equilibrium condition exactly but in an integral sense. In this process, the number of β's will also be reduced and they are also no longer to be uncoupled [93].

We will adopt the former method to enforce the equilibrium condition. On the other hand, the introduction of equilibrium and symmetry on the assumed stress field may add large number of stress parameters to those initially chosen for suppressing the zero-energy deformation modes. It is advisable to relax the equilibrium conditions on some high order terms to keep the number of stress parameters small [94].

3.3.2 Invariant Property

To retain the invariant property of the element has been shown less sensitive to element distortion [93]. Two alternative approaches are also available to achieve this. First, a completeness in polynomial for stress expressions based on the global Cartesian coordinates is used [92]. But for certain elements the number of stress parameters will become impractically high [95].

Invariant property can be always preserved if isoparametric (natural element) coordinates are used. Thus, the alternative approach is first approximated the tensor stress components τ^{ij} which satisfy the equilibrium exactly in a regular shape element based on the natural element coordinates $\xi^i(\xi^1=\xi, \xi^2=\eta, \xi^3=\zeta)$. Then the physical stress components σ^{ij} referring to the global Cartesian coordinates $x^i(x^1=x, x^2=y, x^3=z)$ are obtained by applying the coordinate transformation law

$$\sigma^{ij} = \left(\frac{\partial x^m}{\partial \xi^i}\right)_0 \left(\frac{\partial x^n}{\partial \xi^j}\right)_0 \tau^{mn}, \qquad i,j,m,n=1,2 \qquad (3.29.a)$$

for inplane stress components, and

$$\sigma^{i3} = \left(\frac{\partial x^m}{\partial \xi^i}\right)_0 \left(\frac{\partial x^3}{\partial \xi^3}\right)_0 \tau^{m3}, \quad i,m = 1,2 \tag{3.29.b}$$

$$\sigma^{33} = \left(\frac{\partial x^3}{\partial \xi^3}\right)_0^2 \tau^{33} \tag{3.29.c}$$

for transverse stress components, where

$$\left(\frac{\partial x^m}{\partial \xi^i}\right)_0 = \text{Jacobian of transformation at } \xi^1=\xi^2=\xi^3=0$$

The Jacobian of transformation evaluated at the centroid of the element is to satisfy the patch test for convergence [96]. Because of no inplane stresses be used in the new mixed form model, Eqs. (3.29.b) and (3.29.c) can be simplified as follows:

$$\sigma^{i3} = \left(\frac{\partial x^m}{\partial \xi^i}\right)_0 \tau^{m3}, \quad i,m = 1,2 \tag{3.30.a}$$

$$\sigma^{33} = \left(\frac{\partial x^3}{\partial \xi^3}\right)_0 \tau^{33} \tag{3.30.b}$$

Because of the coordinate transformation, the assumed stress field is no longer satisfied the equilibrium condition exactly but in a weighted sense except for a rectangular shape element. The latter approach is superior than the former one and is adopted in this study.

The second approach by applying internal displacements to enforce the equilibrium condition in section 3.3.1 can also

preserve the invariance by approximating the assumed stress field in terms of isoparametric coordinates. For a four-node two-dimensional element, this approach and the one chosen in this study can arrive the same assumed stress field with 5-β, but a perturbation technique is required for this approach to arrive the result [93].

3.3.3 Kinematic Deformation Modes

For an element to be reliable, all the spurious zero energy (kinematic) modes must be suppressed. A necessary condition for the resulting stiffness matrix to have sufficient rank for the conventional hybrid stress element [97] is

$$m \geq n - r \tag{3.31}$$

where

m = number of independent stress parameter β's

n = number of nodal displacement q's

r = number of rigid body modes

A necessary and sufficient condition for suppressing all kinematic modes and convergence of the element is the so-called 'LBB (Ladyzhenskaya-Babuska-Brezzi)' conditions [98]. Pian and Chen [94] suggested a systematic procedure for the choice of the necessary assumed stresses for suppressing all kinematic modes. It is by selecting the stress parameters in such a way that at

least one β corresponds to each of the strain terms obtained from the strain-displacement relationships.

If the element deformation energy due to the displacements and all six components of assumed stress is U_d, then

$$2U_d = \int_V \sigma^T \varepsilon \, dV \tag{3.32}$$

The displacements $\mathbf{u}$ can also be in terms of n independent deformation modes in the form

$$\mathbf{u} = \begin{bmatrix} \bar{\mathbf{N}}_\alpha & \bar{\mathbf{N}}_R \end{bmatrix} \begin{bmatrix} \alpha \\ \mathbf{R} \end{bmatrix} \tag{3.33}$$

where

α = deformation modes

$\mathbf{R}$ = rigid body modes

$\bar{\mathbf{N}}_\alpha$ = interpolation functions coresponding to α

$\bar{\mathbf{N}}_R$ = interpolation functions corresponding to $\mathbf{R}$

Here, we use an 8-node brick element as an example to illustrate the deformation modes. In 3D analysis, we have 3 d.o.f. per node and total 24 d.o.f. for the brick element. The assumed displacements $\mathbf{u}$ can be expressed as

$$\mathbf{u} = \begin{bmatrix} u \\ v \\ w \end{bmatrix} = \sum_{i=1}^{8} N_i(\xi,\eta,\zeta) \begin{bmatrix} u_i \\ v_i \\ w_i \end{bmatrix} \qquad (3.34.a)$$

where

$$N_i(\xi,\eta,\zeta) = \frac{1}{8}(1+\xi_i\xi)(1+\eta_i\eta)(1+\zeta_i\zeta) \qquad (3.34.b)$$

and u_i, v_i and w_i are nodal displacements at node i

Expanding the assumed displacements **u** into deformation modes α and rigid body modes **R**, we get

$$\begin{aligned} u &= \alpha_1 + \alpha_2\zeta + (\alpha_3 + \alpha_4\zeta)\xi + (\alpha_5 + \alpha_6\zeta)\eta + (\alpha_7 + \alpha_8\zeta)\xi\eta \\ v &= \alpha_9 + \alpha_{10}\zeta + (\alpha_{11} + \alpha_{12}\zeta)\xi + (\alpha_{13} + \alpha_{14}\zeta)\eta + (\alpha_{15} + \alpha_{16}\zeta)\xi\eta \\ w &= \alpha_{17} + \alpha_{18}\zeta + (\alpha_{19} + \alpha_{20}\zeta)\xi + (\alpha_{21} + \alpha_{22}\zeta)\eta + (\alpha_{23} + \alpha_{24}\zeta)\xi\eta \end{aligned} \qquad (3.35)$$

where

the α's are function of the nodal displacements u_i, v_i and w_i

α_1, α_9, α_{17}, $(\alpha_5-\alpha_{11})$, $(\alpha_2-\alpha_{19})$ and $(\alpha_{10}-\alpha_{21})$ are rigid body modes and the rests are deformation modes

Then, the necessary and sufficient condition for absence of kinematic modes is

$$\text{Rank of } \mathbf{G}_\alpha = n - r \qquad (3.36.a)$$

where

$$\mathbf{G}_{\alpha} = \int_{V} \mathbf{P}^{T} \, (\mathbf{D}\,\bar{\mathbf{N}}_{\alpha}) \; dV \qquad (3.36.b)$$

Because the computational effort in formulating the element stiffness matrix is proportional to the dimension of matrices **G** and **H**, it is advantage to keep the number of stress parameters as small as possible. There also exist many examples indicating that overuse of stress parameters will yield over-rigid element and oscillations in resulting stress distribution. Therefore, it is best to keep the number of stress parameters as close to n-r as possible while simultaneously suppressing all kinematic modes.

A new procedure similar to the steps suggested by Pian and Chen [94] to choose the stress terms to suppress the kinematic deformation modes for the new mixed form element is developed in the present section.

We rewrite the element deformation energy into two parts

$$2\,U_{d} = \int_{V} \boldsymbol{\sigma}^{T} \boldsymbol{\varepsilon} \, dV = \int_{V} (\mathbf{t}_{p}^{T} \mathbf{e}_{p} + \mathbf{t}_{t}^{T} \mathbf{e}_{t}) \, dV \qquad (3.37)$$

By introducing Eq. (3.5.a) into Eq. (3.37) and applying the strain-displacement relationships, Eqs. (3.2.e) and (3.2.f), the element deformation energy due to displacements and transverse assumed stresses becomes

$$2\,U_d = \int_V [\,\mathbf{e}_p^T \mathbf{C}_p \mathbf{e}_p + \mathbf{t}_t^T \mathbf{C}_{tp} \mathbf{e}_p + \mathbf{t}_t^T \mathbf{e}_t\,]\; dV \qquad (3.38.a)$$

$$= 2\,(U_{d1} + U_{d2}) \qquad (3.38.b)$$

where

$$U_{d1} = \frac{1}{2}\int_V \mathbf{e}_p^T \mathbf{C}_p \mathbf{e}_p\, dV = \frac{1}{2}\mathbf{q}^T \mathbf{K}_p \mathbf{q} \qquad (3.38.c)$$

= inplane deformation energy

$$U_{d2} = \frac{1}{2}\int_V [\,\mathbf{t}_t^T \mathbf{C}_{tp} \mathbf{e}_p + \mathbf{t}_t^T \mathbf{e}_t\,]\, dV = \frac{1}{2}\beta^T \mathbf{G}\, \mathbf{q} \qquad (3.38.d)$$

= transverse deformation energy and energy coupling between the inplane and transverse components

The element deformation modes α are divided into three parts as

$$\alpha = \begin{bmatrix} \alpha_i \\ \alpha_c \\ \alpha_t \end{bmatrix} \qquad (3.39)$$

where

α_i = deformation modes only related to inplane strains $\mathbf{e}_p$

α_c = deformation modes related to coupling between inplane $\mathbf{e}_p$ and transverse $\mathbf{e}_t$ strains

α_t = deformation modes only related to transverse strains $\mathbf{e}_t$

We continues our previous example here. With Eqs. (3.2.b) and (3.35), the strain field for an 8-node brick element of dimension 1x1x1 with the natural element coordinates ξ, η and ζ parallel to the global Cartesian coordinates x, y and z and the edges can be written as

$$\varepsilon_x = \frac{\partial u}{\partial x} = \alpha_3 + \alpha_4\zeta + (\alpha_7 + \alpha_8\zeta)\,\eta$$

$$\varepsilon_y = \frac{\partial v}{\partial y} = \alpha_{13} + \alpha_{14}\zeta + (\alpha_{15} + \alpha_{16}\zeta)\,\xi$$

$$\gamma_{xy} = \frac{\partial u}{\partial y} + \frac{\partial v}{\partial x} = \alpha_5 + \alpha_6\zeta + (\alpha_7 + \alpha_8\zeta)\,\xi + \alpha_{11} + \alpha_{12}\zeta + (\alpha_{15} + \alpha_{16}\zeta)\,\eta$$

$$\gamma_{yz} = \frac{\partial v}{\partial z} + \frac{\partial w}{\partial y} = \alpha_{10} + \alpha_{12}\xi + \alpha_{14}\eta + \alpha_{16}\xi\eta + \alpha_{21} + \alpha_{22}\zeta + (\alpha_{23} + \alpha_{24}\zeta)\,\xi$$

$$\gamma_{zx} = \frac{\partial u}{\partial z} + \frac{\partial w}{\partial x} = \alpha_2 + \alpha_4\xi + \alpha_6\eta + \alpha_8\,\xi\eta + \alpha_{19} + \alpha_{20}\zeta + (\alpha_{23} + \alpha_{24}\zeta)\,\eta$$

$$\varepsilon_z = \frac{\partial w}{\partial z} = \alpha_{18} + \alpha_{20}\xi + \alpha_{22}\eta + \alpha_{24}\xi\eta \qquad (3.40)$$

Therefore, the three types of deformation modes and rigid body modes are

$$\alpha_i = \left[\alpha_3 \quad \alpha_7 \quad \alpha_{13} \quad \alpha_{15} \quad (\alpha_5 + \alpha_{11})\right]^T$$

$$\alpha_c = \left[\alpha_4 \quad \alpha_6 \quad \alpha_8 \quad \alpha_{12} \quad \alpha_{14} \quad \alpha_{16}\right]^T \qquad (3.41)$$

$$\alpha_t = \left[(\alpha_2 + \alpha_{19}) \quad (\alpha_{10} + \alpha_{21}) \quad \alpha_{18} \quad \alpha_{20} \quad \alpha_{22} \quad \alpha_{23} \quad \alpha_{24} \right]^T$$

$$\mathbf{R} = \left[\alpha_1 \quad \alpha_9 \quad \alpha_{17} \quad (\alpha_5 - \alpha_{11}) \quad (\alpha_2 - \alpha_{19}) \quad (\alpha_{10} - \alpha_{21}) \right]^T$$

Because there is no deformation energy in rigid body modes, we only need to investigate the three types of distinguish deformation mode, α_i, α_c and α_t, together with three components of assumed stresses for possible zero energy (kinematic) deformations. Corresponding to a non-zero finite value for an inplane deformation mode α_i, the inplane strains $\mathbf{e}_p$ will not be zero but the transverse strains $\mathbf{e}_t$ will be zero. Because the elasticity matrix $\mathbf{C}_p$ is positive definite and $\mathbf{e}_p$ is not zero, the inplane deformation energy U_{d1}, Eq. (3.38.c), is non-zero. The deformation energy U_{d2}, Eq. (3.38.d), may be zero under some stress assumptions but the total deformation energy U_d is not because of non-zero value of U_{d1}.

Corresponding to a non-zero value for a coupling mode α_c, both inplane $\mathbf{e}_p$ and transverse $\mathbf{e}_t$ strains will be non-zero. The deformation energy U_{d1} has a non-zero value and U_{d2} may be zero but the total energy U_d is not zero because of U_{d1}.

Corresponding to a non-zero value for a transverse mode α_t, the inplane strains $\mathbf{e}_p$ will be zero but the transverse strains $\mathbf{e}_t$ will not. Then U_{d1} is zero and also under some assumed

stresses U_{d2} may be zero too. Thus, the total deformation energy U_d is possible to be zero.

We can conclude that the only possible source for creating zero energy (kinematic) deformation modes for the present mixed form hybrid stress element under a certain combination of basic modes α is the transverse modes α_t. Summarizing the arguments for possible kinematic modes is listed in Table 3.1.

Table 3.1 Deformation energy with deformation modes

deformation mode Eq. (3.39)	$\alpha_i \neq 0$	$\alpha_c \neq 0$	$\alpha_t \neq 0$
inplane strain $\mathbf{e}_p$ Eq. (3.2.e)	$\neq 0$	$\neq 0$	$= 0$
transverse strain $\mathbf{e}_t$ Eq. (3.2.f)	$= 0$	$\neq 0$	$\neq 0$
inplane deformation energy U_{d1} Eq. (3.38.c)	$\neq 0$	$\neq 0$	$= 0$
transverse deformation energy U_{d2} Eq. (3.38.d)	$= 0$	may be $= 0$	may be $= 0$
Total deformation energy U_d Eq. (3.38.b)	$\neq 0$	$\neq 0$	may be $= 0$

For a plate element, we let

nj = number of nodes

n1 = number of d.o.f. in displacements u and v per node

n2 = number of d.o.f. in displacement w per node

r1 = number of rigid body modes without the rigid body mode of the inplane shear

r = number of rigid body modes

then

$$\text{dimension of } \alpha_i + \alpha_c = (nj-1)*n1-(r-r1) \qquad (3.42.a)$$

$$\text{dimension of } \alpha_t = nj*n2+n1-r1 \qquad (3.42.b)$$

Therefore the necessary condition for the resulting stiffness matrix to have sufficient rank to suppress the kinematic modes for the present mixed form hybrid stress element is

$$m \geq \text{dimension of } \alpha_t = nj*n2+n1-r1 \qquad (3.43)$$

where

m = number of independent stress parameter β's

For pure transverse deformation modes α_t, the deformation energy, Eq. (3.38.a), becomes

$$2\,U_d = \int_V \mathbf{t}_t^T \mathbf{e}_t \; dV = \beta^T \int_V \mathbf{P}^T (\mathbf{D}_t \mathbf{u}) \; dV \qquad (3.44)$$

Rewriting Eqs. (3.33) and (3.39) into the following form

$$\mathbf{u} = \begin{bmatrix} \mathbf{N}_c^* & \mathbf{N}_\alpha^* \end{bmatrix} \begin{bmatrix} \begin{bmatrix} \alpha_i \\ \alpha_c \\ \mathbf{R} \end{bmatrix} \\ \alpha_t \end{bmatrix} \tag{3.45}$$

where

$\mathbf{N}_c^*$ = functions corresponding to α_i, α_c and $\mathbf{R}$

$\mathbf{N}_\alpha^*$ = functions corresponding to α_t

and substituting Eq. (3.45) into Eq. (3.44), we get

$$2U_d = \beta^T \int_V \mathbf{P}^T (\mathbf{D}_t \mathbf{N}_\alpha^*) \, dV \, \alpha_t = \beta^T \mathbf{G}_\alpha \alpha_t \tag{3.46.a}$$

where

$$\mathbf{G}_\alpha = \int_V \mathbf{P}^T (\mathbf{D}_t \mathbf{N}_\alpha^*) \, dV \tag{3.46.b}$$

The matrix $\mathbf{G}_\alpha$ is rank sufficient when there are no zero columns and no columns of linearly dependency and the deformation energy U_d will not be zero. Therefore, the necessary and sufficient condition for absence of kinematic deformation modes is

Rank of $\mathbf{G}_\alpha$ = dimension of α_t = nj*n2+n1-r1 (3.47)

Continuing our previous example, we look at the 8-node brick element as a 4-node plate element. It has two d.o.f. in w and four d.o.f. in u and v per node. Therefore the minimum number of β's is

$$m \geq nj \times n2 + n1 - r1 = 4 \times 2 + 4 - 5 = 7$$

as it is the dimension of α_t in Eq. (3.41). From Eqs. (3.40) and (3.41), we obtain

$$\mathbf{D}_t \mathbf{N}_\alpha^* \alpha_t = \begin{bmatrix} 1 & 0 & 0 & 0 & \zeta & \xi & \xi\zeta \\ 0 & 1 & 0 & \zeta & 0 & \eta & \eta\zeta \\ 0 & 0 & 1 & \xi & \eta & 0 & \xi\eta \end{bmatrix} \alpha_t \qquad (3.48)$$

In order to satisfy Eq. (3.47), we select the stress parameters in such a way that one β corresponds to each of the strain terms in Eq. (3.48). Two possible assumed stress fields which are satisfied the equilibrium and symmetry conditions are presented in the following

$$\mathbf{P} = \begin{bmatrix} 1 & 0 & 0 & 0 & \zeta & \xi & 0 \\ 0 & 1 & 0 & \zeta & 0 & \eta & 0 \\ 0 & 0 & 1 & 0 & 0 & 0 & \xi\eta \end{bmatrix} \tag{3.49}$$

and

$$\mathbf{P} = \begin{bmatrix} 1 & 0 & 0 & 0 & 0 & \xi & 0 \\ 0 & 1 & 0 & 0 & 0 & \eta & 0 \\ 0 & 0 & 1 & \xi & \eta & 0 & \xi\eta \end{bmatrix} \tag{3.50}$$

Substitute Eq. (3.48) and Eq. (3.49) or (3.50) into Eq. (3.47) and carry out the integration, we get

$$\mathbf{G}_\alpha = \begin{bmatrix} 1 & 0 & 0 & 0 & 0 & 0 & 0 \\ 0 & 1 & 0 & 0 & 0 & 0 & 0 \\ 0 & 0 & 1 & 0 & 0 & 0 & 0 \\ 0 & 0 & 0 & \frac{1}{3} & 0 & 0 & 0 \\ 0 & 0 & 0 & 0 & \frac{1}{3} & 0 & 0 \\ 0 & 0 & 0 & 0 & 0 & \frac{2}{3} & 0 \\ 0 & 0 & 0 & 0 & 0 & 0 & \frac{1}{9} \end{bmatrix} \tag{3.51}$$

We can see that the rank of $\mathbf{G}_\alpha$ is 7. Therefore, there will be no kinematic deformation modes in the resulting element stiffness matrix if either Eq. (3.49) or (3.50) is used.

Huang [99] has constructed an 8-node solid element based on the new formulation but he used 8-β rather than 7-β. They are in the form

$$\mathbf{P} = \begin{bmatrix} 1 & 0 & 0 & 0 & 0 & \xi & -\xi & 0 \\ 0 & 1 & 0 & 0 & 0 & \eta & \eta & 0 \\ 0 & 0 & 1 & \xi & \eta & 0 & 0 & \xi\eta \end{bmatrix} \tag{3.52}$$

Eq. (3.52) can be rewritten in the following uncoupled form

$$\mathbf{P} = \begin{bmatrix} 1 & 0 & 0 & 0 & 0 & \xi & 0 & 0 \\ 0 & 1 & 0 & 0 & 0 & 0 & \eta & 0 \\ 0 & 0 & 1 & \xi & \eta & 0 & 0 & \xi\eta \end{bmatrix} \tag{3.53}$$

If Eq. (3.52) is used, the β_7 is redundant because it does not suppress any kinematic mode. But if Eq. (3.53) is used, neither β_6 nor β_7 can be removed because of symmetry. However, it appears that the 8-β stress assumption of Eq. (3.53) is better than Eq. (3.50) which involves an artificial constraint for coupling σ_{xz} and σ_{yz}.

3.3.4 Shear Locking

In a thin plate limit, a low order C^0 plate element by

assumed displacement method performs excessive rigid in general. It is because the element trends to satisfy the kirchhoff hypothesis of Eq. (1.13) for a thin plate. However, in order to satisfy this no shear stress state, the kinematic deformations of the element are constrained by Eq. (1.13) and these constraint equations often eliminate any possible deformation of a low order element. Therefore, the element performs excessive rigid for a thin plate analysis and it is the so-called 'shear locking' phenomenon. 'Selective reduced integration' scheme has been used to avoid this problem in displacement-based model [100].

This over-stiffening phenomenon can be avoided by using hybrid element with carefully chosen assumed stress terms. A convenient way to examine this behavior is to use the method of constraint counting as originally suggested by Malkus and Hughes [101].

The constraint index (CI) is simply defined as [102]

$$CI = NK - NC \tag{3.54}$$

where

NK = number of kinematic d.o.f. brought in by an element when adding to an existing mesh

NC = number of independent kinematic constraint equation of the element in a thin plate limit

A favorable value for the index, i.e. CI $\geq$ 1, suggests that the plate element is expected to be free from locking and CI $\leq$ 0 indicates that failure will occur in a thin plate analysis. NK is related to the degrees of freedom of the element and NC is related to the number of stress terms used in transverse shears. Using high order element and/or less number of stress parameters in the transverse shear parts are the basic strategies to avoid the locking.

For illustration, we use the previous 8-node brick element as an example here. If Eq. (3.49) with a similar 8-β pattern as in Eq. (3.53) is used, NC = 6. For an 8-node brick element, NK = 6 and therefore the resulting element will have shear locking (CI = NK - NC = 6 - 6 = 0 $\leq$ 1). However, if Eq. (3.53) is used, NC = 4 and the resulting element will not have shear locking (CI = NK - NC = 6 - 4 = 2 $\geq$ 1).

On the other hand, the aim of the present mixed form hybird stress element is to attempt to capture the existence of high transverse stress gradients in such solutions as high interlaminar stresses in the boundary layer around a free edge, in a region under concentration lateral loading or in a thick laminated plate. It is necessary to introduce large number of stress parameters for the present analysis. Therefore the constraint index examination will not be made here in this study.

3.4 Two-Dimensional Element

One type I element of a high order and three different orders of type II element based on the new mixed form formulation are constructed and will be tested at a later section. No type I element based on the conventional approach is constructed because of its poor performance in predicting the local stress distributions [33,103]. A family of type II hybrid elements based on the conventional model are also programed. A comparison of the efficiencies and accuracies of the present mixed form and conventional hybrid stress formulations is then made.

A typical two-dimensional laminated plate element is shown in Figure 3.3. It is a subparametric element in general and its coordinates within the element are given by

$$x(\xi) = \sum_{i=1}^{2} l_i(\xi)\ x_i \qquad (3.55.a)$$

$$z(\zeta) = l_2(\zeta)\ z_1 + l_1(\zeta)\ z_{N+1} \qquad (3.55.b)$$

where

x_i = nodal x coordinate at node i

z_1 = z coordinate of the top surface of laminate

z_{N+1} = z coordinate of the bottom surface of laminate

N = number of layers or sub-elements

$$l_1(\xi) = \frac{1}{2}(1-\xi) \qquad (3.55.c)$$

$$l_2(\xi) = \frac{1}{2}(1+\xi) \qquad (3.55.d)$$

3.4.1 Element Displacement Assumption

The nodal parameters are the displacements u and w along the global Cartesian coordinates x and z. The total number of degrees of freedom in individual element or sub-element depends on the order of displacement function in ζ.

3.4.1.1 Type I Element

In type I element, the u displacement distribution along the thickness direction is assumed to be a cubic function in ζ across the whole laminate. It is interpolated in terms of the nodal displacements u at the top, bottom, and 1/3 points of the laminate as shown in Figure 3.4. The displacement w is assumed to be quadratic and expressed in terms of nodal displacements at the top, middle and bottom of the laminate. The displacement distribution between two node-lines is assumed to be linear.

This assumption of displacements u and w is analogous to that of the high order plate theory by Lo, Christensen and Wu [13,14]. The displacement w is assumed to be one order less in ζ than the assumption of displacement w. It is consistent in the sense that the transverse shear strains due to the inplane displacements u and v are of the same order as those due to the transverse displacement w.

The displacement interpolations are as follows:

$$u(\xi,\zeta) = \sum_{i=1}^{2} \sum_{j=1}^{4} l_i(\xi)\, f_j(\zeta)\, u_{ij} \qquad (3.56.a)$$

$$w(\xi,\zeta) = \sum_{i=1}^{2} \sum_{j=1}^{3} l_i(\xi)\, g_j(\zeta)\, w_{ij} \qquad (3.56.b)$$

where

u_{ij} = j^{th} nodal u displacement at node i

w_{ij} = j^{th} nodal w displacement at node i

$$f_1(\zeta) = \frac{1}{16}(-1-\zeta+9\zeta^2+9\zeta^3)$$

$$f_2(\zeta) = \frac{1}{16}(9+27\zeta-9\zeta^2-27\zeta^3)$$

$$f_3(\zeta) = \frac{1}{16}(9-27\zeta-9\zeta^2+27\zeta^3)$$

$$f_4(\zeta) = \frac{1}{16}(-1+\zeta+9\zeta^2-9\zeta^3) \qquad (3.56.c\text{-}i)$$

$$g_1(\zeta) = \frac{1}{2}\zeta(1+\zeta)$$

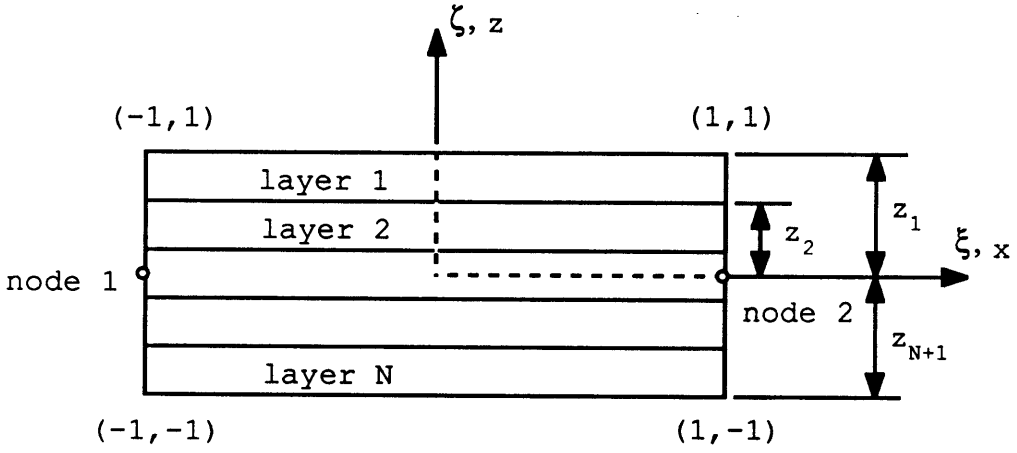

Figure 3.3 Two-dimensional laminated plate element

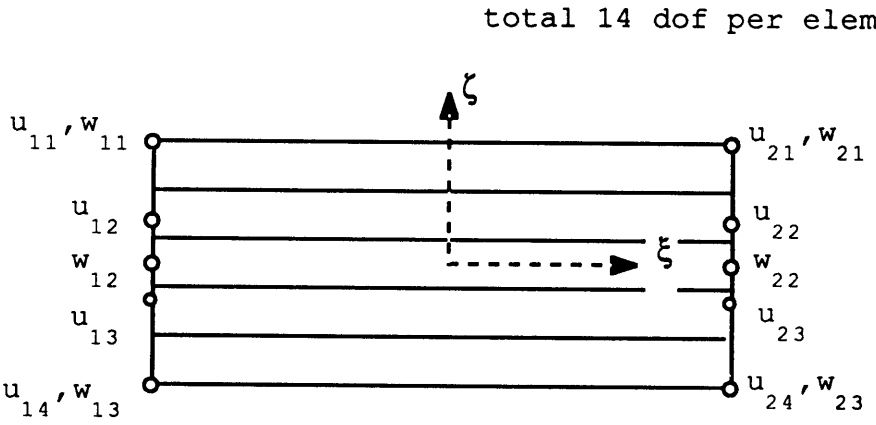

Figure 3.4 Element degrees of freedom for a type I two-dimensional element

$$g_2(\zeta) = (1-\zeta^2)$$

$$g_3(\zeta) = \frac{1}{2}\zeta(-1+\zeta)$$

and $l_1(\zeta)$ and $l_2(\zeta)$ are given by Eqs. (3.55.c-d)

This form of high order displacement distribution is used in the single-layer conventional hybrid stress thick plate element [104] and in the displacement-based model of a symmetrical laminated plate element [30].

3.4.1.2 Type II Element

The nodes and nodal displacements of three sub-elements of different order are shown in Figure 3.5. The displacements are again all assumed to be linear between two node-lines but with different order of ζ_i. These elements are either based on the conventional or the mixed form hybrid stress model.

The one shown in Figure 3.5(a) is of the lowest order and designated as ity=1. The displacements u and w are assumed to vary linearly through the thickness of sub-element and are expressed in terms of the nodal displacements at the top and bottom boundaries. They are written as

$$u^i(\xi,\zeta_i) = \sum_{k=1}^{2}\sum_{j=1}^{2} l_k(\xi)\, l_j(-\zeta_i)\, u^i_{kj} \qquad (3.57.a)$$

$$w^i(\xi,\zeta_i) = \sum_{k=1}^{2}\sum_{j=1}^{2} l_k(\xi)\ l_j(-\zeta_i)\ w^i_{kj} \qquad (3.57.b)$$

where

u^i_{kj} = j^{th} nodal u displacement at node k in sub-element i

w^i_{kj} = j^{th} nodal w displacement at node k in sub-element i

and $l_1(\zeta)$ and $l_2(\zeta)$ are given by Eqs. (3.55.c-d)

Many laminated plate elements which involve this kind of linear displacement behavior in each sub-element have been developed based on the displacement-based model [37-40] and on the conventional hybrid stress model [41,43-45]. The effective stiffness plate theory by Sun and Whitney [21] is also based on this kind of linear displacement assumptions in each lamina.

The second element designated as ity=2 has displacement u to be of order $(\zeta_i)^2$ and expressed in terms of nodal displacements u at the top, middle and bottom of the sub-element (Figure 3.5.b). The displacement w is assumed to be linear in ζ_i and is expressed in terms of nodal displacements at the top and bottom boundaries. They are described as

$$u^i(\xi,\zeta_i) = \sum_{k=1}^{2}\sum_{j=1}^{3} l_k(\xi)\ g_j(\zeta_i)\ u^i_{kj} \qquad (3.58)$$

and $w^i(\xi,\zeta_i)$ is given by Eq. (3.57.b)

This displacement assumption was used by Whitney and Sun [10] in the high order theory for the whole laminated plate.

The last element defined as ity=3 has the highest order of displacement assumption (Figure 3.5.c). Its displacement u is assumed to be of order $(\zeta_i)^3$ and w to be of order $(\zeta_i)^2$. They are identical to the previous type I element and can be expressed as

$$u^i(\xi,\zeta_i) = \sum_{k=1}^{2} \sum_{j=1}^{4} l_k(\xi)\, f_j(\zeta_i)\, u^i_{kj} \qquad (3.59.a)$$

$$w^i(\xi,\zeta_i) = \sum_{k=1}^{2} \sum_{j=1}^{3} l_k(\xi)\, g_j(\zeta_i)\, w^i_{kj} \qquad (3.59.b)$$

This form of high order displacement assumption is also been used in a multilayer hybrid stress thick plate element based on the conventional approach by Spilker [42].

3.4.2 Stress Field Assumption

As previous discussion, the assumed stresses are first approximated in terms of natural coordinates and then transformed into the physical coordinates by applying the coordinate transformation law, Eq. (3.29) or (3.30). Because

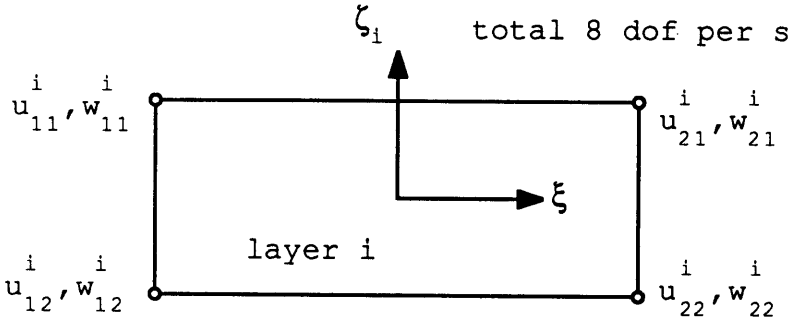

(a) element degrees of freedom for ity=1 sub-element

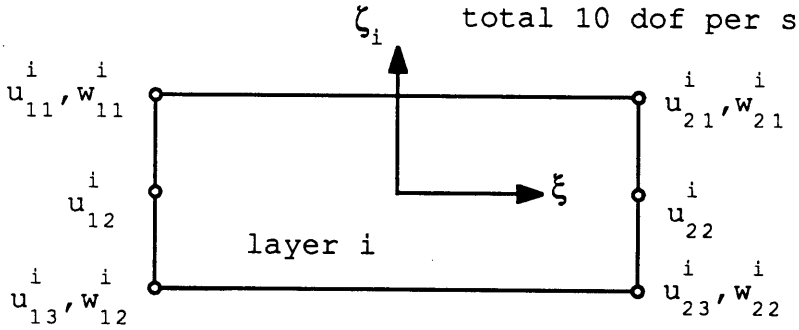

(b) element degrees of freedom for ity=2 sub-element

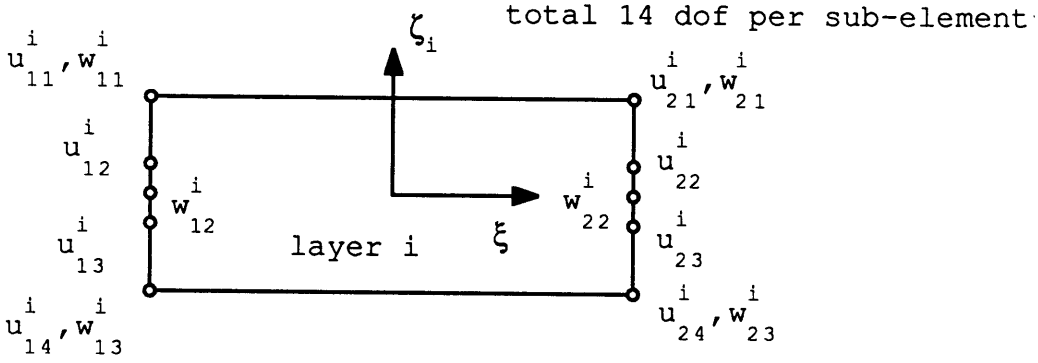

(c) element degrees of freedom for ity=3 sub-element

Figure 3.5 Element degrees of freedom for type II two-dimensional sublayer element

only the two-dimensional rectangular elements are constructed in this study, the assumed stress field is satisfied the equilibrium equations exactly. All kinematic deformation modes are also suppressed.

3.4.2.1 Type I Element

There are three d.o.f. in displacement w and four d.o.f. in displacement u per node-line. With two node-lines in a element, the minimum number of stress parameters m given by Eq. (3.43) is 2 x 3 + 4 - 3 = 7. The two transverse stresses in the present model are assumed as follows

$$\begin{bmatrix}\tau^{13}\\ \tau^{33}\end{bmatrix}=\begin{bmatrix} d_1 & d_1\xi & d_1\xi^2 & d_2 & d_2\xi & d_2\xi^2 & d_3 & d_3\xi & d_3\xi^2 \\ 0 & d_4 & 2d_4\xi & 0 & d_5 & 2d_5\xi & 0 & d_6 & 2d_6\xi \end{bmatrix}\beta \qquad (3.60.a)$$

$$\beta=\begin{bmatrix}\beta_1 & \beta_2 & \beta_3 & \beta_4 & \beta_5 & \beta_6 & \beta_7 & \beta_8 & \beta_9\end{bmatrix}^T \qquad (3.60.b)$$

where

$$d_1(\zeta) = (1 - \zeta^2)$$
$$d_2(\zeta) = \zeta\,(1 - \zeta^2)$$
$$d_3(\zeta) = \zeta^2\,(1 - \zeta^2) \qquad (3.60.c\text{-}h)$$
$$d_4(\zeta) = (\zeta^3 - 3\zeta - 2)/3$$
$$d_5(\zeta) = (\zeta^4 - 2\zeta^2 + 1)/4$$
$$d_6(\zeta) = (3\zeta^5 - 5\zeta^3 - 2)/15$$

Following the procedure in section 3.3.3 for examining the 8-node brick element, one can show that with the first seven β's, the resulting $\mathbf{G}_\alpha$ is rank sufficient. Therefore, there will be no kinematic modes in the resulting element stiffness matrix if at least the first seven stress parameters are used.

The physical stresses in the global Cartesian coordinates are

$$\tau_{xz} = \sigma^{13} = a_1 \tau^{13}$$
$$\sigma_z = \sigma^{33} = c_1 \tau^{33} \qquad (3.61)$$

where

$$a_1 = (x_2 - x_1)/2$$
$$c_1 = (z_{N+1} - z_1)/2$$

and they also satisfy the traction free condition

$$\tau_{xz} = 0 \quad \text{at the top surface}$$
$$\tau_{xz} = \sigma_z = 0 \quad \text{at the bottom surface} \qquad (3.62)$$

3.4.2.2 Type II Element

We begin by assuming the transverse shear stress τ^{13} to be of order $(\zeta_i)^3$ and ξ^2. The remaining stress components are chosen to satisfy the equilibrium equations. Thus, it is

suggested that the transverse normal stress τ^{33} be of order $(\zeta_i)^4$ and ξ and the inplane normal stress τ^{11} be of order $(\zeta_i)^2$ and ξ^3 and a total of 17 stress parameters are used.

In order to enforce the stress continuity and traction free conditions easily, the stress field is rewritten into the form of Eq. (3.23) and can be expressed as

$$\begin{bmatrix} \tau^{11} \\ \tau^{13} \\ \tau^{33} \end{bmatrix}^i = \begin{bmatrix} -\frac{1}{2}\xi & \frac{1}{2}\xi & 2\xi\zeta_i & 1 & \zeta_i & -\frac{3}{4}\xi^2\zeta_i & \frac{3}{4}\xi^2\zeta_i & -\frac{1}{4}s_{10}\xi^2 & \frac{1}{4}s_{11}\xi^2 \\ s_1 & s_2 & s_3 & 0 & 0 & -\frac{3}{4}s_3\xi & \frac{3}{4}s_3\xi & s_{13}\xi & s_{23}\xi \\ 0 & 0 & 0 & 0 & 0 & s_4 & s_5 & s_6 & s_7 \end{bmatrix}$$

$$\begin{bmatrix} -\frac{1}{2}\xi^3\zeta_i & \frac{1}{2}\xi^2\zeta_i & -\frac{1}{6}s_{10}\xi^3 & \frac{1}{6}s_{10}\xi^3 & s_{12}\xi & \zeta_i^2 & \frac{1}{2}s_{12}\xi^2 & \frac{1}{3}s_{12}\xi^3 \\ -\frac{3}{4}s_3\xi^2 & \frac{3}{4}s_3\xi^2 & s_{13}\xi^2 & s_{23}\xi^2 & s_8 & 0 & s_8\xi & s_8\xi^2 \\ 2s_4\xi & 2s_5\xi & 2s_6\xi & 2s_7\xi & 0 & 0 & s_9 & s_9\xi \end{bmatrix}^i \beta^i \qquad (3.63.a)$$

$$\beta^i = \begin{bmatrix} \beta_1^i & \beta_2^i & \beta_3^i & \cdots\cdots\cdots\cdots & \beta_{17}^i \end{bmatrix}^T \qquad (3.63.b)$$

where

$$s_1(\zeta_i) = (1 + \zeta_i)/2$$

$$s_2(\zeta_i) = (1 - \zeta_i)/2$$

$$s_3(\zeta_i) = (1 - \zeta_i^2)$$

$$s_{13}(\zeta_i) = s_1(\zeta_i) - 0.75 \times s_3(\zeta_i)$$

$$s_{23}(\zeta_i) = s_2(\zeta_i) - 0.75 \times s_3(\zeta_i)$$

$$
\begin{aligned}
s_4(\zeta_i) &= (1 + \zeta_i)^2 (2 - \zeta_i)/4 \\
s_5(\zeta_i) &= (1 - \zeta_i)^2 (2 + \zeta_i)/4 \\
s_6(\zeta_i) &= (1 + \zeta_i)^2 (1 - \zeta_i)/4 \\
s_7(\zeta_i) &= -(1 + \zeta_i) (1 - \zeta_i)^2/4 \\
s_8(\zeta_i) &= \zeta_i (1 - \zeta_i^2) \\
s_9(\zeta_i) &= (1 - \zeta_i^2)^2/4 \\
s_{10}(\zeta_i) &= (1 + 3\zeta_i) \\
s_{11}(\zeta_i) &= (1 - 3\zeta_i) \\
s_{12}(\zeta_i) &= (3\zeta_i^2 - 1)
\end{aligned}
\qquad (3.63.c\text{-}p)
$$

For the conventional hybrid stress element, all three stresses are required and for the new mixed form hybrid stress element, only the two transverse stresses are needed.

The minimum number of stress parameters m depends on how many and which kinds of sub-element are used through the thickness direction. It can be determined with the help of Eq. (3.31) or (3.42) after the element layup is decided. Eq. (3.36) or (3.47) should be satisfied in any combination of stress parameters to ensure the reliability of the new super-element. In general, the minimum of stress parameters m cannot be achieved if other considerations are met such as the symmetry condition of the assumed stress field.

The physical stress components in Cartesian coordinates can be obtained by applying Eqs. (3.29) or (3.30). One additional coordinate transformation is required, because the local sub-

element natural coordinates are used. It can be achieved by the change of variable which is given by Eqs. (3.28).

3.4.3 Numerical Examples

To assess the accuracy of the present mixed form hybrid stress element and compare the computational effort and performance with the conventional hybrid stress element, cylindrical bending of a semi-infinite strip has been chosen. The same problem with a two-layer laminate is also studied by the three different orders of type II element based on the new mixed form model. One additional test on the type II ity=3 elements based on the conventional and new mixed form formulations for the free-edge problem will be presented in the later chapter.

The following labels are used for the elements used in the present comparisons:

Hybrid(con) = present mixed form type I hybrid stress element with 7 β's

Hybrid(disc) = present mixed form type II ity=1 hybrid stress element as sub-element

Hybrid(old) = conventional type II ity=1 hybrid stress element as sub-element

Hybrid(ity=1) = present mixed form type II ity=1 hybrid stress element as sub-element for a two-layer laminate

Hybrid(ity=2) = present mixed form type II ity=2 hybrid stress element as sub-element for a two-layer laminate

Hybrid(ity=3) = present mixed form type II ity=3 hybrid stress element as sub-element for a two-layer laminate

3.4.3.1 Cylindrical Bending of a Simply Supported Long Strip

The laminated plate considered herein consists of layers of unidirectional fibrous composite material. The laminate is infinite long in the y direction and simply supported along the two edges. Sinusoidally distributed transverse loading $q_0 \sin(\pi x/L)$ with $q_0=1$ is applied at the top surface of the laminate as shown in Figure 3.6(a). Because of the nature of the problem, the plate is modeled as a plane strain problem in the x-z plane. Finite element analysis is carried out over the left half plane which is subdivided into 10 equal elements as shown in Figure 3.6(b).

Three different thick laminate configurations are considered:

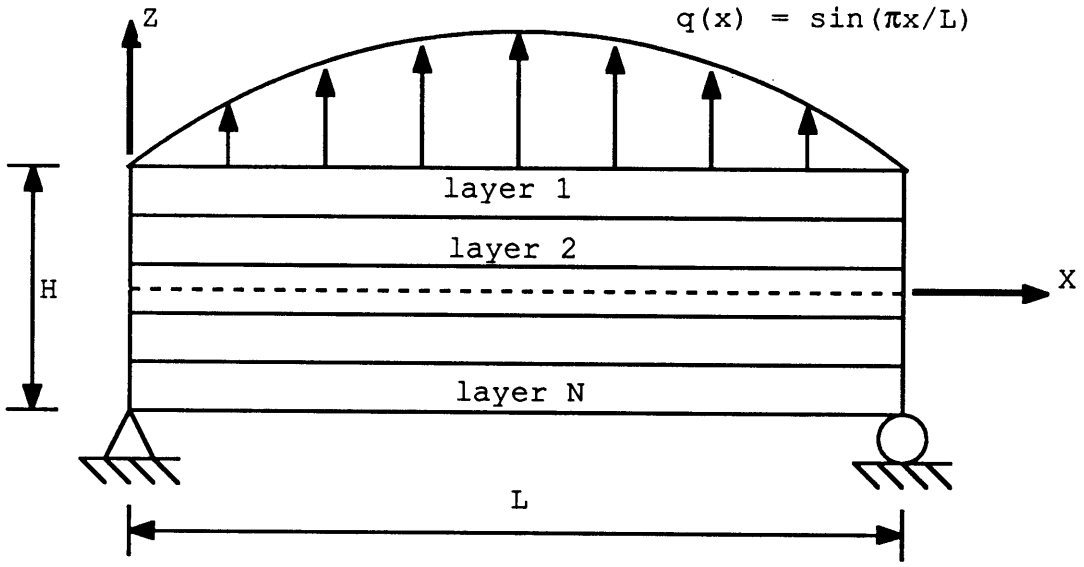

(a) plane of analysis (side view)

$E_L = 25 \times 10^6$ psi

$E_T = 10^6$ psi

$G_{LT} = 0.5 \times 10^6$ psi

$G_{ZT} = 0.2 \times 10^6$ psi

$\nu_{LT} = \nu_{ZT} = 0.25$

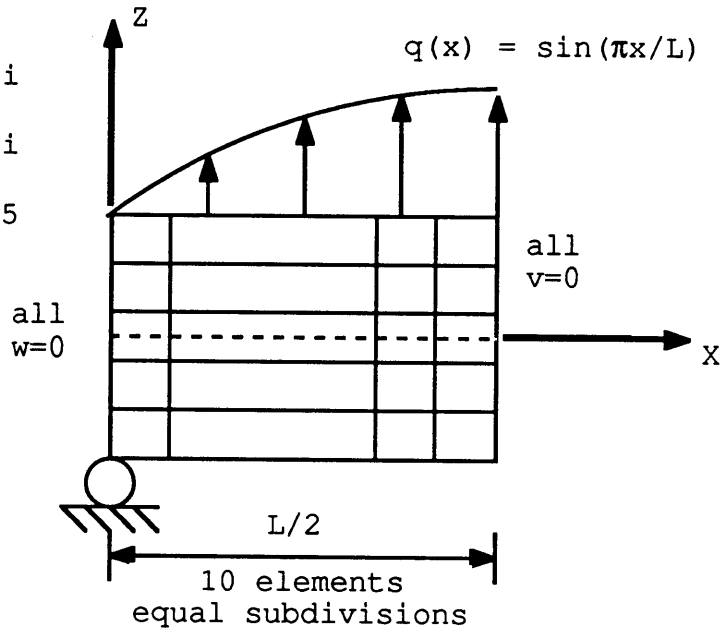

(b) finite element mesh and property definition

Figure 3.6 Problem description and finite element model for a semi-infinite cross-ply lmainated plate subjected to cylindrical bending (L/H=4)

(1) a twenty-layer cross ply laminate $[90/0]_{10T}$ with layers of equal thickness.

(2) a two-layer cross ply laminate $[90/0]_{T}$ with layers of equal thickness.

(3) a three-layer cross ply laminate $[0/90/0]_{T}$ with layers of equal thickness.

The angle is measured with respect to the x-axis (i.e. 0 degree implies fibers are parallel to the axis x). The elasticity solutions for this plane-strain problem have been determined using the method given by Pagano [105]. The results based on classical lamination plate theory (CPT), which is independent of the span-to-thickness ratio, are also presented in Case 2 and 3.

In all the problems, the material properties for each lamina are shown in Figure 3.6(b) and span-to-thickness ratio (L/H) is four. The numerical results are presented in terms of normalized values which are defined as

$$\begin{aligned}
\bar{\sigma}_x &= \sigma_x(L/2, z/H)/q_0 \\
\bar{\sigma}_z &= \sigma_z(L/2, z/H)/q_0 \\
\bar{\tau}_{xz} &= \tau_{xz}(0, z/H)/q_0 \\
\bar{u} &= \frac{E_T}{H\ q_0}\ u\ (0, z/H)
\end{aligned} \tag{3.64}$$

Because of the large number of laminae in case 1, it is computationally inefficient to use any type II element. Therefore, only the Hybrid(con) element is tested. The results for twenty-layer, H/L=4, are in excellent agreement with the elasticity solutions for inplane displacement u, inplane normal stress σ_x and transverse normal stress σ_z as shown in Figures 3.7(a,b,d). The transverse shear τ_{xz} appears to be of less accuracy compared with the other stress components (Figure 3.7.c). However, the maximum values in all those stresses and displacement are in very good agreement with elasticity solutions.

For case 2 and 3, each layer is modeled by one sub-element. The numbers of stress parameters used for each layer are the first eleven β's of Eq. (3.63.a) for Hybrid(old) element and the first nine non-zero β's in the last two rows for Hybrid(disc) element. After enforcing the traction free condition at the top and bottom surfaces of the laminate and stress continuity at the interlayer boundaries, the actual numbers of stress parameters being used for the two-layer and three-layer models are listed in the following table

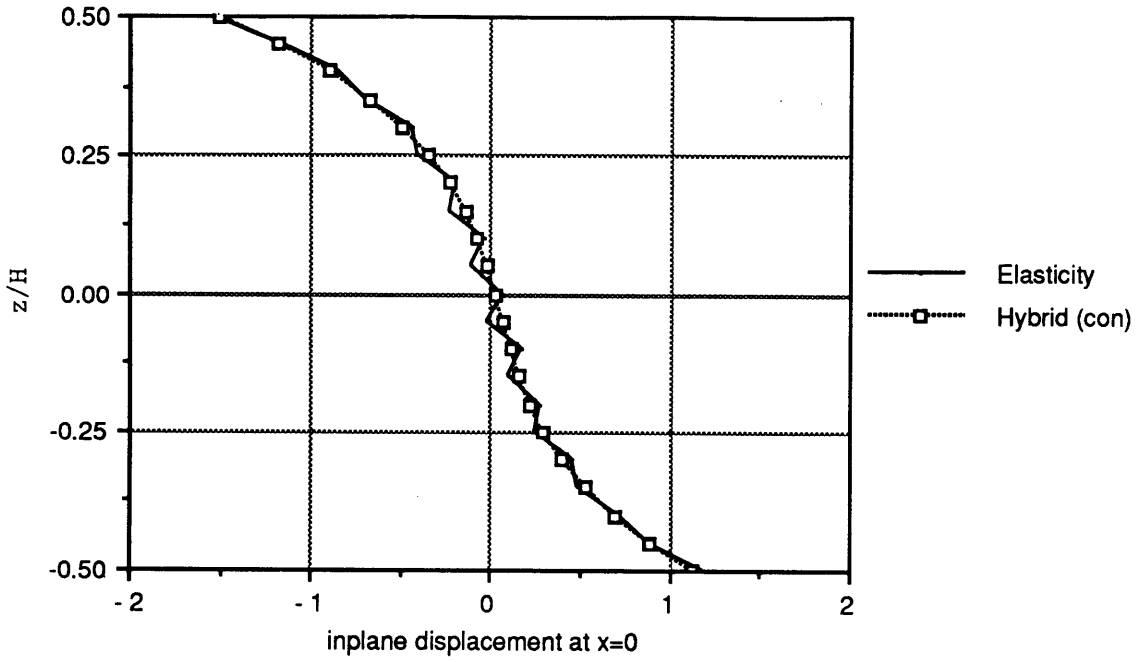

(a) inplane displacement $\bar{u}$ (0, z/H)

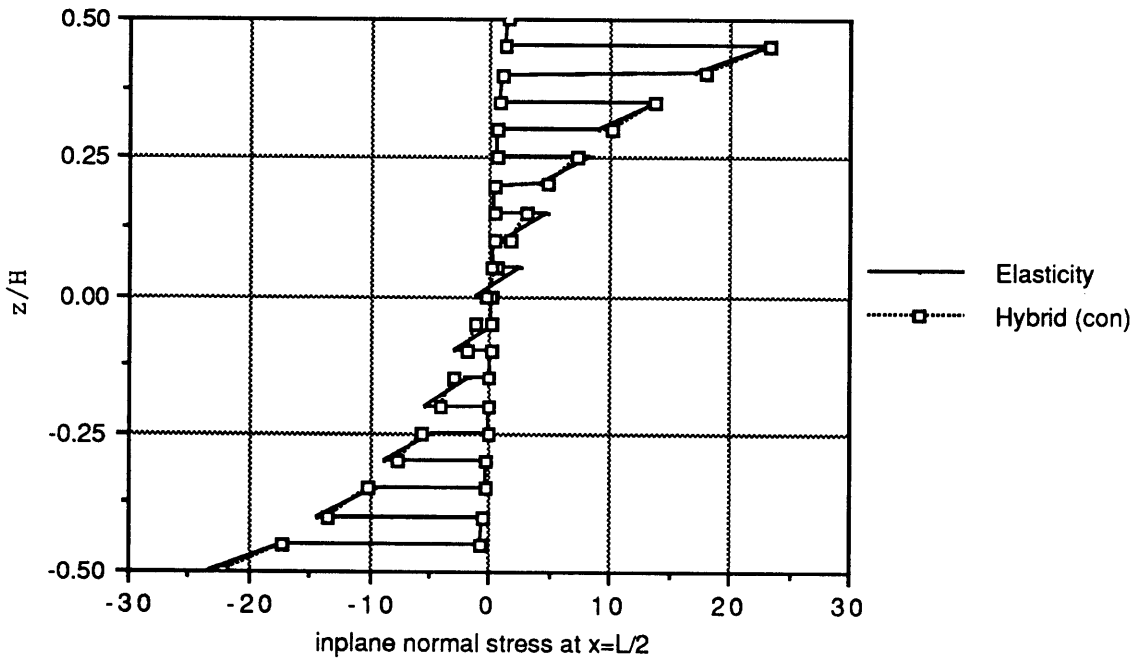

(b) inplane normal stress $\bar{\sigma}_x$ (L/2, z/H)

Figure 3.7 Solutions for a 20-layer $[90/0]_{10T}$ laminate at L/H=4

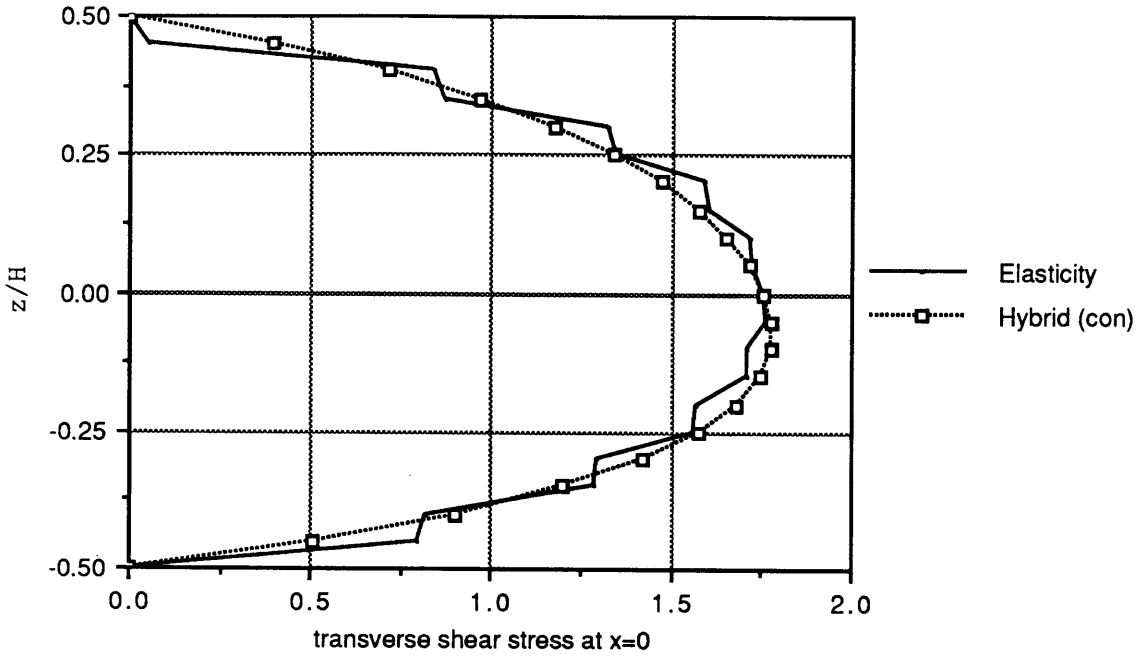

(c) transverse shear stress $\bar{\tau}_{xz}$ (0, z/H)

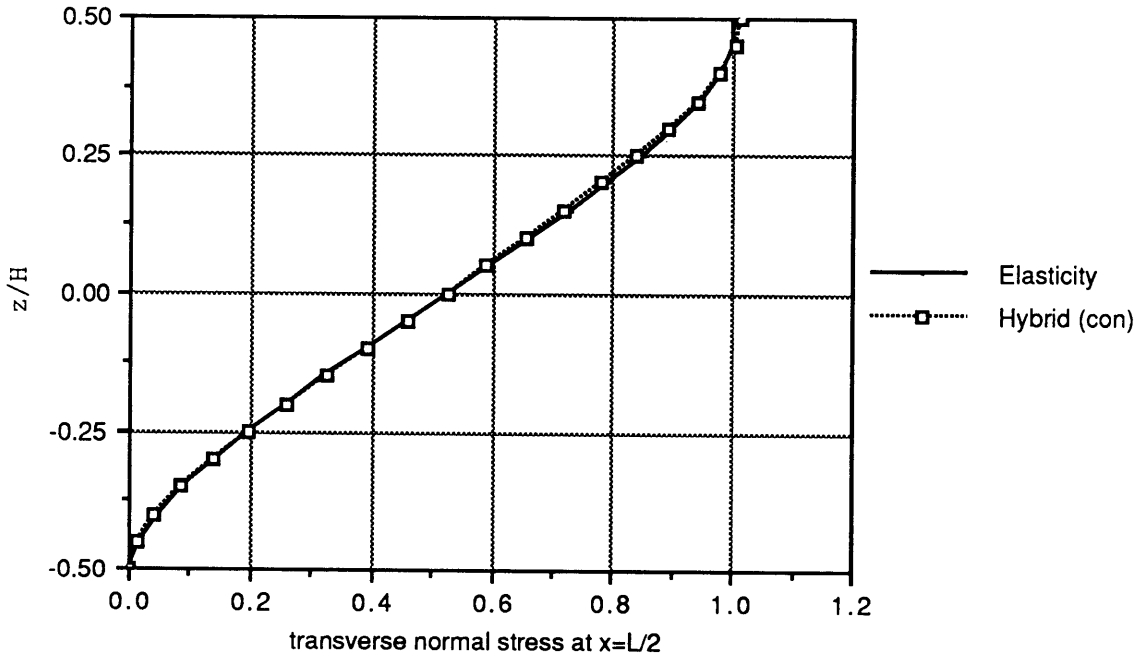

(d) transverse normal stress $\bar{\sigma}_z$ (L/2, z/H)

Figure 3.7 Solutions for a 20-layer $[90/0]_{10T}$ laminate at L/H=4

Table 3.2 Number of β's used in the 2D model

Element type	Case 2	Case 3
Hybrid(disc)	8 (6)*	13 (9)
Hybrid(old)	12 (9)	19 (13)

* the number in the parenthesis is the minimum number of β's needed to suppress the kinematic modes

Results obtained for case 2 and 3 are shown in Figures 3.8 and 3.9, respectively. It is seen that there is no significant cross section warping in case 2 and the CPT solutions are in good agreement with the elasticity solutions for case 2. This is not so in case 3.

Results obtained by the Hybrid(disc) and Hybrid(old) elements are indistinguishable for both cases. The inplane displacement u, inplane normal stress σ_x and transverse normal stress σ_z are all in very good agreement with the elasticity solutions. The transverse shear τ_{xz} is in reasonable agreement, although in both cases the interlaminar shear stresses are slightly underestimated at the interfaces of the laminates. The inplane displacement u, given in Figure 3.9(a), indicates the severe cross-sectional warping for case 3.

Results obtained by the Hybrid(con) element are also presented in Figures 3.8 and 3.9 for both cases. Because of the smoothness of the stress assumptions, the transverse shear stress at the laminate interfaces are slightly overestimated.

For constructing one element stiffness matrix, the Hybrid(disc) element requires approximately twenty-five percent less computational effort than the Hybrid(old) element for the two-layer model and approximately thirty-five percent less for the three-layer model. On the other hand, the construction of the Hybrid(disc) element requires approximately the same effort as that of the Hybrid(con) element for the three-layer model and approximately twenty-five percent less for the two-layer model. We can see that the new mixed form hybrid stress element is computationally efficient compared with the conventional hybrid stress element and the type I element for the new mixed form model becomes very efficient when the number of layer is larger than three.

3.4.3.2 Cylindrical Bending of a Two-layer Laminate

In order to compare the performances of the three different orders of type II element based on the new mixed form model, the elements, denoted as Hybrid(ity=1), Hybrid(ity=2) and Hybrid(ity=3) elements, are used to re-examine the case 2 of the

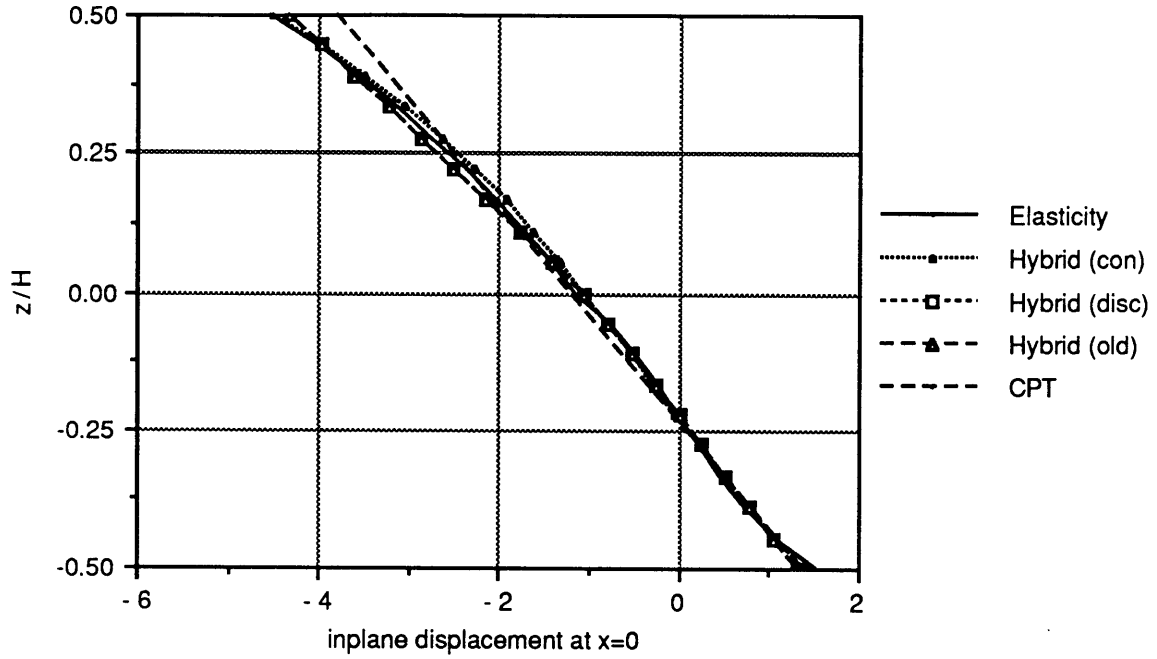

(a) inplane displacement $\bar{u}$ (0,z/H)

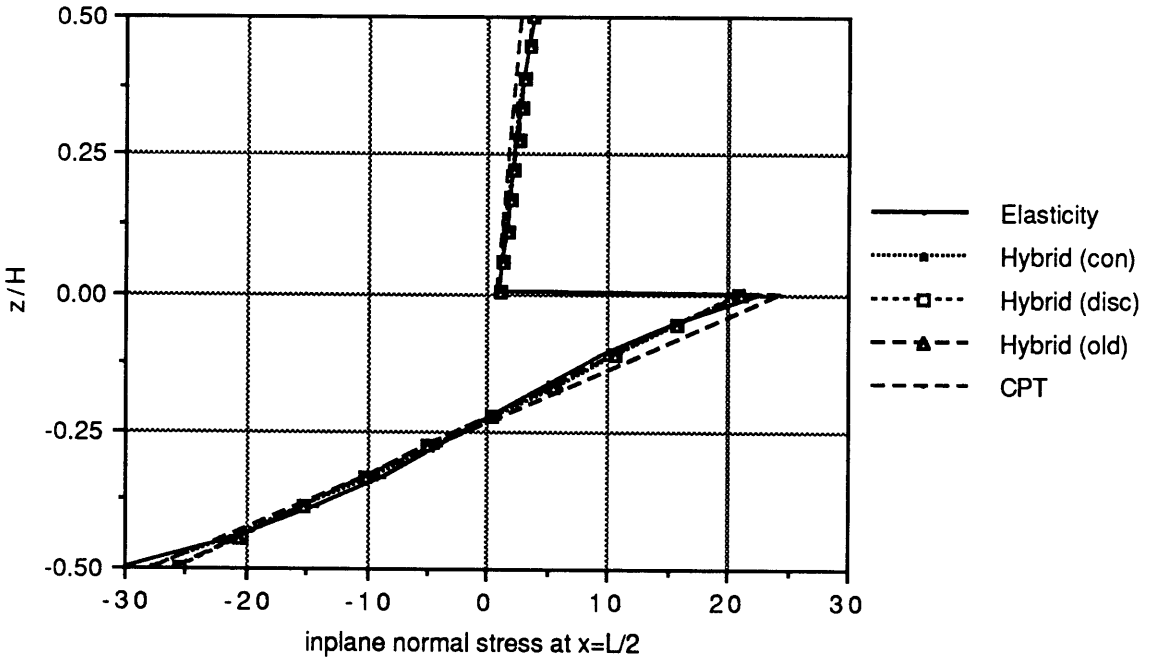

(b) inplane normal stress $\bar{\sigma}_x$ (L/2,z/H)

Figure 3.8 Solutions for a 2-layer $[90/0]_T$ laminate at L/H=4

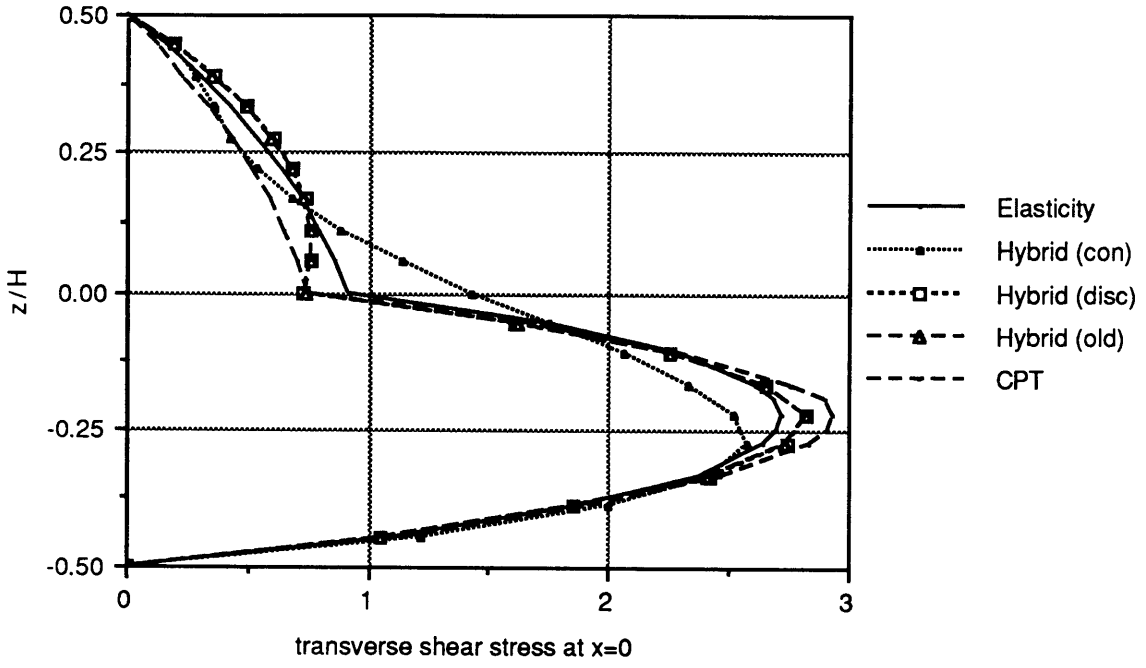

(c) transverse shear stress $\bar{\tau}_{xz}$ (0, z/H)

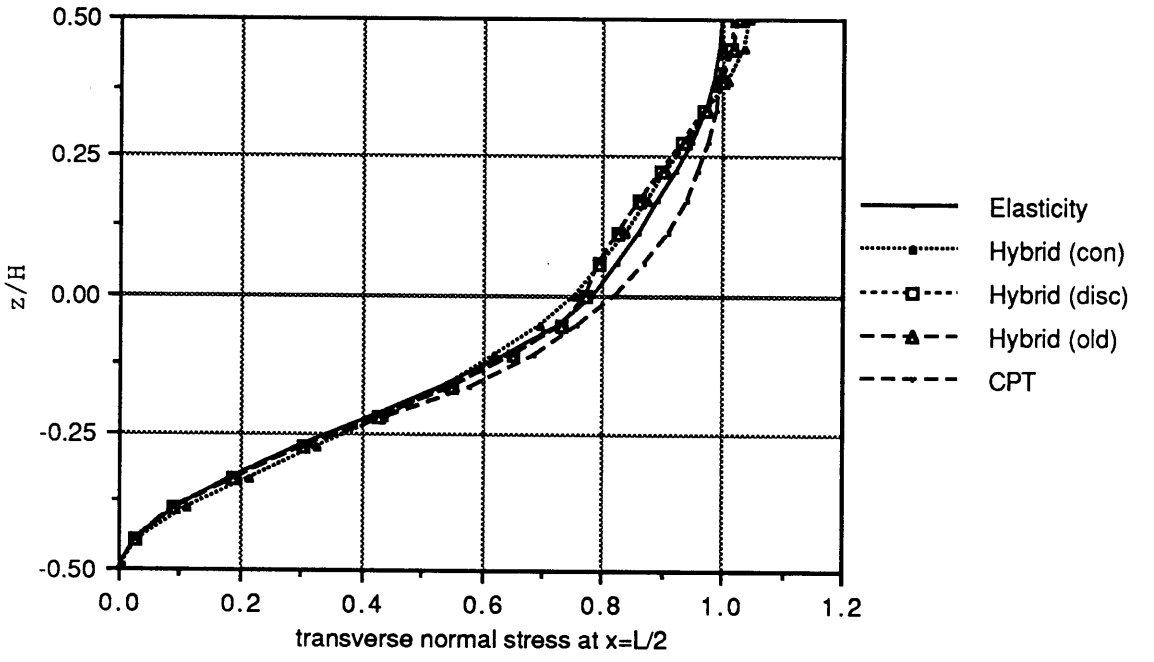

(d) transverse normal stress $\bar{\sigma}_z$ (L/2, z/H)

Figure 3.8 Solutions for a 2-layer $[90/0]_T$ laminate at L/H=4

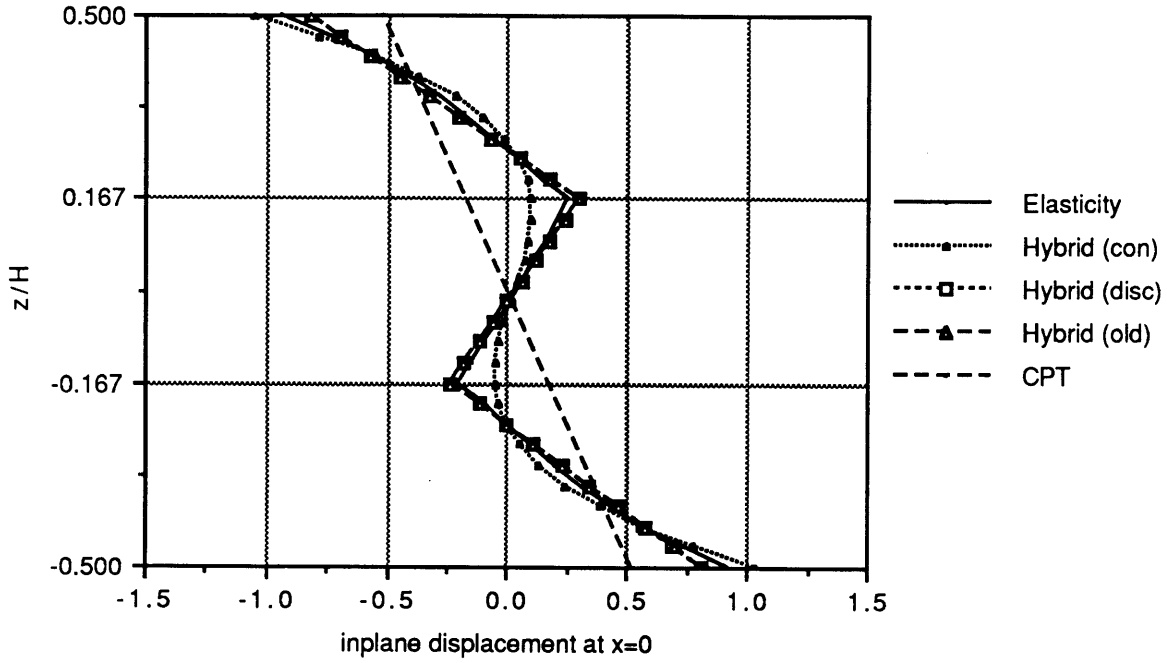

(a) inplane displacement $\bar{u}$ (0,z/H)

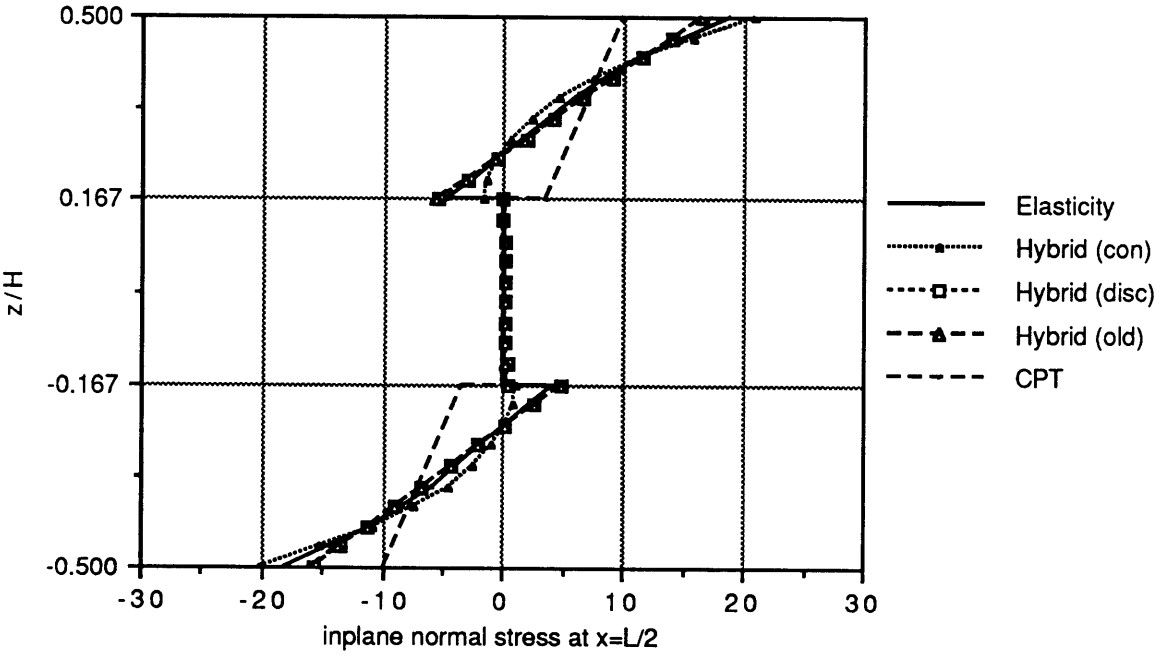

(b) inplane normal stress $\bar{\sigma}_x$ (L/2,z/H)

Figure 3.9 Solutions for a 3-layer $[0/90/0]_T$ laminate at L/H=4

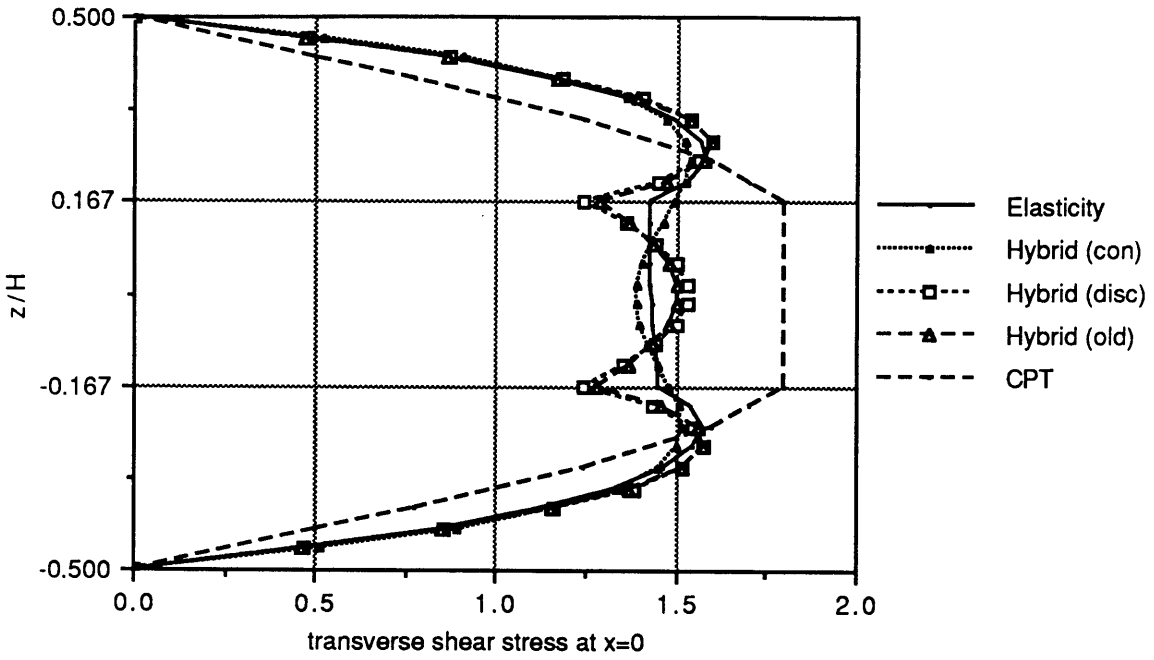

(c) transverse shear stress $\bar{\tau}_{xz}$ (0, z/H)

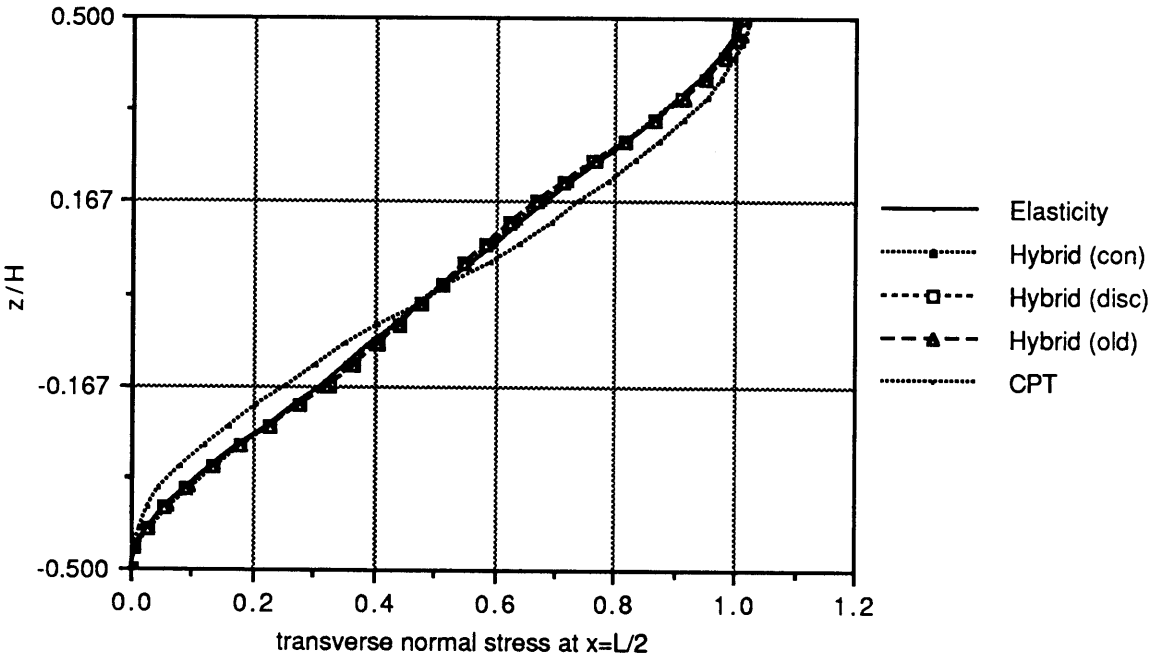

(d) transverse normal stress $\bar{\sigma}_z$ (L/2, z/H)

Figure 3.9 Solutions for a 3-layer $[0/90/0]_T$ laminate at L/H=4

previous example. A five-element mesh is adopted rather than a ten-element mesh as previously used.

Each layer is modeled by one sub-element. The numbers of stress parameters used for each layer are the first nine non-zero β's in the last two rows of Eq. (3.63.a) for Hybrid(ity=1) element and first twelve non-zero β's for Hybrid(ity=2) element. For Hybrid(ity=3) element, it is the all fourteen non-zero β's in the last two rows of Eq. (3.63.a) and one additional term in order to suppress the kinematic modes. It is

$$\begin{bmatrix} \tau^{13} \\ \tau^{33} \end{bmatrix}^i = \begin{bmatrix} \zeta_i^2 (1 - \zeta_i^2) \\ 0 \end{bmatrix}^i \beta_{15}^i$$

After enforcing the stress continuity and traction free conditions, the actual numbers of stress parameters used are 8, 11 and 17 for Hybrid(ity=1), Hybrid(ity=2) and Hybrid(ity=3) elements for a two-layer model, respectively. They are summarized in the Table 3.3.

In order to determine the optimal stress pattern, one additional Hybrid(ity=1) element with a larger number of β's is studied. In this element combination, the first eleven non-zero β's in the last two rows of Eq. (3.63.a) for each layer and a total of 13 β's are used for the two-layer model.

Table 3.3 Number of β's used in the 2D two-layer model

Element	(ity=1)	(ity=2)	(ity=3)
Number of β's for each layer	9	12	15
Actual number of β's for the two-layer model	8	11	17
Minimum number of β's to suppress the kinematic modes	6	8	14

Results obtained for all cases are shown in Figure 3.10. They are presented in normalized quantities which are given by Eqs. (3.64). For all cases, the inplane normal stress σ_x results are indistinguishable and in very good agreement with the elasticity solution. All the results for the transverse normal stress σ_z are in very good agreement with the exact solutions for the lower lamina region and in reasonable agreement for the upper region (Figure 3.10-c).

Results in the transverse shear stress τ_{xz} are very different from one another. The Hybrid(ity=3) element result is superior to those obtained by the others and in excellent agreement with the elasticity solution as predicted. The Hybrid(ity=2) element result is similar to the one obtained by the Hybrid(con) element with ten-element mesh (Figures 3.8-c and 3.10-c) but it is not better than the one obtained by the lower

order Hybrid(ity=1) element. As we mentioned before, oscillation of stress results may occur if overuse of stress parameters. It is clear that this happens while we are only increasing the number of β's but without increasing the d.o.f. of Hybrid(ity=1) element.

The computational effort compared with the Hybrid(ity=1) element mesh, for the Hybrid(ity=3) element case requires 120% more than that for the Hybrid(ity=1) case and the Hybrid(ity=2) element case requires thirty percent more.

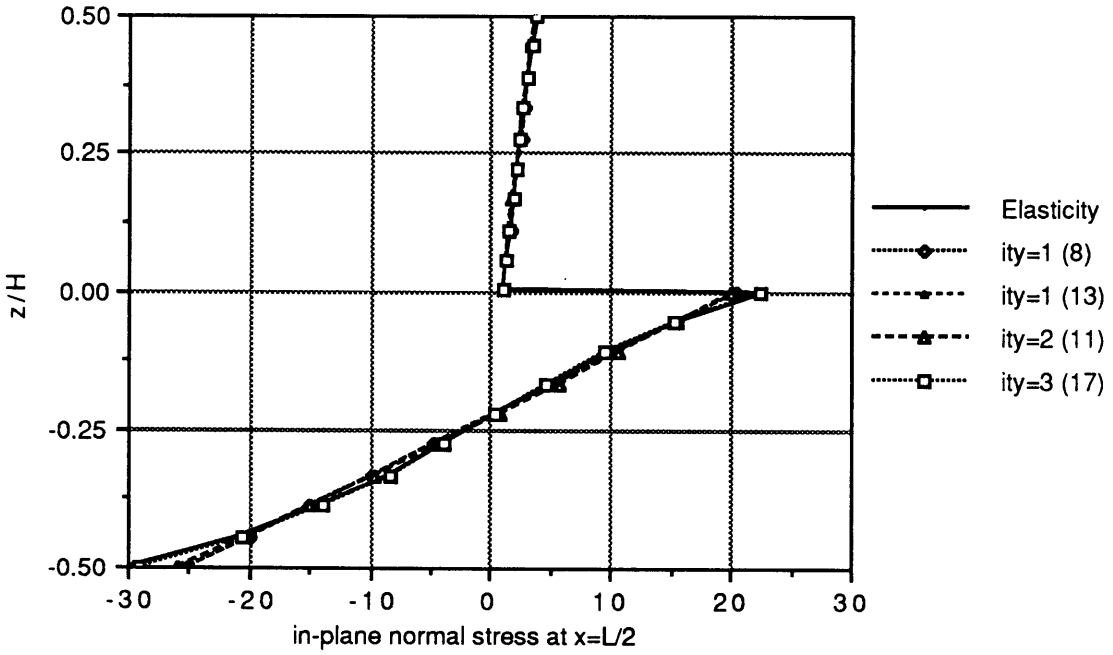

(a) inplane normal stress $\bar{\sigma}_x$ (L/2, z/H)

Figure 3.10 Solutions for a 2-layer $[90/0]_T$ laminate at L/H=4 with three different orders of type II element

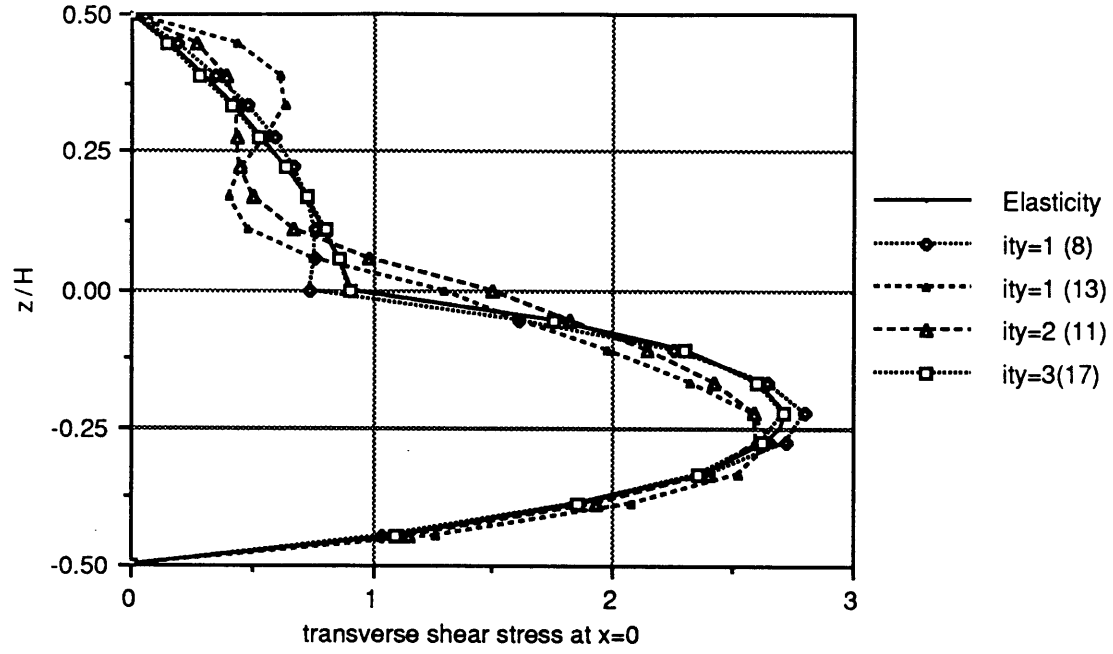

(b) transverse shear stress $\bar{\tau}_{xz}(0, z/H)$

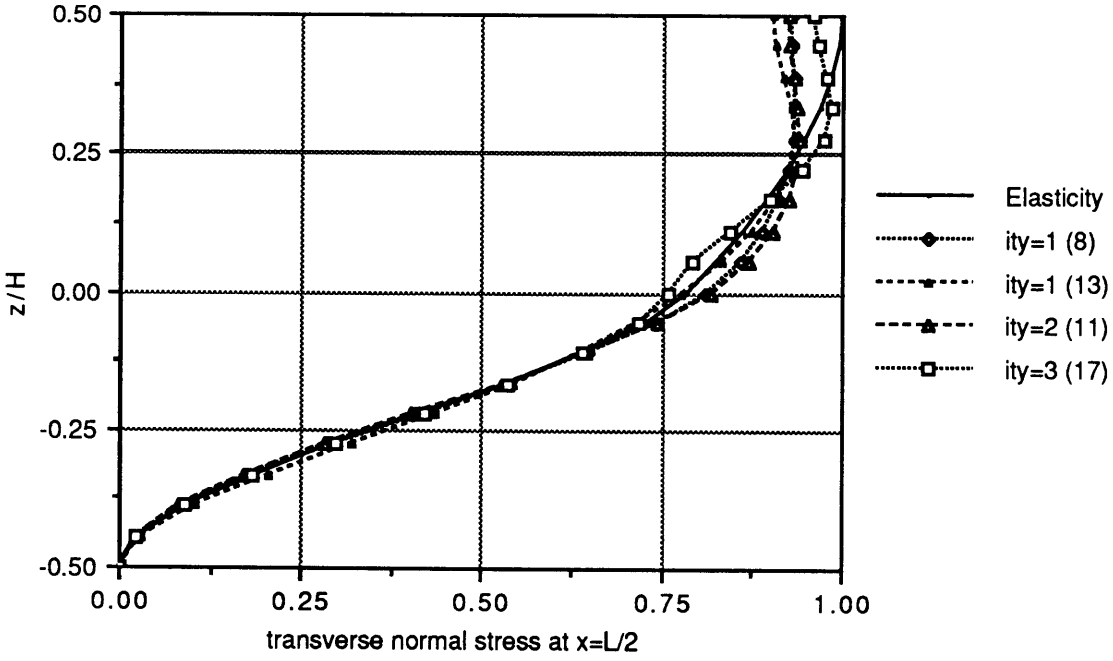

(c) transverse normal stress $\bar{\sigma}_z(L/2, z/H)$

Figure 3.10 Solutions for a 2-layer $[90/0]_T$ laminate at L/H=4 with three different orders of type II element

3.5 Three-Dimensional Element

Using in essence the same procedures as in two-dimensional element, the three-dimensional hybrid stress element based on the new mixed form model can be constructed. No three-dimensional hybrid stress element based on the conventional approach is formulated in this study.

A typical three-dimensional four-node laminated plate element is shown in Figure 3.11. As the 2D element, the element is also a subparametric element. Its coordinates can be expressed as

$$x(\xi,\eta) = \sum_{i=1}^{4} N_i(\xi,\eta)\ x_i \qquad (3.65.a)$$

$$y(\xi,\eta) = \sum_{i=1}^{4} N_i(\xi,\eta)\ y_i \qquad (3.65.b)$$

where

$$N_i(\xi,\eta) = \frac{1}{4}(1+\xi_i\xi)(1+\eta_i\eta) \qquad (3.65.c)$$

and $z(\zeta)$ is given by Eq. (3.55.b)

3.5.1 Element Displacement Assumption

The order of ζ in displacement assumption for all three-

dimensional elements is exactly the same as that of those two-dimensional elements.

3.5.1.1 Type I Element

The displacement u is assumed to be of order ζ^3 and displacement w is assumed to be of order ζ^2. The displacement behavior assumed in the x-y plane is bi-linear

The displacement can be written as

$$u(\xi,\eta,\zeta) = \sum_{i=1}^{4}\sum_{j=1}^{4} N_i(\xi,\eta)\ f_j(\zeta)\ u_{ij} \qquad (3.66.a)$$

$$v(\xi,\eta,\zeta) = \sum_{i=1}^{4}\sum_{j=1}^{4} N_i(\xi,\eta)\ f_j(\zeta)\ v_{ij} \qquad (3.66.b)$$

$$w(\xi,\eta,\zeta) = \sum_{i=1}^{4}\sum_{j=1}^{3} N_i(\xi,\eta)\ g_j(\zeta)\ w_{ij} \qquad (3.66.c)$$

where

u_{ij} = j^{th} nodal u displacement at node i

v_{ij} = j^{th} nodal v displacement at node i

w_{ij} = j^{th} nodal w displacement at node i

f_j and g_j are given by Eqs. (3.56.c-i)

and N_i is given by Eq. (3.65.c)

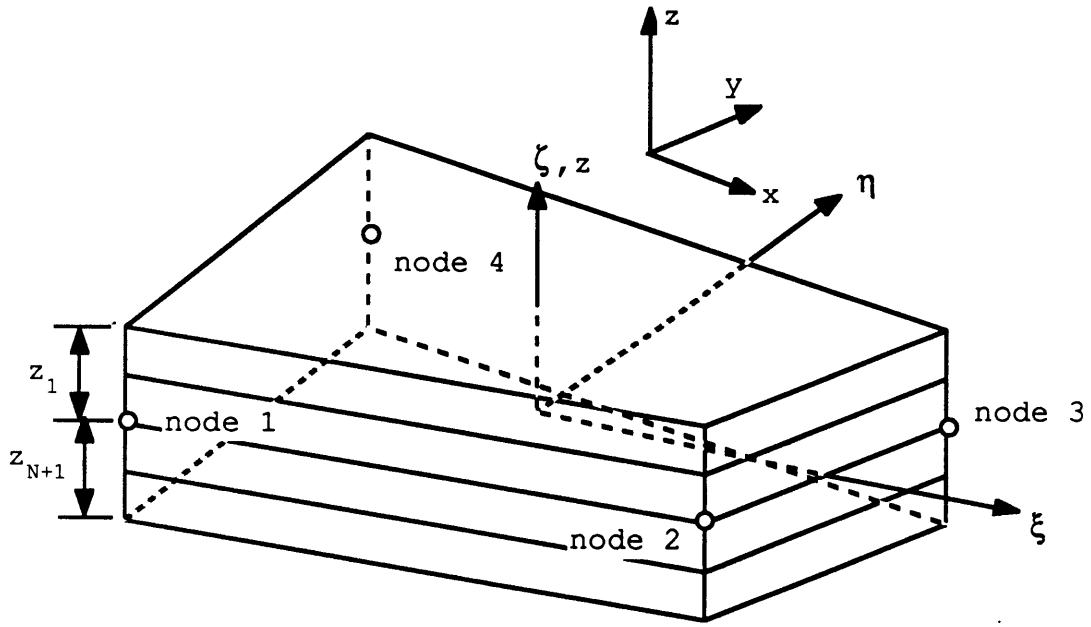

Figure 3.11 Three-dimensional laminated plate element

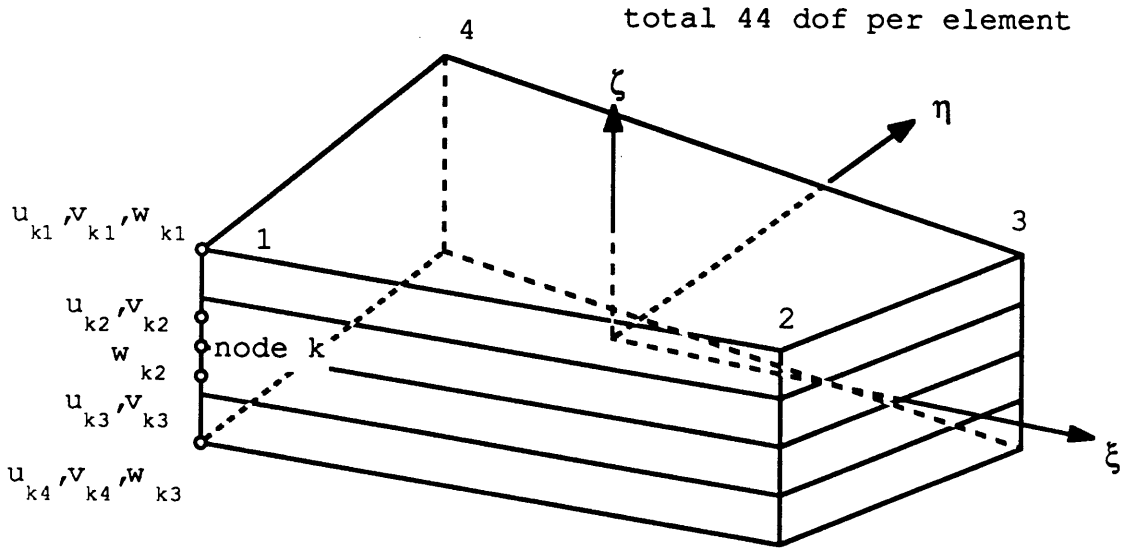

Figure 3.12 Element degrees of freedom for a type I three-dimensional element

3.5.1.2 Type II Element

From the last numerical example in two-dimensional study, we have found that the second element (ity=2) preforms poorly in predicting the transverse shear stress compared with other two elements. Therefore, only two different orders of 3D element are actually constructed and tested. They are shown in Figure 3.13. The displacement assumed in the x-y plane is bi-linear as the type I element.

The first element is assumed to be linear through the thickness of sub-element in displacements u, v and w. The displacement is expressed as

$$u^i(\xi,\eta,\zeta_i) = \sum_{k=1}^{4}\sum_{j=1}^{2} N_k(\xi,\eta)\ l_j(-\zeta_i)\ u^i_{kj} \qquad (3.67.a)$$

$$v^i(\xi,\eta,\zeta_i) = \sum_{k=1}^{4}\sum_{j=1}^{2} N_k(\xi,\eta)\ l_j(-\zeta_i)\ v^i_{kj} \qquad (3.67.b)$$

$$w^i(\xi,\eta,\zeta_i) = \sum_{k=1}^{4}\sum_{j=1}^{2} N_k(\xi,\eta)\ l_j(-\zeta_i)\ w^i_{kj} \qquad (3.67.c)$$

where

u^i_{kj} = j^{th} nodal u displacement at node k in sub-element i

v^i_{kj} = j^{th} nodal v displacement at node k in sub-element i

w^{i}_{kj} = j^{th} nodal w displacement at node k

in sub-element i

and l_j and N_i are given by Eqs. (3.55.c-d) and (3.65.c), respectively

It is shown in Figure 3.13(a) and defined as ity=1.

A higher order element with displacements u and v to be of order $(\zeta_i)^3$ and displacement w to be of order $(\zeta_i)^2$ as two-dimensional element. The displacement is in the form

$$u^{i}(\xi,\eta,\zeta_i) = \sum_{k=1}^{4}\sum_{j=1}^{4} N_k(\xi,\eta)\ f_j(\zeta_i)\ u^{i}_{kj} \qquad (3.68.a)$$

$$v^{i}(\xi,\eta,\zeta_i) = \sum_{k=1}^{4}\sum_{j=1}^{4} N_k(\xi,\eta)\ f_j(\zeta_i)\ v^{i}_{kj} \qquad (3.68.b)$$

$$w^{i}(\xi,\eta,\zeta_i) = \sum_{k=1}^{4}\sum_{j=1}^{3} N_k(\xi,\eta)\ g_j(\zeta_i)\ w^{i}_{kj} \qquad (3.68.c)$$

Because of the extensive computational effort required in 3D analysis, no element based on this high-order displacement assumptions has ever been constructed and tested in the literature.

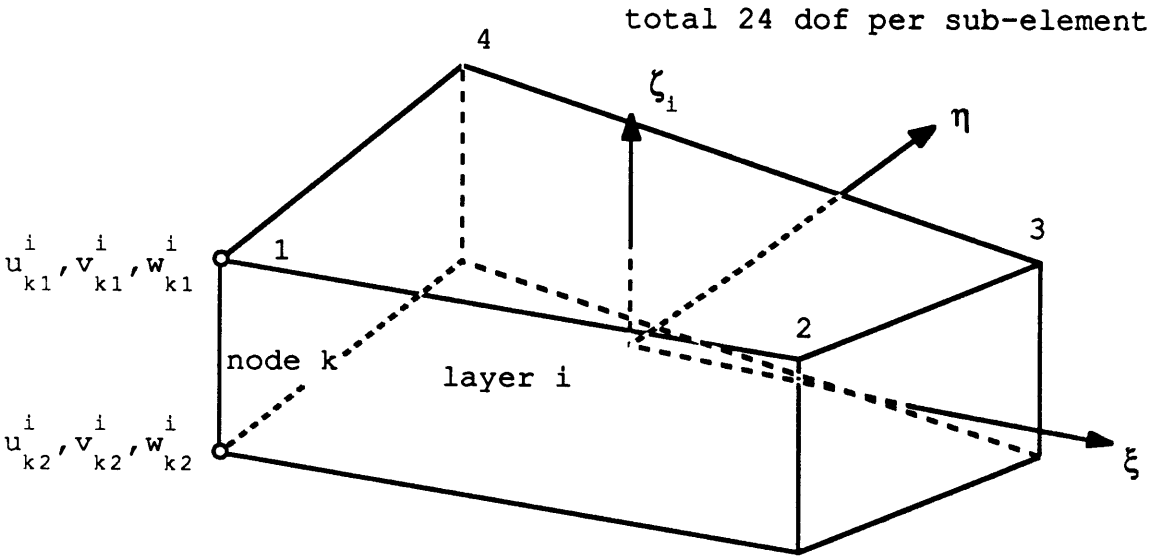

(a) Element degrees of freedom for ity=1 sub-element

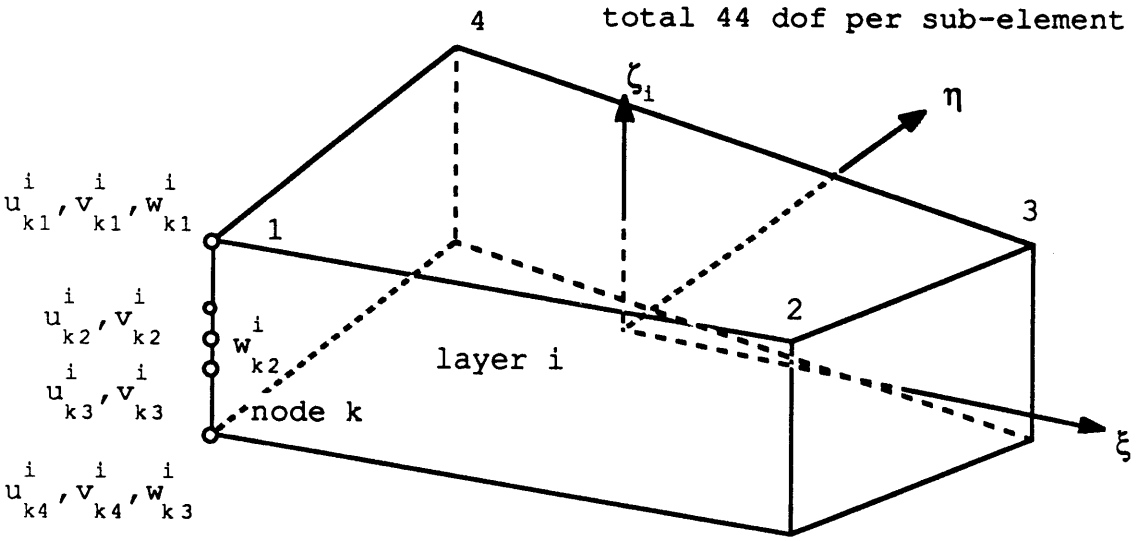

(b) Element of freedom for ity=3 sub-element

Figure 3.13 Element degrees of freedom for type II three-dimensional sublayer element

3.5.2 Stress Field Assumption

The assumed stresses are very similar to all those used in two-dimensional analysis except that they satisfy the equilibrium equations only in an integral sense. In general, more than the minimum number of stress parameters m is used.

3.5.2.1 Type I Element

There are three d.o.f. in displacement w and four d.o.f. in displacements u and v per node. With four node-lines in a element, the minimum number of stress parameters m is 4 x 3 + 8 - 5 = 15. The three transverse stresses are assumed in the form

$$\begin{bmatrix} \tau^{23} \\ \tau^{31} \\ \tau^{33} \end{bmatrix} = \begin{bmatrix} d_1 & 0 & d_1\xi & 0 & d_1\eta & 0 & d_2 & 0 & d_2\xi & 0 & d_2\eta & 0 \\ 0 & d_1 & 0 & d_1\eta & 0 & d_1\xi & 0 & d_2 & 0 & d_2\eta & 0 & d_2\xi \\ 0 & 0 & 0 & 0 & d_4 & d_4 & 0 & 0 & 0 & 0 & d_5 & d_5 \end{bmatrix}$$

$$\begin{bmatrix} d_3 & 0 & d_3\xi & 0 & d_1\xi\eta & 0 & d_1\eta^2 & 0 \\ 0 & d_3 & 0 & d_3\eta & 0 & d_1\xi\eta & 0 & d_1\xi^2 \\ 0 & 0 & 0 & 0 & d_4\xi & d_4\eta & 2d_4\eta & 2d_4\xi \end{bmatrix} \beta \qquad (3.69)$$

$$\beta = \begin{bmatrix} \beta_1 & \beta_2 & \beta_3 & \cdots\cdots\cdots & \beta_{19} & \beta_{20} \end{bmatrix}^T$$

where

$d_i(\zeta)$ in Eqs. (3.60)

A total of twenty stress parameters are used. There are five pairs of stress parameter suppressing the same deformation mode. They are (β_3,β_4), (β_5,β_6), (β_9,β_{10}), (β_{11},β_{12}) and (β_{15},β_{16}). For maintaining symmetry of the assumed stress field, both terms in each pair must be taken simultaneously. Therefore, five more stress parameter than the minimum number of β's are used. The last four stress parameters in Eq. (3.69) are added purely for the purpose to suppress the kinematic modes.

It is noted that the traction free condition at the top and bottom surfaces of the laminate are satisfied.

3.5.2.2 Type II Element

Based on Eq. (3.63), the assumed stresses can easily be extended into three-dimensional stress field. Many high order terms are added in order to suppress the kinematic modes for the high order element (ity=3) but in order to keep the number of β's small, globally, the equilibrium equations are relaxed in some of these terms. a total of forty stress parameters are used. The actual number of β's being used depends on the element layup in the direction of thickness. They are in the form

$$
\begin{bmatrix} \tau^{23} \\ \tau^{31} \\ \tau^{33} \end{bmatrix}^i = \begin{bmatrix}
0 & 0 & 0 & 0 & 0 & 0 & s_1 & s_1\xi & s_2 & s_2\xi & s_3 & s_3\xi \\
s_1 & s_1\eta & s_2 & s_2\eta & s_3 & s_3\eta & 0 & 0 & 0 & 0 & 0 & 0 \\
0 & 0 & 0 & 0 & 0 & 0 & 0 & 0 & 0 & 0 & 0 & 0
\end{bmatrix}
$$

$$
\begin{bmatrix}
-\frac{3}{8}s_3\eta & \frac{3}{8}s_3\eta & 0 & 0 & s_{13}\eta & s_{23}\eta & 0 & 0 & 0 \\
-\frac{3}{8}s_3\xi & \frac{3}{8}s_3\xi & s_{13}\xi & s_{23}\xi & 0 & 0 & s_{13}\xi\eta & s_{23}\xi\eta & s_{13}\xi^2 \\
s_4 & s_5 & s_6 & s_7 & s_6 & s_7 & s_6\eta & s_7\eta & 2s_6\xi
\end{bmatrix}
$$

$$
\begin{bmatrix}
0 & s_{13}\xi\eta & s_{23}\xi\eta & s_{13}\eta^2 & s_{23}\eta^2 & 0 & 0 & 0 & 0 \\
s_{23}\xi^2 & 0 & 0 & 0 & 0 & 0 & 0 & 0 & 0 \\
2s_7\xi & s_6\xi & s_7\xi & 2s_6\eta & 2s_7\eta & s_4\xi & s_4\eta & s_5\xi & s_5\eta
\end{bmatrix}
$$

$$
\begin{bmatrix}
0 & 0 & s_8 & s_8\xi & 0 & s_8\eta & 0 & 0 & 0 & s_9 \\
s_8 & s_8\eta & 0 & 0 & s_8\xi & 0 & 0 & 0 & s_9 & 0 \\
0 & 0 & 0 & 0 & s_9 & s_9 & s_9\xi & s_9\eta & 0 & 0
\end{bmatrix}^i \beta^i \qquad (3.70)
$$

$$
\beta^i = \begin{bmatrix} \beta_1^i & \beta_2^i & \beta_3^i & \cdots\cdots\cdots\cdots & \beta_{39}^i & \beta_{40}^i \end{bmatrix}^T
$$

where

$s_i(\zeta_i)$ in Eqs. (3.64)

It is seen that the six high order terms β_{27} to β_{30}, β_{37} and

β_{38} in above equation do not satisfy the equilibrium. They are needed to suppress all kinematic modes.

3.5.3 Numerical Examples

Three examples have been chosen to validate the accuracy of the present elements. The first two are a simply supported plate under sinusoidal loading and the third one is a laminated plate under cylindrical bending. One additional test on the type II ity=3 element based on the new mixed form formulation for the free-edge problem will be presented in the later chapter.

3.5.3.1 Bending of a Square Laminated Plate

We consider here a bi-directional laminated square plate. The laminate configuration is a three-layer cross ply laminate $[0/90/0]_T$ with layers of equal thickness. The angle is measured with respect to the axis x (i.e. 0 degree implies fibers are parallel to the axis x). The material properties are the same as those in the two-dimensional examples. The laminate is simply supported along all its edges and sinusoidally distributed transverse loading $q_0\cos(\pi x/L)\cos(\pi y/L)$ with $q_0=1$ is applied at the top surface of the laminate as shown in Figure 3.14. The span-to-thickness ratio is four as before. Because

of symmetries along the axes x and y, the finite element analysis is carried out over a quarter of the plate which is subdivided into 4 equal elements on each side.

Each layer is modeled by a present mixed form type II ity=1 hybrid stress element. The number of stress parameters used for each layer is twenty-two. They are the β_1 to β_{18}, and β_{27} to β_{30} in Eq. (3.70). After enforcing the stress continuity and traction free conditions, the number of stress parameters for the three-layer model is reduced to thirty-three. The minimum number of β's required to suppress the kinematic modes is nineteen. For maintaining symmetry of the assumed stress field, the actual number of β's being used is quite large compared with the minimum number of β's.

The results are compared with the elasticity solutions by Pagano [106], classical lamination plate theory [106] and conventional hybrid stress element by Mau, Tong and Pian [41]. The numerical results are presented in terms of normalized values which are given by Eq. (3.64).

Results obtained by the present element and Mau's element are very similar to each other (Figure 3.15). Their behaviors are also analogy to 2D three-layer example. They are in good agreement with the elasticity solutions and the transverse shear stress τ_{xz} is trend to underestimate at the interlayer boundaries. The CPT results are in poor agreement with the

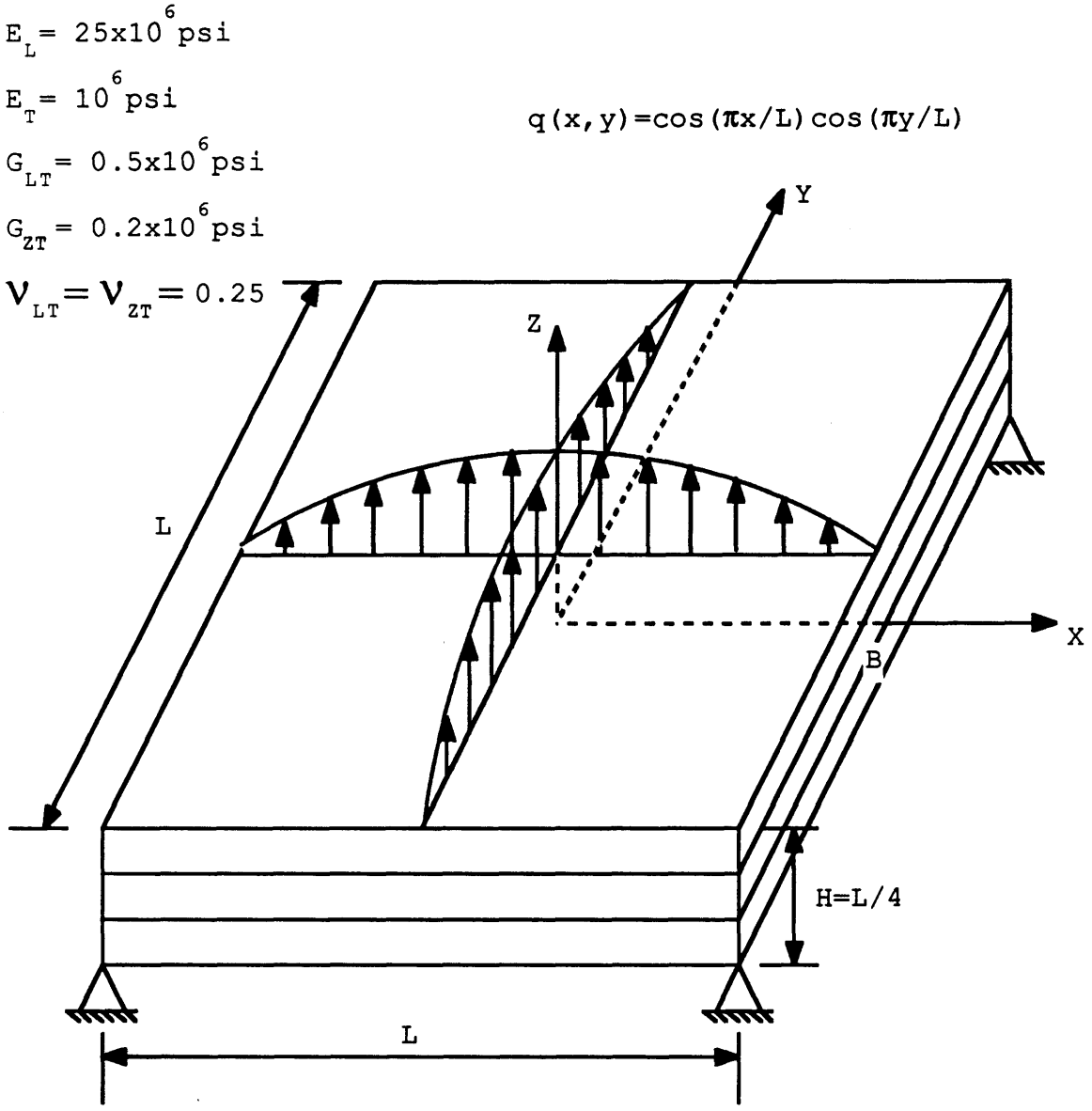

Figure 3.14 A simply supported square laminated plate under sinusoidal loading

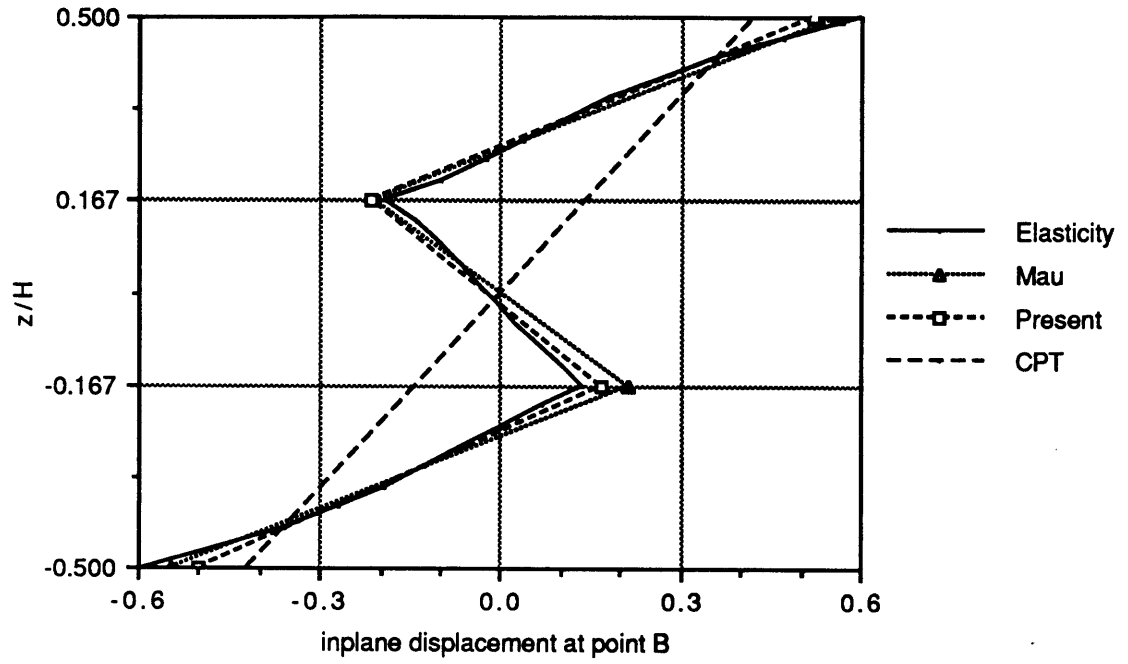

(a) inplane displacement $\bar{u}$ (0, z/H)

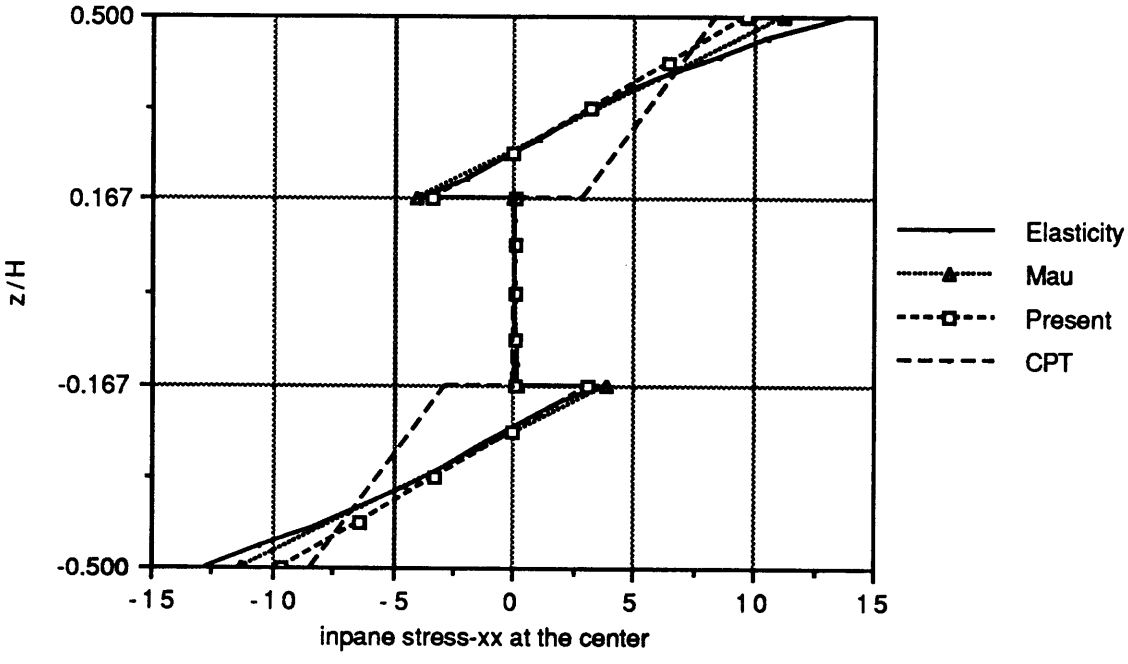

(b) inplane normal stress $\bar{\sigma}_x$ (L/2, z/H)

Figure 3.15 Solutions for a simply supported square plate of 3-layer $[0/90/0]_T$ laminate at L/H=4

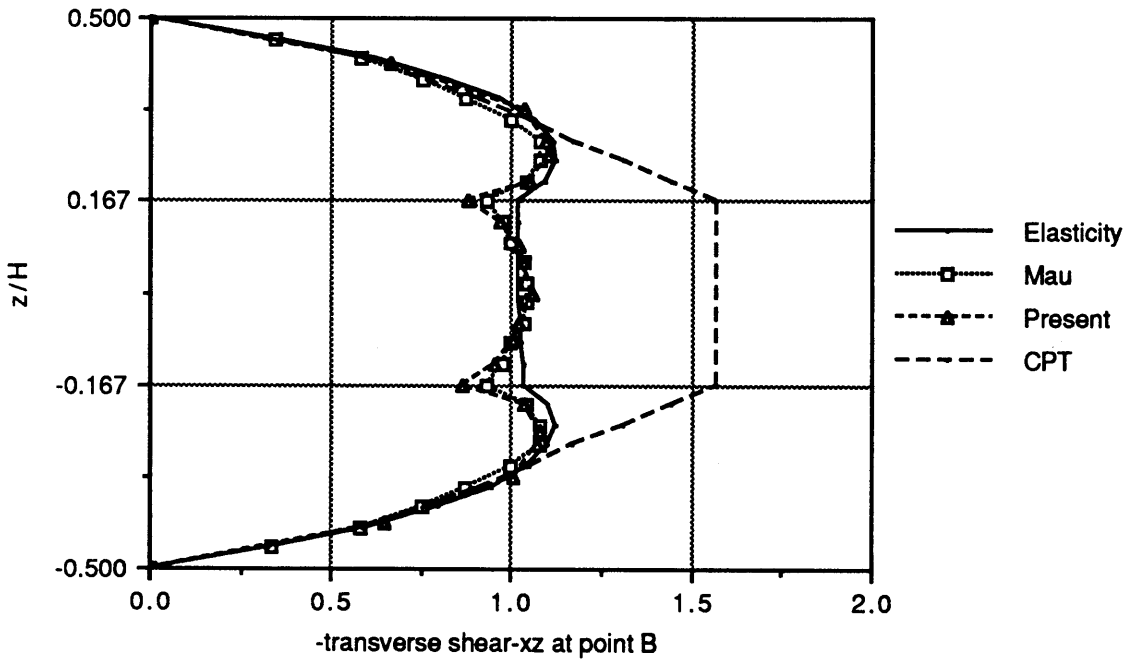

(c) transverse shear stress $\bar{\tau}_{xz}(0, z/H)$

Figure 3.15 Solutions for a simply supported square plate of 3-layer $[0/90/0]_T$ laminate at L/H=4

elasticity solutions as the 2D analysis because of its incapable to predict the cross-section warping.

3.5.3.2 Bending of a Square Sandwich Plate

We consider here a simply supported square sandwich plate under the distributed loading considered in the preceding example and the span-to-thickness ratio is four as shown in Figure 3.14. The material of the face sheets is the same as that in the preceding example and the core material is transversely isotropic with respect to z. The material properties are shown in Figure 3.16. The thickness of each face sheet is H/10.

The finite element mesh and the type of element are both the same as those used in the preceding example. The following quantities are normalized with respect to q_0. Selected results of the analysis are presented in Table 3.4.

The maximum inplane stresses obtained by the present mixed form hybrid stress element are in reasonable agreement with the elasticity solutions and the maximum transverse shear stresses are in good agreement. Once again, the CPT solutions are poor at the interface boundaries because of its incapability to capture the cross-section warping.

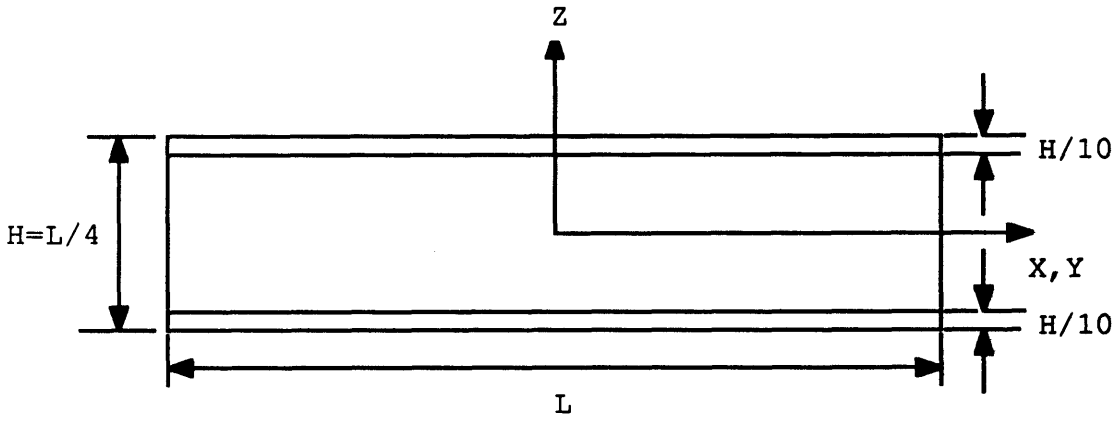

Property of face sheet

$E_L = 25 \times 10^6$ psi

$E_T = 10^6$ psi

$G_{LT} = 0.5 \times 10^6$ psi

$G_{ZT} = 0.2 \times 10^6$ psi

$\nu_{LT} = \nu_{ZT} = 0.25$

Property of core material

$E_x = E_y = 0.04 \times 10^6$ psi

$E_z = 0.5 \times 10^6$ psi

$G_{xz} = G_{yz} = 0.06 \times 10^6$ psi

$G_{xy} = 0.016 \times 10^6$ psi

$\nu_{zx} = \nu_{zy} = \nu_{xy} = 0.25$

Figure 3.16 Dimension and property definition for a sandwich plate (L/H=4)

Table 3.4 Maximum stresses in square sandwich plate

Solution Technique	$\bar{\sigma}_x(0,0,\pm H/2)$	$\bar{\sigma}_x(0,0,\pm .4H)$	$\bar{\sigma}_y(0,0,\pm H/2)$
Elasticity	24.896	-3.728	4.152
	-24.192	3.136	-4.053
Present	20.377	-0.870	3.418
Finite Element	-21.384	1.613	-3.659
CPT	±17.552	±14.048	±0.869

Solution Technique	$\bar{\tau}_{xz}(L/2,0,0)$	$\bar{\tau}_{yz}(0,L/2,0)$
Elasticity	-0.956	-0.429
Present	-0.929	-0.417
CPT	-1.296	-0.118

3.5.3.3 Distortion Study

The case chosen for the distortion study is a three-dimensional model of the previous 2D examples, a simply supported long strip under cylindrical bending as shown in

Figure 3.17. The laminate is a three-layer cross ply $[0/90/0]_T$ with layers of equal thickness. To demonstrate the effect of element distortion, a 4x4 mesh of the same elements for the three-layer model of the previous two examples is used. Figure 3.18 defines the distortion parameter a. Full triangularization occurs for a=3.

The displacement w along the axis y at the top and bottom surfaces versus distortion is shown in Figure 3.19(a). The maximum inplane normal stress σ_x along the axis y at the top surface and the maximum transverse shear stress τ_{xz} along the simply supported edge at z=H/4 versus distortion are shown in Figures 3.19(a-b). The results indicate a severe deterioration in inplane normal stress when the element becomes a triangular element. However, the rest of the results shows relatively small deterioration in comparison with the solution obtained by the undistorted finite element mesh.

3.6 Summary

Overall, the previous two- and three-dimensional examples demonstrate the computational efficiency of the present mixed form hybrid stress elements. The type II ity=3 element has the best accuracy within its family. Type II element should be used whenever the laminate is less than four layers. On the other

Boundary Conditions:
All u=0 along side ABDC
All v=0 along side ABFE
and CDIG
All w=0 along side EFIG

$E_L = 25 \times 10^6$ psi

$E_T = 10^6$ psi

$G_{LT} = 0.5 \times 10^6$ psi

$G_{ZT} = 0.2 \times 10^6$ psi

$\nu_{LT} = \nu_{ZT} = 0.25$

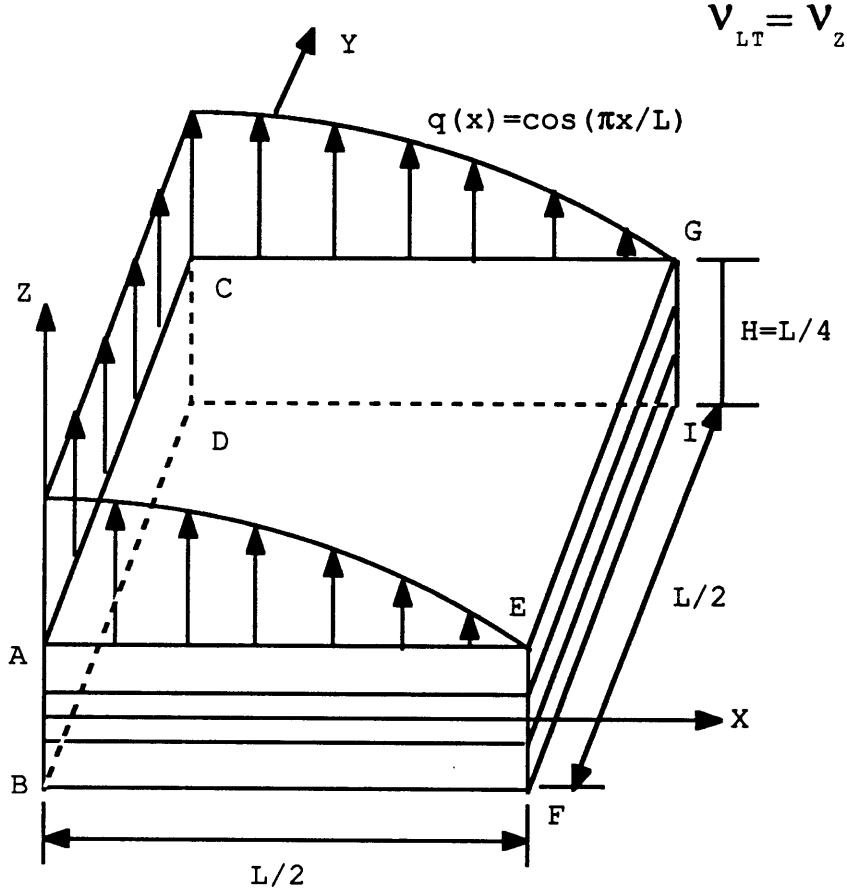

Figure 3.17 Problem description for a semi-infinite three-layer cross-ply laminated plate subjected to cylindrical bending (L/H=4)

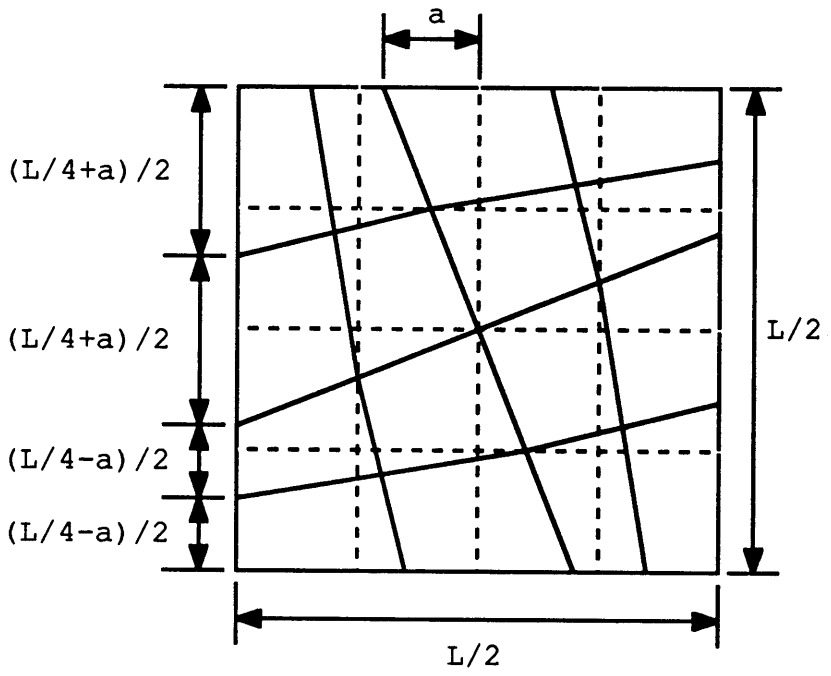

Figure 3.18 Finite element mesh for distortion study of a rectangular plate under cylindrical bending (L=12)

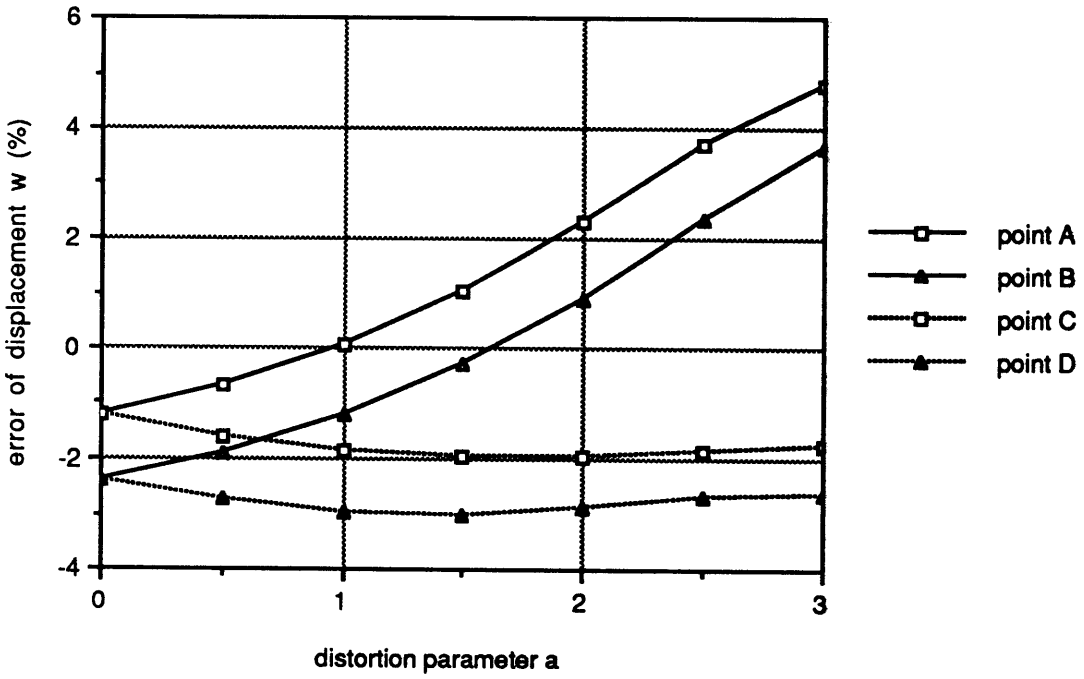

(a) transverse displacement $w(L/2,y,\pm H/2)$

Figure 3.19 Solutions for distortion study of a laminate under cylindrical bending

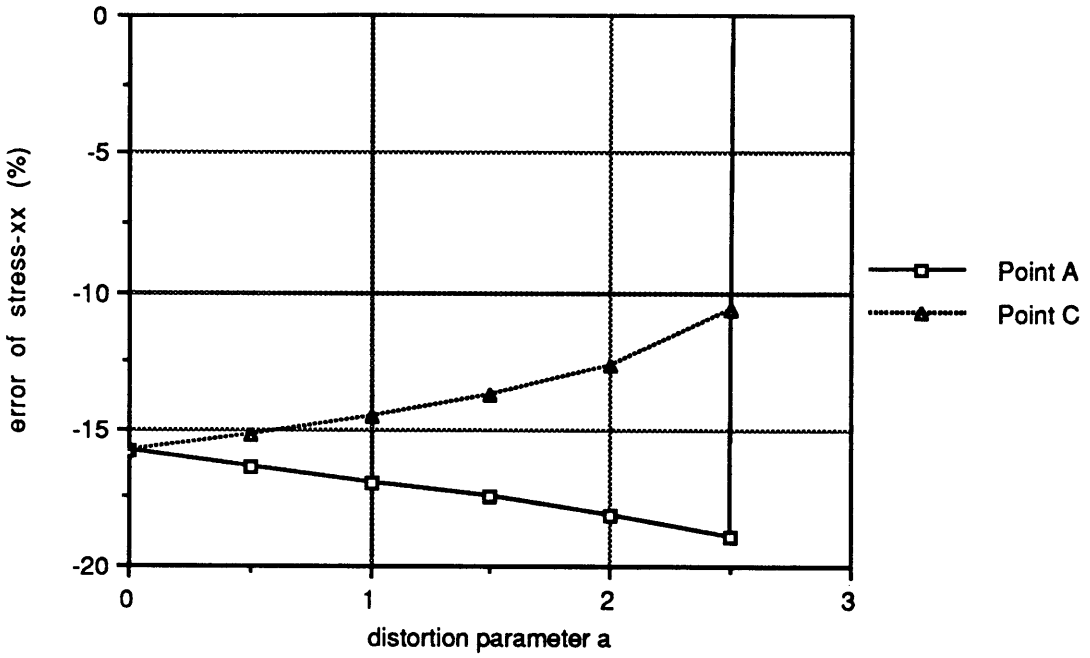

(b) inplane normal stress $\bar{\sigma}_x$ (0,y,H/2)

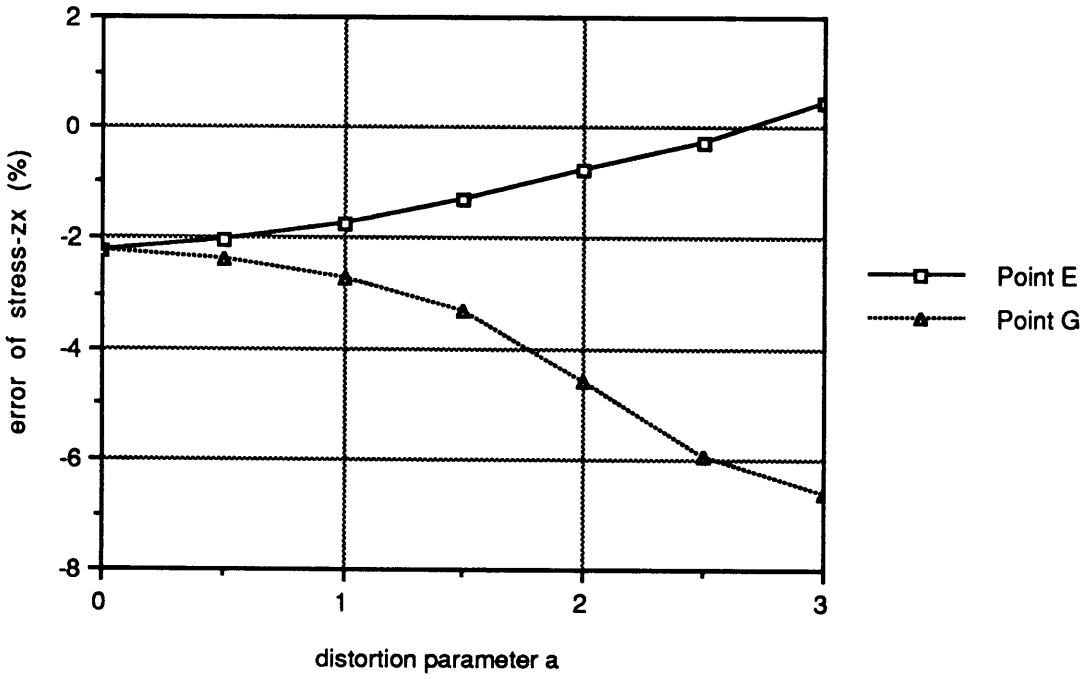

(c) transverse shear stress $\bar{\tau}_{xz}$ (L/2,y,H/4)

Figure 3.19 Solutions for distortion study of a laminate under cylindrical bending

hand, to avoid oscillation of stress results the number of stress parameters should be kept as minimum as possible and simultaneously suppressing all the kinematic modes.

CHAPTER FOUR

SMOOTHING OF STRESS AND STRAIN FIELDS

The solution of an elasticity problem given by the displacement-based, assumed stress and assumed strain formulations all provide discontinuous stress and strain fields along the inter-element boundaries.

On the other hand, the mixed model in which the stresses or strains and the displacements are used as primary variables with irreducible forms provides the solution with continuous displacement and stress or strain fields for homogeneous mediums and often demonstrated better accuracy than other formulations when applied to a similar element mesh. However, the increased number of unknowns entering the computation has in general made its application in practice not cost effective and particularly the equation system containing a zero diagonal term has also made the equation not well conditioned and difficult to solve numerically.

A number of techniques has been used to deal with such discontinuous fields, for example, nodal mean values, Gaussian point values, extrapolations and iteration technique. The most effective of these is based on a combination of stress or strain

'smoothing' and iteration techniques. Application of certain smoothing procedures and iteration scheme for maintaining the continuity of interlaminar stresses along the interfaces of laminated composite plates is to be investigated here.

Oden and Reddy [107] used a 'conjugate' approximations of stresses in the displacement formulation to arrive a smooth stress field in regions in which high stress gradients are experienced. Some improvement in accuracy of the stresses is obtained.

Hinton and Campbell [108] employed the least square method for discontinuous stress field smoothing in the displacement formulation. The least squares smoothing procedure may be carried out globally over the whole of the finite element domain or locally over each individual element. They have demonstrated the advantages of using the least square smoothing procedure on some two-dimensional and plate problems.

Loubignac, Cantin and Touzot [109,110] presented an iterative algorithm based on an initial stress field for building a continuous stress and displacement solution. Starting from the solution of a classical displacement finite element analysis and using simple nodal mean value to obtain the smoothed stress field, however, the smoothed stress field does not satisfy the original equilibrium condition. They proposed an iteration scheme to obtain a continuous stress field which

also satisfies the principle of virtual work. A number of examples has shown the efficiency of the method.

Stein and Ahmad [111] proposed an equilibrium method for stress smoothing calculation using the displacement model. After the nodal displacements are calculated, the nodal stress values are then determined by the principle of virtual work with the assumptions of some forms of stress distributions and corresponding virtual displacements at element boundaries. However, in general, the equation system is nonquadratic and Gauss's transformation procedure is needed to produce a symmetric, positive definite band matrix. Various examples of plane stress, plate bending and shell problems have shown better accuracy of stresses in comparison with conventional methods.

Chen [112] studied the use of the Hellinger-Reissner principle as a smoothing tool with an iteration scheme cited in References 109 and 110 for constructing a continuous stress field in the assumed stress model. However, the results have shown divergence instead of convergence for plane stress problems. On the other hand, the use of the nodal mean stress value or the weighted-by-volume nodal mean stress with the iteration scheme based on initial stresses for restoring the equilibrium in the smoothed stress field has shown some promising results.

Zienkiewicz, Li and Nakazawa [76] presented a 'consistent'

stress and strain smoothing procedures along with the 'Loubignac-Cantin' equilibrium iteration technique. They have shown that the stress or strain smoothing combined with the iteration scheme corresponds precisely to the solution of mixed model. The procedure promises to add considerable accuracy to F.E.M. results by some additional effort.

An application of the mixed model to study the interlaminar stresses near curved boundaries of laminate composite plates has been presented by Hwang and Sun [113]. They used the three inplane strains and three transverse stresses as primary variables while solving the system equations by an iteration scheme which is similar to the 'Loubignac-Cantin' equilibrium iteration scheme.

Certain stress and strain smoothing procedures along with the equilibrium iteration algorithm will be discussed in the following section. Assessments for these techniques in an elastic body with isotropic and orthotropic materials will followed. A study of their applications in the laminated composite plates and a discussion are presented at the end of this chapter.

4.1 Stress Smoothing Procedures and Iteration Technique

The use of a 'consistent' and a 'lumping' stress smoothing

schemes cited in Reference 76 for the displacement formulation and their extensions to the conventional hybrid stress formulation are described as follows:

The problem is solved first by either the conventional displacement or hybrid stress finite element method and the nodal displacements $\mathbf{q}$ are obtained by

$$\mathbf{K}\,\mathbf{q} = \mathbf{Q} \tag{4.1.a}$$

where

$\mathbf{K}$, $\mathbf{q}$ and $\mathbf{Q}$ are global matrices assembled from element matrices

$$\mathbf{k} = \int_{V_n} \mathbf{B}^T\,\mathbf{C}\,\mathbf{B}\,dV \tag{4.1.b}$$

V_n = spatial domain of element n

$$\mathbf{B} = \mathbf{D}\,\mathbf{N} = \text{strain matrix} \tag{4.1.c}$$

for the assumed displacement element and

$$\mathbf{k} = \mathbf{G}^T\,\mathbf{H}^{-1}\,\mathbf{G} \tag{4.1.d}$$

for the conventional hybrid stress element and $\mathbf{C}$, $\mathbf{D}$, $\mathbf{N}$, $\mathbf{G}$, $\mathbf{H}$ and $\mathbf{Q}$ are given in Eqs. (3.1), (3.2), (3.14) and (3.15)

Second, the stresses σ are computed by

$$\boldsymbol{\sigma} = \mathbf{C}\,\mathbf{B}\,\mathbf{q} \tag{4.2.a}$$

for the assumed displacement element and

$$\boldsymbol{\sigma} = \mathbf{P}\,\boldsymbol{\beta} \tag{4.2.b}$$

for the conventional hybrid stress element, where

$$\boldsymbol{\beta} = \mathbf{H}^{-1}\,\mathbf{G}\,\mathbf{q} \tag{4.2.c}$$

Third, a stress field $\boldsymbol{\sigma}^*$ is interpolated in terms of nodal stresses $\mathbf{p}$,

$$\boldsymbol{\sigma}^* = \mathbf{N}\,\mathbf{p} \tag{4.3}$$

where

$\mathbf{N}$ = the same shape functions used for the displacement field

Thus, $\boldsymbol{\sigma}^*$ will be continuous over the entire domain. Then, the nodal stress parameters $\mathbf{p}$ are determined by the condition that the integral of the difference between $\boldsymbol{\sigma}$ and $\boldsymbol{\sigma}^*$ when weighted by the shape functions $\mathbf{N}$ is zero, i.e.

$$\sum_{n} \int_{V_n} \mathbf{N}^T (\boldsymbol{\sigma} - \boldsymbol{\sigma}^*)\, dV = \mathbf{0} \tag{4.4}$$

where

n is the total number of elements

Substituting Eq. (4.3) into above equation, we obtain

$$\mathbf{p} = \mathbf{M}^{-1} \sum_{n} \int_{V_n} \mathbf{N}^T \boldsymbol{\sigma} \, dV \qquad (4.5.a)$$

where

$$\mathbf{M} = \sum_{n} \int_{V_n} \mathbf{N}^T \mathbf{N} \, dV \qquad (4.5.b)$$

The matrix $\mathbf{M}$ has the same form as a classical consistent mass matrix. The computation of Eq. (4.5.a) is done separately for each component of stresses.

To avoid inverting the consistent matrix, a simple iteration method can be used to obtain the nodal stress parameters $\mathbf{p}$ by rewriting Eq. (4.5.a) into the following form

$$\mathbf{p}_i = \mathbf{M}_L^{-1} \left[\sum_{n} \int_{V_n} \mathbf{N}^T \boldsymbol{\sigma} \, dV - (\mathbf{M} - \mathbf{M}_L) \, \mathbf{p}_{i-1} \right] \qquad (4.6)$$

where

$\mathbf{M}_L$ has the same form as a classical lump mass matrix

i is the number of iterations

This converges reasonably fast. The alternative approach is to replace the consistent matrix $\mathbf{M}$ by the lump matrix $\mathbf{M}_L$. Both approaches are cited in Reference 76.

However, for consistency, Eq. (4.5.a) should be replaced by the following equation if the lump matrix $\mathbf{M}_L$ is used,

$$\mathbf{p} = \mathbf{M}_L^{-1} \left[\sum_{i=1}^{n} \sum_{j=1}^{nj} (m_L)_j^i \, \sigma_j^i \right] \tag{4.7}$$

where

$(m_L)_j^i$ = lump value at node j in element i

σ_j^i = value of σ at node j in element i

n = total number of elements

nj = total number of nodes in element i

and it was not done in Reference 76. When the lumped values of a high order element, for example an 8-node two-dimensional element, are not explicit, nodal mean value can be used to resolve this difficulty. On the other hand, the computational effort of this operation is trivial compared with that using the consistent matrix.

However, the computed smoothed stress field σ^* does not satisfy the original equilibrium condition and it is desirable that the following equation

$$\sum_n \int_{V_n} \mathbf{B}^T \, \sigma^* \, dV = \mathbf{Q} \tag{4.8}$$

should be satisfied. Loubignac and his colleagues [109,110] proposed the following iteration scheme for restoring the equilibrium condition. The algorithm is as follows:

First, assuming that the structure is subjected to inbalance forces based on the difference between the smoothed stress field σ^* and $\mathbf{Q}$, therefore, the displacement increments $\Delta\mathbf{q}$ for restoring the equilibrium are obtained by

$$\Delta\mathbf{q}_i = \mathbf{K}^{-1} \left(\mathbf{Q} - \sum_n \int_{V_n} \mathbf{B}^T \sigma_i^* \, dV \right) \qquad (4.9)$$

where

i = the number of iterations (-1,0,1,2....)

$\sigma_{-1}^* = \mathbf{0}$ for starting value

Then, the nodal displacements $\mathbf{q}$ and stresses σ are updated by the following equations

$$\mathbf{q}_{i+1} = \mathbf{q}_i + \Delta\mathbf{q}_i \qquad (4.10.a)$$

$$\sigma_{i+1} = \mathbf{C}\,\mathbf{B}\,\mathbf{q}_{i+1} \qquad (4.10.b)$$

for the assumed displacement element and

$$\sigma_{i+1} = \mathbf{P} \left(\mathbf{H}^{-1}\,\mathbf{G}\,\mathbf{q}_{i+1} \right) \qquad (4.10.c)$$

for the conventional hybrid stress element, where

$\mathbf{q}_{-1} = \mathbf{0}$ for starting value

Again, one can apply certain stress smoothing procedure to re-compute the continuous stress field σ^* if convergence is not reached.

The criterion of convergence adopted in this study is that if the following equation is satisfied, we assume that the convergence is reached.

$$\frac{\sum_{i=1}^{nd} (q_{i,0})^2}{\sum_{i=1}^{nd} (\Delta q_{i,j})^2} \geq k \qquad (4.11)$$

where

$q_{i,0}$ = nodal displacement q_i at the 0^{th} iteration

$\Delta q_{i,j}$ = nodal displacement increment Δq_i at the j^{th} iteration

nd = total number of degrees of freedom

k is an arbitrary coefficient

The original stress smoothing scheme can no longer be applied to laminated structures because of the discontinuity of the inplane stresses σ_x, σ_y and τ_{xy} in the direction of the plate thickness. However, because of the continuity of the inplane strains ε_x, ε_y and ε_{xy}, the stress smoothing for the inplane stresses can be replaced by the corresponding inplane strains. Therefore, in the problems of laminated structures the smoothing

scheme is again divided into inplane and transverse parts. For the inplane portion, it is to smooth the strains $\mathbf{e}_p$ and for the transverse portion, it is to smooth the stresses $\mathbf{t}_t$. The stresses $\mathbf{t}_t$ and the strains $\mathbf{e}_p$ are given in Eqs. 3.3(d) and 3.3(e).

The smoothing and iteration procedures are replaced by the following steps:

After the nodal displacements $\mathbf{q}$ are solved by either the conventional assumed displacement or hybrid stress method, the inplane strains $\mathbf{e}_p$ and the transverse stresses $\mathbf{t}_t$ are computed by

$$\mathbf{e}_p : \varepsilon = (\mathbf{DN})\ \mathbf{q}, \text{ and } \mathbf{t}_t : \sigma = \mathbf{C}\ (\mathbf{DN})\ \mathbf{q} \qquad (4.12.a)$$

for the assumed displacement element and

$$\mathbf{t}_t : \sigma = \mathbf{P}\ \beta, \text{ and } \mathbf{e}_p : \varepsilon = \mathbf{S}\ \sigma \qquad (4.12.b)$$

for the conventional hybrid stress element

where

$\mathbf{C}$, $\mathbf{S}$, $\mathbf{D}$, $\mathbf{N}$, $\mathbf{P}$ and β are given in Eqs. (3.1), (3.2), (3.14), (3.13) and (3.14)

Once again, the continuous strain field $\mathbf{e}_p^*$ and stress field $\mathbf{t}_t^*$ are in terms of nodal strains $\mathbf{b}$ and nodal stresses $\mathbf{p}$, respectively,

$$\mathbf{e}_p^* = \mathbf{N}\ \mathbf{b}, \text{ and } \mathbf{t}_t^* = \mathbf{N}\ \mathbf{p} \qquad (4.13)$$

Then, the nodal strain parameters **b** and the nodal stress parameters **p** are determined by the similar condition of Eq. (4.4), i.e.,

$$\sum_n \int_{V_n} \mathbf{N}^T (\mathbf{e}_p - \mathbf{e}_p^*) \, dV = \mathbf{0} \qquad (4.14.a)$$

and

$$\sum_n \int_{V_n} \mathbf{N}^T (\mathbf{t}_t - \mathbf{t}_t^*) \, dV = \mathbf{0} \qquad (4.14.b)$$

Substituting Eq. (4.13) into above two equations, we obtain

$$\mathbf{b} = \mathbf{M}^{-1} \sum_n \int_{V_n} \mathbf{N}^T \mathbf{e}_p \, dV \qquad (4.15.a)$$

and

$$\mathbf{p} = \mathbf{M}^{-1} \sum_n \int_{V_n} \mathbf{N}^T \mathbf{t}_t \, dV \qquad (4.15.b)$$

where

M is given in Eq. (4.5.b)

and the computation of Eqs. (4.15.a) and (4.15.b) is done separately for each component of inplane strains and transverse stresses.

If the lump matrix $\mathbf{M}_L$ is used, the above equations are replaced by the following equations,

$$\mathbf{b} = \mathbf{M}_L^{-1} \left[\sum_{i=1}^{n} \sum_{j=1}^{nj} (m_L)_j^i \, (\mathbf{e}_p)_j^i \right] \qquad (4.16.a)$$

and

$$\mathbf{p} = \mathbf{M}_L^{-1} \left[\sum_{i=1}^{n} \sum_{j=1}^{nj} (m_L)_j^i \, (\mathbf{t}_t)_j^i \right] \qquad (4.16.b)$$

where

$(m_L)_j^i$ = lump value at node j in element i

$(\mathbf{e}_p)_j^i$ = value of $\mathbf{e}_p$ at node j in element i

$(\mathbf{t}_t)_j^i$ = value of $\mathbf{t}_t$ at node j in element i

n = total number of elements

nj = total number of nodes in element i

The displacement increments $\Delta\mathbf{q}$ for restoring the equilibrium are then obtained by

$$\Delta\mathbf{q}_i = \mathbf{K}^{-1} \left(\mathbf{Q} - \sum_n \int_{V_n} \{ (\mathbf{D}_p\mathbf{N})^T [\mathbf{C}_p (\mathbf{e}_p^*)_i + \mathbf{C}_{pt} (\mathbf{t}_t^*)_i] + (\mathbf{D}_t\mathbf{N})^T (\mathbf{t}_t^*)_i \} \, dV \right) \qquad (4.17)$$

where

i = the number of iterations (-1,0,1,2.....)

$(\mathbf{e}_p^*)_{-1} = (\mathbf{t}_t^*)_{-1} = \mathbf{0}$ for starting value

$\mathbf{C}_p$ and $\mathbf{C}_{pt}$ are given in Eq. (3.5)

4.2 Numerical Examples

In the following, the three different stress smoothing procedures described in the previous section based on the conventional assumed displacement and hybrid stress models along with the iteration for restoring the original equilibrium are studied. After the best scheme is determined, it will be applied to laminated composite plates and the results are compared with those obtained by the high order laminated plate element will be made.

In this study, only the two-dimensional 4-node 5-β and the three-dimensional 8-node 18-β elements for the conventional hybrid stress model [93,114] and the two-dimensional 4-node and three-dimensional 8-node isoparametric elements for the assumed displacement model are used.

The first four examples are plane stress problems with isotropic materials. Then, two three-dimensional problems, one with isotropic and one with anisotropic material, will follow. The last example is a two-layer cross ply unsymmetrical laminate subjected to cylindrical bending.

Some of the labels for the elements used in the present comparisons are listed in the following:

Hybrid (c) = conventional hybrid stress element with consistent stress smoothing scheme

Hybrid (l) = conventional hybrid stress element with lumped stress smoothing scheme

Displacement (c) = assumed displacement element with consistent stress smoothing scheme

Displacement (l) = assumed displacement element with lumped stress smoothing scheme

* the number in the parenthesis is the number of equilibrium iteration steps used

4.2.1 Plane Isotropic Cantilever Beam under End Tip Loading

The first problem defined in Figure 4.1(a) is taken from Reference 76. A cantilever beam is represented by ten 4-node isoparametric elements. Convergence studies on the tip displacement and the stretching stress σ_x at point B are shown in Figure 4.2. The shear locking phenomenon is relieved by all three stress smoothing procedures with a few equilibrium iteration steps. In this example, no analysis is carried out by the hybrid stress model because the present type of locking phenomenon does not exist in the hybrid model.

The results obtained by the ones with consistent and lumped stress smoothing schemes are very similar to each other in the aspect of accuracy. They are labelled as 'Consistent' and

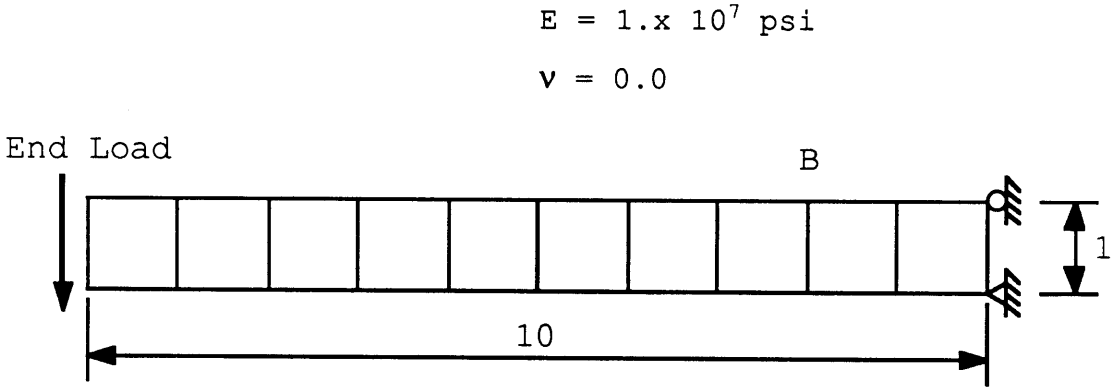

(a) geometry and finite element mesh

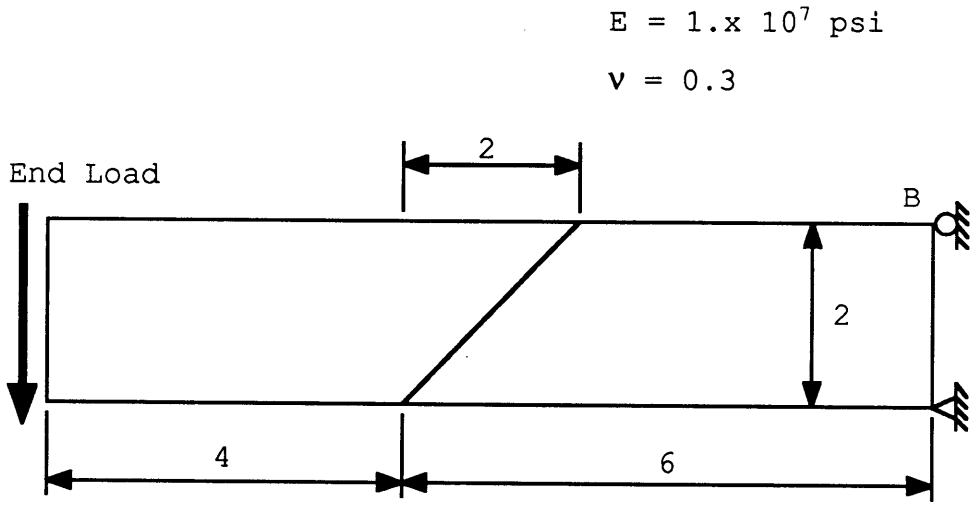

(b) geometry and finite element mesh for study of distortion of element geometry

Figure 4.1 Isotropic cantilever beam under end tip loading

'Lumped', respectively. However, the one with lumped stress is more computationally efficient than the one with consistent stress. Although the one with consistent stress smoothing scheme and solving it iteratively with 3 iteration steps of Eq. (4.6) labeled as 'Consist.(3-iter)' shows convergence, it seems that it may not be reliable when only a few equilibrium iteration steps is used except that large number of iteration steps of Eq. (4.6) is applied. Based on this example, the one with lumped stress is clearly a better choice in the aspects of efficiency.

The second example is a distortion study of element geometry on a cantilever beam as shown in Figure 4.1(b). The beam is modeled by two distorted elements. Both conventional displacement and hybrid stress models have been used. Convergence studies on the tip displacement and the stretching stress σ_x at point B are shown in Figure 4.3. For the hybrid stress model, the deterioration caused by the distortion of element geometry is diminishing with equilibrium iteration by both consistent and lumped stress smoothing schemes. On the other hand, the exact solutions is recovering very slowly if the displacement model is used. Although the smoothing procedure with consistent stress is slightly better than the one with lumped stress, the smoothing procedure with lumped stress is still a better choice from the cost consideration.

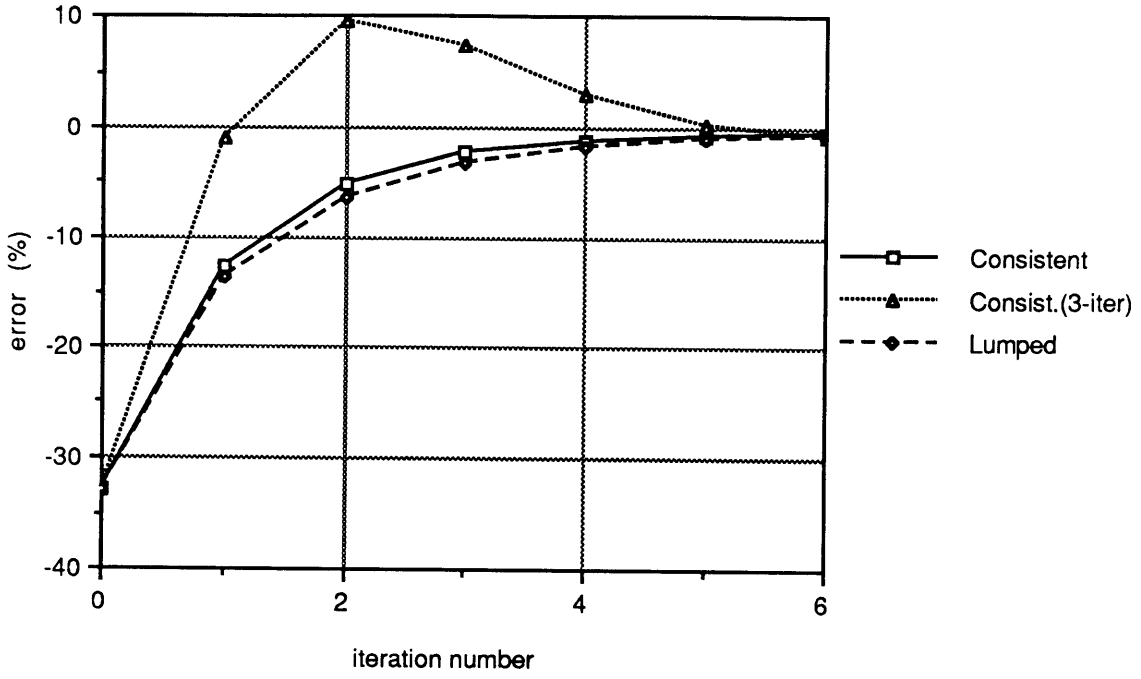

(a) tip displacement

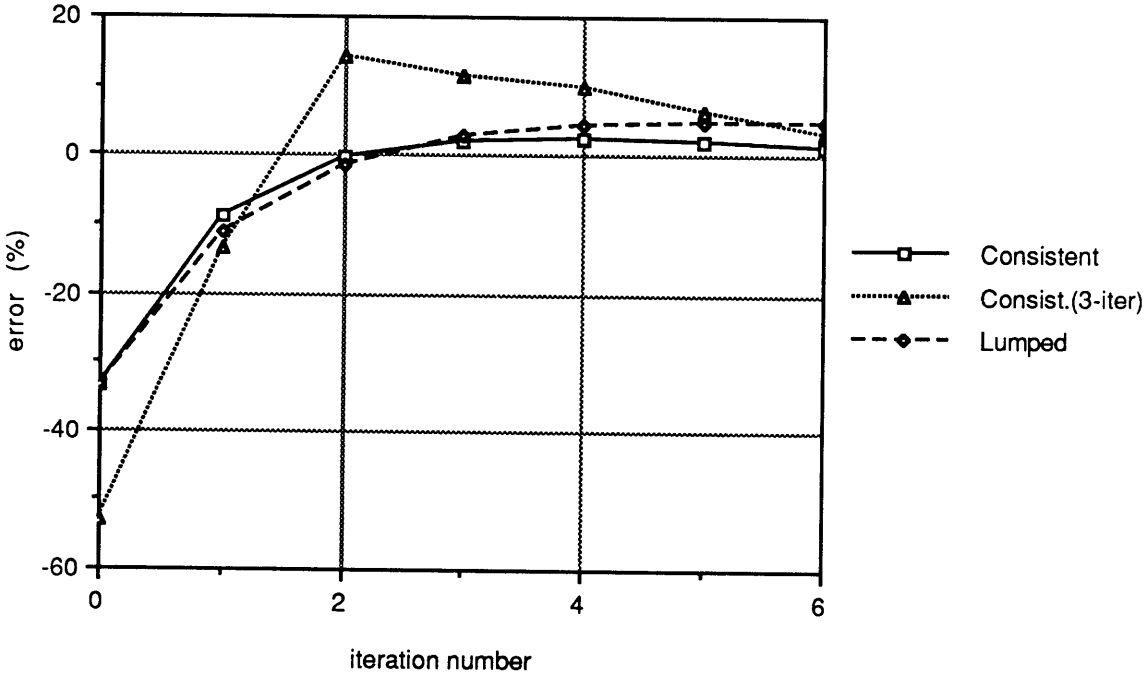

(b) inplane stress σ_x at point B

Figure 4.2 Convergence study of cantilever beam under end tip load with 10 assumed displacement elements and different smoothing schemes

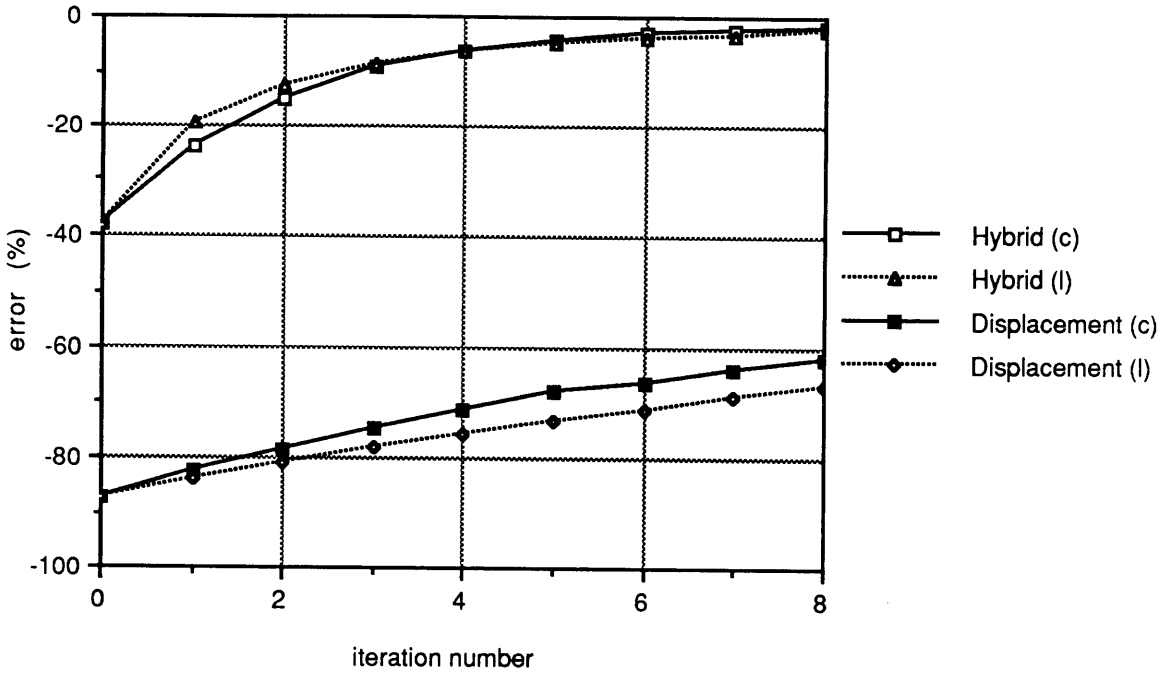

(a) tip displacement

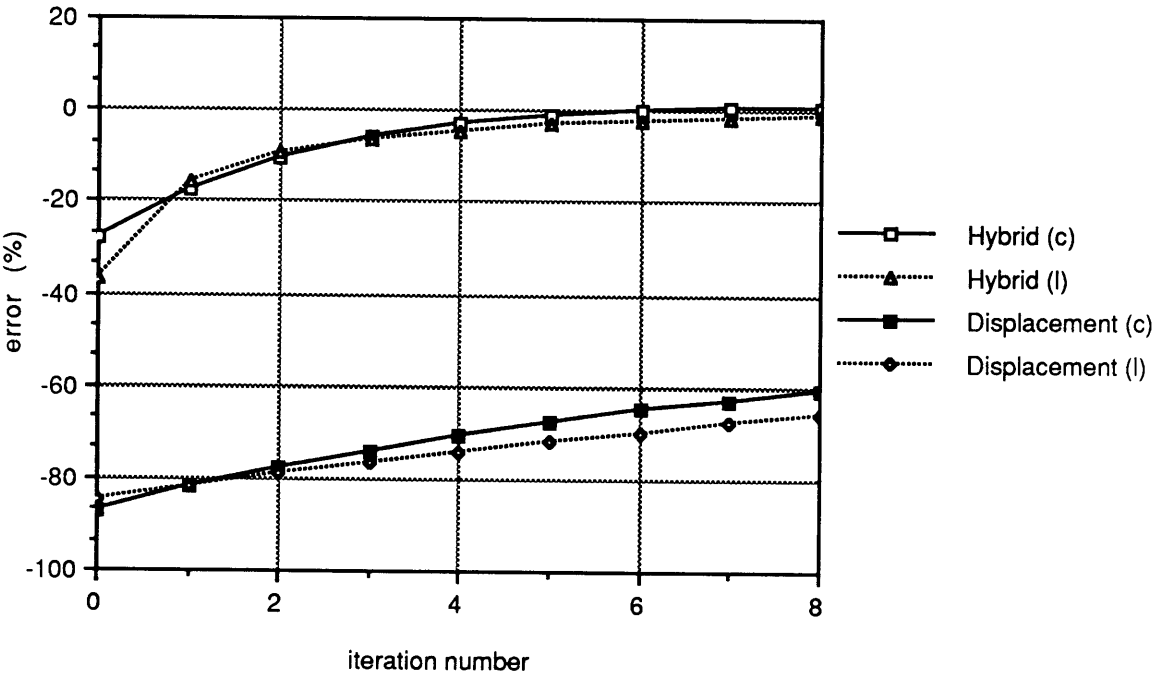

(b) inplane stress σ_x at point B

Figure 4.3 Convergence study of distortion of element geometry for cantilever beam under end tip loading

4.2.2 Finite Width Strip with a Circular Hole under Pure Tension

A finite width strip with a circular hole subjected to pure tension and the finite element model for one quarter of the structure are presented in Figure 4.4. Convergence study on the stress concentration factor at point A is shown in Figure 4.5. Reference value of the factor is 4.32p where p is the applied tensile force [115]. By applying the stress smoothing procedure, improved results again are obtained. However, they do not converge to the reference value.

On the other hand, in this example the one with lumped stress smoothing scheme leads to better results than the one with consistent stress scheme. Because almost no variation is allowed in the x direction of stress σ_x in the 4-node 5-β hybrid stress element at point A, the 'averaging' effect over the span of the element in the x direction always makes the results of the stress concentration factor less accurate than the one obtained by the assumed displacement model. On the other hand, the difference between the two models is diminishing when the stress smoothing and equilibrium iteration procedures are used.

4.2.3 Elastic Elliptic Membrane under Outward Pressure

This elliptic membrane problem is defined in Figure 4.6 and

is taken from Reference 116. Two finite element meshes, a 2x6 mesh and a 4x6 mesh, are used as shown in Figure 4.7. Convergence studies on the stress concentration at point C for mesh #1 and mesh #2 are presented in Figures 4.8(a) and 4.8(b), respectively. Equation 4.11 has been used as an indicator for terminating the iteration and the coefficient k is chosen to be 100. In this example, the one with consistent stress smoothing scheme is convergence faster than the one with $\mathbf{M}_L$. However, for the displacement model, the latter yields better results than the former. On the other hand, for the conventional hybrid stress model, the tendency is the reverse.

Results of the radial stress along side CD obtained by mesh #2 are given in Figures 4.8(c,d). Figure 4.8(c) is solutions without any stress smoothing scheme. Clearly the analysis based on the hybrid stress model is closer to the reference value cited in Reference 116 than the analysis based on the displacement model. The results obtained by the two stress smoothing schemes are shown in Figure 4.8(d). The number in the parenthesis is the number of equilibrium iteration steps being used.

Based on the four two dimensional examples, it is decided that the lumped stress smoothing scheme with the equilibrium iteration procedure is the more suitable algorithm and will be employed in the rest of this study.

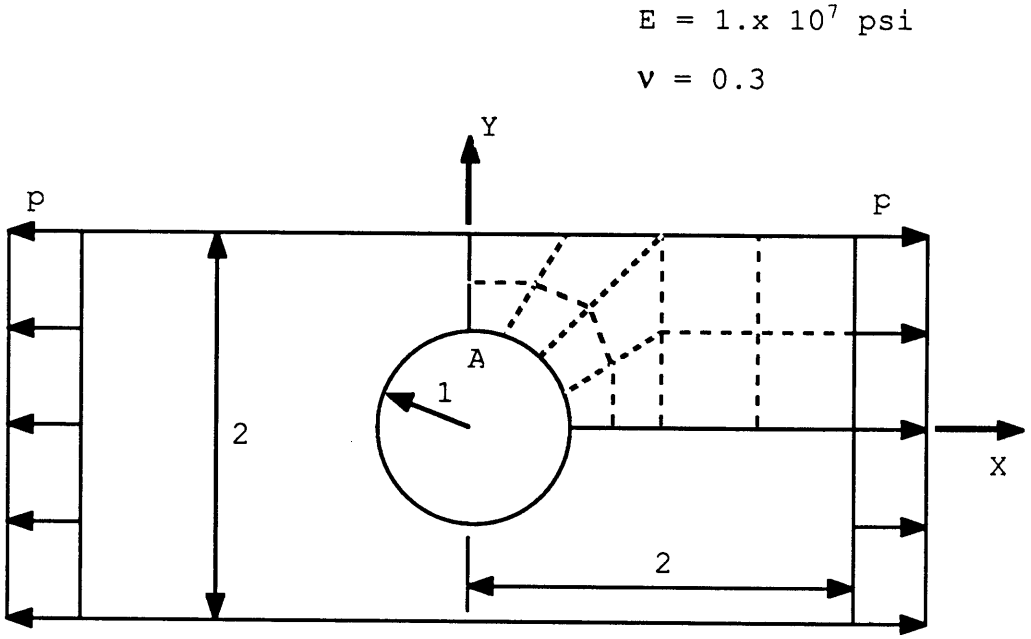

Figure 4.4 Circular hole in a finite width strip

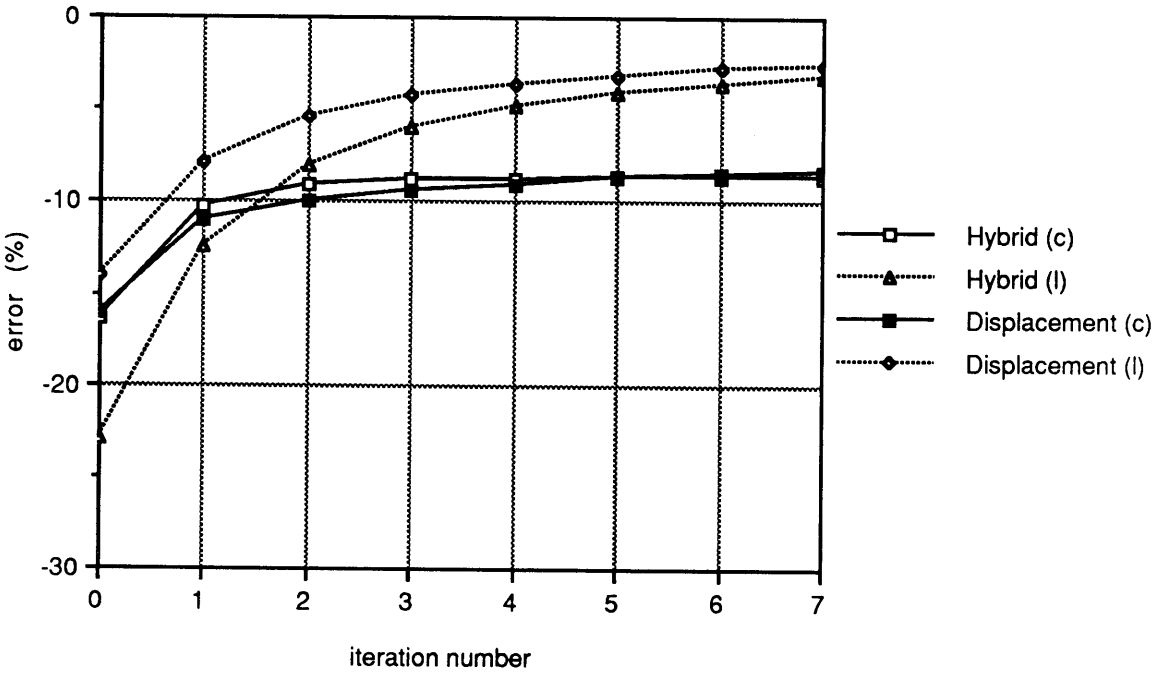

Figure 4.5 Stress concentration results for a finite width strip with a circular hole problem

$E = 210 \times 10^3$ MPa

$\upsilon = 0.3$

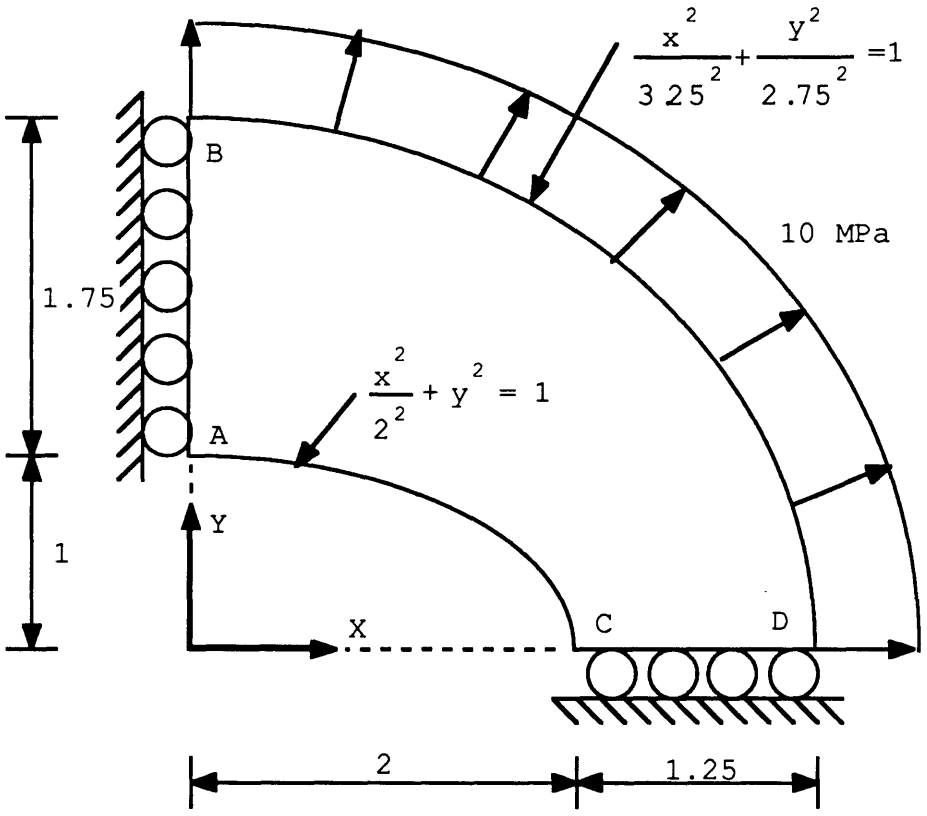

All dimensions is metres and thickness = 0.1

Figure 4.6 Elastic elliptic membrane under outward pressure

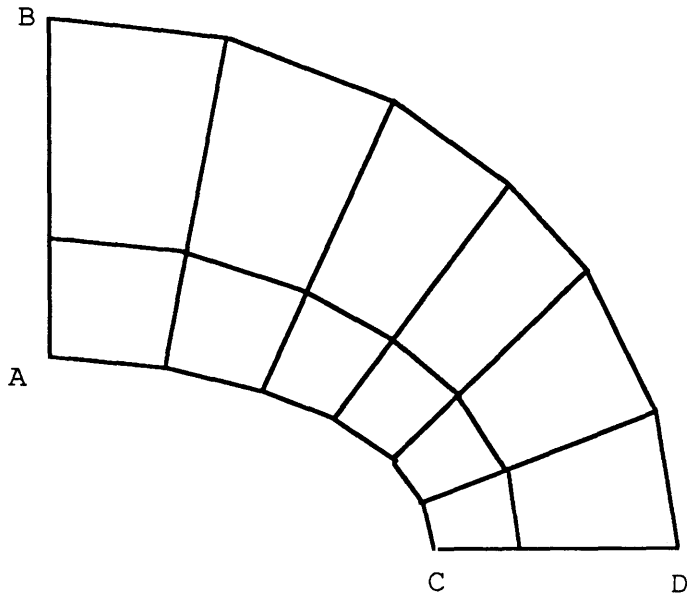

(a) mesh #1 (2x6)

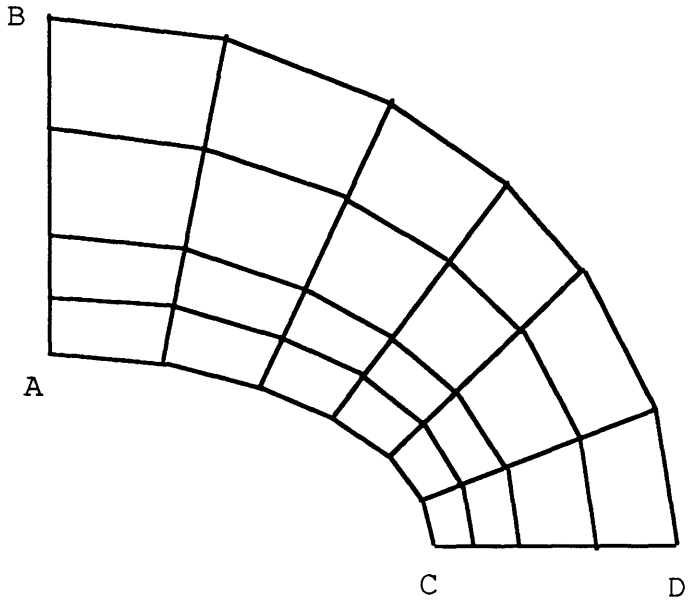

(b) mesh #2 (4x6)

Figure 4.7 Finite element model for elliptic membrane

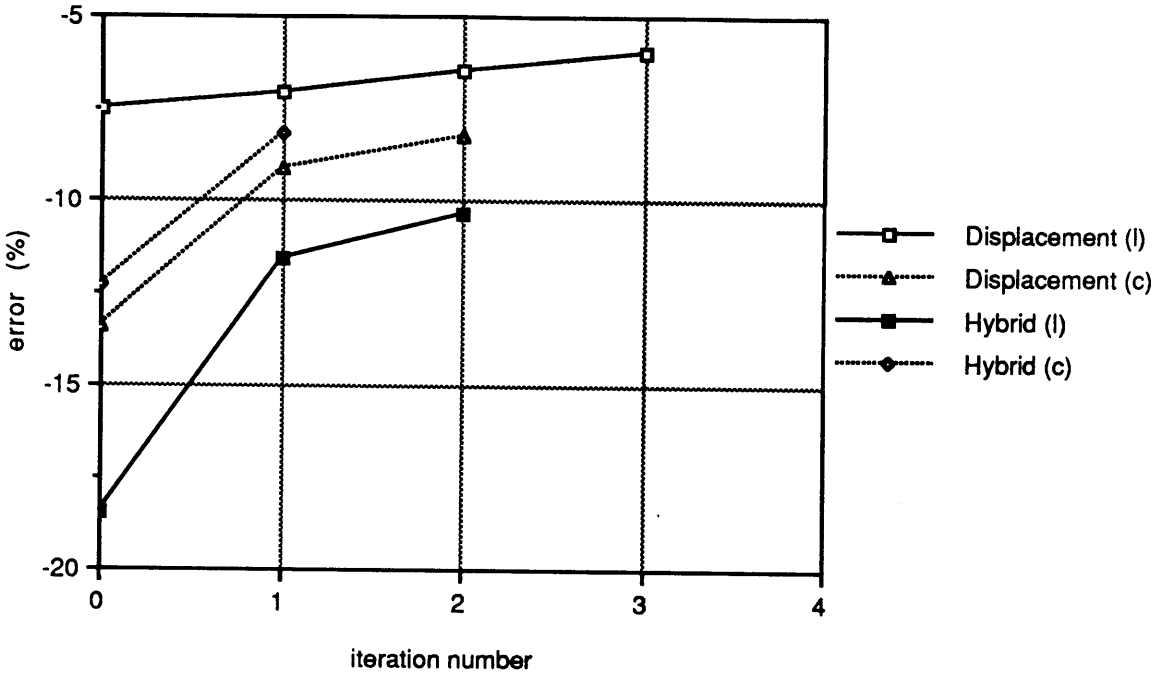

(a) tangential stress σ_θ at point C for mesh #1

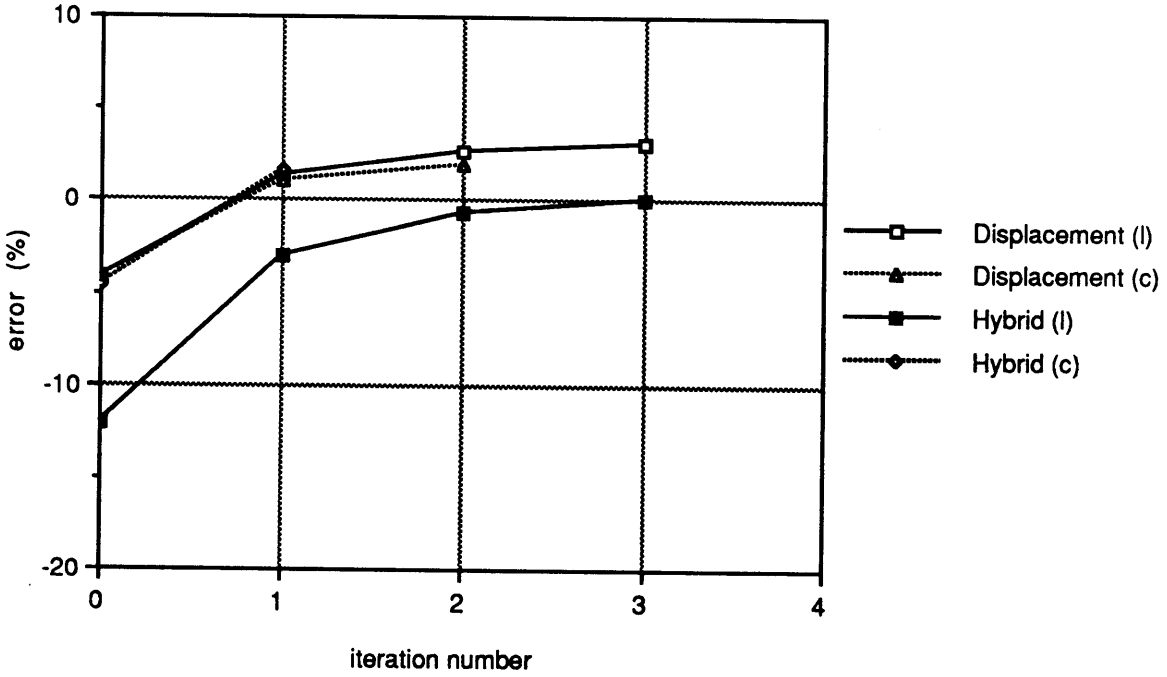

(b) tangential stress σ_θ at point C for mesh #2

Figure 4.8 Solutions of elliptic membrane under outward pressure

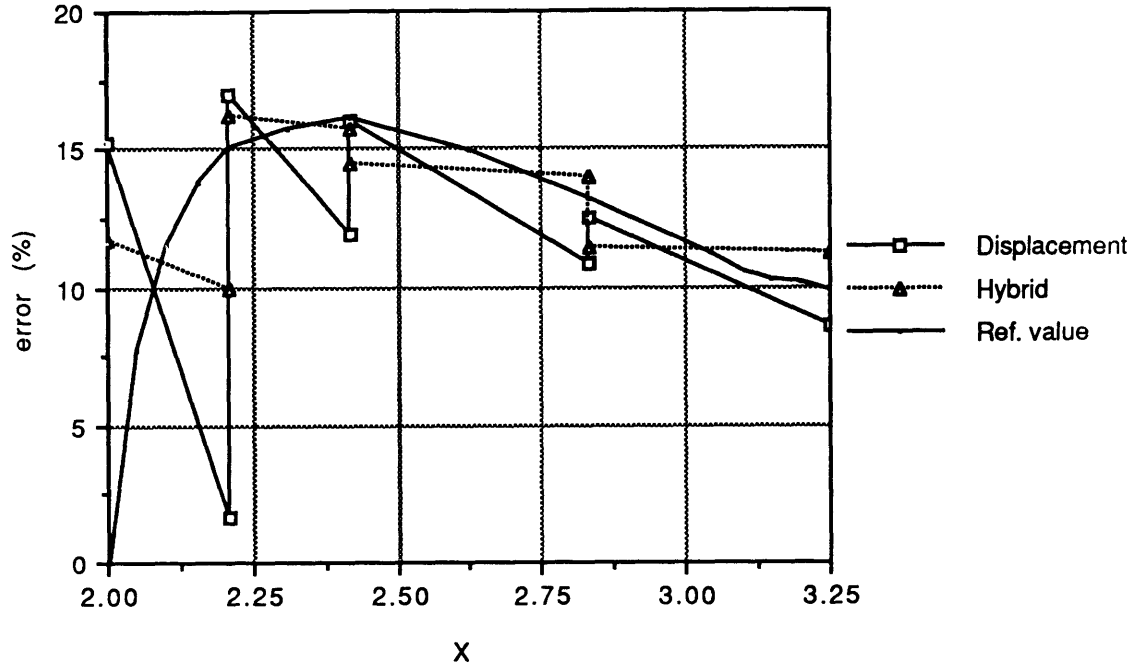

(c) radial stress σ_r along side CD for mesh #2 without iteration

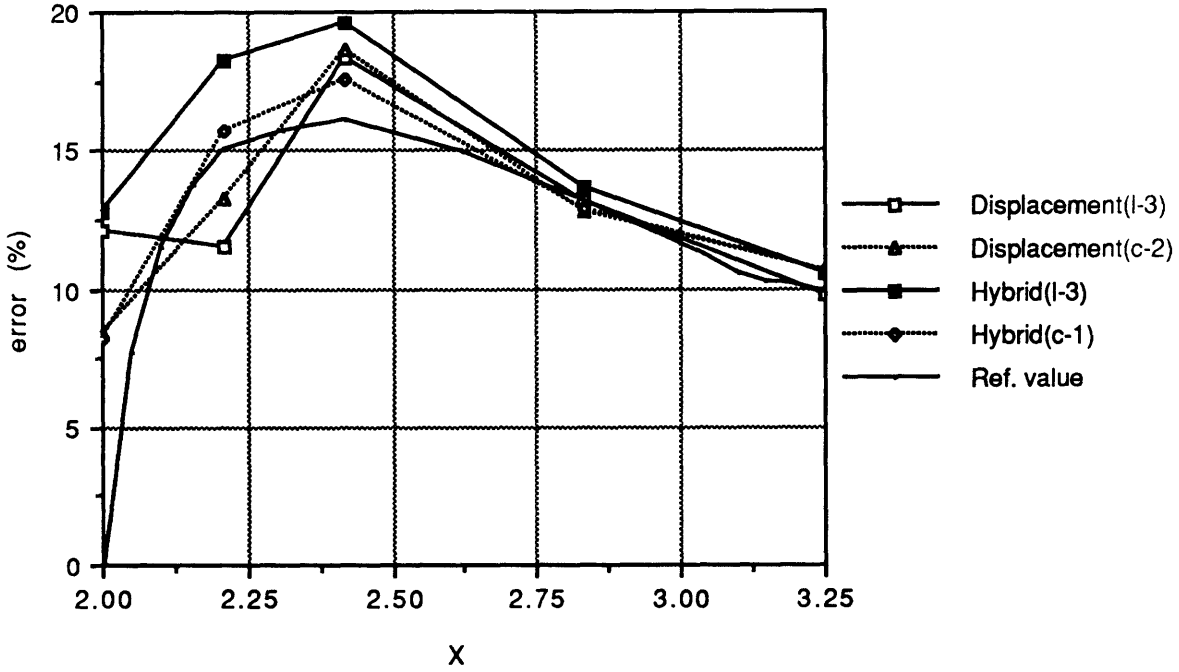

(d) radial stress σ_r along side CD for mesh #2 with iteration

Figure 4.8 Solutions of elliptic membrane under outward pressure

4.2.4 Distortion Study of Solid Isotropic Cantilever Beam under Pure Bending

To study the effectiveness of the stress smoothing for 3D solid elements with geometric distortion, the problem of bending of cantilever beam is selected. The geometry and elastic properties are shown in Figure 4.9. The tip displacement error versus the number of equilibrium iteration steps are plotted in Figure 4.10(a). The results and convergence rate are similar to those obtained in the two-dimensional distortion study (Figure 4.3). Also presented are comparisons of the resulting stretching stress σ_x, obtained with and without any equilibrium iteration procedures, along sides AC and BD which are located at the top surface of the beam. Comparison of the conventional hybrid stress model is shown in Figure 4.9(a) and comparison of the assumed displacement model, in Figure 4.9(b).

4.2.5 Anisotropic Solid Cantilever Beam under Pure Bending

MacNeal and Harder proposed a set of problems to test accuracy of finite element programs [117]. The test problems do take into account many parameters which affect accuracy, for example loading, element geometry, problem geometry and material properties. However, in the parameter of material properties, only the use of nearly incompressible material is examined.

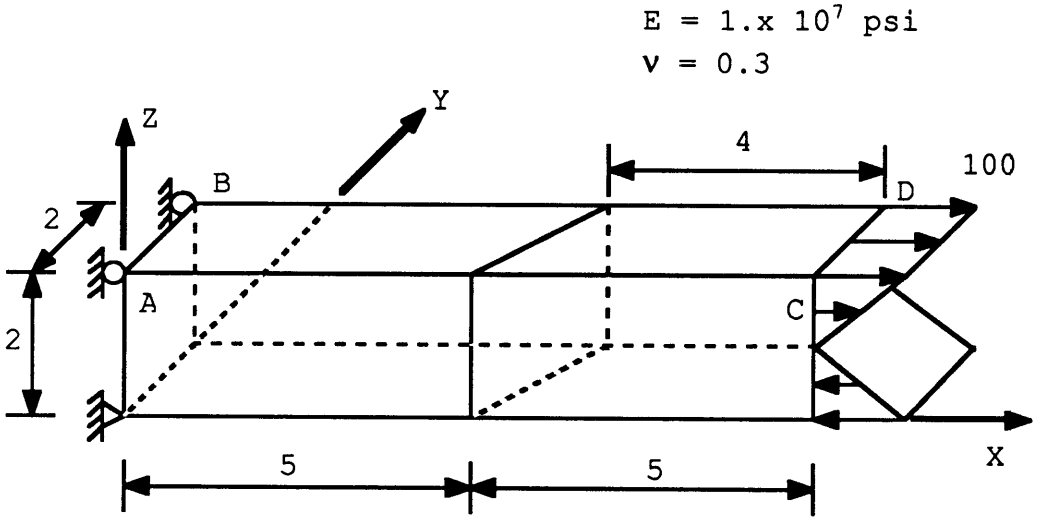

Figure 4.9 Distortion study of solid cantilever beam under pure bending

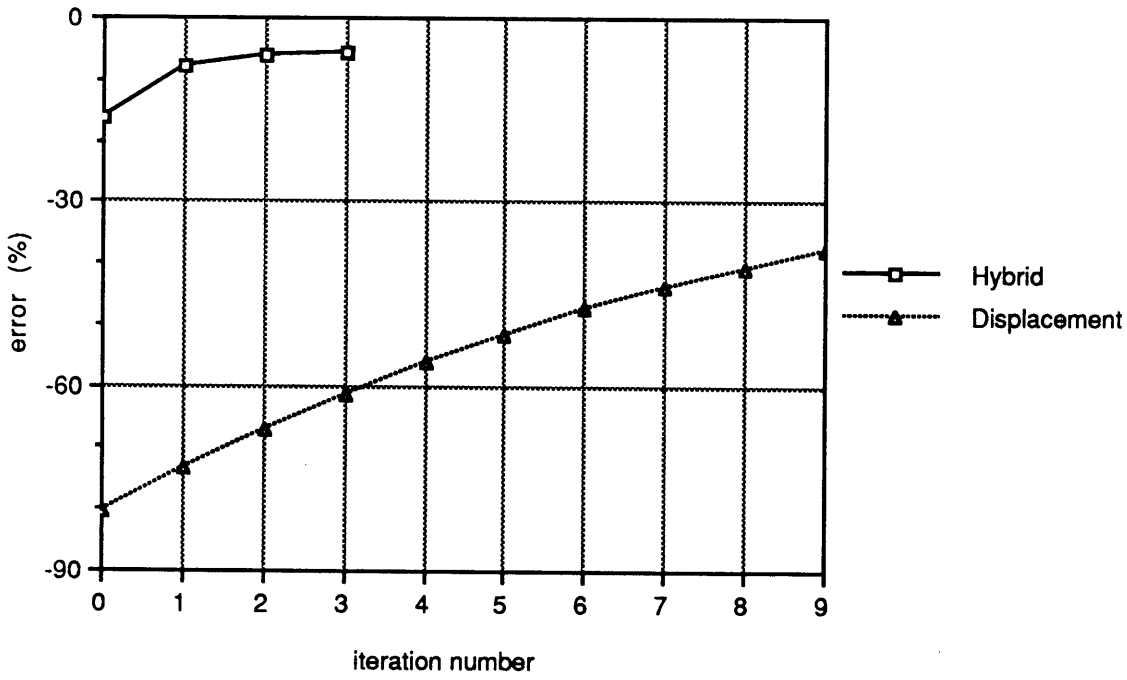

(a) tip displacment error

Figure 4.10 Solutions of solid cantilever beam under pure bending - study of effect of distortion of element geometry

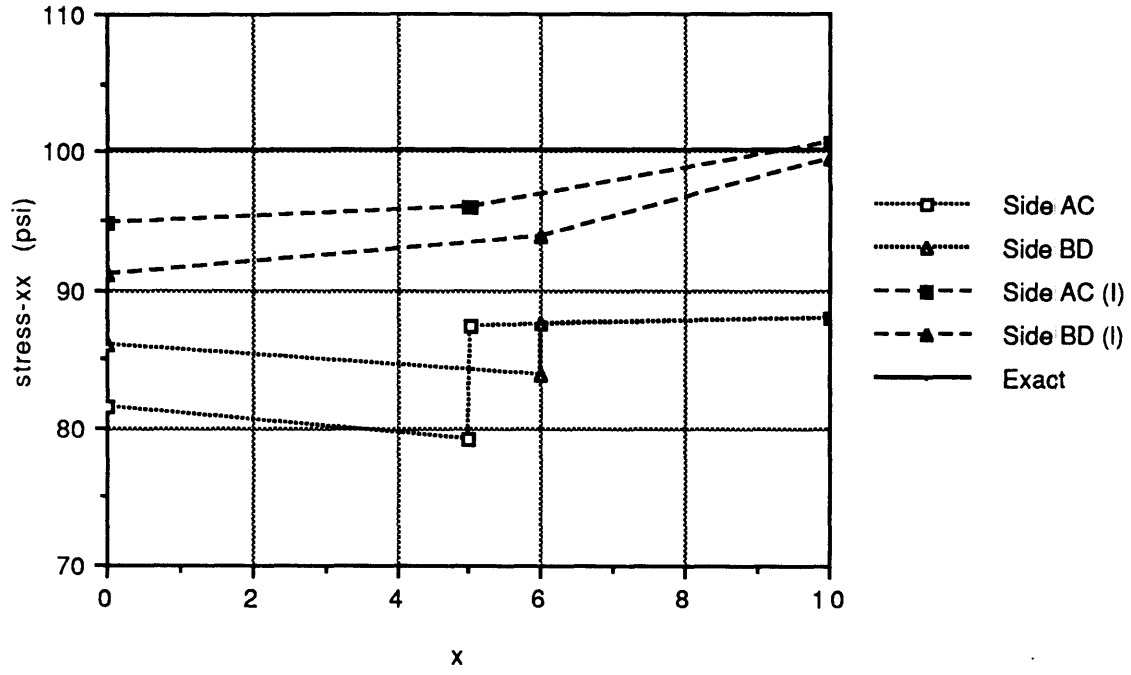

(b) inplane stress σ_x with hybrid stress element

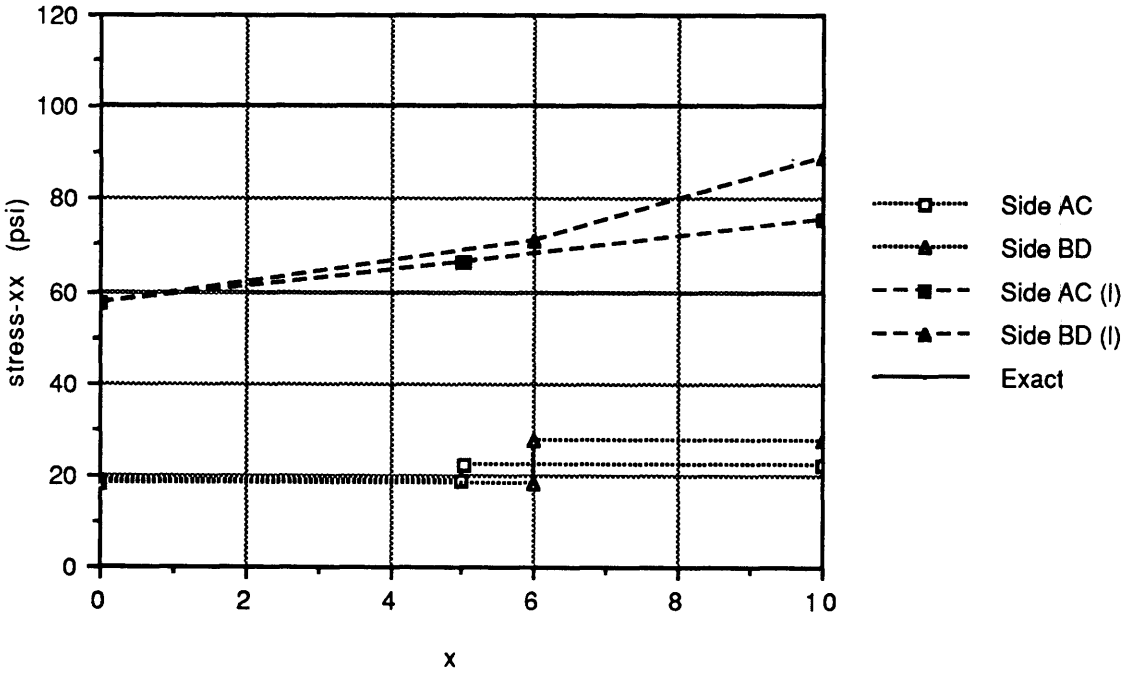

(c) inplane stress σ_x with displacment-based element

Figure 4.10 Solutions of solid cantilever beam under pure bending - study of effect of distortion of element geometry

Anisotropic material properties also plays an important role on element accuracy which have not be studied.

In this section, a primary examination of the effect of the anisotropy on the conventional assumed displacement and hybrid stress models is presented first and the study of the stress smoothing procedure in the application of anisotropic material properties will follow.

The problem is an anisotropic cantilever beam subjected to pure bending. The geometry and material properties are shown in Figure 4.11(a). Two displacement variables located at the central axis of the beam shown in Figure 4.11(b) are selected as parameters to indicate the performance of the finite element models. They are the central deflection w_c at the free end and the angle of twisting per unit of length θ_c. The elasticity solutions in Reference 88 of the problem are based on the well-known principle of Saint-Venant. It states that the restriction to warping at the fixed end is highly localized and will not affect the elasticity solutions which describe the behavior of the beam away from the support.

The error of deflection w_c versus the ply angle is presented in Figure 4.12(a). Similar to the isotropic material, when the assumed displacement model is used, the deflection w_c of the beam is constrained by the shear locking effect and the

$E_L = 25 \times 10^6$ psi

$E_T = 10^6$ psi

$G_{LT} = 0.5 \times 10^6$ psi

$G_{ZT} = 0.2 \times 10^6$ psi

$\nu_{LT} = \nu_{ZT} = 0.25$

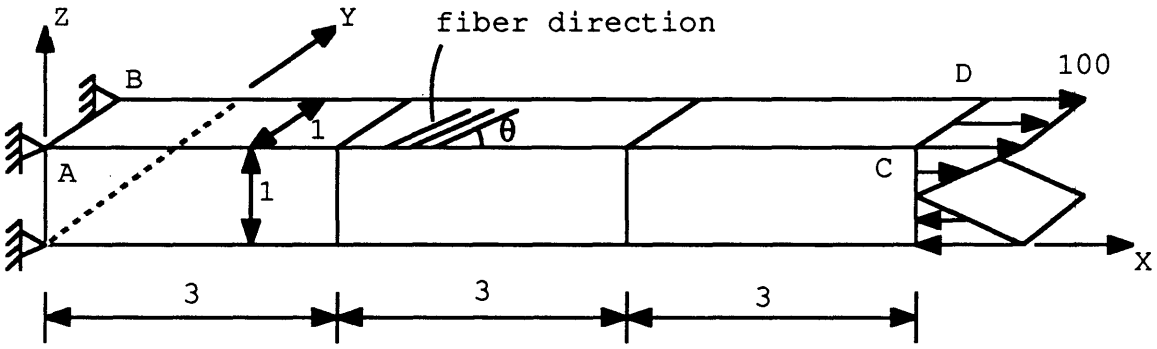

(a) geometry of the solid beam

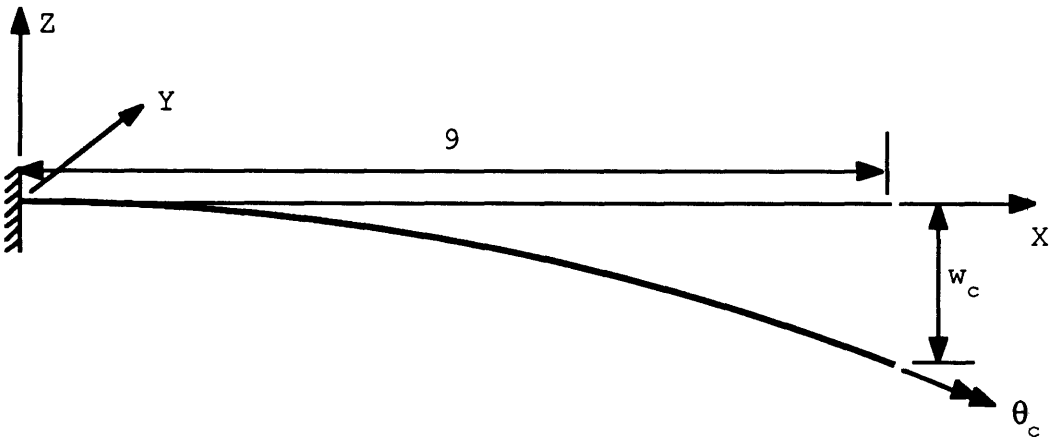

(b) displacement definition

Figure 4.11 Anisotropic solid cantilever beam under pure bending

structure becomes very rigid. On the other hand, the deflection w_c is only slightly affected in the hybrid stress model.

The degree of the shear locking is a function of the ratio of shear modulus in the xz plane to the longitudinal modulus in the x direction (S_{55}/S_{11}) as plotted in Figure 4.12(c) when the structural parameters and loading are kept unchanged. We can see that the ratio of S_{55}/S_{11} becomes smaller when the ply angle is increasing from the 0^0 and is stabilized when the ply angle reaches 30^0. When the two elastic moduli are closer to each other, more strain energy plunges into the shear strain portion compared to the bending portion. Therefore, the structure becomes more rigid when the ply angle increases and the deterioration is stabilized when the ply angle reaches 30^0.

The error of twisting angle θ_c versus the ply angle is plotted in Figure 4.12(b). If the material is isotropic, the twisting angle will be zero. Therefore, one may use this twisting angle as a parameter to justify the sensitivity of the element with respect to the anisotropy. Once again, the element based on the hybrid stress model is not sensitive to the anisotropic material properties and the element based on the assumed displacement model is. In order to maintain the same order of magnitude in the deflection and the twisting angle at the free end, the error of θ_c is normalized by multiplying a factor, |S11/S16|*(span of the beam).

When the structural parameters and loading are kept unchanged, the twist angle is only a function of the coupling elastic modulus S_{16}. The ratio of S_{16} to S_{11} is plotted in Figure 4.12(c). When the ratio of S_{16}/S_{11} is large, more twisting of the beam compared to the deflection occur. At the same time, more error occur in the assume displacement element.

In this example, we have demonstrated that the hybrid stress model is less sensitive to anisotropic material properties than the assumed displacement model. Now, we continue a study of the effect of stress smoothing and iteration procedures improve the accuracy of the analysis. We choose the structure with ply angle equal to 15^0 in this example. Convergence studies on the deflection w_c and twisting angle θ_c are shown in Figure 4.13(a) and 4.13(b), respectively.

Since the errors of the results obtained by the hybrid stress model are small, the improvements by the stress smoothing and iteration schemes are insignificant. On the other hand, the errors of the results obtained by the assumed displacement model do improve significantly when the smoothing procedure is used. Within ten iteration steps, the error of deflection w_c reduces four times from the beginning 46% error and the error of twisting almost disappears from the beginning 37% error. Once again, the results demonstrate that the exact solutions are not guaranteed by applying the iteration procedure.

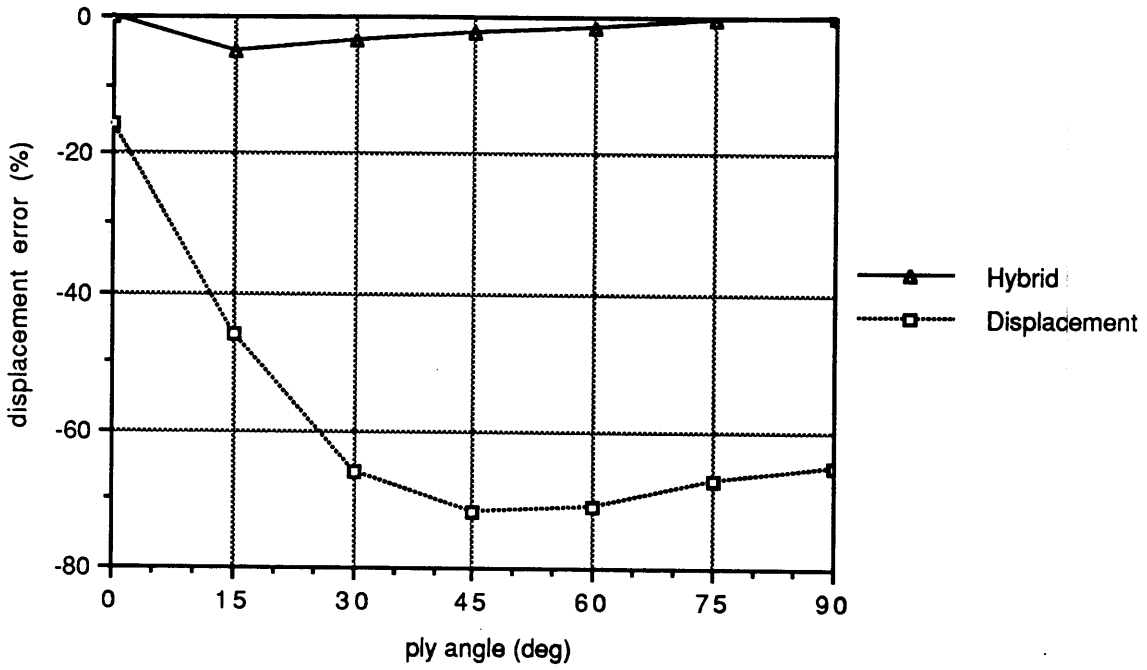

(a) central axis displacement w_c at the free end

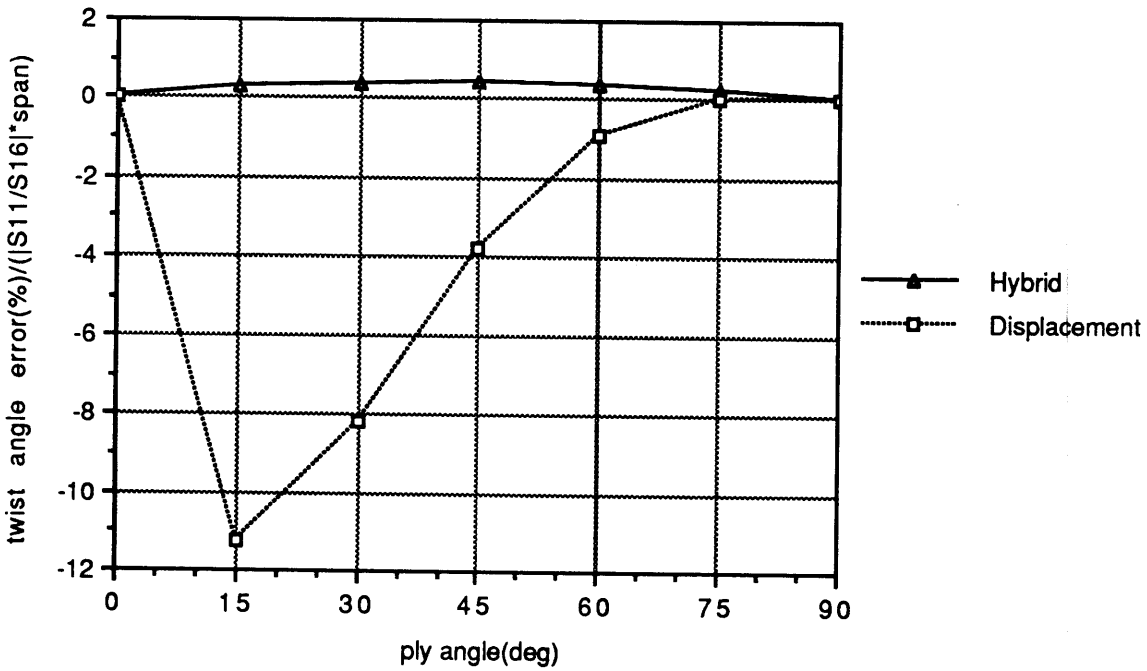

(b) normalized angle of twisting per unit of length θ_c

Figure 4.12 Solutions of anisotropic solid beam under pure bending - study of effect of anisotropic material properties

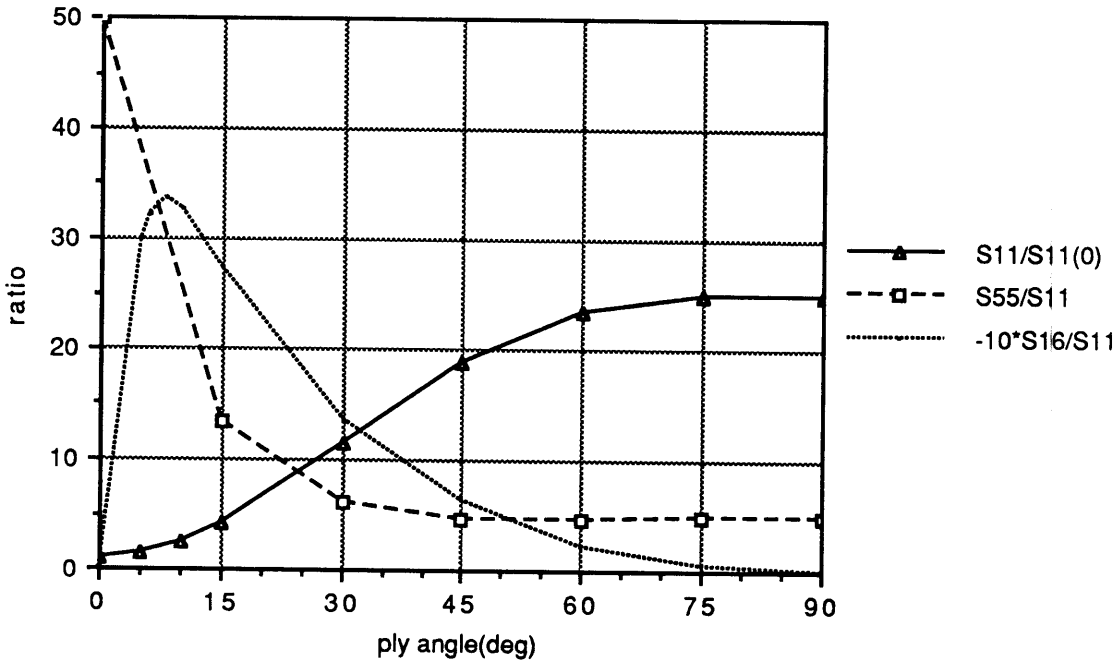

(c) ratio of elastic properties

Figure 4.12 Solutions of anisotropic solid beam under pure bending - study of effect of anisotropic material properties

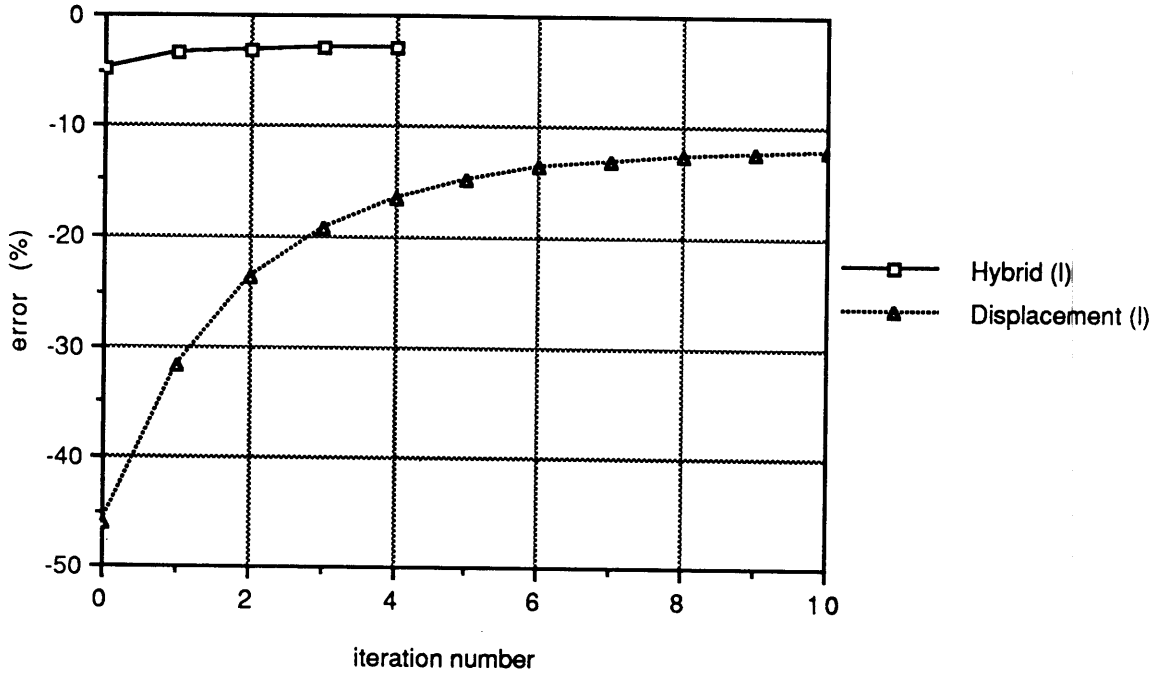

(a) central axis displacement w_c at the free end

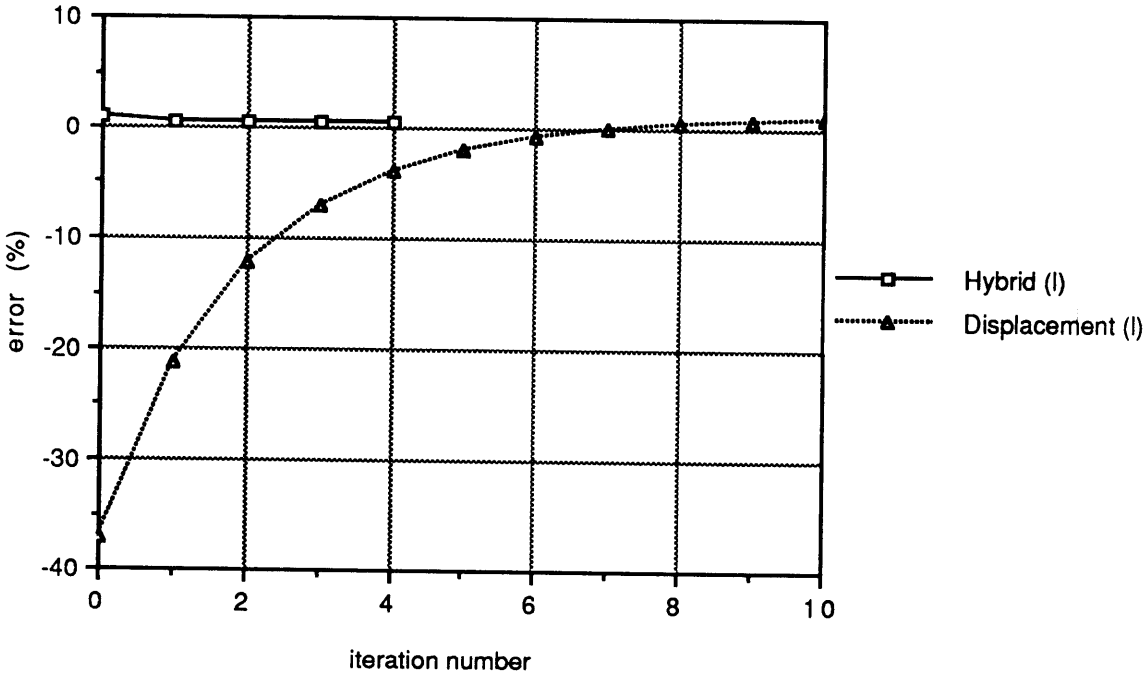

(b) angle of twisting per unit of length θ_c

Figure 4.13 Convergence study of anisotropic cantilever beam under pure bending with ply angle = 15^0

4.2.6 Two-layer Cross Ply Laminate under Cylindrical Bending

Application of the smoothing and iteration schemes for maintaining the continuity of inplane strain and transverse stress conditions along the interlaminar boundaries is studied here. A two-layer cross ply laminate subjected to cylindrical bending which has been studied previously is used. The geometry of the problem, the material properties of the laminate and the finite element model are shown in Figure 3.6. However, only 5 finite element mesh is used instead of 10. The results obtained by the new mixed form type II ity=3 hybrid stress sub-element are chosen as reference solutions while compared to iterative results. Each layer is modeled by one sub-element as previously.

In order to compare the accuracy and the efficiency with similar orders of degrees of freedom through the thickness direction of the layer and the span of the laminate, each layer is modeled by three 4-node 5-β hybrid stress elements in the direction of the thickness and five elements in the direction of the span as shown in Figure 4.14.

As the previous chapter, the numerical results are presented in terms of normalized values which are defined in Eq. (3.64) and the ones obtained by the new mixed form type II ity=3 hybrid stress sub-element are labelled as 'Hybrid (ity=3)'. Results obtained by the conventional hybrid stress model without

any iteration scheme are labelled as 'Hybrid (w/o)' and the ones with lumped inplane strain and transverse stress smoothing scheme and three equilibrium iteration steps are labelled as 'Hybrid (w)'. The computational efforts of the one with the mixed form elements and the one with iteration scheme are almost the same as each other. On the other hand, the computational effort of the one without any iteration step is about one half of those of the two other methods.

The results of the inplane stress σ_x shown in Figure 4.15(a) do not indicate any significant differences between the three methods and the elasticity solution. However, the results of the two transverse stresses τ_{xz} and σ_z obtained by the mixed form high order hybrid stress plate element show better accuracy than those obtained by the conventional hybrid stress elements with and without any iteration scheme as shown in Figure 4.15(b) and 4.15(c). Although the model with iteration scheme trends to recover the shapes of interlaminar stress distributions of the elasticity solutions and the traction free conditions at the top and bottom surfaces of the laminate, its accuracy is limited by the assumption of linear smoothed stress field $\mathbf{t}_t^*$ within each element.

The results show that for computing the interlaminar stress distributions through the thickness of the laminates the previous mixed form of high order hybrid stress laminated plate element is a better choice.

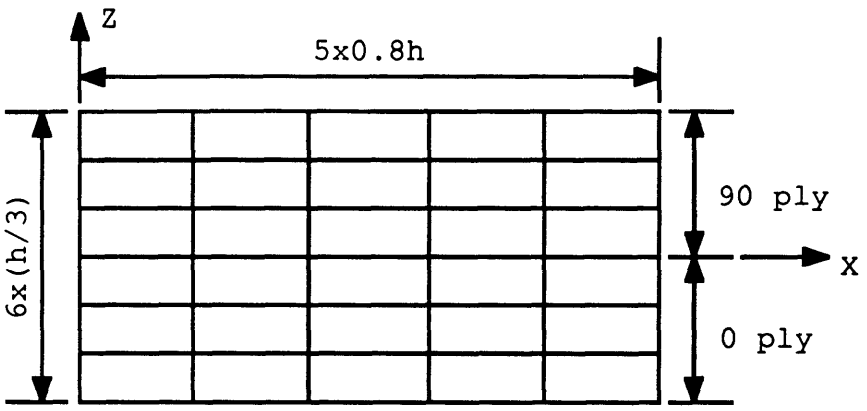

Figure 4.14 Finite element mesh for a 2-layer $[90/0]_T$ laminate at L/H=4 under cylindrical bending with partial stress and strain smoothing schemes

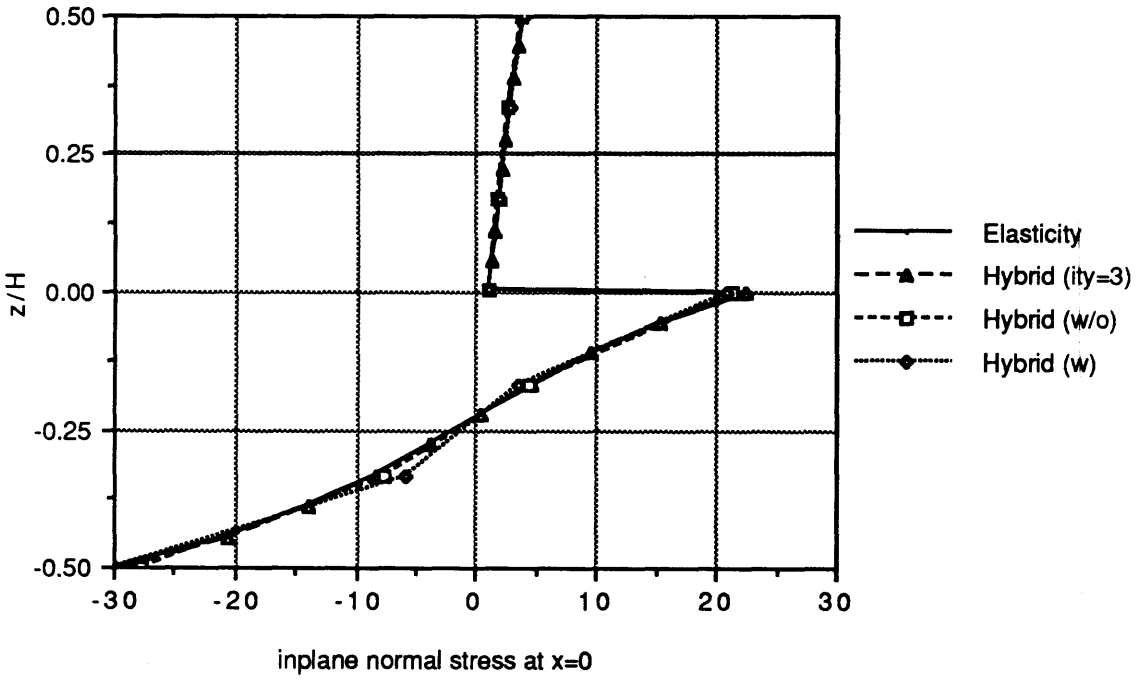

(a) inplane normal stress $\bar{\sigma}_x$ (L/2, z/H)

Figure 4.15 Solutions for a 2-layer $[90/0]_T$ laminate at L/H=4 with partial stress and strain smoothing schemes

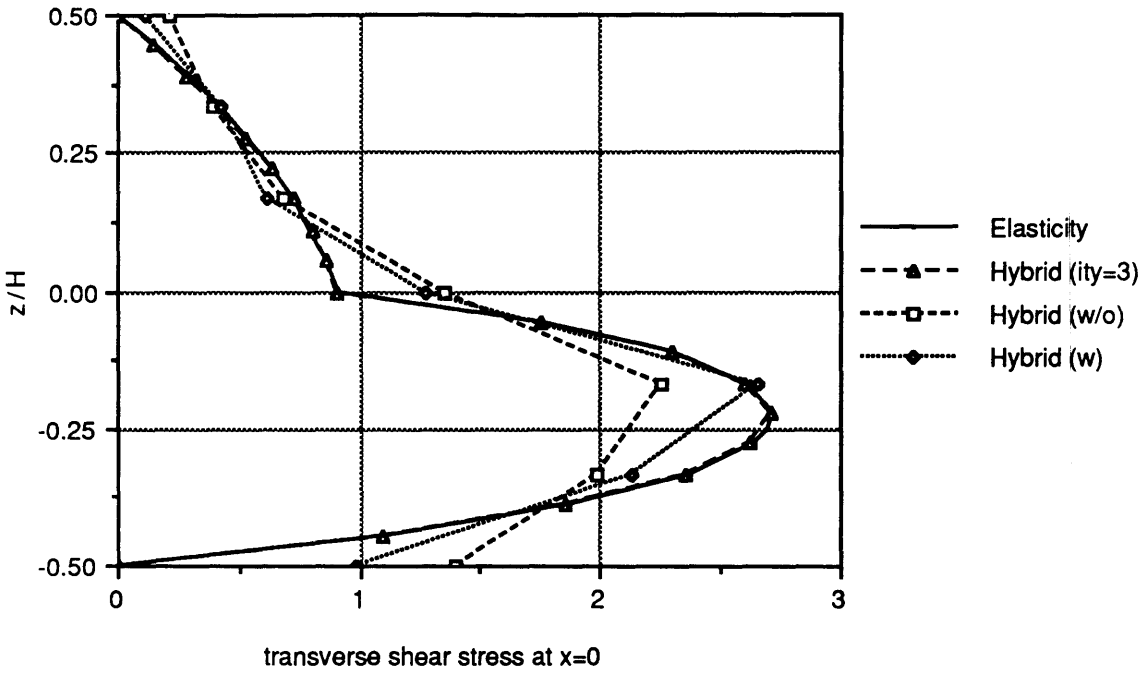

(b) transverse shear stress $\bar{\tau}_{xz}$ (0, z/H)

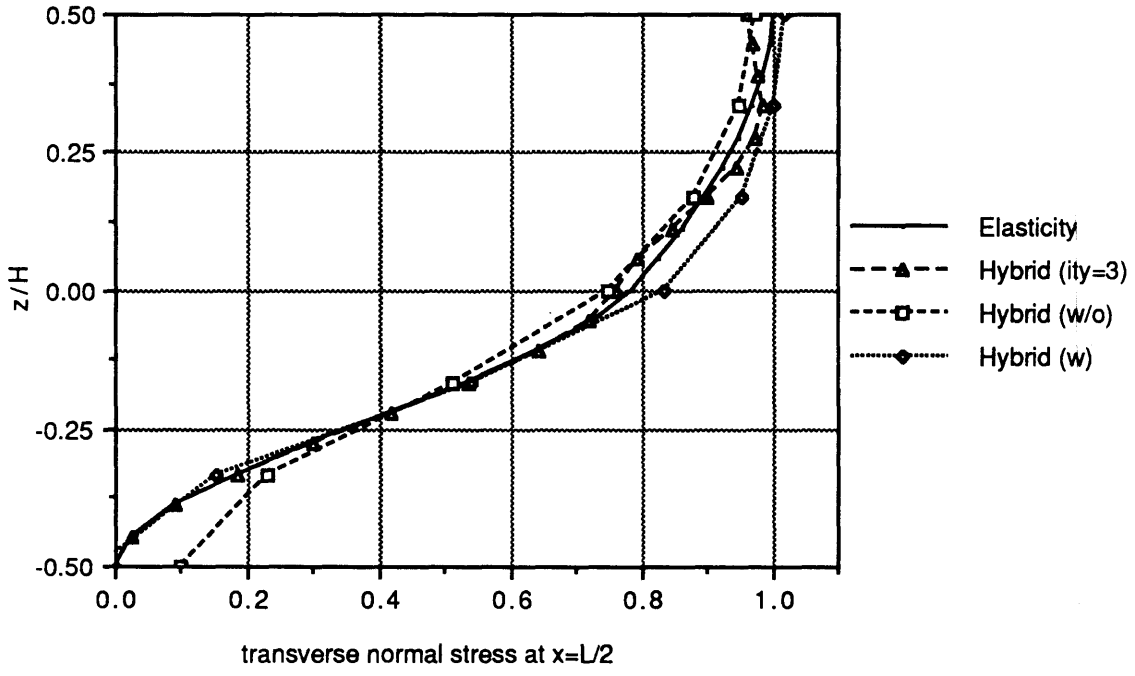

(c) transverse normal stress $\bar{\sigma}_z$ (L/2, z/H)

Figure 4.15 Solutions for a 2-layer $[90/0]_T$ laminate at L/H=4 with partial stress and strain smoothing schemes

4.3 Summary and Discussion

The application of the smoothing and iteration procedure based on the conventional hybrid stress model for maintaining continuity along the inter-element boundaries of the laminates does not appear to have better accuracy than the one with the mixed form of high order hybrid stress laminated plate elements under the same computational effort.

The results have demonstrated that the shear locking phenomenon, the deterioration caused by the element distortion and the effect of anisotropic material properties can always be relieved at least partially if not completely by the stress smoothing and equilibrium iteration procedures. The consistent stress smoothing scheme does not appear to be superior to the lumped stress smoothing scheme. Furthermore, the lumped scheme is more computationally efficient than the consistent one. Therefore, the lumped smoothing scheme should be used rather than the consistent scheme. On the other hand, they do not guarantee that the results will converge to the exact solutions.

Loubignac and his colleges [109,110] suggested that the use of actual boundary stresses instead of nodal stress parameters **p** obtained by smoothing at nodal points located on the boundary of the structure will speed up the convergence. They have used a thick cylinder loaded with a uniform pressure as an example to

support their statement. However, enforcing the actual traction free boundary condition along the circular arc in the previous example of a strip with a circular hole, the results are deteriorated rather than improved. It is because the inbalance forces in Eq. (4.9) along the boundaries which are based on the difference between the smoothed stress field $\boldsymbol{\sigma}^*$ and $\mathbf{Q}$ trend to recover the actual boundary force conditions. If the actual boundary stresses instead of the computed nodal stress parameters $\mathbf{p}$ are used, the forces which trend to recover the actual boundary conditions disappear and the results may be deteriorated rather than improved.

On the other hand, in problems of plasticity and geometry nonlinear analysis, the present algorithm will be highly efficient because the iterations can be done simultaneously with those required by the non-linearity.

CHAPTER FIVE

GLOBAL AND LOCAL FINITE ELEMENT METHOD

Finite element analysis of a structure with a crack or cut-out requires large number of elements in the regions of steep stress distribution if conventional assumed displacement or hybrid stress elements are used, and thus, consequently, a great amount of computational effort. To reduce the effort, one can use elements that satisfy exactly the traction boundary condition on the surface of a crack or a cut-out with some forms of analytical asymptotic solution in the assumed stress field as cited at the end of chapter two. However, elements based on the new mixed formulation are impossible to impose any traction boundary condition on the inplane stresses because the assumed stress field in the new mixed form does not include any inplane stresses.

Alternatively, one can use some forms of 'global-local' technique [50,70,118-120] to reduce the cost of computation.

For example, in the application of finite element analysis, Wang and Crossman [50] proposed a 'sub-structuring' technique and in the application of laminated plate theory, Pagano and Soni [70] suggested a 'global-local' laminate model to study the

edge problems of laminates. Both schemes have been reviewed in chapter two and will not be repeated here.

Luckings, Hoa and Sankar [120] employed a scheme that is similar to 'sub-structuring' technique [50] to analyze laminates with circular holes. The solutions were obtained in three steps. The first step is a global analysis in the whole structure using a coarse mesh. The second step is a analysis of a smaller local region with refined finite element meshes using the global displacement solutions as boundary conditions for the local region. The third step is to apply the local analysis one more time with further smaller region and refined mesh. Satisfied accuracy in the region of interest near the hole was achieved. The three-step scheme is designated as multi-step global-local finite element method in this study.

Sun and Mao [118] suggested a scheme that is similar to multi-step global-local finite element method [120] in the analysis of a structure with the application of parallel computations. The computing scheme consists of two steps of computation. The first step is a global displacement analysis which is the same as the global analysis of the multi-step global-local finite element method. The second step is the stress analysis of some smaller local regions which are the regions of interest with refined finite element meshes. The computations of the local regions are performed simultaneously on different processors in the computer to save the

computational effort. They have demonstrated the advantages of using the 'global-local' scheme in the stress analysis of a thick laminated beam and a center-crack panel.

Dong [119] presented another kind of global-local finite element method to reduce the number of degrees of freedom. The scheme is to simultaneously utilize the conventional finite element method which has the capability in modeling complicated geometry and inhomogeneous materials with the classical Rayleigh-Ritz approximations which involve far less computation than the finite element method for achieving a comparable level of accuracy in a simply-shaped domain. Structures are divided into some subregions which are modeled by either the finite element method or the Rayleigh-Ritz approximation. The continuity of displacements between dissimilar subregions is enforced by means of constraint equations and the governing equations of motion are derived based on the Hamilton principle. The advantage of this approach has been demonstrated in a fracture mechanics problem and problems involving a far field.

The computational efficiency and accuracy of the application of the multi-step global-local modeling technique with the conventional and mixed form hybrid stress laminated plate elements to laminated plate problems will be examined here. The problems which have been selected in this study are the stress analysis of laminates with straight or curvilinear free edges.

5.1 Multi-Step Global-Local Finite Element Method

As cited in Reference 120, the multi-step global-local finite element method consists of at least two steps of computation. The first step is the global analysis of the whole structure. A coarse mesh is used in most of the structure and a slightly finer mesh is employed in the local region which includes the region of interest and its surrounding area as shown in Figure 5.1(a) where the shaded area is considered as the region of interest. The second step is local stress field analysis with a much more refined mesh in the local region with the global displacement solutions as prescribed displacement boundary conditions along the interfaces between the global and local regions as shown in Figure 5.1(b). Additional local analyses can be performed if higher accuracy in the region of interest is sought.

As suggested by Sun and Mao [118] and illustrated in Figure 5.1, in order to minimize errors in the global solutions propagated into the local analysis, the local region should be at least one element away from the region of interest as shown by the region CDFE.

After the mesh in the local region is refined, additional nodal degrees of freedom are introduced. The prescribed

displacements at the refined nodes, for example along the edges CD and DF in Figure 5.1(b), are obtained by employing the shape function of the original finite element used in the global analysis. Therefore, for the local analysis, the displacements at nodes between two original global nodes are completely determined by interpolation.

Displacement boundary conditions rather than stress conditions are used along the edges between the global and local regions because numerical studies have indicated that the displacement field converges more rapidly than the stress field in the finite element analysis.

On the other hand, if displacement and traction boundaries of the original structure are also part of the boundaries of the local region, for example edges CE and EF in Figure 5.1(b), then the actual boundary conditions should be used in the local analysis rather than the solutions obtained by the global study.

5.2 The Straight Free Edge Problem

To assess the accuracy and effectiveness of the multi-step global-local finite element method with the conventional and mixed form hybrid stress laminated plate elements to laminated plate problem, the straight free edge problem of a composite laminate subjected to uniform inplane strain is chosen as the

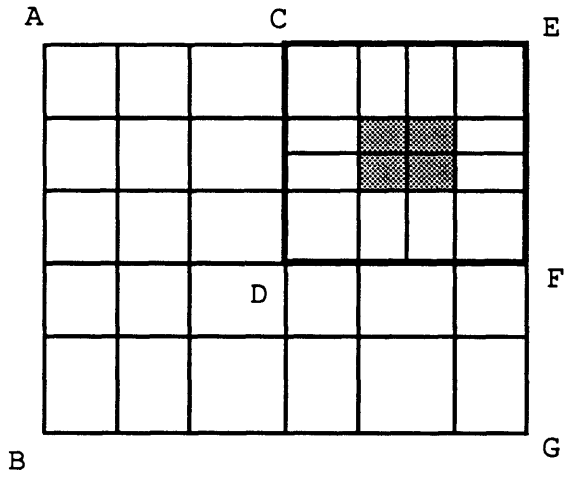

(a) global finite element mesh

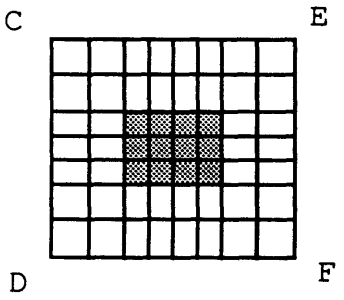

Boundary conditions of local analysis:
Sides CE and EF --
displacement or force boundary conditions from the original structure
Sides CD and DF --
precribed displacement boundary conditions derived from the global solutions

(b) local finite element mesh

Figure 5.1 Multi-step global-local finite element method

first example (Figure 5.2). Results for this kind of problems have been presented by a number of investigators [46-57, 59-61, 63-65, and 67-74] and have been reviewed in chapter two. The majority of analytical and numerical studies are based on modeling each layer as a homogeneous anisotropic material. A more realistic approach from the micromechanics veiwpoint is to provide a thin matrix interply at the interlaminar boundaries. The effect of the presence of the matrix thin layer will also be investigated here in the local analysis. The material properties for each lamina and the matrix thin layer which is assumed to be isotropic are also shown in Figure 5.2.

5.2.1 Global Analysis

The laminate to be analyzed is a four layer symmetric cross-ply structure $[0/90]_s$ with layers of equal thickness and shown in Figure 5.3(a). Because of the symmetry about the y and z axes, it is only necessary to consider one quadrant of an x=constant plane. A global finite element analysis is carried out over the upper right quadrant and the mesh is shown in Figure 5.3(b). Along the z-axis, the displacement v is zero on the z axis and along the y-axis, the displacement w is zero.

Two studies have been made. One is employed the conventional hybrid stress plate element and the other employed the present mixed form hybrid stress plate element. Each layer

laminate material properties:

$E_L = 20.0 \times 10^6$ psi

$E_T = 2.1 \times 10^6$ psi

$G_{LT} = G_{ZT} = 0.85 \times 10^6$ psi

$\nu_{LT} = \nu_{ZT} = 0.21$

matrix material properties:

$E = 0.5 \times 10^6$ psi

$\nu = 0.35$

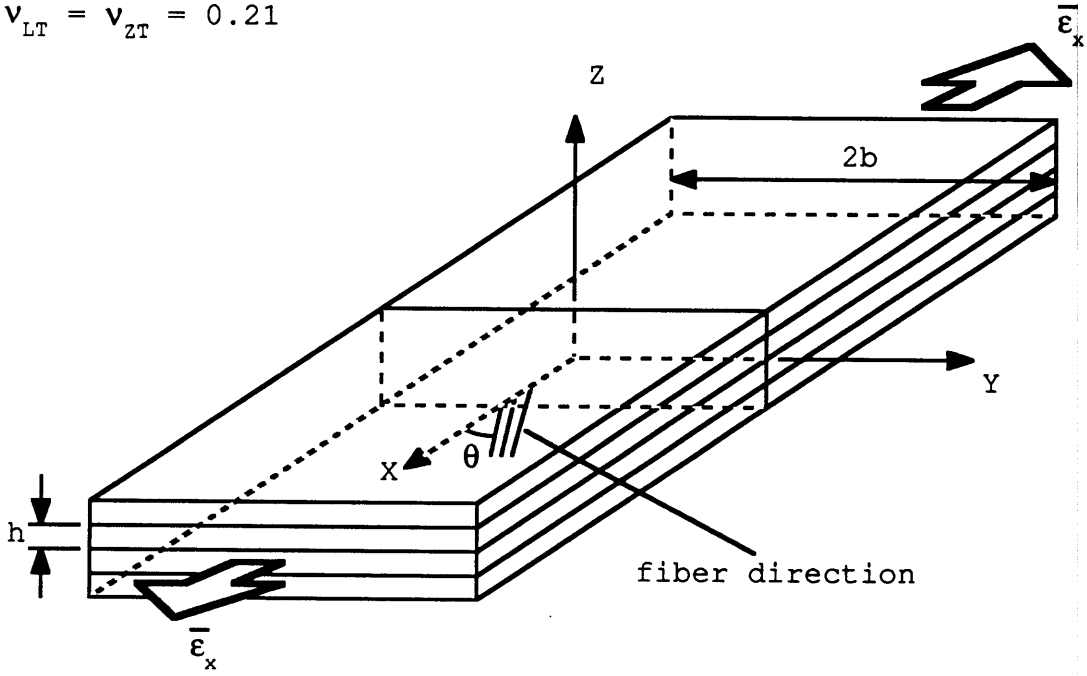

Figure 5.2 Configuration of laminate subjected to uniform inplane strain $\bar{\varepsilon}_x$

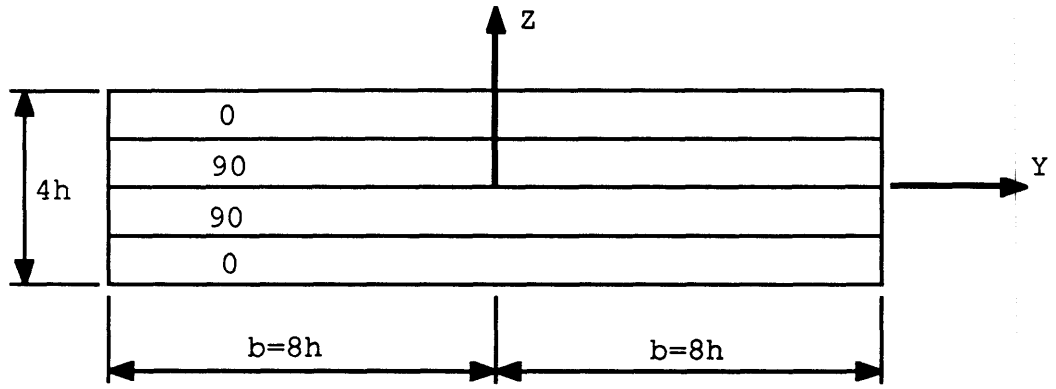

(a) plane view of a four-layer laminate

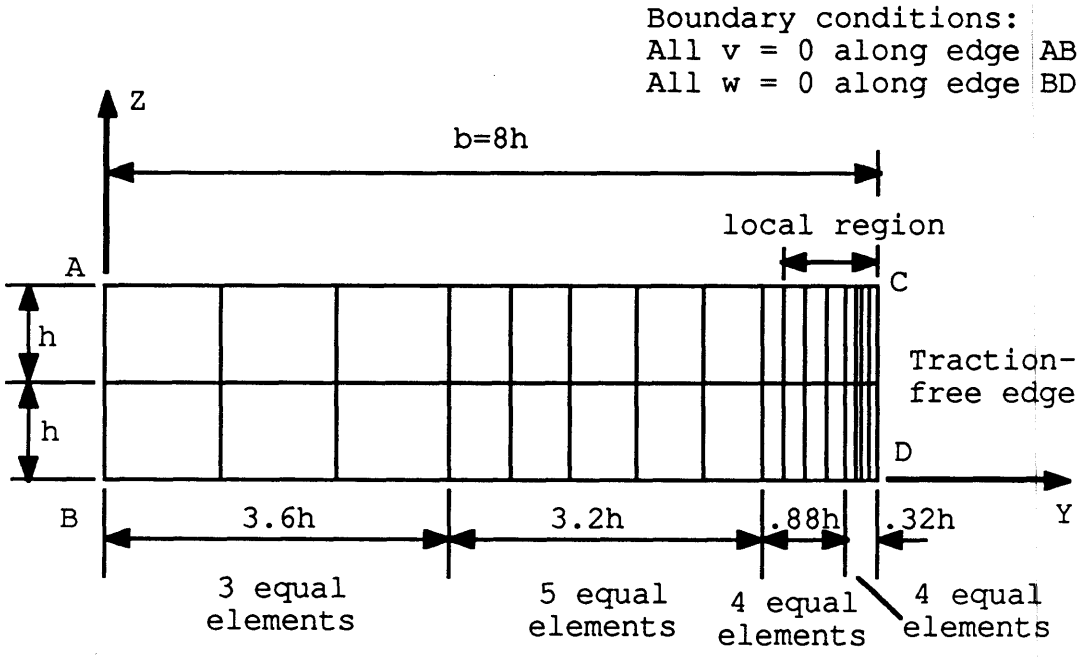

(b) two-layer finite element model

Figure 5.3 Geometry and finite element model of a $[0/90]_s$ laminate for the global study

is modeled by one 2D type II ity=3 hybrid stress sub-element (Figure 3.5.c). The number of stress parameters β used for each layer is fourteen in the last two rows of Eq. (3.63.a) and one additional term in order to suppress the kinematic modes for the mixed form 2D type II ity=3 hybrid stress sub-element. It is

$$\begin{bmatrix} \tau^{23} \\ \tau^{33} \end{bmatrix}^i = \begin{bmatrix} \zeta_i^2 (1-\zeta_i^2) \\ 0 \end{bmatrix}^i \beta_{15}^i \qquad (5.1)$$

For the conventional 2D type II ity=3 sub-element, it is the all seventeen β's in the equation of (3.63.a) and two additional terms for suppressing the kinematic modes. They are

$$\begin{bmatrix} \tau^{22} \\ \tau^{23} \\ \tau^{33} \end{bmatrix}^i = \begin{bmatrix} 2\zeta_i(2\zeta_i^2-1)\eta & \zeta_i^3 \\ \zeta_i^2(1-\zeta_i^2) & 0 \\ 0 & 0 \end{bmatrix}^i \begin{bmatrix} \beta_{18} \\ \beta_{19} \end{bmatrix}^i \qquad (5.2)$$

It should be noted that the hybrid stress field in Eq. (3.63) is in terms of x and z coordinates and the stress field in the present study is in terms of y and z coordinates.

After enforcing the stress continuity and traction free conditions, the actual numbers of stress parameters used are 17 and 25 for the mixed form and conventional 2D hybrid stress sub-

elements, respectively for a two-layer model. They are summarized in the following table

Table 5.1 Number of β's used in the 2D type II ity=3 sub-element for a two-layer model

Element	mixed form	conventional
Number of β's for each layer	15	19
Actual number of β's for the two-layer model	17	25
Minimum number of β's to suppress the kinematic modes	14	21

A fine mesh has been used near the free edge region in order to evaluate the accuracy of the present mixed form hybrid stress element. A total of 16 elements and 204 degrees of freedom are used. For actual global analysis, a coarser mesh can be used.

The results are compared with the assumed displacement finite element solutions by Wang and Crossman [49], conventional hybrid stress element by Spilker [51] and singular hybrid stress element by Lee, Rhiu and Wong [56]. Wang and Crossman [49] used 392 constant strain triangular elements and a total of 452 degrees of freedom in their study. Spilker [51] used 30 2D high

order hybrid stress laminated plate elements which have the same d.o.f. as the present 2D type II ity=3 element but with different assumed stress field. A total of 527 degrees of freedom is used to model one half of the structure instead of one quadrant of it. Lee and his colleagues [56] used a special singular hybrid stress element at the free edge region and conventional 4-node 7-β hybrid stress elements in the rest of the structure. A total of 318 degrees of freedom has been used in their model.

The following labels are used for the elements used in the present comparisons:

Hybrid (n-17) = mixed form two-layer 2D type II ity=3 hybrid stress element with 17 β's

Hybrid (n-13) = mixed form two-layer 2D type II ity=3 hybrid stress element with 13 β's used near the region of free edge and element with 17 β's used in the rest of the structure

Hybrid (o-25) = conventional two-layer 2D type II ity=3 hybrid stress element with 25 β's

Displ. (Wang) = constant strain triangle assumed displacement element

Hybrid (Spilker) = conventional three-layer 2D high order hybrid stress laminated plate element with 40 β's

Hybrid (Lee) = conventional 4-node 7-β hybrid stress element with a special singular element

Elements with 17 and 25 β's do not contain any kinematic deformation mode and element with 13 β's contains two.

The numerical results which are presented in Figure 4.5(a-f) are in terms of normalized values which are defined as

$$\bar{v} = \frac{v}{\varepsilon_x h}$$

$$(\bar{\sigma}_y, \bar{\sigma}_z, \bar{\tau}_{yz}) = \frac{(\sigma_y, \sigma_z, \tau_{yz})}{\bar{\varepsilon}_x x 10^6 \text{ psi}} \qquad (5.3)$$

Results obtained by the Hybrid (n-17) and Hybrid (o-25) elements are indistinguishable in all Figures 5.4(a-f). In Figure 5.4(a), the results of inplane displacement v along the top surface of the laminate z=2h obtained by the Hybrid (n-17), Hybrid (o-25) and Hybrid (n-13) are in very good agreement with the Wang and Crossman's solutions.

The distribution of σ_y along the ply interface z=h is shown in Figure 4.5(b). Results obtained by the Hybrid (Lee), Hybrid (n-17) and Hybrid (o-25) indicate that the absolute value of σ_y are all increasing when approaching the free edge region.

However, results obtained by Hybrid (n-17) and (o-25) do not satisfy the traction free conditions exactly.

The transverse normal stress σ_z distributions along the interface z=h and the midplane z=0 obtained by the first five models are presented in Figures 4.5(c) and 4.5(d), respectively. They are all in very good agreement with each other.

Figure 5.4(e) shows the distribution of transverse shear stress τ_{yz} along the laminar interfaces obtained by the six models. A closer look of these results near the free edge is presented in Figure 4.5(f). It attains maximum value very near the free edge. Results by all the hybrid stress elements drop to zero or close to zero at the free edge. On the other hand, solutions obtained by the displacement model do not. Spilker's element performs the worst among all the six models. As expected, the Lee et.al's solution has the highest stress value near the free edge because their element does contain the singular stress field. On the other hand, the one with 13 β's obtains a slightly better results than the one with 17 β's.

The computational effort required for the Hybrid (n-17) element is 44% less than that by the Hybrid (o-25) element and the effort by the Hybrid (n-13) element is fifty percent less. This again demonstrates the computational efficiency of the present mixed form hybrid stress element over the conventional hybrid stress element.

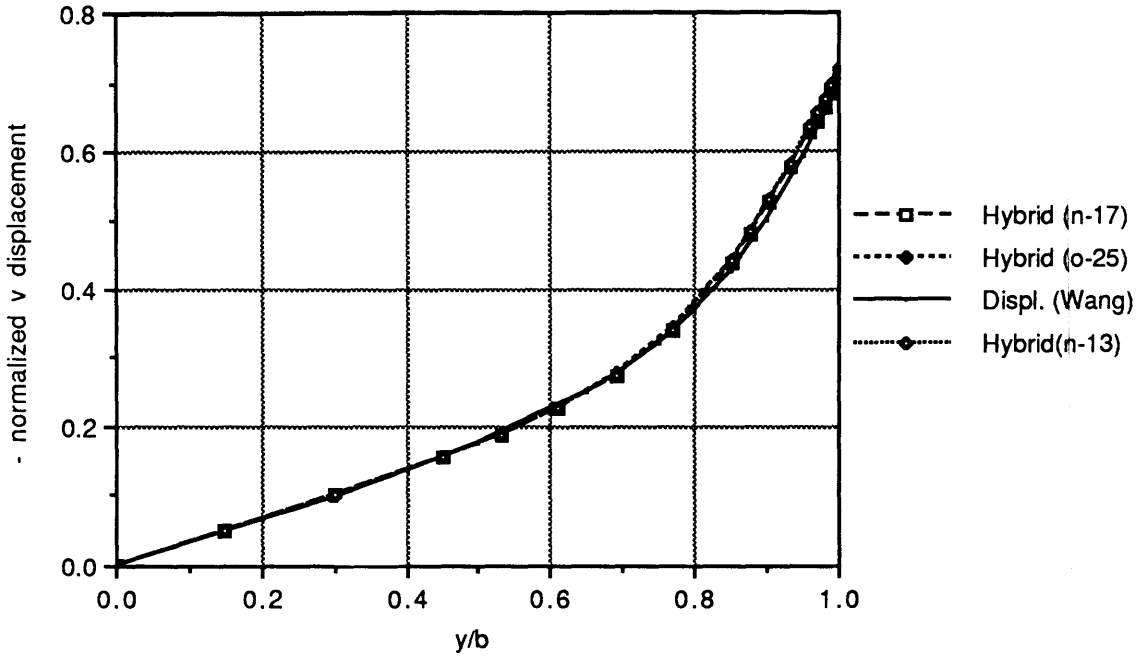

(a) normalized $\overline{v}$ distributions along the top interface z=2h

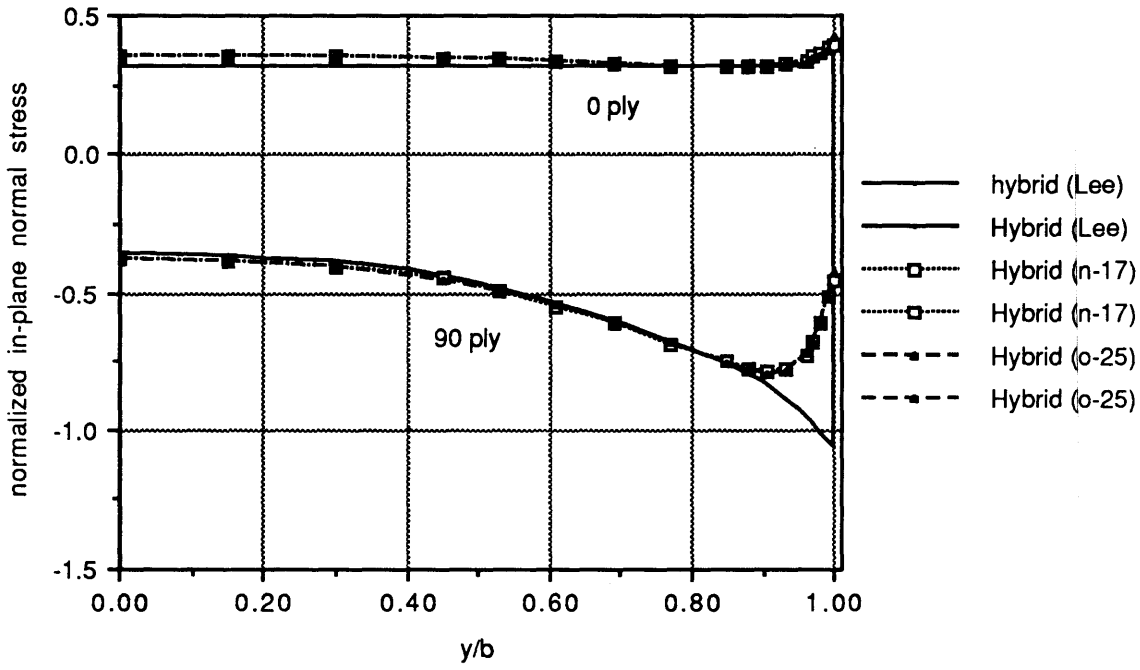

(b) normalized $\overline{\sigma}_y$ distributions along the ply interface z=h in the 0 and 90 plies

Figure 5.4 Solutions of stress distribution for a $[0/90]_s$ laminate - global study

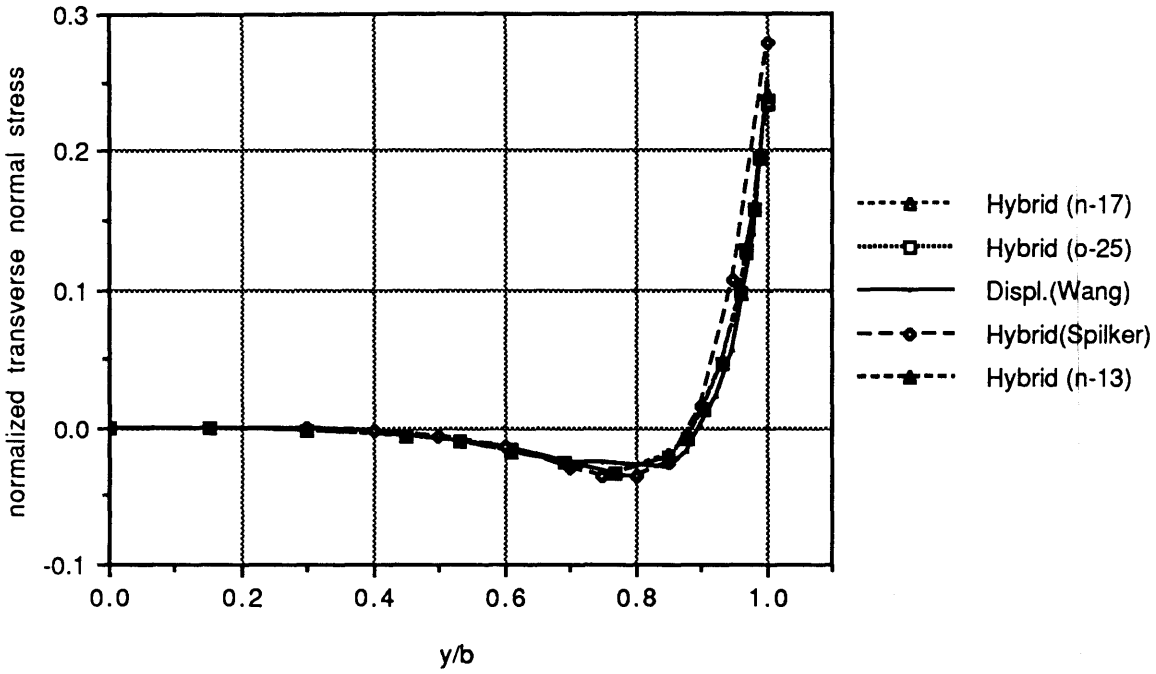

(c) normalized $\bar{\sigma}_z$ distributions along the ply interface z=h

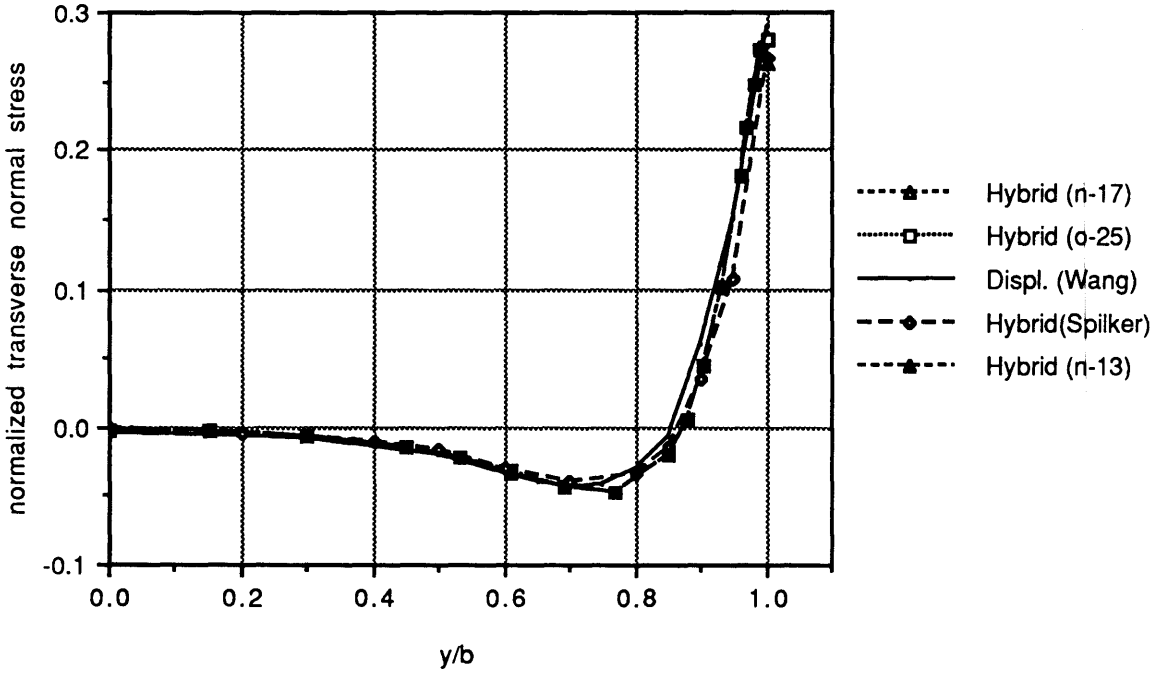

(d) normalized $\bar{\sigma}_z$ distributions along the midplane z=0

Figure 5.4 Solutions of stress distribution for a $[0/90]_s$ laminate - global study

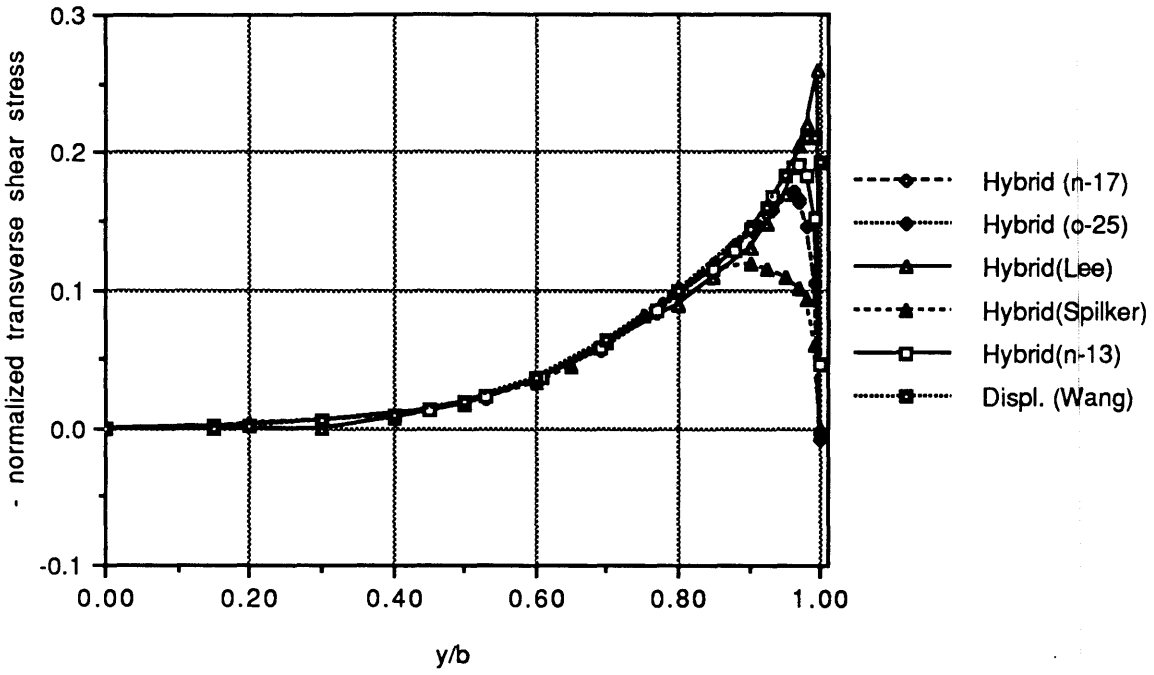

(e) normalized $\bar{\tau}_{zy}$ distributions along the ply interface z=h

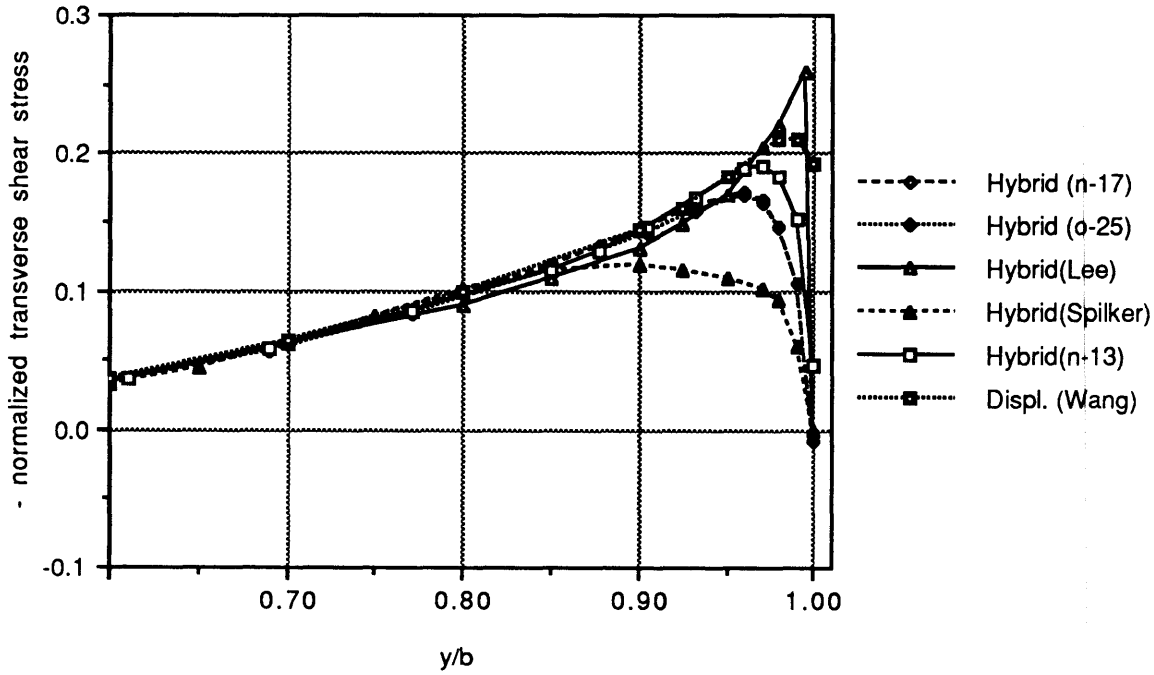

(f) normalized $\bar{\tau}_{zy}$ distributions along the ply interface z=h around the free edge region

Figure 5.4 Solutions of stress distribution for a $[0/90]_s$ laminate - global study

5.2.2 Local Analysis

Two finite element meshes have been adopted and are shown in Figure 5.5. In mesh A, only the conventional 2D 4-node 5-β hybrid stress element is used. In mesh B, the new mixed form high order 2D type II ity=3 hybrid stress sub-element with total 17 β's for a two-layer model is used in the region adjacent to the laminar interface in order to enforce the stress continuity along the interface and conventional 4-node 5-β hybrid stress element in the rest of the local region. A total of 278 degrees of freedom in mesh A and 256 in mesh B are used. The computational time required for Mesh A is 12% less than that for Mesh B.

A study is made of the effect of the presence of a matrix thin layer between two anisotropic lamina. For Mesh A, the thin layer is modeled by a conventional 4-node 5-β element and for Mesh B, it is modeled by a special mixed form 2D type II ity=1 sub-element in which the transverse stresses σ_z and τ_{yz} are not allowed any variation in the direction of laminate thickness. The thickness of the matrix thin layer is taken as 4% of the thickness of the lamina and the total thickness of the laminate is kept unchanged. In general, the thickness of the matrix thin layer is a function of fiber volume fraction and fiber diameter.

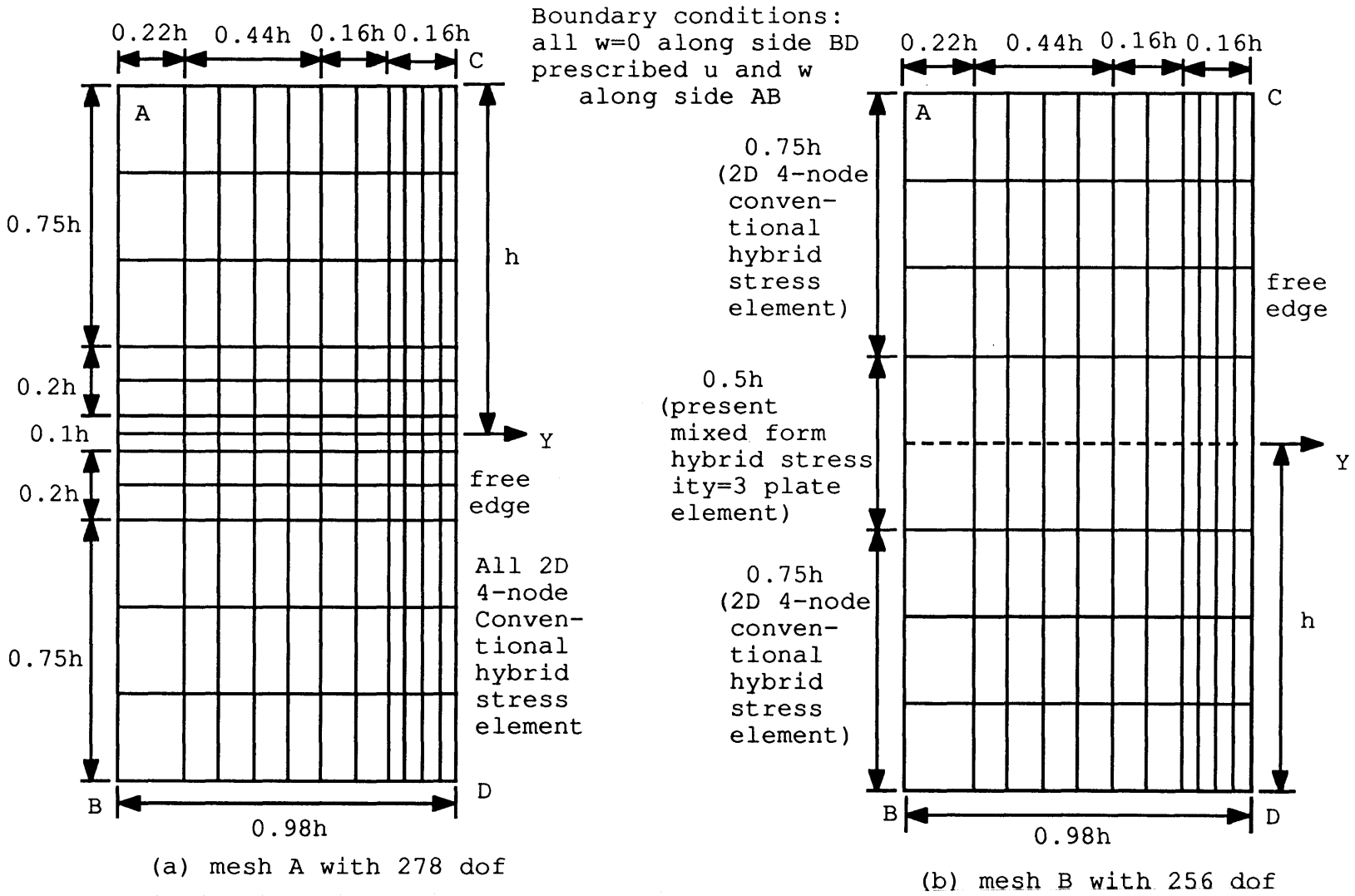

Figure 5.5 Two-layer finite element model for local study

Numerical results are again presented in normalized form defined in Eq. (5.3) and shown in Figures 5.6(a-f). Through-the-thickness stress distributions of σ_z are compared with the results obtained by Raju and Crews [52]. For a study of the same problem but with slightly different geometry, Raju and Crews used 576 8-node 2D isoparametric elements with a total of 3666 degrees of freedom. Results of stress distributions along the ply interface z=h are also compared with the solutions obtained by Lee, Rhiu and Wong [56].

The following labels are used for the elements used in the present comparison:

Mesh A (w/o) = conventional 4-node 5-β hybrid stress element in mesh A and without the matrix thin layer

Mesh A (w) = conventional 4-node 5-β hybrid stress element in mesh A and with the matrix thin layer

Mesh B (w/o) = mixed form 2D type II ity=3 hybrid stress sub-element with 17 β's and conventional 4-node 5-β hybrid stress element in mesh B and without the matrix thin layer

Mesh B (w) = mixed form 2D type II ity=3 hybrid stress sub-element with 17 β's and conventional 4-node 5-β hybrid stress element in mesh B and with the matrix thin layer

Displacement = 8-node 2D isoparametric element with a total of 3688 d.o.f. and without the matrix thin layer

Hybrid (Lee) = conventional 4-node 7-β hybrid stress element with a special singular element and without the matrix thin layer

Figure 5.6(a) presents through-the-thickness stress distributions of σ_z for a laminate without thin layer of matrix material obtained by Mesh A and Mesh B. The results are in good agreement with those obtained by Raju and Crews. However, the one obtained by mesh B shows better agreement than the one obtained by mesh A. The total degree of freedom used in the global and local analyses in mesh B is 460 d.o.f. compared with 3688 d.o.f. in one global analysis used by Raju and Crews. It clearly shows that the computational effort can be reduced significantly by the use of global-local finite element method. The one with the matrix layer is shown in Figure 5.6(b) and the value of σ_z at the interface drops slightly.

Results of the transverse normal stress σ_z, the shear stress τ_{yz}, the inplane normal stresses σ_y in the 0^0 and 90^0 plies along the interlayer boundary are presented in Figures 5.6(c-f), respectively. The ones with the thin layer of matrix material are plotted at the location of the interface between the lamina and the matrix interply. Results all indicate that the one with

the matrix layer trends to decrease its values compared with the one without the matrix thin layer.

The results of σ_z obtained by Mesh A and Mesh B are in good agreement with each other as shown in Figure 5.6(c). However, because an elastic singularity is expected at the free edge, the resulting values right at the free edge is dependent significantly on the element size used near the edge. Therefore, higher value in Mesh A is observed because a smaller size of the element is used. In Figure 5.6(d), results obtained by Mesh B of the transverse shear τ_{yz} are in better agreement with the Hybrid(Lee) solutions than the one with Mesh A.

Results of the inplane normal stress σ_y are shown in Figures 5.6(e) and 5.6(f). For the stresses in the 0^0 ply, the one obtained by Mesh B is in better agreement with the Hybrid(Lee) solutions than the one obtained by Mesh A. On the other hand, for the case of the 90^0 ply the one obtained by Mesh A is better.

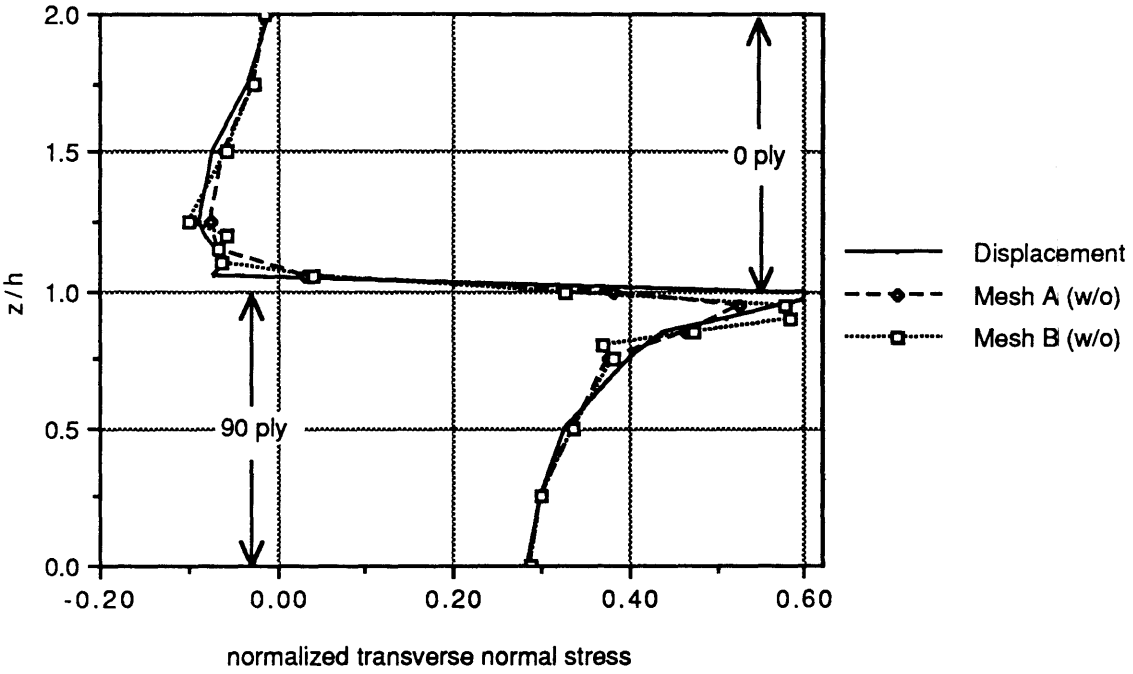

(a) normalized $\bar{\sigma}_z$ distributions through the laminate thickness at the free edge y=b without matrix thin layer

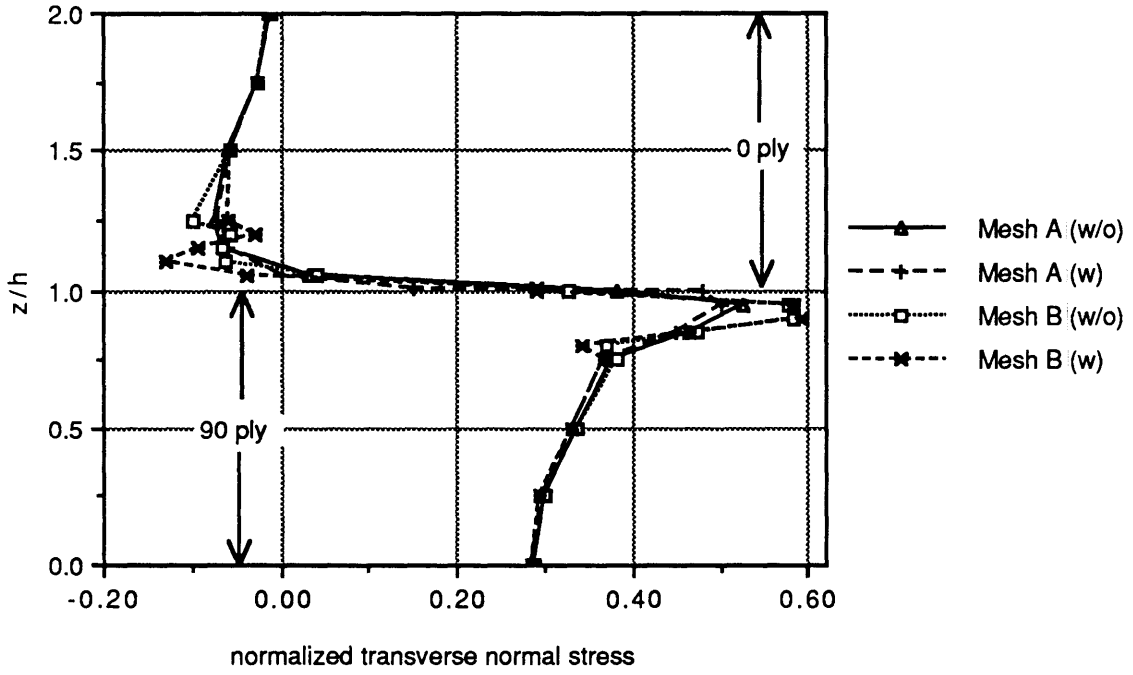

(b) normalized $\bar{\sigma}_z$ distributions through the laminate thickness at the free edge y=b with and without matrix thin layer

Figure 5.6 Solutions of stress distribution for a $[0/90]_s$ laminate - local study

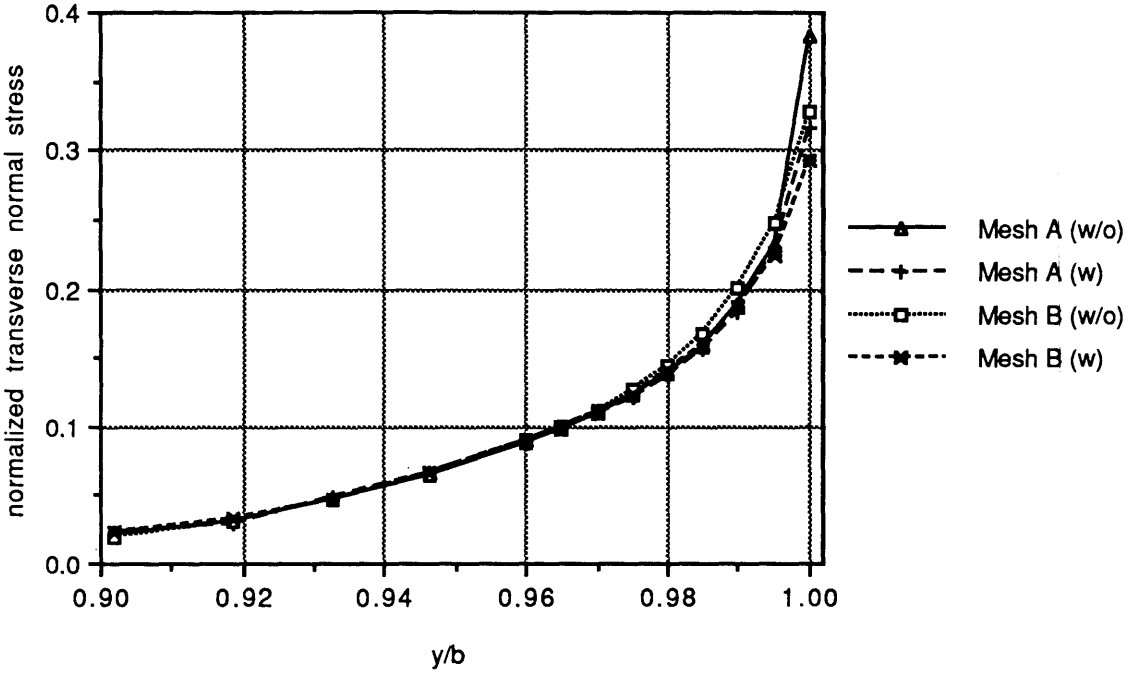

(c) normalized $\overline{\sigma}_z$ distributions along the ply interface z=h with and without matrix thin layer

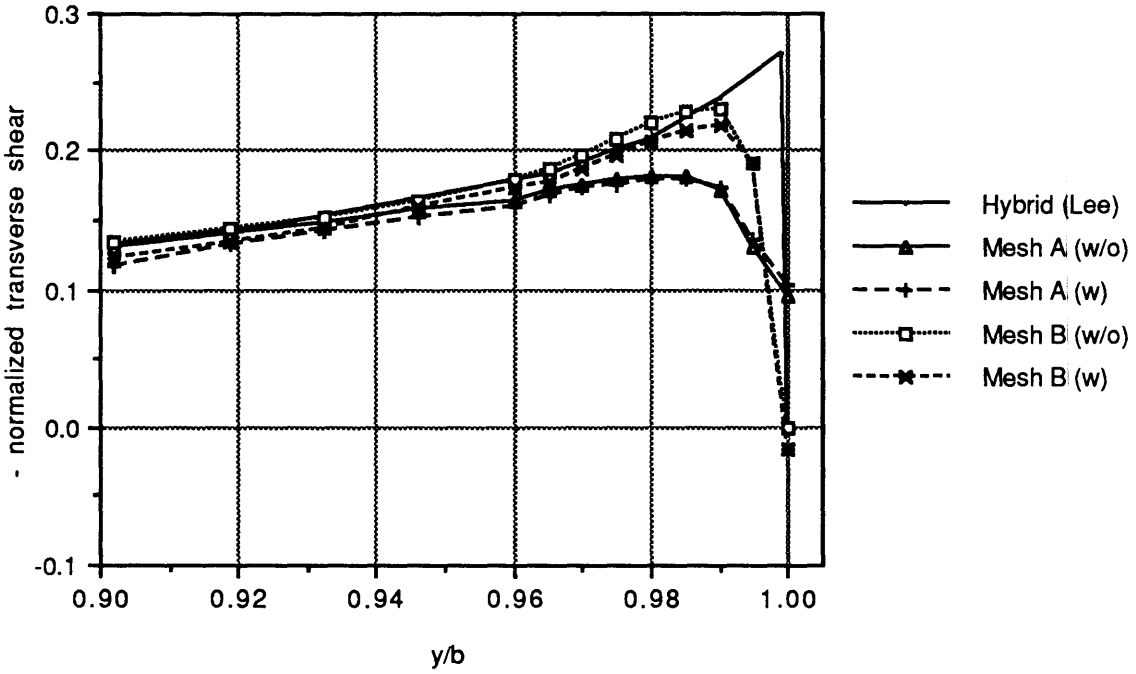

(d) normalized $\overline{\tau}_{zy}$ distributions along the ply interface z=h with and without matrix thin layer

Figure 5.6 Solutions of stress distribution for a $[0/90]_s$ laminate - local study

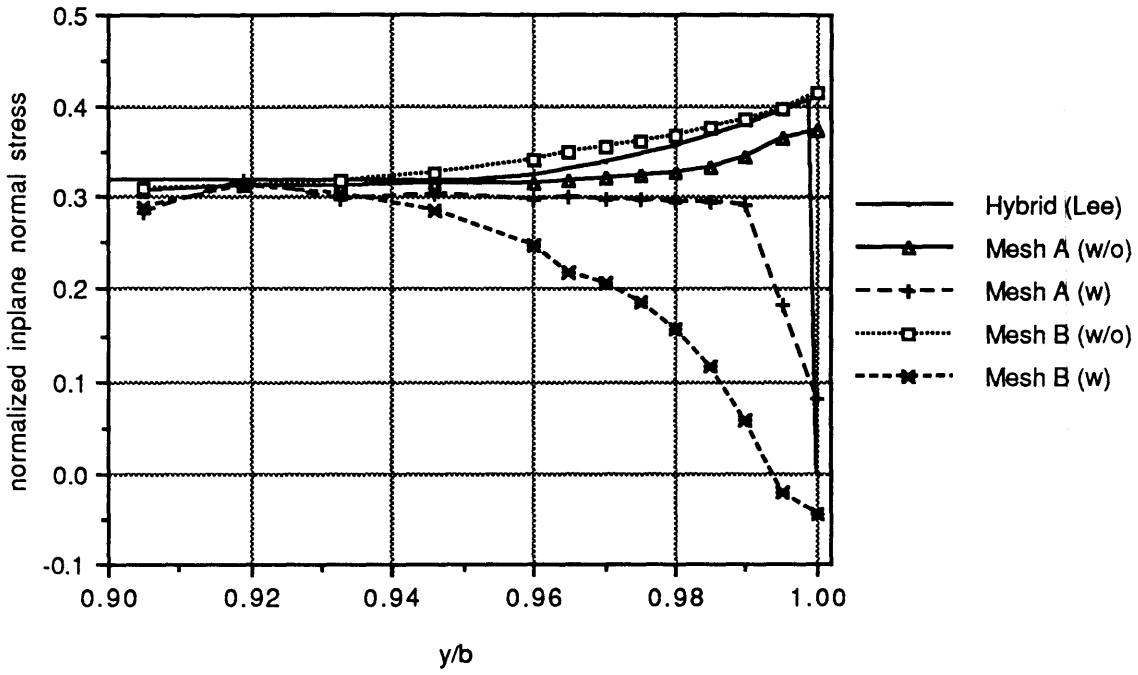

(e) normalized $\overline{\sigma}_y$ distributions along the ply interface z=h in the 0 ply with and without matrix thin layer

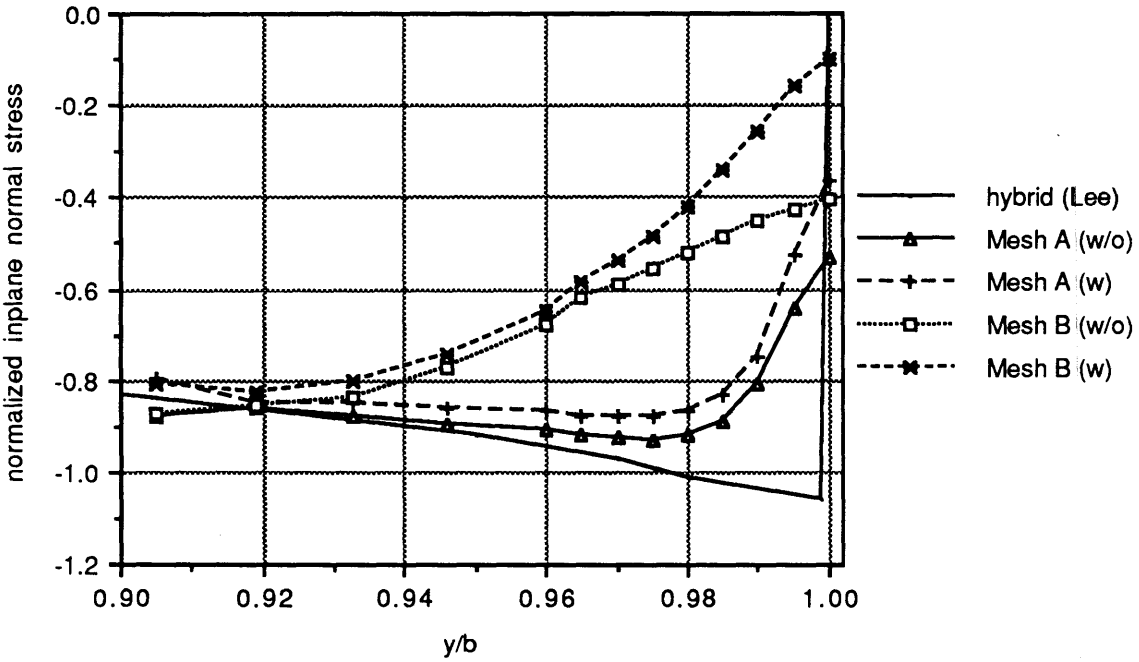

(f) normalized $\overline{\sigma}_y$ distributions along the ply interface z=h in the 90 ply with and without matrix thin layer

Figure 5.6 Solutions of stress distribution for a $[0/90]_s$ laminate - local study

5.3 The Curvilinear Free Edge Problem

The second example chosen to validate the accuracy and computational efficiency of the global-local finite element method to laminated plate problem is a cross ply composite laminate with a circular cut-out. It is subjected to uniform inplane stress σ_0 and is illustrated in Figure 5.7.

Results for this kind of problems have been presented by a number of investigators [62,66,75,120,122]. Tang [62] used a boundary layer theory formulated in cylindrical coordinates to analyze the problem. Bar-Yoseph and Avrashi [66] used a method based on a variational perturbation and hybrid stress finite element method. Nishioka and Atluri [75] presented a special traction free hybrid stress element to deal with the problem. Instead of development any special element or approximate technique, Luckings, Hoa and Sankar [120] and Raju and Crews [122] used the 20-node isoparametric element with a very fine mesh to study the problem.

The laminate consists of four-layer cross ply $[0/90]_s$ with layers of equal thickness and the loading is imposed as uniform pressures σ_0 applied to the surfaces at $x = \pm L$. The angle is measured with respect to the axis x (i.e. 0 degree implies fibers are parallel to the axis x). Because of the symmetry along the planes xy, yz and zx, the analysis is carried out over

$E_L = 21.0 \times 10^6$ psi

$E_T = 1.55 \times 10^6$ psi

$G_{LT} = 0.65 \times 10^6$ psi

$G_{ZT} = 0.52 \times 10^6$ psi

$\nu_{LT} = 0.31$

$\nu_{ZT} = 0.49$

t = 4h
W = 8R
L = 10R

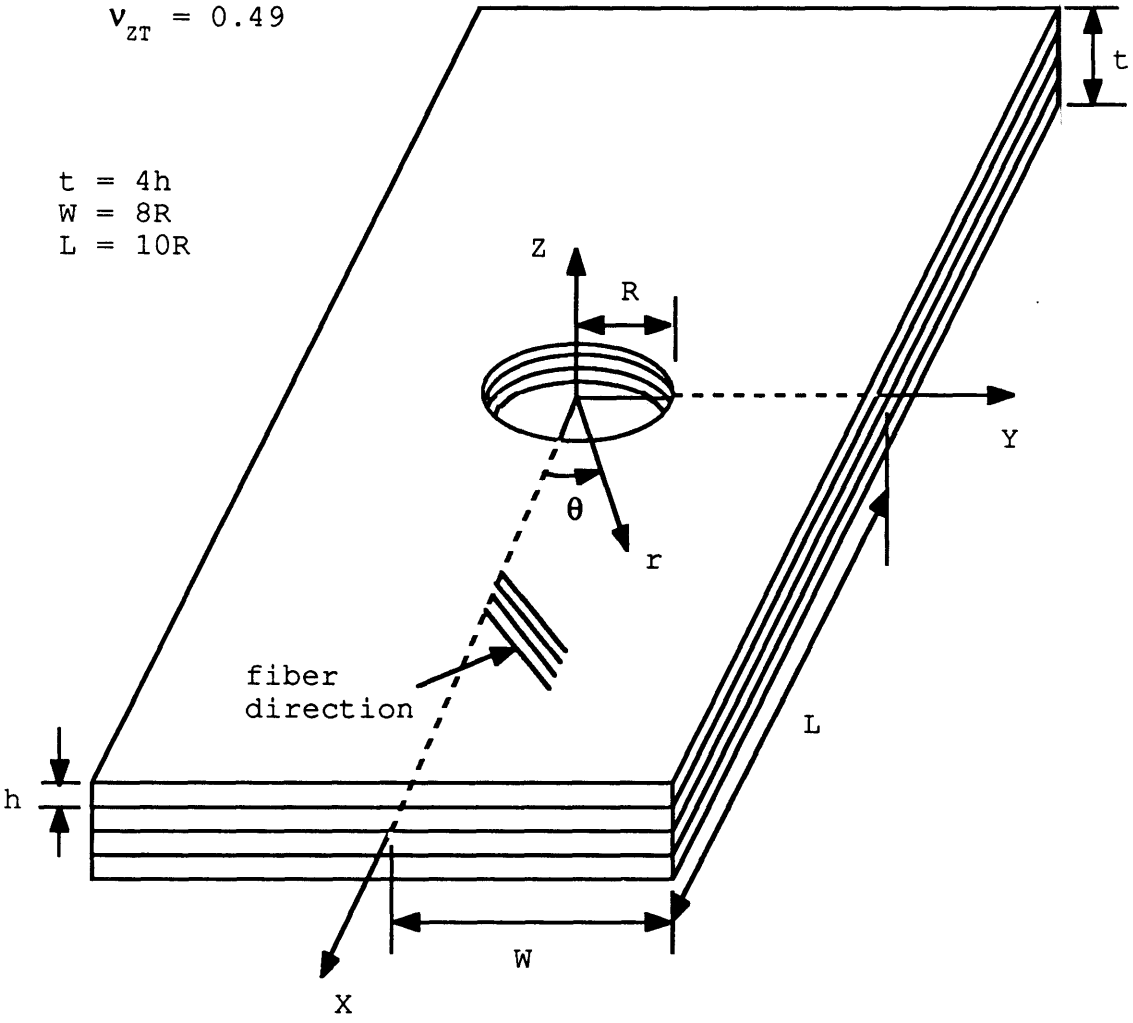

Figure 5.7 Configuration of laminate with a circular hole subjected to uniform inplane stress σ_o in the x direction

one eighth of the structure. The displacements u, v and w are zero on the planes yz, zx and xy, respectively.

Each layer is modeled by a mixed form 3D type II ity=3 hybrid stress sub-element as shown in Figure 3.13(b). The number of stress parameters β used in Eq. (3.70) for each layer is forty. After enforcing the stress continuity and traction free conditions, the number of stress parameters for the two-layer model is reduced to forty-four. The minimum number of β's required to suppress the kinematic modes is twenty-nine. Once again, for maintaining symmetry of the assumed stress field, the actual number of β's being used is quite large compared with the minimum number of β's.

Two laminates with two different hole radius to laminate thickness ratios R/t are considered. The one with R/t equal to 1 is designated as case 1 and the other with R/t equal to 5 is designated as case 2. For the global analysis, 48 elements are used for each cases as shown in Figure 5.8(a). The element is constructed by two mixed form 3D type II ity=3 hybrid stress sub-elements and a total of 1197 d.o.f. is used.

This analysis is conducted by three steps. The first local region which is designated as local region #1 has an outer radius equal to 2.15R and the finite element mesh is shown in Figure 5.8(b). It has 60 elements and a total of 1482 d.o.f. For case 1, the smallest size of the element in r direction is

0.4h where h is the laminar thickness. However, for case 2, the smallest size of the element is 2h.

Similar to the problem involving a straight edge which is traction free, the present problem also has stress singularity along the inner boundary which is stress free. Thus, the accuracy of the stresses at the free edge is dependent on the element size used near the edge. Therefore, for case 2, a subsequent local region designated as local region #2 is used as shown in Figure 5.8(b) which has an outer radius of 1.25R. The finite element mesh used in the local region #2 has a similar mesh as the one used in the local region #1. They have the same numbers of elements and d.o.f. On the other hand, the smallest size of the element in r direction in the present finite element mesh is 0.4h which is the same size as the one for case 1 used in the local region #1.

The results are compared with the assumed displacement finite element solutions obtained by Lucking, Hoa and Sankar [120]. As mentioned before, they used the 20-node 3D isoparametric element with the same global-local finite element scheme that is adopted in the present study. The numbers of elements used in the global and the two subsequent local region analyses are 220, 200 and 180 and the total numbers of d.o.f. are 4149, 3507 and 3129, respectively.

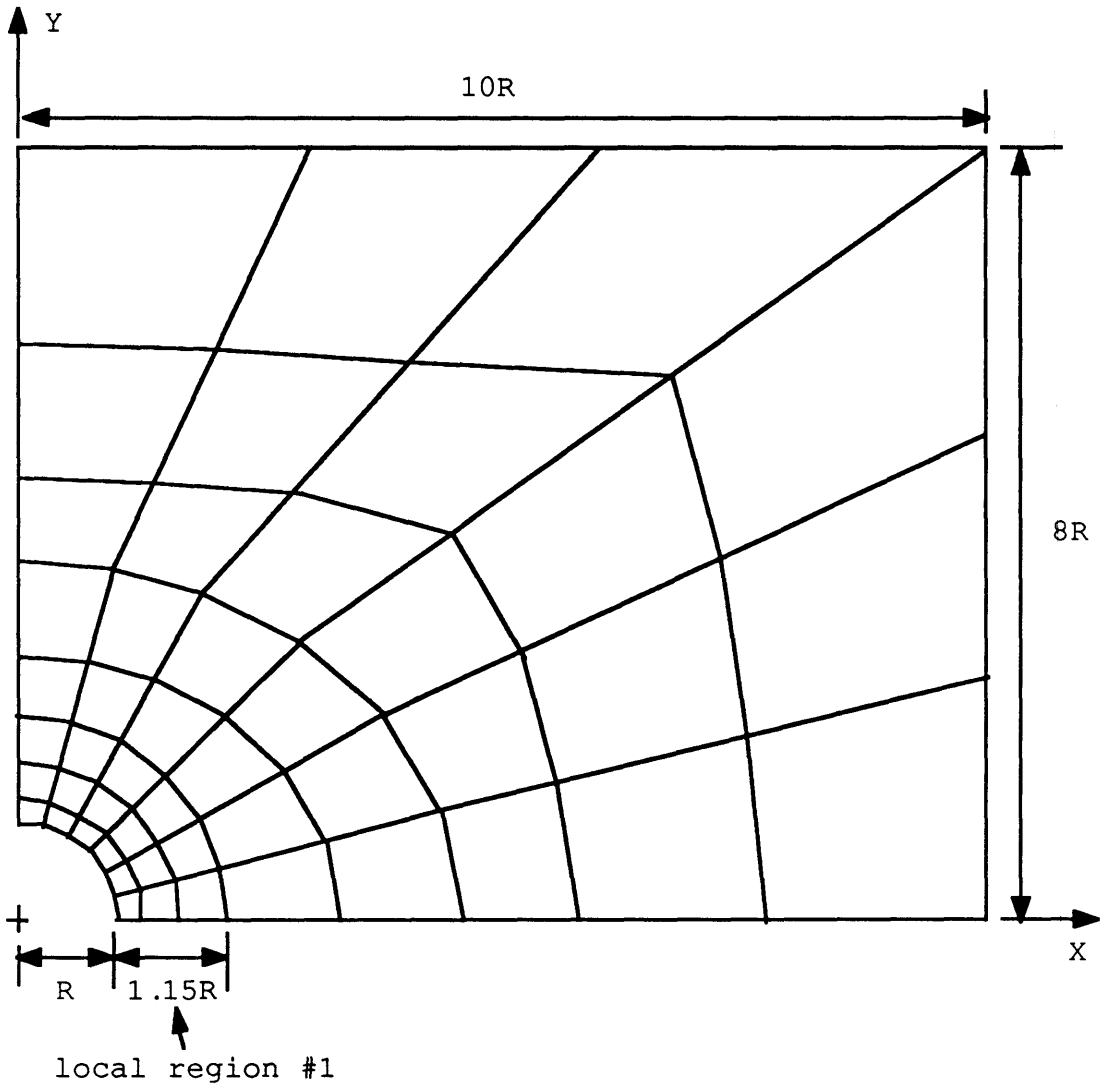

(a) model for global study

Figure 5.8 Finite element model of a $[0/90]_s$ laminate with a circular hole

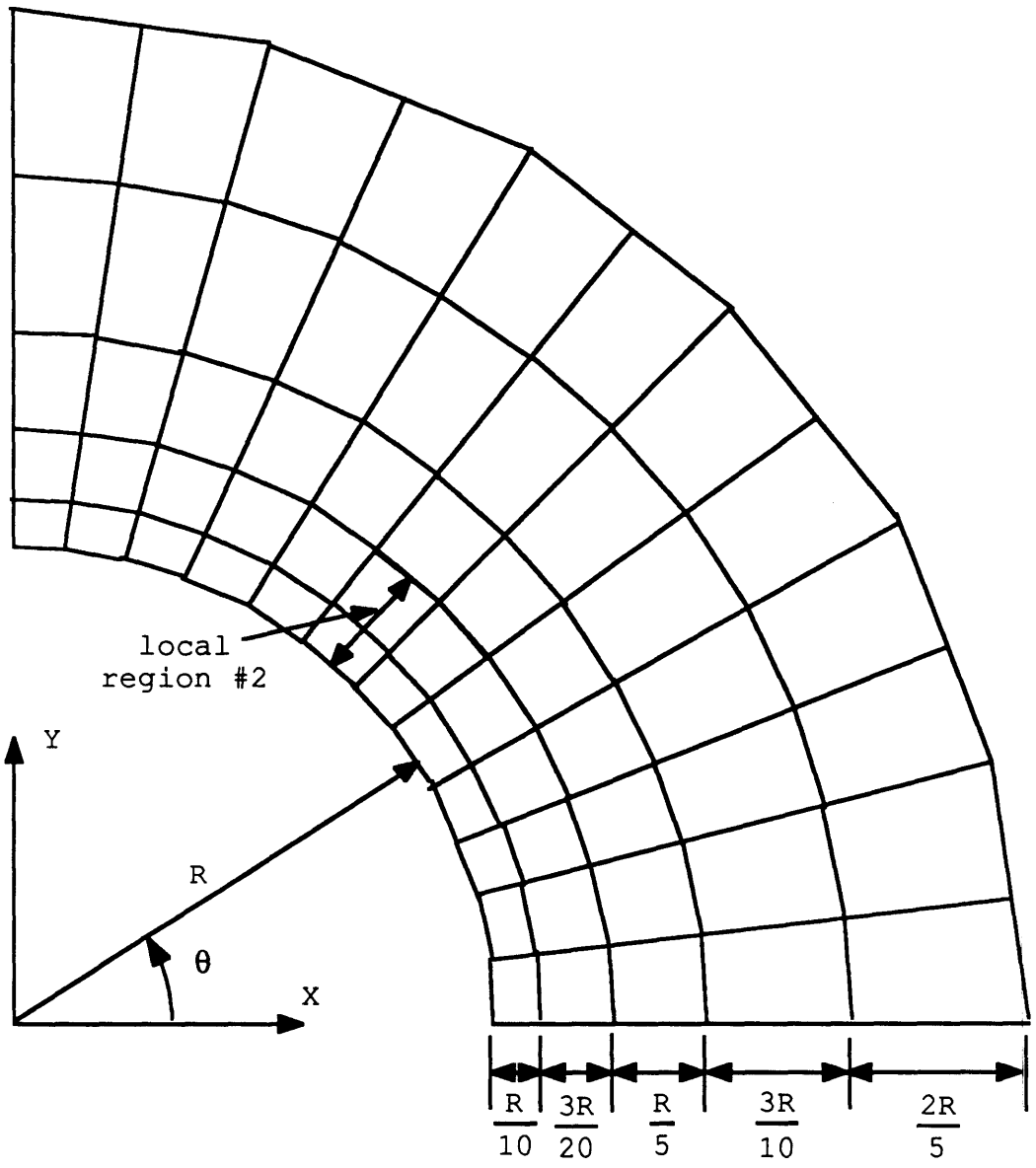

(b) model for local study

Figure 5.8 Finite element model of a $[0/90]_s$ laminate with a circular hole

Because the in-core memory of the computer used in this study is limited to only 1Mb, the present calculation is performed in single precision rather than double precision which has been used in the all previous calculations. The numerical results which are shown in Figures 5.9(a-n) are presented in terms of normalized values which are defined as

$$(\bar{\sigma}_\theta, \bar{\sigma}_z, \bar{\tau}_{\theta z}, \bar{\tau}_{rz}) = \frac{(\sigma_\theta, \sigma_z, \tau_{\theta z}, \tau_{rz})}{\sigma_0} \qquad (5.4)$$

where

σ_0 is the far field tensile stress

The following labels are used for the elements used in the present comparisons:

Hybrid-1 = mixed form two-layer 3D type II ity=3 hybrid stress element with the local region #1

Hybrid-2 = mixed form two-layer 3D type II ity=3 hybrid stress element with the local region #2

Displacement = 20-node 3D isoparametric element with the global-local finite element method used by Lucking, Hoa and Sankar.

CLT = using classical lamination theory to determine the far field stresses in the individual lamina of an infinite laminate and the 2D solutions from Reference 122 for holes in anisotropic plates.

* the number in the parenthesis is the ply angle

The results of the hoop stress distributions σ_θ around the hole boundary at the center of each plies obtained by the Hybrid-1 element for the cases 1 and 2 are shown in Figures 5.9(a) and 5.9(b), respectively. They are in good agreement with the solutions by the Displacement element. It shows that the hoop stresses σ_θ are not sensitive to the R/t ratio. Through-the-thickness distributions of σ_θ at θ equal to 0^0, 45^0 and 90^0 are compared with the CLT solutions as shown in Figures 5.9(c) and 5.9(d).

The results of the largest of the three interlaminar stresses $\tau_{\theta z}$ are plotted in Figures 5.9(e) and 5.9(f) for the cases 1 and 2, respectively. The results obtained by the Hybrid-1 for case 1 and the Hybrid-2 for case 2 are in very good agreement with the solutions by the Displacement elements. The results indicate that the magnitude of $\tau_{\theta z}$ increases with R/t and its maximum's position slightly shifts. Also, results obtained for case 2 by the Hybrid-1 element clearly show that the accuracy of the stresses at the free edge is significantly affected by the element size used near the edge.

Figures 5.9(g) and 5.9(h) and Figure 5.9(i) and 5.9(j) show the interlaminar normal stress σ_z around the hole boundary at the interface and at the midplane, respectively. Once again, the results obtained by the Hybrid-1 for case 1 and Hybrid-2 for

case 2 are in reasonable agreement with the solutions by the Displacement elements.

Through-the-thickness distributions of $\tau_{\theta z}$ and σ_z at $\theta=45^0$ and r/R=1 are plotted in Figure 5.9(k) and 5.9(l) for cases 1 and 2, respectively. They have the same shapes as the one obtained by Raju and Crews [122]. However, they obtained a much higher value at the interface because the element size as small as h/500 was used in their study.

The distributions of interlaminar shear stresses $\tau_{\theta z}$ and τ_{rz} along r direction at the ply interface and $\theta=45^0$ are plotted in Figures 5.9(m) and 5.9(n) for cases 1 and 2, respectively. For the case 1, the results obtained by the Hybrid-1 are in excellent agreement with the solutions obtained by the Displacement element.

5.4 Summary and Discussion

The two numerical examples has clearly demonstrated the computational efficiency and accuracy achieved by the multi-step global-local finite element method. Once again, they also show that the present mixed form 2D and 3D hybrid stress sub-elements have a desirable performance and are more computationally efficient than the conventional hybrid stress elements.

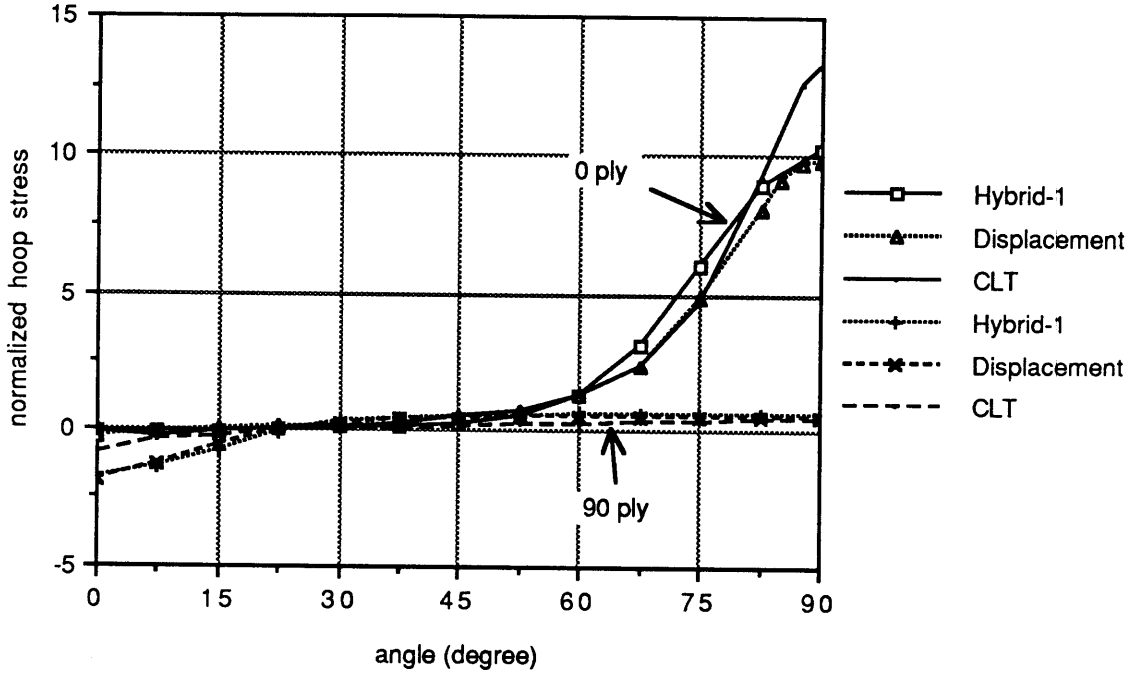

(a) normalized $\overline{\sigma}_\theta$ distributions around hole at the center of the plies z = 0.5h and 1.5h (R/t=1)

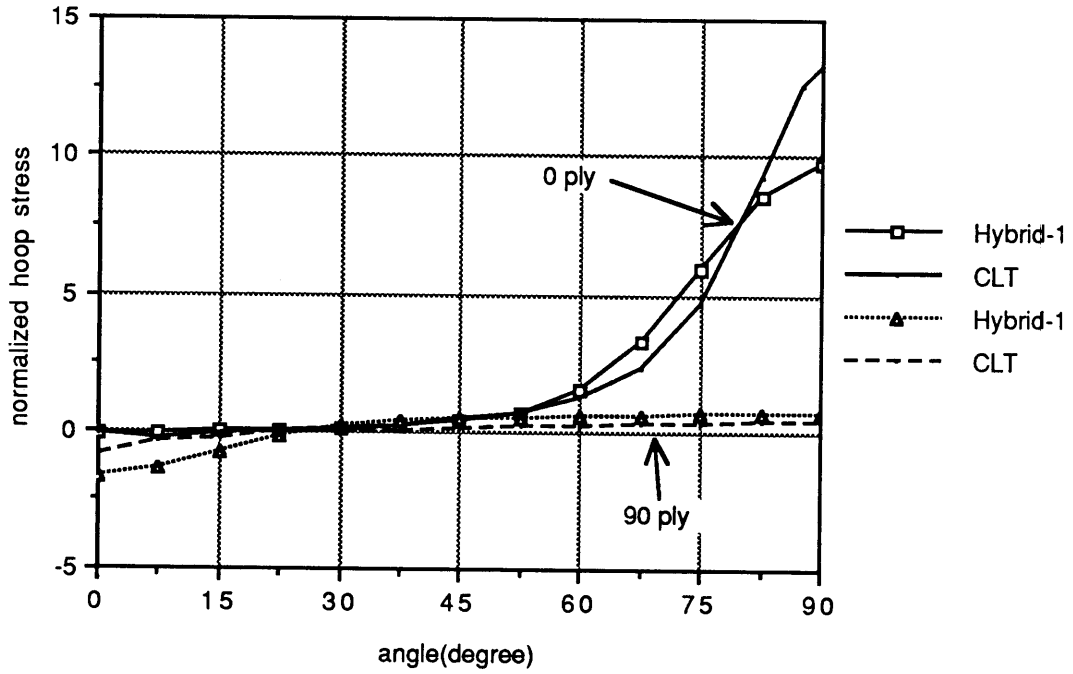

(b) normalized $\overline{\sigma}_\theta$ distributions around hole at the center of the plies z = 0.5h and 1.5h (R/t=5)

Figure 5.9 Solutions of stress distribution for a $[0/90]_s$ laminate with a hole

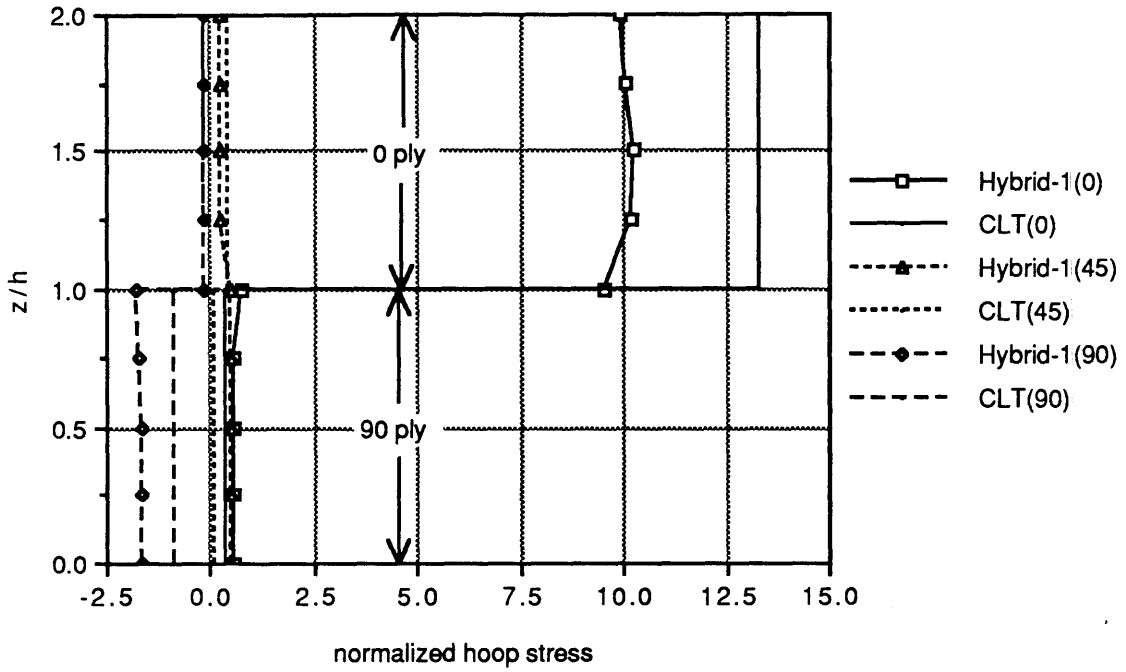

(c) normalized $\bar{\sigma}_\theta$ distributions through the laminate thickness at the hole boundary r/R=1 (R/t=1)

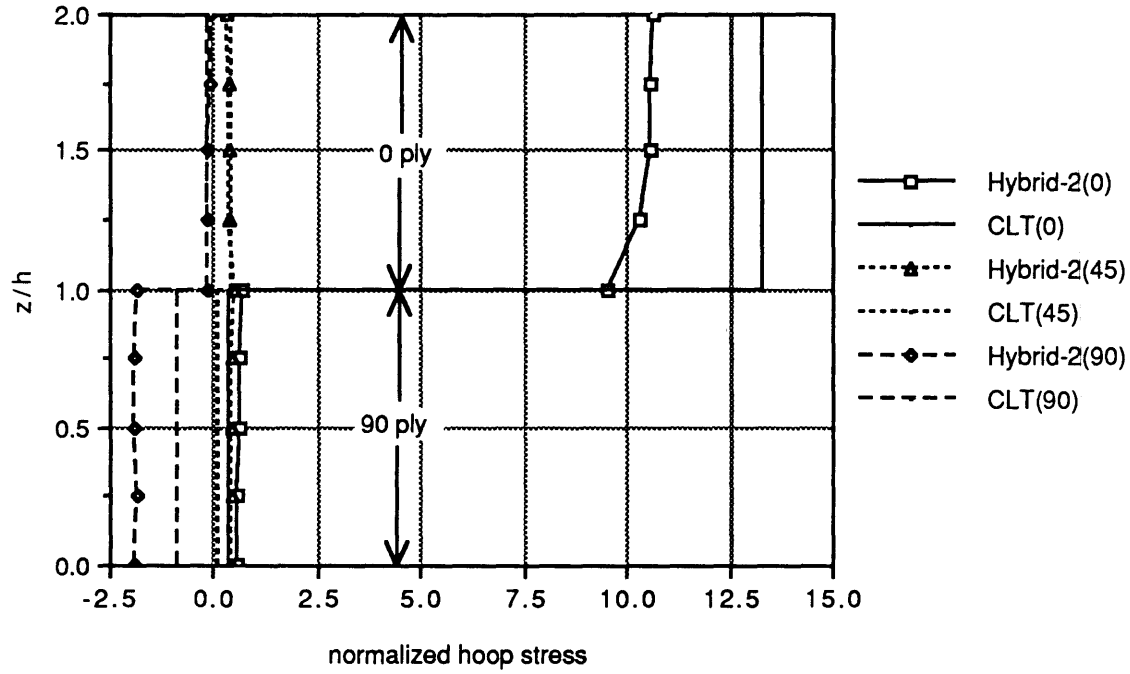

(d) normalized $\bar{\sigma}_\theta$ distributions through the laminate thickness at the hole boundary r/R=1 (R/t=5)

Figure 5.9 Solutions of stress distribution for a $[0/90]_s$ laminate with a hole

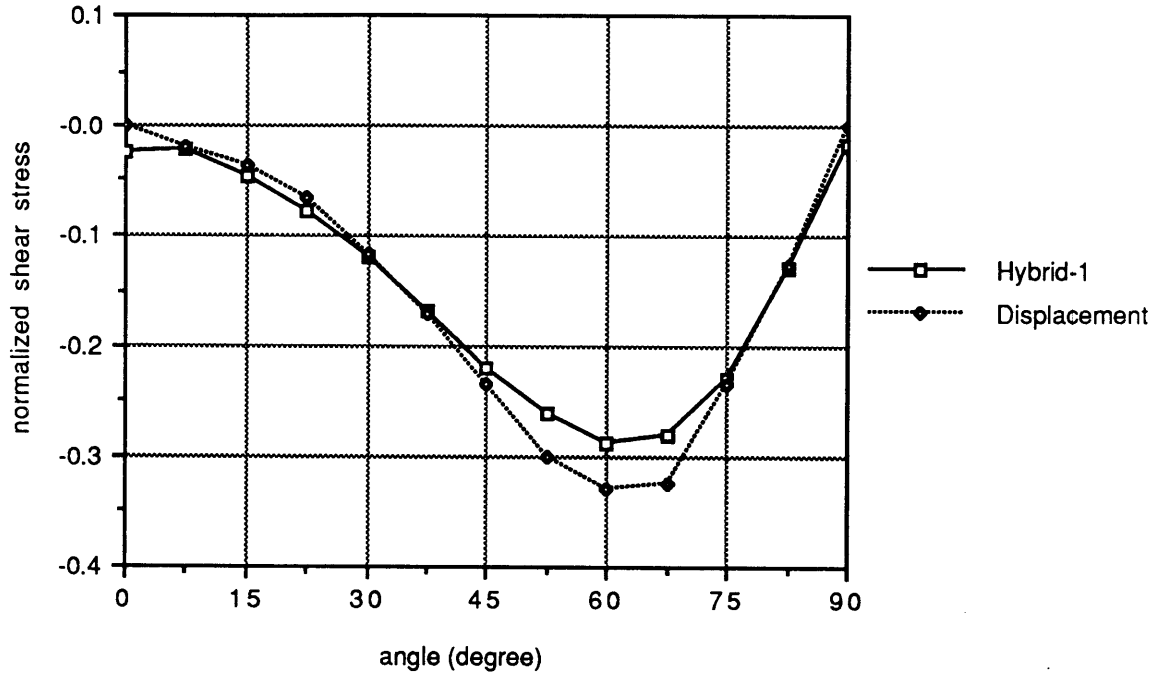

(e) normalized $\overline{\tau}_{\theta z}$ distributions around hole at the ply interface z=h (R/t=1)

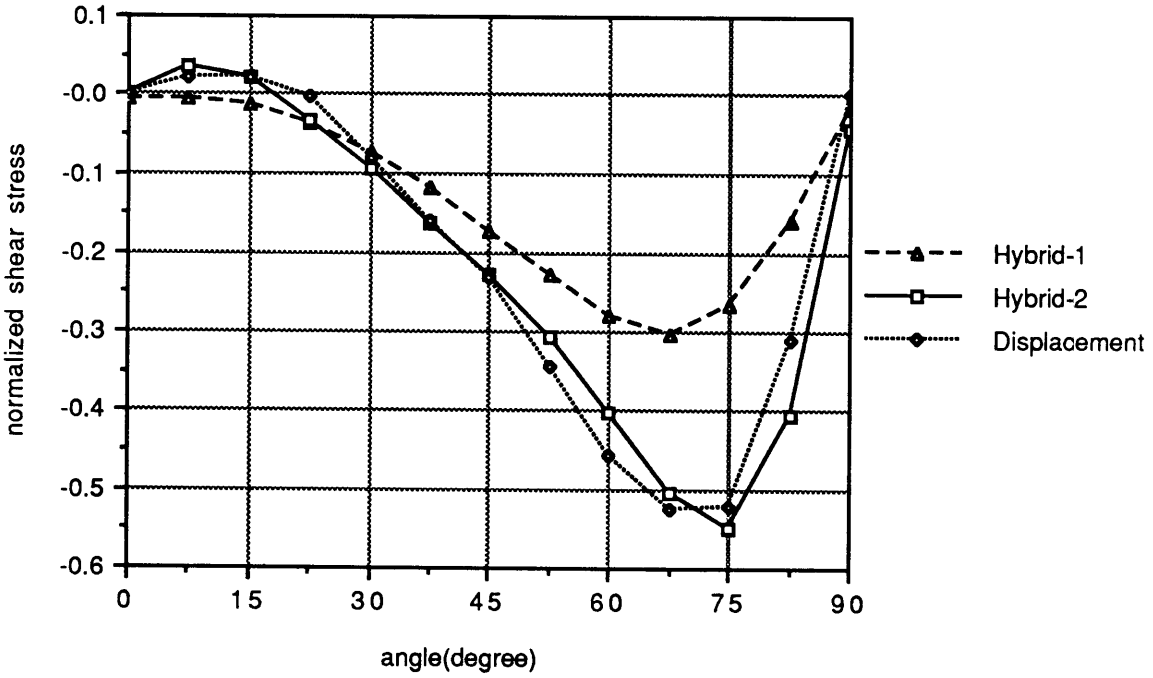

(f) normalized $\overline{\tau}_{\theta z}$ distributions around hole at the ply interface z=h (R/t=5)

Figure 5.9 Solutions of stress distribution for a $[0/90]_s$ laminate with a hole

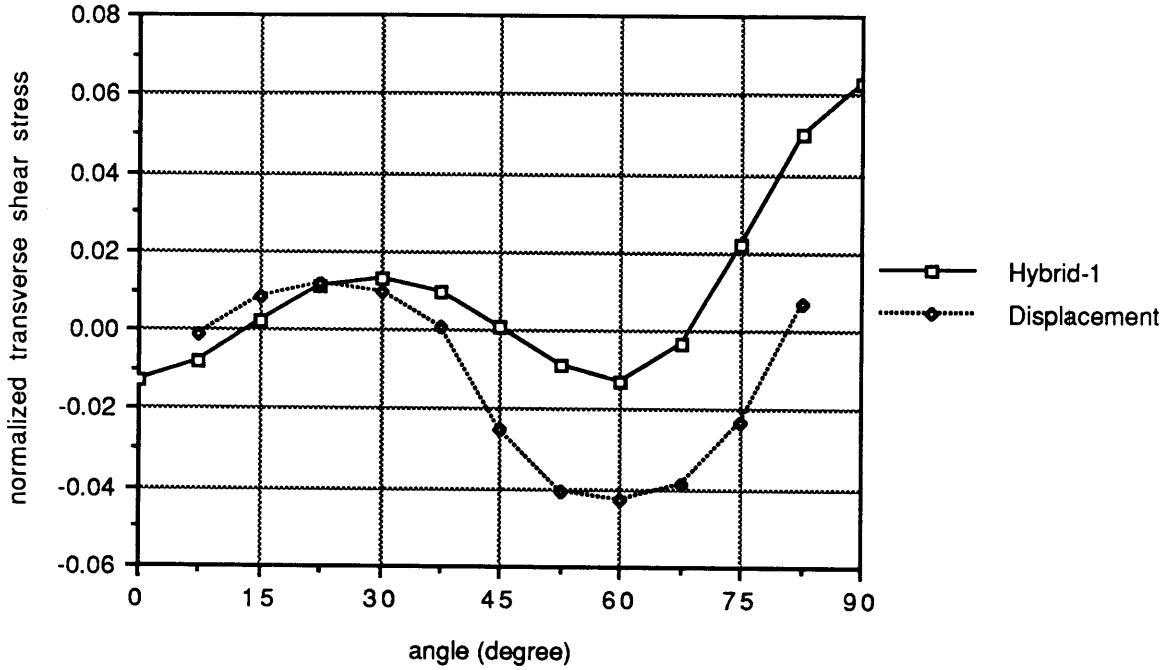

(g) normalized $\overline{\sigma}_z$ distributions around hole at the ply interface z=h (R/t=1)

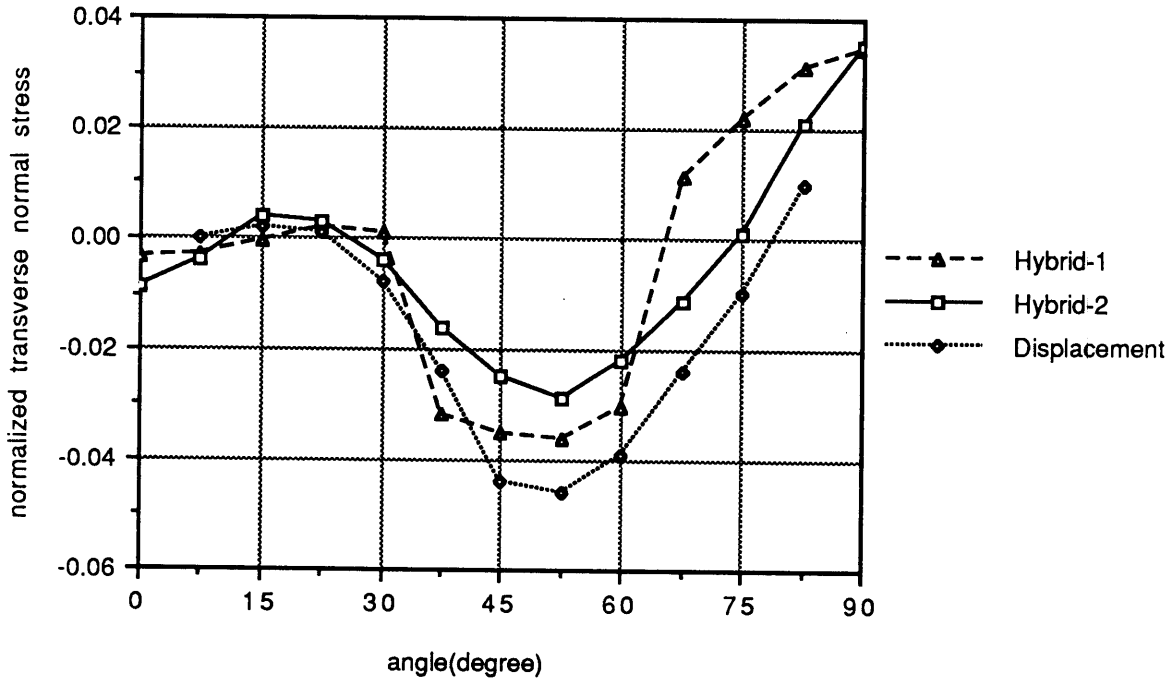

(h) normalized $\overline{\sigma}_z$ distributions around hole at the ply interface z=h (R/t=5)

Figure 5.9 Solutions of stress distribution for a $[0/90]_s$ laminate with a hole

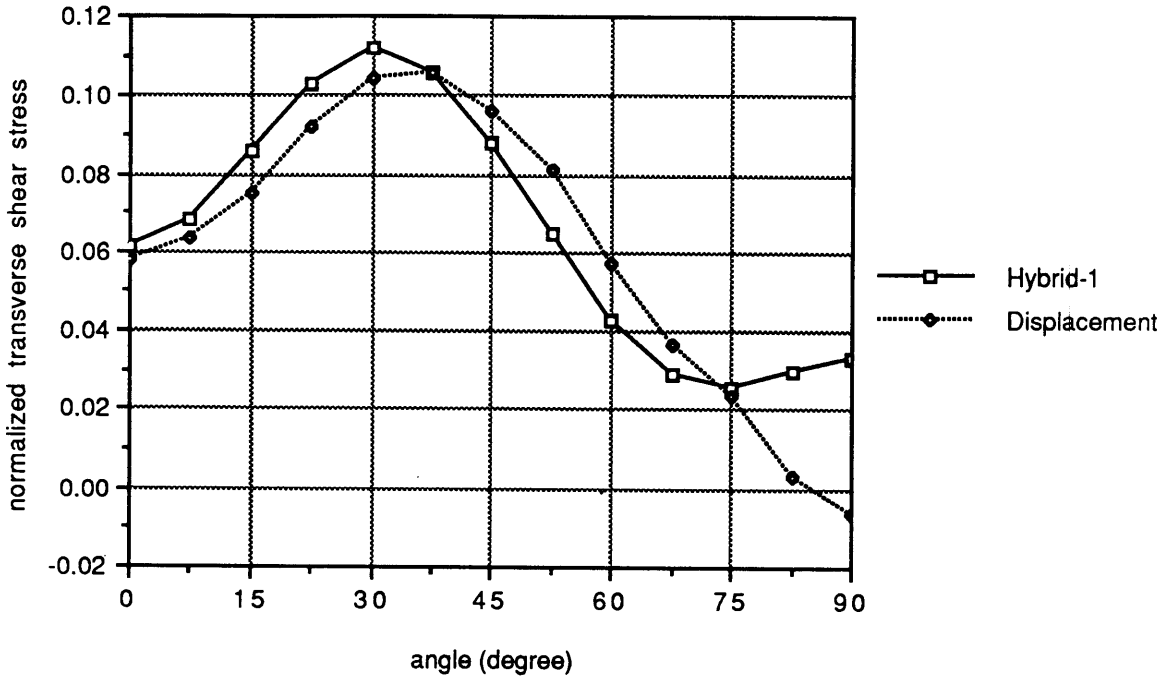

(i) normalized $\bar{\sigma}_z$ distributions around hole at the midplane z=0 (R/t=1)

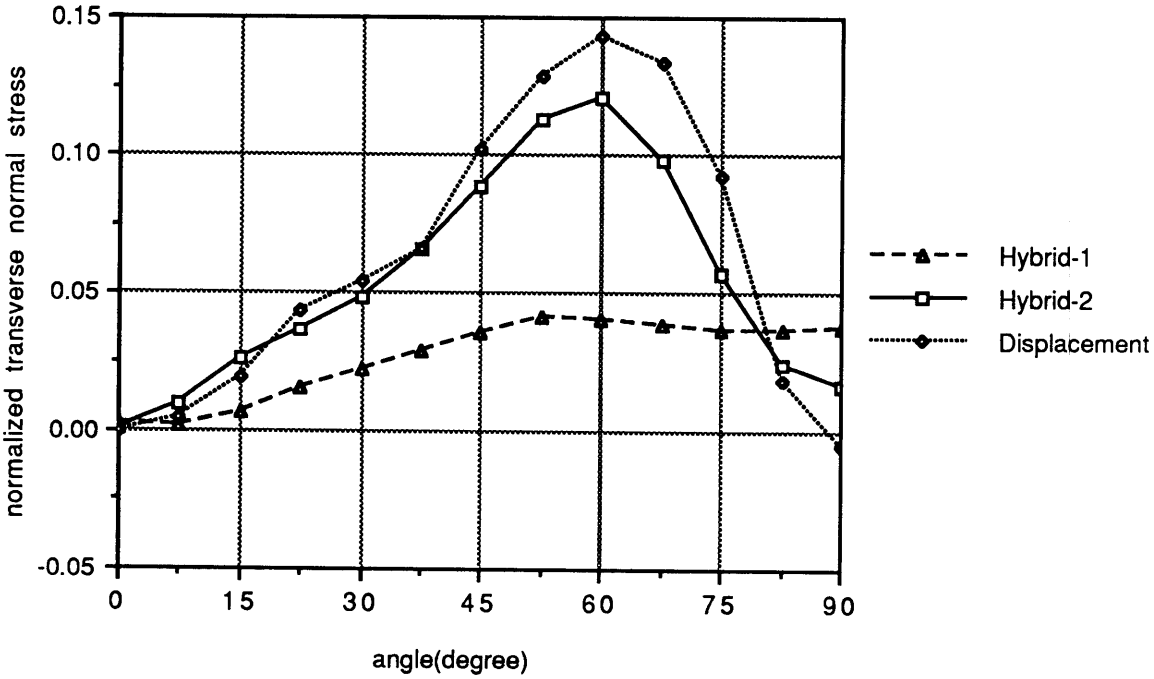

(j) normalized $\bar{\sigma}_z$ distributions around hole at the midplane z=0 (R/t=5)

Figure 5.9 Solutions of stress distribution for a $[0/90]_s$ laminate with a hole

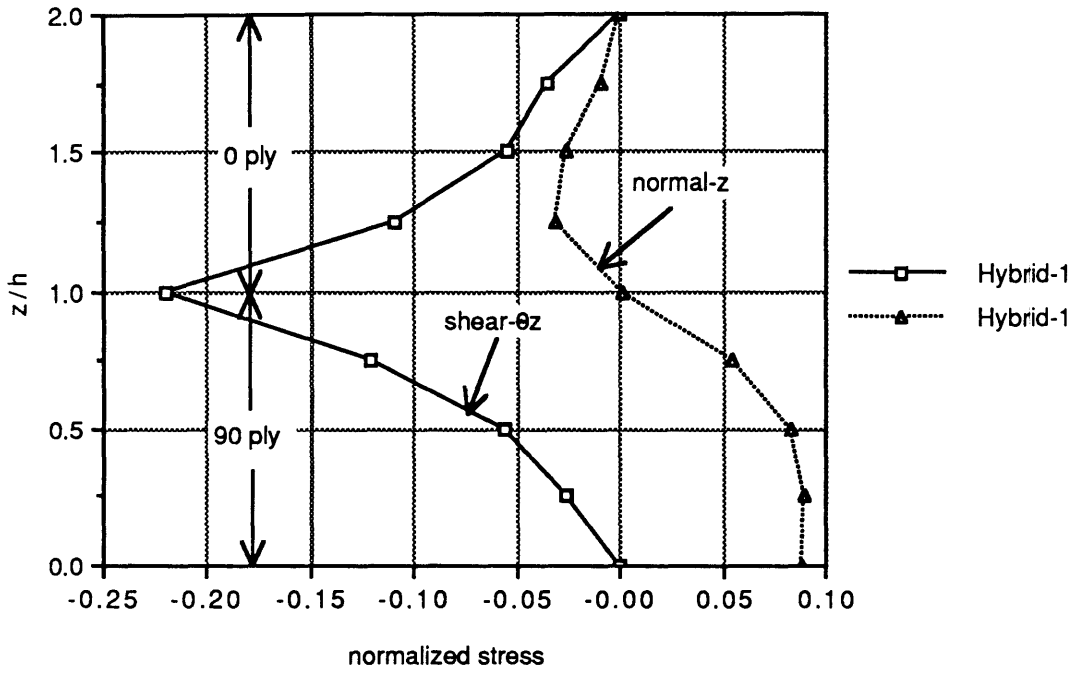

(k) normalized $\bar{\tau}_{\theta z}$ and $\bar{\sigma}_z$ distributions through the laminate thickness at the hole boundary r/R=1 and $\theta=45^0$ (R/t=1)

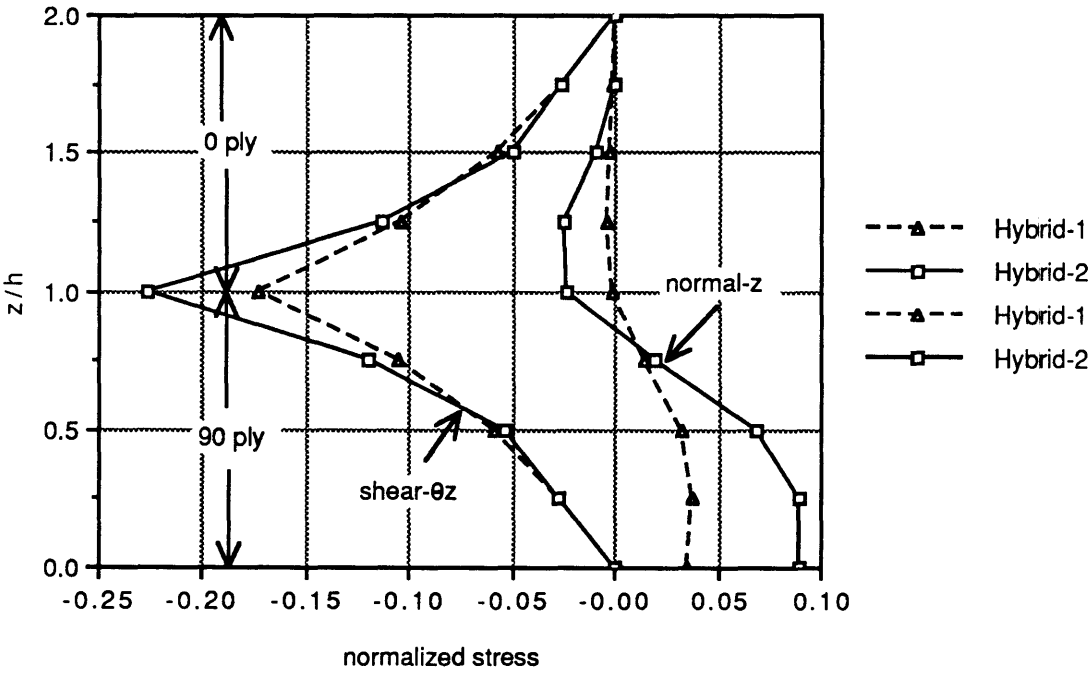

(l) normalized $\bar{\tau}_{\theta z}$ and $\bar{\sigma}_z$ distributions through the laminate thickness at the hole boundary r/R=1 and $\theta=45^0$ (R/t=5)

Figure 5.9 Solutions of stress distribution for a $[0/90]_s$ laminate with a hole

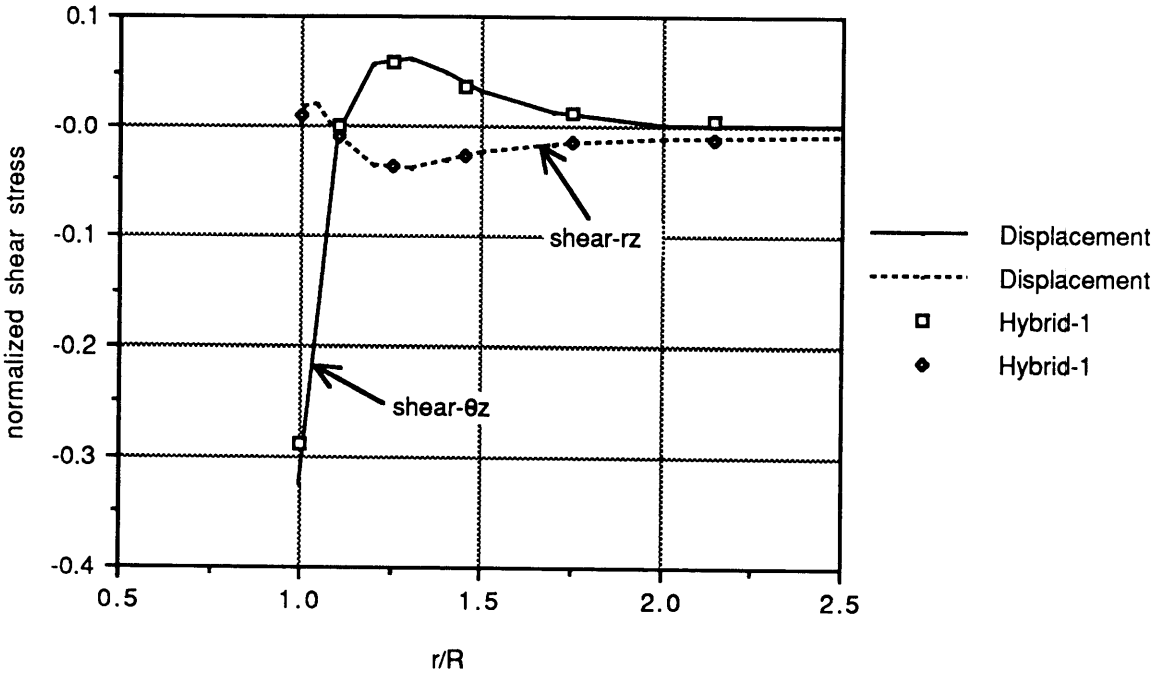

(m) normalized $\bar{\tau}_{\theta z}$ and $\bar{\tau}_{rz}$ distributions at the ply interface z=h and $\theta=63^0$ (R/t=1)

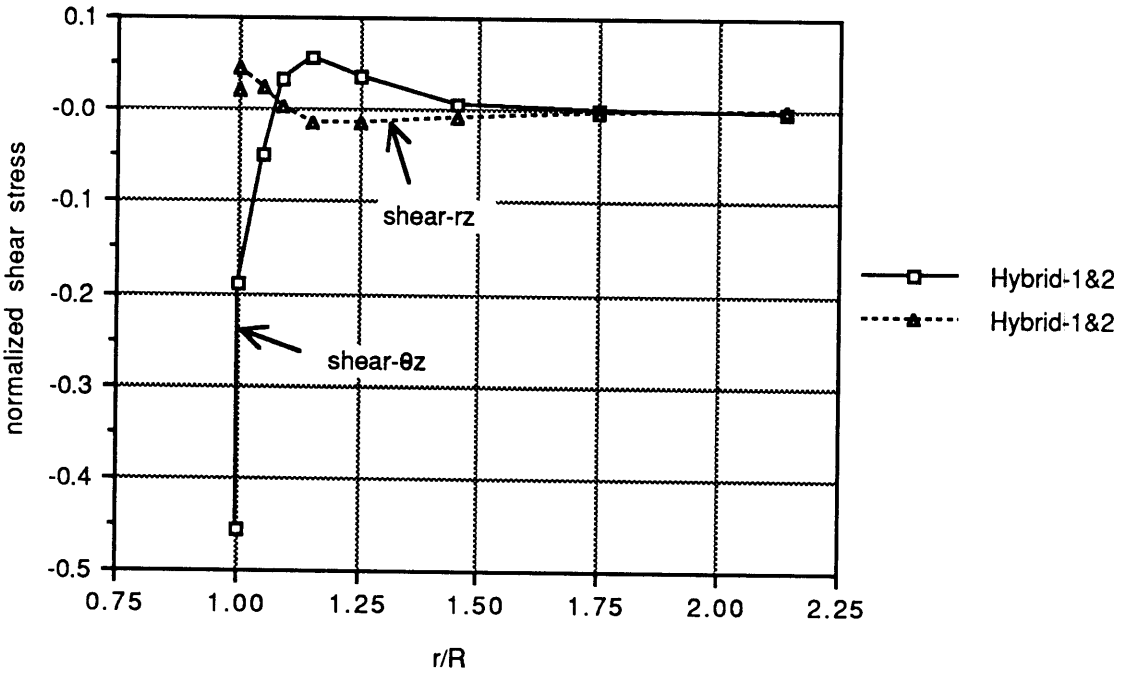

(n) normalized $\bar{\tau}_{\theta z}$ and $\bar{\tau}_{rz}$ distributions at the ply interface z=h and $\theta=63^0$ (R/t=5)

Figure 5.9 Solutions of stress distribution for a $[0/90]_s$ laminate with a hole

The study also indicates that the interlaminar stresses at the interlaminar boundary near the free edge decreases if the interlaminar boundary is modeled by a very thin matrix rich layer.

The study of a 4-layer cross ply laminate with a hole clearly indicates that the magnitude of the interlaminar stresses $\tau_{\theta z}$ and σ_z at the hole boundary is dependent on the mesh refinement because of the existence of stress singularity at the free edge. The optimum size of the element in r direction used adjacent to the free edge is about four-tenths of the layer thickness at least in the two cases considered here.

The accuracy of the stress analysis of the region of interest may be very sensitive to the size of the local region. If it is the case, a reasonable fine mesh in the global analysis and more transition region between the region of interest and the boundary of the local region should be used. On the other hand, it is not recommended to use too many consecutive local analyses because the errors propagated into each analysis may become very large in the final analysis.

In the application of the global-local finite element method to the laminated structures which contain many layers, the mixed form type I hybrid stress element should be used in the global analysis instead of the type II element that has been

used in this study as shown in Figure 5.10(a) because of its computational efficiency. On the other hand, in order to avoid the errors that limited the warping of the cross section of each layer near the region of interest because continuous functions through the laminate thickness are used in the assumed displacement field of the type I element, a through-the-thickness local region is recommended. For example, in Figure 5.10(b) region ADHE should be used as local region instead of region BCGF. In order to maintain the computational efficiency of the model, the mixed form type I hybrid stress element should be used in the region of local model that at least one layer away from the region of interest, for example regions ABFE and CDHG in Figure 5.10(b). On the other hand, in the region of interest and its neighboring area, mixed form type II element should be used.

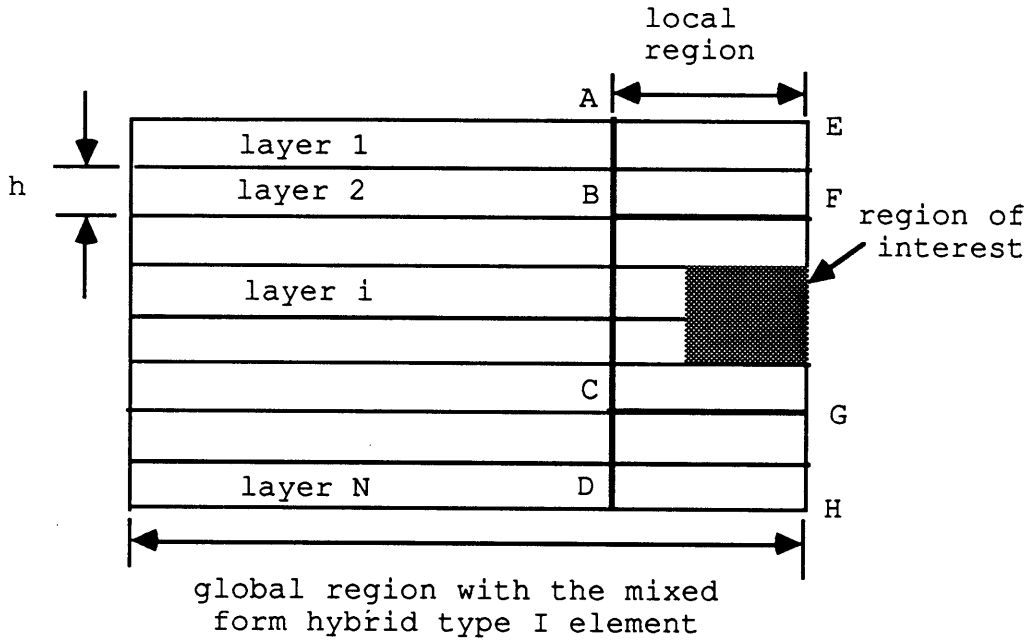

(a) model for global study

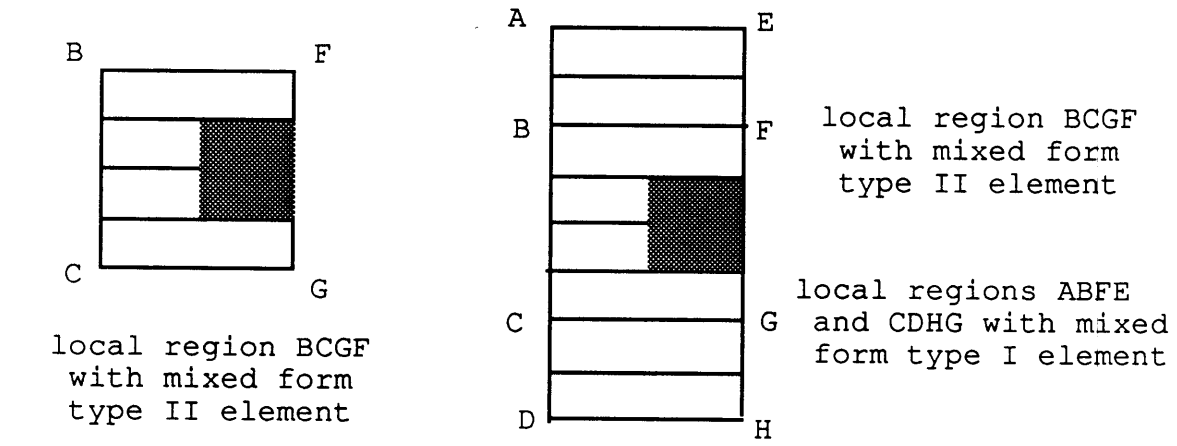

(b) model for local study

Figure 5.10 Suggestion of global and local finite element models for laminates having many layers

CHAPTER SIX

CONCLUSIONS AND RECOMMENDATIONS

6.1 Conclusions

A development has been made of two families, type I and type II, of mixed form hybrid stress elements for laminated composite plate analysis based on a mixed form of Hellinger-Reissner principle which is a function of three displacement components and three transverse stresses. The performances of these elements are verified by a large number of illustrative examples. Furthermore, the computational efficiency and accuracy of these elements along with the multi-step global-local finite element method for the laminated plate problems and various stress smoothing schemes for isotropic solids as well as laminated structures using the conventional hybrid stress model are also investigated.

The following conclusions are drawn from the present investigation:

1. The accuracy of the conventional hybrid stress element is less sensitive to the effect of

anisotropic material properties than that of the assumed displacement element.

2. For the case of laminate having large number of layers, the family of the mixed form type I hybrid stress laminated plate elements is the most computationally efficient element in predicting the interlaminar stresses compared to other laminated plate finite elements in the global analysis.

3. The mixed form type II hybrid stress laminated plate elements are much more computationally efficient than the type II hybrid stress laminated plate elements with all six components of stress and in some cases, the saving can be up to 45%.

4. The present mixed form hybrid stress elements along with the multi-step global-local finite element method is a very cost effective scheme in predicting the interlaminar stress distributions around the free edge regions of laminates.

5. The stress smoothing and equilibrium iteration schemes promise to add considerable accuracy to the existent finite element results by a relative small additional expenditure. However, they are not as computationally efficient as the present mixed form hybrid stress elements in application to laminated plates.

6.2 Suggestion for Future Work

The following subjects are recommended for future work:

1. The two families of mixed form hybrid stress laminated plate elements should be extended to laminated shell and sandwich plate structures.

2. Development of low order mixed form type I laminated plate hybrid stress elements with free of shear locking phenomenon in a thin plate limit and its extension to nonlinear analysis should be performed.

3. Examples in studying the effect of anisotropic material properties on the accuracy of various finite element model should be extended.

4. A study of an investigation of the effectiveness should be made of the multi-step global-local method for laminates having a large number of layers.

REFERENCES

1. J.M. Whitney, "The Effect of Transverse Shear Deformation on the Bending of Laminated Plates", J. Comp. Mater., Vol. 6, pp. 534-547, 1969.

2. A.K. Noor, "Stability of Multilayered Composite Plates", Fibre Sci. Tech., Vol. 8, pp. 81-89, 1974.

3. C. Wang, "Finite Element and Experimental Studies of Buckling of Laminated Thin-wall Structures", Sc.D. Thesis, Mass. Inst. of Tech., 1986.

4. S.P. Joshi and C.T. Sun, "Impact Induced Fracture in a Laminated Composite", J. Comp. Mater., vol. 19, pp. 51-68, 1985.

5. E. Reissner and Y. Stavsky, "Bending and Stretching of Certain Types of Heterogeneous Aeolotropic Plates", J. Appl. Mech. Vol. 28, pp. 402-408, 1961.

6. E. Reissner, "The Effect of Transverse Shear Deformation on the Bending of Elastic Plates", J. Appl. Mech., Vol. 12, pp. 69-77, 1945.

7. R.D. Mindlin, "Influence of Rotatory Inertia and Shear on Flexural Motions of Isotropic, Elastic Plates", J. Appl. Mech., Vol. 18, pp. 31-38, 1951.

8. P.C. Yang, C.H. Norris and Y. Stavsky, "Elastic Wave Propagation in heterogeneous Plates", Int. J. Solids Struct., Vol. 2, pp. 665-684, 1966.

9. F. Essenburg, "On the Significance of the Inclusion of the Effect of Transverse Normal Strain in Problems Involving Beams with Surface Constraints", J. Appl. Mech., Vol. 42, pp. 127-132, 1975.

10. J.M. Whitney and C.T. Sun, "A Higher Order Theory for Extension Motions of Laminated Plates", J. Sound Vibrat., Vol. 30, pp. 85-97, 1973.

11. R.B. Nelson and D.R. Lorch, "A Refined Theory of Laminated Orthotropic Plates", J. Appl. Mech., Vol. 41, pp.177-183, 1974.

12. E. Reissner, "On the Transverse Bending of Plates, Including the Effects of Transverse Shear Deformation", Int. J. Solids Struct., Vol. 11, pp. 569-573, 1975.

13. K.H. Lo, R.M. Christensen and E.M. Wu, "A High-order Theory of Plate Deformation, Part I: Homogeneous Plates", J. Appl. Mech., Vol. 44, pp. 663-668, 1977.

14. K.H. Lo, R.M. Christensen and E.M. Wu, "A High-order Theory of Plate Deformation, Part II: Laminated Plates", J. Appl. Mech., Vol. 44, pp. 669-676, 1977.

15. M. Levinson, "An Accurate Simple Theory of the Static and Dynamics of Elastic Plates", Mech. Res. Communications, Vol. 7, pp. 343-350, 1980.

16. M.V.V. Murthy, "An Improved Transverse Shear for Laminated Anisotropic Plates", NASA Technical Paper 1903, 1981.

17. J.N. Reddy, "A Refined Nonlinear Theory of Plates with Transverse Shear Deformation", Int. J. Solids Struct., Vol. 20, pp. 881-896, 1984.

18. J.N. Reddy, "A Simple Higher-order Theory for Laminated Composite Plates", J. Appl. Mech., Vol. 51, pp. 745-752, 1984.

19. A. Bhimaraddi and L.K. Stevens, "A Higher Order Theory for Free Vibration of Orthotropic, Homogeneous, and Laminated

Rectangular Plates", J. Appl. Mech., Vol. 51, pp. 195-198, 1984.

20. A.V. Krishna Murty and S. Vellaichamy, "On the Higher Order Shear Deformation Theory of Laminated Composite Panels", Composite Structure, Vol. 8, pp. 247-270, 1987.

21. C.T. Sun and J.M. Whitney, "Theories for the Dynamic Response of Laminated Plates", AIAA J., Vol.11, pp. 178-183, 1973.

22. S. Srinivas, "A Refined Analysis of composite Laminates", J. Sound Vibrat., Vol. 30, pp. 495-, 1973.

23. C.W. Pryor and R.M. Barker, "A Finite-Element Analysis Including Transverse Shear Effects for Applications to Laminated Plates", AIAA J., Vol. 9, pp. 912-917, 1971.

24. A.K. Noor and M.D. Mathers, "Finite Element Analysis of Anisotropic Plates", Int. J. Num. Meth. Engng., Vol. 11, pp. 289-307, 1977.

25. S.C. Panda and R. Natarajan, "Finite Element Analysis of Laminated Composite Plates", Int. J. Num. Meth. Engng., Vol. 14, pp. 69-79, 1979.

26. J.N. Reddy, "A Penalty Plate-Bending Element for the Analysis of Laminated Anisotropic Composite Plates", Int. J. Num. Meth. Engng., Vol. 15, pp. 1187-1206, 1980.

27. H.V. Lakshminarayana and S.S. Murthy, "A Shear-Flexible Triangular Finite Element Model for Laminated Composite Plates", Int. J. Num. Meth. Engng., Vol. 20, pp. 591-623, 1984.

28. J.J. Engblom and O.O. Ochoa, "Through-the-Thickness Stress Predictions for Laminated Plates of Advanced Composite Materials", Int. J. Num. Meth. Engng., Vol. 21, pp. 1759-1776, 1985.

29. J.J. Engblom and O.O. Ochoa, "Finite Element Formulation Including Interlaminar Stress Calculations", Comput. Struct., Vol. 23, pp. 241-249, 1986.

30. B.N. Pandya and T. Kant, "Flexural Analysis of Laminated Composites Using Refined Higher-Order C^0 Plate Bending Elements", Comput. Meth. Appl. Mech. Engng., Vol. 66, pp. 173-198, 1988.

31. N.S. Putcha and J.N. Reddy, "A Refined Mixed Shear Flexible Finite Element for the Nonlinear Analysis of Laminated Plates", Comput. Struct., Vol. 22, pp. 529-538, 1986.

32. Y.K. Kwon and J.E. Akin, "Analysis of Layered Composite Plates Using a High-Order Deformation Theory", Comput. Struct., Vol. 27, pp. 619-623, 1987.

33. R.L. Spilker, S.C. Chou and O. Orringer, "Alternate Hybrid Stress Elements for Analysis of Multilayer Composite Plates", J. Comp. Mater., Vol. 11, pp. 51-70, 1977.

34. R.L. Spilker and M. Jakobs, "Hybrid Stress Reduced-Mindlin Elements for Thin Multilayer Plates", Int. J. Num. Meth. Engng., Vol. 23, pp. 555-578, 1986.

35. D.J. Haas and S.W. Lee, "A Nine-Node Assumed-Strain Finite Element for Composite Plates and Shells", Comput. Struct., Vol. 26, pp. 445-452, 1987.

36. A.S. Mawenya and J.D. Davies, "Finite Element Bending Analysis of Multilayer Plates", Int. J. Num. Meth. Engng., Vol. 8, pp. 215-225, 1974.

37. R.A. Chaudhuri, "An Equilibrium Method for Prediction of Transverse Shear Stresses in a Thick Laminated Plate", Comput. Struct., Vol. 23, pp. 139-146, 1986.

38. R.A. Chaudhuri and P. Seide, "An Approximate Semi-analytical Method for Prediction of Interlaminar Shear Stresses in an Arbitrarily Laminated Thick Plate", Comput. Struct., Vol. 25, pp. 627-636, 1987.

39. D.R.J. Owen and Z.H. Li, "A Refined Analysis of Laminated Plates by Finite Element Displacement Methods--I. Fundamentals and Static Analysis", Comput. Struct., Vol. 26, pp. 907-914, 1987.

40. D.R.J. Owen and Z.H. Li, "A Refined Analysis of Laminated Plates by Finite Element Displacement Methods--II. vibration and Stability", Comput. Struct., Vol. 26, pp. 915-923, 1987.

41. S.T. Mau, P. Tong and T.H.H. Pian, "Finite Element Solutions for Laminated Thick Plates", J. Comp. Mater., Vol. 6, pp. 304-311, 1972.

42. R.L. Spilker, "A Hybrid-stress Finite-element Formulation for Thick Multilayer Laminates", Comput. Struct., Vol. 11, pp. 507-514, 1980.

43. R.L. Spilker, "An Invariant Eight-Node Hybrid-Stress Element for Thin and Thick Multilayer Laminated Plates", Int. J. Num. Meth. Engng., Vol. 20, pp. 573-587, 1984.

44. W.J. Liou and C.T. Sun, "A Three-dimensional Hybrid Stress Isoparametric Element for the Analysis of Laminated Composite Plates", Comput. Struct., Vol. 25, pp. 241-249, 1987.

45. K. Moriya, "Laminated Plate and Shell Elements for Finite Element Analysis of Advanced Fiber Reinforced Composite Structures" (in Japanese), Nippon Kikai Gakkai Ronbunshu, A Hen, Vol. 52, No. 478, pp. 1600-1607, 1986.

46. R.B. Pipes and N.J. Pagano, "Interlaminar Stresses in Composite Laminates Under Uniform Axial Extension", J. Comp. Mater., Vol. 4, pp. 538-548, 1970.

47. E. Altus, A. Rotem and M. Shmueli, "Free Edge Effect in Angle-ply Laminates - A New Three-Dimensional Finite Difference Solution", J. Comp. Mater., Vol. 14, pp. 21-30, 1980.

48. E.F. Rybicki, "Approximate Three-Dimensional Solutions for Symmetric Laminates Under Inplane Loading", J. Comp. Mater., Vol. 5, pp. 354-360, 1971.

49. A.S.D. Wang and F.W. Crossman, "Some New Results on Edge Effect in Symmetric Composite Laminates", J. Comp. Mater., vol. 11, pp. 92-106, 1977.

50. A.S.D Wang and F.W. Crossman, "Calculation of Edge Stresses in Multi-Layer Laminates by Sub-Structuring", J. Comp. Mater., Vol. 12, pp. 76-83, 1978.

51. R.L. Spilker, "A Traction-Free-Edge Hybrid-Stress Element for the Analysis of Edge Effects in Cross-ply Laminates", Comput. Struct., Vol. 12, pp. 167-179, 1980.

52. I.S. Raju and J.H. Crews, "Interlaminar Stress Singularities at a Straight Free Edge in Composite Laminates", Comput. Struct., Vol. 14, pp. 21-28, 1981.

53. S.S.Wang and F.G. Yuan, "A Singular Hybrid Finite Element Analysis of Boundary-Layer Stresses in Composite Laminates", Int. J. Solids and Struct., Vol. 19, pp. 825-837, 1983.

54. S.S. Wang and I. Choi, "Boundary-Layer Effects in Composite Laminates: Part I - Free Edge Stress Singularities", J. Appl. Mech., Vol. 49, pp. 541-548, 1982.

55. S.S. Wang and I. Choi, "Boundary-Layer Effects in Composite Laminates: Part II - Free Edge Stress Solutions and Basic Characteristics", J. Appl. Mech., Vol. 49, pp. 549-560, 1982.

56. S.W. Lee, J.J. Rhiu and S.C. Wong, "Hybrid Finite Element Analysis of Free Edge Effect in Symmetric Composite Laminates", UMAE TR 83-3, Dept. of Aerospace Engng., Univ. of Maryland, June 1983.

57. J.R. Yeh and I.G. Tadjbakhsh, "Stress Singularity in Composite Laminates by Finite Element Method", J. Comp. Mater., Vol. 20, pp. 347-364, 1986.

58. Y. Yamada and H. Okumura, "Finite Element Analysis of Stress and Strain Singularity Eigenstate in Inhomogeneous Media or Composite Materials", Hybrid and Mixed Finite Element Method, Edited by S.N. Atluri, R.H. Gallagher and O.C. Zienkiewicz, 1983.

59. P.L.N. Murthy and C.C. Chamis, "A Study of Interply Layer Effects on the Free Edge Stress Field of Angleplied Laminates", Comput. Struct., Vol. 20, pp. 431-441, 1985.

60. S. Tang, "A Boundary Layer Theory - Part I: Laminated Composite in Plane Stress", J. Comp. Mater., Vol. 9, pp. 33-41, 1975.

61. S. Tang and A. Levy, "A Boundary Layer Theory - Part II: Extension of Laminated Finite Strip", J. Comp. Mater., Vol. 9, pp. 42-50, 1975.

62. S. Tang, "Interlaminar Stresses Around Circular Cutouts in Composite Plates Under Tension", AIAA J., vol. 15, pp. 1631-1637, 1977.

63. P.W. Hsu and C.T. Herakovich, "Edge Effects in Angle-Ply Composite Laminates", J. Comp. Mater., Vol. 11, pp. 422-428, 1977.

64. P. Bar-Yoseph and J. Avrashi, "New Variational-Asymptotic Formulations for the Interlaminar Stress Analysis in Laminated Plates", J. Appl. Math. Phys. (ZAMP), Vol. 37, pp. 305-321, 1986.

65. P. Bar-Yoseph and J. Avrashi, "On the Nature of the Free Edge Stress Singularity in Composite Laminated Plates", Int. J. Num. Meth. Engng., Vol. 26, pp. 1507-1523, 1988.

66. P. Bar-Yoseph and J. Avrashi, "Interlaminar Stress Analysis for Laminated Plates containing a Curvilinear Hole", Comput. Struct., Vol. 21, pp. 917-932, 1985.

67. P. Bar-Yoseph and G. Siton, "The Effect of Material Nonlinearity on the Interlaminar Stress Field in Composite Laminates", Comput. Struct., vol. 21, pp. 1105-1118, 1985.

68. R.I. Zwiers, T.C.T. Ting and R.L. Spilker, "On the Logaritmic Singularity of Free-Edge Stress in Laminated Composites Under Uniform Extension", J. Appl. Mech., Vol. 49, pp. 561-569, 1982.

69. N.J. Pagano, "Stress Fields in Composite Laminates", Int. J. Solids Struct., Vol. 14, pp. 385-400, 1978.

70. N.J. Pagano and S.R. Soni, "Global-Local Laminate Variational Model", Int. J. Solids Struct., Vol. 19, pp. 207-228, 1983.

71. J.T.S. Wang and J.N. Dickson, "Interlaminar Stresses in Symmetric Composite Laminates", J. Comp. Mater., Vol. 12, pp. 390-402, 1978.

72. G.K. Mandell, "Analysis of Free-Edge Effects in Composite Laminates by an Assumed-Stress Method", M.S. Thesis, Mass. Inst. of Tech., 1970.

73. C. Kassapoglou and P.A. Lagace, "Closed Form Solutions for the Interlaminar Stress Field in Angle-Ply and Cross-Ply Laminates", J. Comp. Mater., Vol. 21, pp. 292-308, 1987.

74. C. Kassapoglou and P.A. Lagace, "An Efficient Method for the Calculation of Interlaminar Stresses in Composite Materials", J. Appl. Mech., Vol. 53, pp. 744-750, 1986.

75. T. Nishioka and S.N. Atluri, "Stress Analysis of Holes in Angle-Ply Laminates: An Efficient Assumed Stress "Special-Hole-Element" Approach and A Simple Estimation Method", Comput. Struct., Vol. 15, pp. 135-147, 1982.

76. O.C. Zienkiewicz, X.K. Li and S. Nakazawa, "Iterative Solution of Mixed Problems and the Stress Recovery Procedures", Communications in Appl. Num. Meth., Vol. 1, pp.3-9, 1985.

77. J.D. Whitcomb, I.S. Raju and J.G. Goree, "Reliability of the Finite Element Method for Calculating Free Edge Stresses in Composite Laminates", Comput. Struct., Vol. 15, pp. 23-37, 1982.

78. J. Storch and G. Strang, "Paradox Lost: Natural Boundary Conditions in the Ritz-Galerkin Method", Int. J. Num. Meth. Engng., Vol. 26, pp. 2255-2266, 1988.

79. T.H.H. Pian, P. Tong and C.H. Luk, "Elastic Crack Analysis by a Finite Element Method", Proc. Third Conf. on Matrix Methods in Structural Mechanics, AFFDL-TR-71-160, Wright-Patterson AFB, PP. 661-682, 1971.

80. E. Schnack and M. Wolf, "Application of Displacement and Hybrid Stress Methods to Plane Notch and Crack Problems", Int. J. Num. Meth. Engng., Vol. 12, pp. 963-975, 1978.

81. E. Reissner, "On a Certain Mixed Variational Theorem and a Proposed Application", Int. J. Num. Meth. Engng., Vol. 20, pp. 1366-1368, 1984.

82. E. Reissner, "On a Mixed Variational Theorem and on Shear Deformable Plate Theory", Int. J. Num. Meth. Engng., vol. 23, pp. 193-198, 1986.

83. Q. Huang, "Variational Principle of Hybrid Energy and the Fundamentals of 3-D Laminate Theory -- A New Approach for the Analysis of Interlaminar Stresses in Composite Laminates", Appl. Math. Mech. (English ed.), Vol. 9, pp. 649-666, 1988.

84. T.H.H. Pian and D.P. Chen, "Alternative Ways for Formulation of Hybrid Stress Elements", Int. J. Num. Meth. Engng., Vol. 18, pp. 1679-1684, 1982.

85. K. Washizu, Variational Method in Elasticity and Plasticity, 3rd edition, Pergamon Press, 1982.

86. T.H.H. Pian, "Derivation of Element Stiffness Matrices by Assumed Stress Distributions", AIAA Journal, No.2, pp. 1333-1336, 1964.

87. T.H.H. Pian and P. Tong, "Basis of Finite Element Methods for Solid Continua", Int. J. Num. Meth. Engng., Vol. 1, pp. 3-28, 1969.

88. S.G. Lekhnitskii, Theory of Elasticity of an Anisotropic Elastic Body, Holden-Day, Inc., 1963

89. B.M. Fraeijs de Veubeke, "Displacement and Equilibrium Models in Finite Element Method", in Stress Analysis,

Edited by O.C. Zienkiewicz and G.S. Holister, Wiley, pp. 145-197, 1964.

90. H. Stolarski and T. Belystschko, "Limitation Principles for Mixed Finite Elements Based on the Hu-Washizu Variational Formulation", in Hybrid and Mixed Finite Element Methods edited by R.L. Spilker and K.W. Reed, The Applied Mechanics Division, ASME, AMD-Vol. 73, pp. 123-132, 1985.

91. D. Kang, "C^0 Continuity Elements by Hybrid Stress Method", M.S. Thesis, Mass. Inst. of Tech., 1982.

92. R.L. Spilker, S.M. Maskeri and E. Kania, "Plane Isoparametric Hybrid-stress Elements: Invariance and Optimal Sampling", Int. J. Num. Meth. Engng., Vol. 18, pp. 445-465, 1982.

93. T.H.H. Pian and K. Sumihara, "Rational Approach for Assumed Stress Finite Elements", Int. J. Num. Meth. Engng., Vol. 20, pp. 1685-1695, 1984.

94. T.H.H. Pian and D.P. Chen, "On the Suppression of Zero Energy Deformation Modes", Int. J. Num. Meth. Engng., Vol. 19, pp. 1741-1752, 1983.

95. T.H.H. Pian, D.P. Chen and D. Kang, "A New Formulation of Hybrid/mixed Finite Element", Comput. Struct., Vol. 16, pp. 81-87, 1983.

96. B. Irons and S. Ahmad, Techniques of Finite Elements, Ellis Horwood, 1980.

97. P. Tong and T.H.H. Pian, "A Variational Principle and the Convergence of the Finite Element Method Based on Assumed Stress Distribution", Int. J. Solids Struct., Vol. 5, pp. 436-472, 1969.

98. W.M. Xue and S.N. Atluri, "Existence and Stability, and Discrete BB and Rank Conditions, for General Mixed-hybrid

Finite Elements in Elasticity", in Hybrid and Mixed Finite Element Methods edited by R.L. Spilker and K.W. Reed, The Applied Mechanics Division, ASME, AMD-Vol. 73, pp. 91-112, 1985.

99. Qian Huang, "Three Dimensional Composite Finite Element for Stress Analysis of Anisotropic Laminate Structures", Ph.D. Thesis, Concordia University, 1989.

100. O.C. Zienkiewicz, The Finite Element Method, 3rd edition, McGraw-Hill, 1977.

101. D.S. Malkus and T.J.R. Hughes, "Mixed Finite Element Methods--Reduced and Selective Integration Techniques: a Unification of Concepts", Comput. Meth. Appl. Mech. Engng., Vol. 15, pp.63-81, 1978.

102. A.F. Saleeb and T.Y. Chang, "An Efficient Quadrilateral Element for Plate Bending Analysis", Int. J. Num. Meth. Engng., Vol. 24, pp. 1123-1155, 1987.

103. R.L. Spilker, "Hybrid-stress Eight-node Elements for Thin and Thick Multilayer Laminated Plates", Int. J. Num. Meth. Engng., Vol. 18, pp. 801-828, 1982.

104. R.L. Spilker, "High-order Three-dimensional Hybrid-stress Elements for Thick Plate analysis", Int. J. Num. Meth. Engng., Vol. 17, pp. 53-69, 1981.

105. N.J. Pagano, "Exact Solutions for Composite Laminates in Cylindrical Bending", J. Comp. Mater., Vol. 3, pp. 398-411, 1969.

106. N.J. Pagano, "Exact Solutions for Rectangular Bidirectional Composites and Sandwich Plates", J. Comp. Mater., Vol. 4, pp. 20-34, 1970.

107. J.T. Oden and J.N. Reddy, "Note on an Approximate Method for Computing Consistent Conjugate Stresses in Elastic

Finite Elements", Int. J. Num. Meth. Engng., Vol. 6, pp. 55-61, 1973.

108. E. Hinton and J. Campbell, "Local and Global Smoothing of Discontinuous Finite Element Functions Using a Least Square Method", Int. J. Num. Meth. Engng., Vol. 8, pp. 461-480, 1974.

109. G. Loubrignac, G. Cantin and G. Touzot, "Continuous Stress Field in Finite Element Analysis", AIAA J., Vol. 15, pp. 1645-1647, 1977.

110. G. Cantin, G. Loubrignac and G. Touzot, "An Iterative Algorithm to Build Continuous Stress and Displacement Solutions", Int. J. Num. Meth. Engng., Vol. 12, pp. 1493-1506, 1978.

111. E. Stein and R. Ahmed, "An Equilibrium Method for Stress Calculation Using Finite Element Displacement Models", Comput. Meths. Appl. Mech. and Engng., Vol. 10, pp. 175-198, 1977.

112. C.K. Chen, "Studies of Stress Smoothing in Finite Element Analysis", M.S. Thesis, Mass. Inst. of Tech., 1983.

113. W.C. Hwang and C.T. Sun, "Analysis of Interlaminar Stresses near Curved Free-Edges of Laminates Composites Using Iterative Finite Element Method", Comput. Struct., Vol. 28, pp. 461-467, 1988.

114. T.H.H. Pian and P. Tong, "Relations Between Incompatible Displacement Model and Hybrid Stress Model", Int. J. Num. Meth. Engng., vol. 22, pp. 173-181, 1986.

115. K. Kafie, "Traction Free Finite Elements with the Assumed Stress Medel", M.S. Thesis, Mass. Inst. of Tech., 1981.

116. Z. Pammer, "P-Extended Finite Elements Are Tested", Benchmark by NAFEMS (National Agency for Finite Element Methods and Standards, UK), pp. 18-21, April 1988.

117. R.H. MacNeal and R.L. Harder, "A Proposed Standard Set of Problems to Test Finite Element Accuracy", Finite Element in Analysis and Design, Vol. 1, pp. 3-20, 1985.

118. C.T. Sun and K.M. Mao, "A Global-Local Finite Element Method Suitable for Parallel Computations", Comput. Struct., Vol. 29, pp. 309-315, 1988.

119. S.B. Dong, "Global-Local Finite Element Methods", State-of-the-Art Surveys on Finite Element Technology, Edited by A.K. Noor and W.D. Pilkey, 1983.

120. W.M. Luckings, S.V. Hoa and T.S. Sankar, "The Effect of Geometry on Interlaminar Stresses of $[0/90]_s$ Composite Laminates with Circular Holes", J. Comp. Struct., Vol. 18, pp. 188-198, 1984.

121. G.N. Savin, "Stress Distributions Around Holes", Pergamon Press, 1961.

122. I.S. Raju and J.H. Crews, "Three Dimensional Analysis of $[0/90]_s$ and $[90/0]_s$ Laminates with a Central Circular Hole", NASA-TM-83300, 1982.

APPENDIX

FORMULATION FOR UNIFORM INPLANE STRAIN OF CROSS PLY LAMINATES

Formulation of cross ply laminates subjected to prescribed uniform inplane strain $\bar{\varepsilon}_x$ is presented here and shown in Figure 5.2. As a result of the symmetry of the structures, the material property matrix of the laminates **S** is reduced to the form of Eq. (3.24) and the analysis is reduced to the plane yz as shown in Figure 5.3(b). The displacements **u** in the x, y and z directions are assumed to be in the form

$$\mathbf{u} = \begin{bmatrix} x\bar{\varepsilon}_x \\ v(y,z) \\ w(y,z) \end{bmatrix} \tag{A.1}$$

As a result of the form of Eq. (A.1), the following shear strains and stresses vanish,

$$\gamma_{xz} = \gamma_{xy} = 0 \quad \text{and} \quad \sigma_{xz} = \sigma_{xy} = 0 \tag{A.2}$$

The inplane normal stress σ_x is also eliminated by requiring that the corresponding inplane strain calculated from the stresses be equal to the prescribed value $\bar{\varepsilon}_x$. Therefore

$$\sigma_x = (\bar{\varepsilon}_x - S_{12}\sigma_y - S_{13}\sigma_z)/S_{11} \qquad (A.3)$$

Substitution of Eqs. (A.1) to (A.3) into the following Hellinger-Reissner principle which involves all displacements and stresses in the form

$$\pi_R(\mathbf{u},\sigma) = \int_V [-\frac{1}{2}\sigma^T \mathbf{S}\sigma + \sigma^T(\mathbf{D}\mathbf{u})]dV = \text{stationary} \qquad (A.4)$$

where

σ, $\mathbf{S}$, $\mathbf{D}$ and $\mathbf{u}$ are given in Eq. (3.1)

we obtain

$$\pi_R(\tilde{\mathbf{u}},\tilde{\sigma}) = \int_A [-\frac{1}{2}\tilde{\sigma}^T \tilde{\mathbf{S}}\,\tilde{\sigma} + \tilde{\sigma}^T(\tilde{\mathbf{D}}\tilde{\mathbf{u}})]dA - \bar{\varepsilon}_x \int_A \tilde{\sigma}^T \begin{bmatrix} \frac{S_{12}}{S_{11}} \\ 0 \\ \frac{S_{13}}{S_{11}} \end{bmatrix} dA \qquad (A.5)$$

where

$$\tilde{\mathbf{u}} = \{v, w\}^T$$

$$\tilde{\sigma} = \{\sigma_y, \tau_{yz}, \sigma_z\}^T$$

$$\tilde{\mathbf{S}} = \begin{bmatrix} (S_{22} - \frac{S_{12}^2}{S_{11}}) & 0 & (S_{23} - \frac{S_{12}S_{13}}{S_{11}}) \\ 0 & S_{44} & 0 \\ (S_{23} - \frac{S_{12}S_{13}}{S_{11}}) & 0 & (S_{33} - \frac{S_{13}^2}{S_{11}}) \end{bmatrix}$$

$$\tilde{\mathbf{D}} = \begin{bmatrix} \frac{\partial}{\partial y} & 0 \\ 0 & \frac{\partial}{\partial z} \\ \frac{\partial}{\partial z} & \frac{\partial}{\partial y} \end{bmatrix}$$

A = area of the continuum in the plane yz

We begin by dividing the stresses and strains into the inplane and transverse parts, as

$$\tilde{\sigma} = \begin{bmatrix} \tilde{\mathbf{t}}_p \\ \tilde{\mathbf{t}}_t \end{bmatrix} \qquad \text{(A.6.a)}$$

$$\tilde{\varepsilon} = \tilde{\mathbf{D}}\,\tilde{\mathbf{u}} = \begin{bmatrix} \tilde{\mathbf{e}}_p \\ \tilde{\mathbf{e}}_t \end{bmatrix} \qquad \text{(A.6.b)}$$

$$\tilde{\mathbf{t}}_p = \{ \sigma_y \} \qquad \text{(A.6.c)}$$

$$\tilde{\mathbf{t}}_t = \{ \tau_{yz}, \sigma_z \}^T \qquad \text{(A.6.d)}$$

$$\tilde{\mathbf{e}}_p = \{ \varepsilon_y \} = \tilde{\mathbf{D}}_p \tilde{\mathbf{u}} \qquad \text{(A.6.e)}$$

$$\tilde{\mathbf{e}}_t = \{ \gamma_{yz}, \varepsilon_z \}^T = \tilde{\mathbf{D}}_t \tilde{\mathbf{u}} \qquad \text{(A.6.f)}$$

where

$$\tilde{\mathbf{D}}_p = \begin{bmatrix} \frac{\partial}{\partial y} & 0 \end{bmatrix}$$

$$\tilde{\mathbf{D}}_t = \begin{bmatrix} \frac{\partial}{\partial z} & \frac{\partial}{\partial y} \\ 0 & \frac{\partial}{\partial z} \end{bmatrix}$$

Furthermore, the stress-strain relation can be expressed as

$$\begin{bmatrix} \tilde{\mathbf{e}}_p \\ \tilde{\mathbf{e}}_t \end{bmatrix} = \begin{bmatrix} \tilde{\mathbf{S}}_p & \tilde{\mathbf{S}}_{pt} \\ \tilde{\mathbf{S}}_{pt}^T & \tilde{\mathbf{S}}_t \end{bmatrix} \begin{bmatrix} \tilde{\mathbf{t}}_p \\ \tilde{\mathbf{t}}_t \end{bmatrix} + \bar{\varepsilon}_x \begin{bmatrix} \frac{S_{12}}{S_{11}} \\ 0 \\ \frac{S_{13}}{S_{11}} \end{bmatrix} \qquad (A.7)$$

Substituting Eqs. (A.6) and (A.7) into Eq. (A.5), we get

$$\pi_R(\tilde{\mathbf{u}}, \tilde{\mathbf{t}}_p, \tilde{\mathbf{t}}_t) = \int_A [-\frac{1}{2}\tilde{\mathbf{t}}_p^T \tilde{\mathbf{S}}_p \tilde{\mathbf{t}}_p - \tilde{\mathbf{t}}_p^T \tilde{\mathbf{S}}_{pt} \tilde{\mathbf{t}}_t - \frac{1}{2}\tilde{\mathbf{t}}_t^T \tilde{\mathbf{S}}_t \tilde{\mathbf{t}}_t + \tilde{\mathbf{t}}_p^T \tilde{\mathbf{e}}_p +$$

$$\tilde{\mathbf{t}}_t^T \tilde{\mathbf{e}}_t] dA - \bar{\varepsilon}_x \int_A \{ \tilde{\mathbf{t}}_p \frac{S_{12}}{S_{11}} + \tilde{\mathbf{t}}_t^T \begin{bmatrix} 0 \\ \frac{S_{13}}{S_{11}} \end{bmatrix} \} dA \qquad (A.8)$$

From the first half of Eq. (A.7), we can solve for $\tilde{\mathbf{t}}_p$ in terms of $\tilde{\mathbf{e}}_p$, $\tilde{\mathbf{t}}_t$ and $\bar{\varepsilon}_x$

$$\tilde{t}_p = \tilde{C}_p \tilde{e}_p + \tilde{C}_{pt} \tilde{t}_t - \bar{\varepsilon}_x \frac{S_{12}}{S_{11}} \tilde{C}_p \tag{A.9}$$

where

$$\tilde{C}_p = \tilde{S}_p^{-1}$$

$$\tilde{C}_{pt} = -\tilde{C}_p \tilde{S}_{pt} = \tilde{C}_{tp}^T$$

Substitution of Eq. (A.9) into Eq. (A.8) yields the following mixed variational functional for an uniform inplane strain $\bar{\varepsilon}_x$

$$\pi_{mR}(\tilde{u}, \tilde{t}_t) = \int_A [\frac{1}{2} \tilde{e}_p^T \tilde{C}_p \tilde{e}_p + \tilde{t}_t^T \tilde{C}_{tp} \tilde{e}_p - \frac{1}{2} \tilde{t}_t^T \tilde{S}_t^* \tilde{t}_t + \tilde{t}_t^T \tilde{e}_t] dA$$

$$- \bar{\varepsilon}_x \int_A \{ \tilde{e}_p^T \frac{S_{12}}{S_{11}} \tilde{C}_p + \tilde{t}_t^T [\frac{S_{12}}{S_{11}} \tilde{C}_{pt}^T + \begin{bmatrix} 0 \\ \frac{S_{13}}{S_{11}} \end{bmatrix}] \} dA \tag{A.10}$$

where

$$\tilde{S}_t^* = \tilde{S}_t - \tilde{S}_{pt}^T \tilde{C}_p \tilde{S}_{pt}$$

with the constraint equations (A.6.e), (A.6.f) and (A.9).

Once again, we rewrite the mixed variational principle into a modified form for the finite element formulation

$$\pi_{mR}^* = \sum_n \{ \int_{A_n} [\frac{1}{2} \tilde{e}_p^T \tilde{C}_p \tilde{e}_p + \tilde{t}_t^T \tilde{C}_{tp} \tilde{e}_p - \frac{1}{2} \tilde{t}_t^T \tilde{S}_t^* \tilde{t}_t + \tilde{t}_t^T \tilde{e}_t] dA$$

$$-\bar{\varepsilon}_x \int_{A_n} \{ \tilde{\mathbf{e}}_p^T \frac{S_{12}}{S_{11}} \tilde{\mathbf{C}}_p + \tilde{\mathbf{t}}_t^T [\frac{S_{12}}{S_{11}} \tilde{\mathbf{C}}_{pt}^T + \begin{bmatrix} 0 \\ \frac{S_{13}}{S_{11}} \end{bmatrix}] \} dA \} \qquad (A.11)$$

where

n = number of element

A_n = spatial domain of element n

The displacement and stress fields are expressed as

$$\tilde{\mathbf{u}} = \mathbf{N}\ \mathbf{q} \qquad (A.12.a)$$

$$\tilde{\mathbf{t}}_t = \mathbf{P}\ \beta \qquad (A.12.b)$$

where

$\mathbf{N}$ = matrix of shape functions

$\mathbf{q}$ = nodal displacements

$\mathbf{P}$ = matrix of assumed polynomials

β = set of stress parameters

Introducing Eq. (A.12) into Eq. (A.11), the functional is reduced to the form

$$\pi^*_{mR} = \sum_n \{ \frac{1}{2} \mathbf{q}^T \mathbf{k}_p \mathbf{q} + \beta^T \mathbf{G} \mathbf{q} - \frac{1}{2} \beta^T \mathbf{H} \beta - \beta^T \mathbf{f}_t - \mathbf{q}^T \mathbf{f}_p \} \qquad (A.13)$$

where

$$\mathbf{k}_p = \int_{A_n} (\tilde{\mathbf{D}}_p \mathbf{N})^T \tilde{\mathbf{C}}_p (\tilde{\mathbf{D}}_p \mathbf{N})\, dA$$

$$\mathbf{G} = \int_{A_n} \mathbf{P}^T [\tilde{\mathbf{C}}_{tp} (\tilde{\mathbf{D}}_p \mathbf{N}) + \tilde{\mathbf{D}}_t \mathbf{N}]\, dA$$

$$\mathbf{H} = \int_{A_n} \mathbf{P}^T \tilde{\mathbf{S}}_t^* \mathbf{P}\, dA$$

$$\mathbf{f}_t = \bar{\varepsilon}_x \int_{A_n} \mathbf{P}^T \left[\frac{S_{12}}{S_{11}} \tilde{\mathbf{C}}_{pt}^T + \begin{bmatrix} 0 \\ \frac{S_{13}}{S_{11}} \end{bmatrix}\right] dA$$

$$\mathbf{f}_p = \bar{\varepsilon}_x \int_{A_n} \frac{S_{12}}{S_{11}} \mathbf{N}^T \tilde{\mathbf{C}}_p\, dA$$

Applying the stationary condition to Eq. (A.13) with respect to β, i.e. $\partial\pi/\partial\beta = \mathbf{0}$, we obtain

$$\mathbf{G}\,\mathbf{q} - \mathbf{H}\,\beta - \mathbf{f}_t = \mathbf{0}$$

and rewritten as

$$\beta = \mathbf{H}^{-1}(\mathbf{G}\,\mathbf{q} - \mathbf{f}_t) \qquad \text{(A.14)}$$

Substituting Eq. (A.14) into Eq. (A.13) and applying the stationary condition with respect to $\mathbf{q}$, i.e. $\partial\pi/\partial\mathbf{q} = \mathbf{0}$, we obtain

$$\mathbf{K}\,\mathbf{q} = \mathbf{Q} \qquad \text{(A.15)}$$

where

$\mathbf{K}$, $\mathbf{q}$ and $\mathbf{Q}$ are global matrices assembled from element matrices

$$\mathbf{k} = \mathbf{k}_p + \mathbf{G}^T \mathbf{H}^{-1} \mathbf{G}$$

$$\mathbf{Q} = \mathbf{f}_p + \mathbf{G}^T \mathbf{H}^{-1} \mathbf{f}_t$$